Winter 2019

# An Adaptive Hilbert-Huang Transform System

Joshua Letterman
*University of New Hampshire, Durham*

# AN ADAPTIVE HILBERT-HUANG TRANSFORM SYSTEM

BY
JOSHUA C. LETTERMAN

Bachelor of Science in Computer Engineering
University of New Hampshire, 2017

THESIS

Submitted to the University of New Hampshire

In Partial Fulfillment of the

Requirements for the Degree of

MASTER OF SCIENCE
IN
ELECTRICAL ENGINEERING

DECEMBER, 2019

This thesis has been examined and approved in partial fulfillment of the requirements for the degree of Master of Science in Electrical Engineering by:

Thesis Director, Dr. Richard Messner, Associate Professor of Electrical and Computer Engineering,
University of New Hampshire

Dr. Kent Chamberlin, Professor of Electrical and Computer Engineering,
University of New Hampshire

Dr. Nicholas Kirsch, Associate Professor of Electrical and Computer Engineering,
University of New Hampshire

Dr. Ron Croce, Professor of Kinesiology,
University of New Hampshire

# ACKNOWLEDGEMENTS

There is no way this thesis is completed without the support of my lovely and loving wife, Olga Letterman. An Applied Mathematician who listened to me ranting about function shapes, reviewed an endless series of plots that I couldn't quite make up my mind about, helped me think through problems, and generally just being there as a sounding board when I needed it most.

In addition to her support, I thank Dr. Messner for his gracious time listening to me drone on and on about the things I've done, the results I've gotten, and to validate or invalidate my thinking with respect to those results. It was a fun time bandying ideas about.

Thanks to Dr. Chamberlain and Dr. Croce both for their time, their input on the paper for which this research was able to provide a comparison and validation, and just to generally provide feedback whenever I needed it with no complaints. Incredibly supportive.

Thanks to Dr. Kirsch and Dr. Al-Badrawi for their time and domain expertise in Empirical Mode Decomposition research. Dr. Al-Badrawi's input both conversationally and with literature references generated significant changes to the research I completed and much of the work provided in this thesis came about due to his support.

Thanks to Dr. Michelle Cappozoli for her considerate donation of time and mental energy helping me understand some of the trickier statistical aspects of the results presented in this thesis. Without her help, at least one very serious error would have been committed on my part.

# PREFACE

The research presented in this thesis actually came about by chance. I was very interested in doing research work in the field of Brain-Computer Interfaces. While I was working through literature, I came across this thing called the Empirical Mode Decomposition and how a couple of researchers had great success using it in a BCI-type scheme for wheelchair control. My initial intention was to use the EMD decompositions to support further work in pattern recognition towards the larger goal of building a BCI system that could work reliably with new EEG thought patterns (such as might exist with imagining colors or other imagery).

But as I was in the middle of establishing the framework for the project, the EMD kept performing terribly for the purposes I needed. So, I started digging deeper and deeper until it sort of took on a life of its own. First, I experimented with various multivariate EMD schemes. Then I started digging into the EMD itself and why it behaved as it did. Finally, I was in full scale warfare with this decomposition method.

It was from this need-a-tool-build-a-tool that the current research found its genesis. Nevertheless, it was fun and rewarding work.

# TABLE OF CONTENTS

# LIST OF FIGURES

# LIST OF TABLES

# ABSTRACT

**An Adaptive Hilbert-Huang Transform System**

by

Joshua C. Letterman
University of New Hampshire, December 2019

This thesis presents a system which can be used to generate Intrinsic Mode Functions and the associated Hilbert spectrum resulting from techniques based on the Empirical Mode Decomposition as pioneered by N. E. Huang at the end of the 20$^{th}$ century. Later dubbed the Hilbert-Huang Transform by NASA, the process of decomposing data manually through repetitive detrending and subtraction followed by applying the Hilbert transform to the results was presented as a viable alternative to the wavelet transform which was gaining traction at the time but had shown significant limitations. In the last 20 years, the Hilbert-Huang Transform has received a lot of attention, but that attention has been miniscule relative to the amount of attention received by wavelet transformation. This is, in part, due to the limitations of the Empirical Mode Decomposition and also in part due to the difficulty in developing a theoretical basis for the manner in which the Empirical Mode Decomposition works. While the question of theoretical foundations is an important and tricky one, this thesis presents a system that breaks many of the previously known limits on band-width resolution, mode mixing, and viable decomposable frequency range relative to sampling frequency of the Empirical Mode Decomposition.

Many recent innovations do not simply improve on N. E. Huang's algorithm, but rather provide new approaches with different decompositional properties. By choosing the best technique at each step, a superior total decomposition can be arrived at. Using the Hilbert-Huang Transform itself during the

decomposition as a guide as suggested by R. Deering in 2005, the final HHT can show distinct improvements. The AHHT System utilizes many of the properties of various Empirical Mode Decomposition techniques from literature, includes some novel innovations on those techniques, and then manages the total decomposition in an adaptive manner.

The Adaptive Hilbert-Huang Transform System (AHHT) is demonstrated successfully on many different artificial signals, many with varying levels of noise down to -5dB SNR, as well as on an electrocardiogram and for comparison with a surface electromyographic study which found biopotential frequency-shifting associated with the fatigue of fast-twitch muscle fibers.

# INTRODUCTION

The EMD as part of the larger Hilbert-Huang Transform (HHT) was first proposed by N. Huang twenty years ago in a series of papers beginning in 1998 [1]. The Empirical Mode Decomposition (EMD) is an algorithm that decomposes signals, in a purely data-driven way, into a series of constituent Intrinsic Mode Functions (IMF) and a final leftover residual. An IMF is characterized by satisfying two properties: 1) the number of zero crossings and the number of local extrema may differ by no more than one, and 2) the local mean of the IMF must be zero. The completeness property of the EMD ensures that the original signal can be reconstituted by summing the IMFs together with the remaining residual.

The greatest benefit of the EMD, and by extension, the HHT, is the ability to analyze non-stationary and nonlinear signals in the time-frequency spectrum for which the DFT (Discrete Fourier Transform), STFT (Short-Time Fourier Transform), or CWT/DWT (Continuous/Discrete Wavelet Transform) may not be not well-suited. The DFT is unsuitable for nonstationary and nonlinear signals, while the STFT has been shown to be of limited use for such signals. Wavelet transformation provides for more granular time resolution, but not equally across all frequencies, and further requires *a priori* knowledge of the underlying signal in order to choose proper wavelets in the transform.

By decomposing signals into IMFs, the Hilbert transform may be applied to each mode revealing their instantaneous amplitudes and instantaneous phases. Instantaneous frequency vs. time may then be derived by $\omega_t = \frac{d\theta_t}{dt}$, where $d\theta_t$ represents instantaneous phase. The entire process of extracting IMFs

via the EMD and transforming them into instantaneous frequency vs amplitude vs time is often referred to as the Hilbert-Huang Transform (HHT). Since the decomposition is ordered, in that it extracts components of higher frequency first, the EMD may also be used in a filtering capacity. This is often applied in denoising schemes. Indeed, more than one researcher has shown that the EMD behaves as a dyadic filter bank in noise [2] [3].

Over the last two decades, the EMD has gained increasing attention and analysis, highlighting limitations and problems, and proposing mitigations and/or improvements. Many problems associated with the EMD include a) Types I and II Mode Mixing, b) limited bandwidth resolution, c) upper bounds on frequency decomposition relative to the Nyquist frequency, d) Phantom or transient IMFs, e) poor metrics for differentiating good decompositions from bad decompositions, f) poor mathematical modeling/definition of the algorithm, and g) difficulty in adequately decomposing multidimensional data [4].

Despite the improvements and mitigations that have been proposed by various researchers, the EMD continues to exhibit many of these problems. The goals of this research are to provide an alternative approach to the EMD and the HHT that improves on many of these limitations, to provide more meaningful decompositions, and to provide two improved metrics by which the decompositions of artificial signals can be evaluated.

EMD is no longer a single technique with one algorithmic version clearly superior to any other, but rather a group of techniques, each with the same fundamental principle; detrending and separation, but with disparate properties. Recognizing this, a system can be devised that decomposes signals into more meaningful, high-resolution IMFs and, ultimately, more meaningful frequency/amplitude/time representations. Developed and presented in this thesis is one such rudimentary system called the AHHT System. The AHHT System developed shows that Type-I and Type-II Mode Mixing can be surprisingly

reduced. In addition, bandwidth resolution can be improved beyond any known approach to-date. Examples shown suggest that the heretofore known limitations respecting the sampling frequency vs the highest decomposable spectral content via EMD are not as stringent as formerly believed, and that better data-driven metrics can be developed for quantitatively analyzing the decomposition of artificial signals.

However, it should be noted that AHHT was only tested on the signals described in this thesis and how it behaves on other real-world signals beyond those presented here is unclear. Many of the artificial signals in this thesis were generated at two different sampling frequencies so as to demonstrate the effect of higher resolution sampling on the overall decompositions and the associated comparisons between the various algorithms.

# Chapter 1

# BACKGROUND

The research detailed in this paper employs several distinct methods. This system utilizes various modifications to the EMD and HHT along with blind clustering in an attempt to optimize the decomposition process. Additionally, two Quality of Decomposition (QoD) metrics are used to compare the decompositions against noise-assisted variants of the EMD and the UPEMD. This chapter details relevant background information related to each of these.

## 1.1 EMPIRICAL MODE DECOMPOSITION

The original Empirical Mode Decomposition (EMD) and all variants of this algorithm rely on the fundamental principle of *sifting*—that is, repeatedly detrending a given signal in order to produce an Intrinsic Mode Function (IMF). After generating a mean trend via some interpolation scheme, the trend is subtracted from the signal and the remainder is tested for IMF sufficiency.

Sufficiency, or sifting stop criteria, is often not defined as simply conforming to the two IMF properties (local mean = 0, difference between extrema count and zero crossings <= 1) and/or a hard limit (no more than *k* sifting iterations), but via other criteria depending on the researcher, such as:

1) While at least two extrema are present, a threshold defined by the ratio of the standard deviation of two consecutive sifting results [1].

2) $k_2$ consecutive sifting iterations with the first IMF property satisfied [5]

3) Two threshold values $\theta_1$ and $\theta_2$. Let *mode amplitude* $a(t) := (e_{\max}(t) - e_{min}(t))/2$ and let the *evaluation function* be defined as $\sigma(t) := \left|\frac{m(t)}{a(t)}\right|$. "…sifting is iterated until $\sigma(t) < \theta_1$ for some prescribed fraction of $(1-\alpha)$ of the total duration, while $\sigma(t) < \theta_2$ for the remaining fraction. One can typically set $\alpha \approx 0.05$, $\theta_1 \approx 0.05$, and $\theta_2 \approx 10\theta_1$" [6] [7].

4) A ratio of the squared Euclidean norm of the envelope mean of the and the squared Euclidean norm of the proto-IMF is below some predetermined threshold [8].

Whatever the stopping criterion, ultimately, this *sifting* process results in an IMF which is then subtracted from the original signal and the decomposition continues until all IMFs have been extracted or some decomposition stop criterion has been met (again, dependent on the researcher's algorithm).

The original EMD algorithm (referred to in this thesis as the Classical EMD sifting algorithm or simply Classic EMD) is simple and elegant. First, the Sift function follows these steps:

1) Find the upper and lower extrema of the signal separately.

2) Create an *envelope* of the signal by interpolating the upper extrema using cubic spline interpolation. Repeat for the lower extrema.

3) Find the *envelope mean* at all index points by taking the average of the upper and lower interpolations.

4) Subtract the envelope mean from the signal.

5) If the sifting stop criterion has not yet been reached, repeat from step 1 on the detrended signal from step 4.

The Sift algorithm produces a single IMF. The full decomposition is likewise simple and elegant:

1) IMF = Sift(signal)

2) signal = signal - IMF

3) If the decomposition stop criterion has not yet been reached, repeat from step 1 on the reduced signal from step 2.

A single iteration of sifting is demonstrated in Fig. [1-1]. The full algorithm is detailed in the pseudocode in Algorithm 1.1, where details such as boundary extrema extrapolation or interpolation have been excluded for clarity.

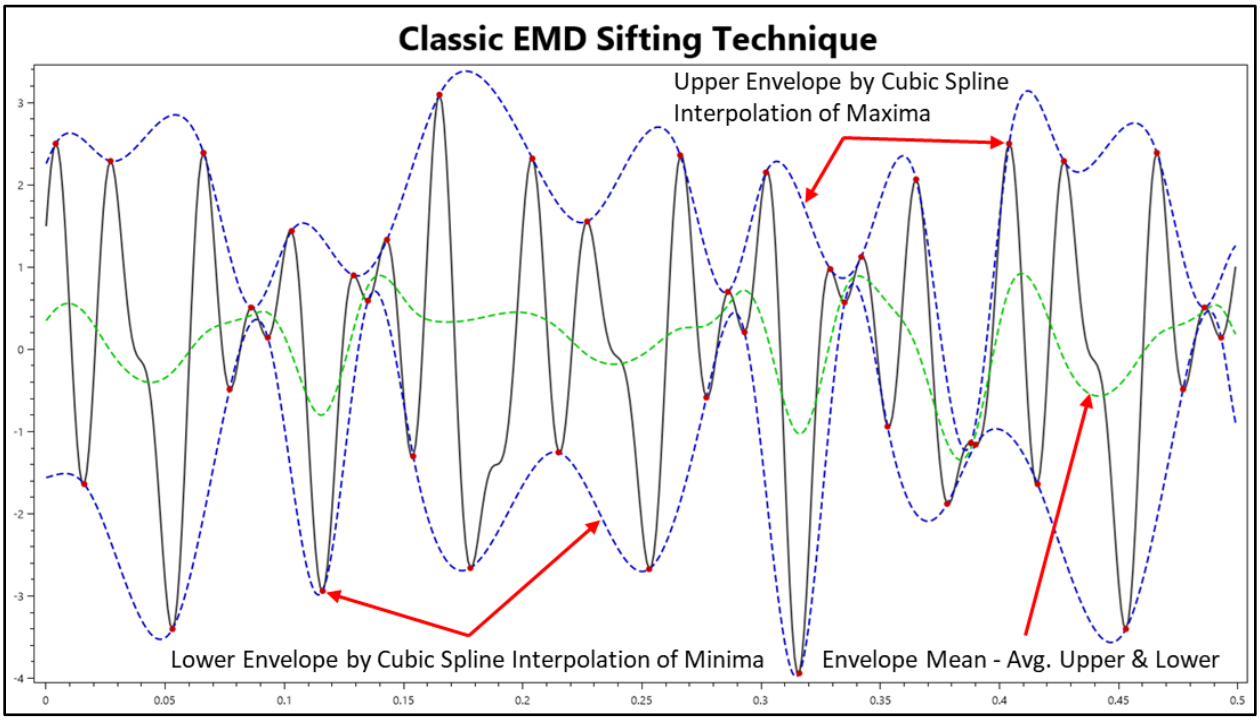


***Figure 1-1 Envelope Mean Development in the Classical EMD Sifting Technique***

**Algorithm 1.1: Classical EMD**

```
1:  function double[,] EMD (double[] x(t))
2:
3:  // Let x(t) be the decomposable signal.
4:  // Let r(t) represent a residual
5:  //   (the signal or residual minus the last IMF extracted from that signal or residual).
6:  // Let m_k(t) represent the k^th IMF of the decomposition
7:
8:  k = 0;
9:  do {
10:   r(t) = x(t);
11:   // The following do-while implements the Sift subroutine
12:   do {
13:     env^u = CubicSplineInterp(maxima(r(t)));
14:     env^l = CubicSplineInterp(minima(r(t)));
15:     env^μ = (env^u + env^l) / 2;
16:     r(t) -= env^μ;
17:   } while (not done sifting)
18:   m_k(t) = r(t);     // r(t) now holds the IMF signal, save it
19:
20:   // What remains is assigned to be decomposed in the next iteration
21:   x(t) -= r(t);     // subtract the IMF from the original signal
22:   k++;
23: } while (not done decomposing)
24:
25: // m(t) now holds all of the IMFs
26: // What remains in x(t) is the residual of the decomposition
```

Although the residual may satisfy the requirements to allow the application of the Hilbert transform, it may not, and therefore it is not strictly correct to transform them. However, in the HHT plots throughout this thesis, the Hilbert transform of the residual will be included except in the case where the residual is a straight line. Fig. [1-2.A] shows a simple two-tone signal. Fig. [1-2.B-C] shows the IMFs from its decomposition by the EMD implementation provided in MATLAB™ 2018b's Signal Processing Toolbox [9] and Fig. [1-2.D] shows the HHT of the signal. Signal #1 will be examined in more detail later but is introduced here to familiarize the reader with the EMD and HHT plots presented throughout this thesis. Note, the residual is not included in the IMF plots. Also note, signals in this thesis are characterized as having been sampled at 1 kHz to reduce the need for fractional frequencies in equations.

Signal #1 is extremely simple. There is one constant frequency component at 255 Hz and another 65 Hz frequency which appears over a short time interval. The EMD decomposed the signal in Fig. [1-2.A] and produced the IMFs seen in Figs. [1-2.B-C]. The Hilbert transform was applied to each IMF and the derived amplitude/frequency/time plot is depicted in the *heat line* plot of Fig. [1-2.D]. The *heat line* plot thus depicted is a multiline plot where the lines are colored according to a third dimensional scale (in the case of the HHT, the color bar is defined by amplitude, while the x-axis is time and the y-axis is frequency). Unlike heat maps which define values for the entire field (typically zero unless specified otherwise), heat line plots only give meaningful value to plot lines. As a result, heat line plots are often able to be generated much faster and are pedantically more accurate.

In this HHT plot, the two components of Signal #1 appear as two mostly straight red lines at 255 Hz and 65 Hz respectively. The 255 Hz line is constant while the 65 Hz line appears only over the interval where that component exists in the original signal. Both are a red color that matches to the value 1 on the colorbar to indicate amplitude 1.

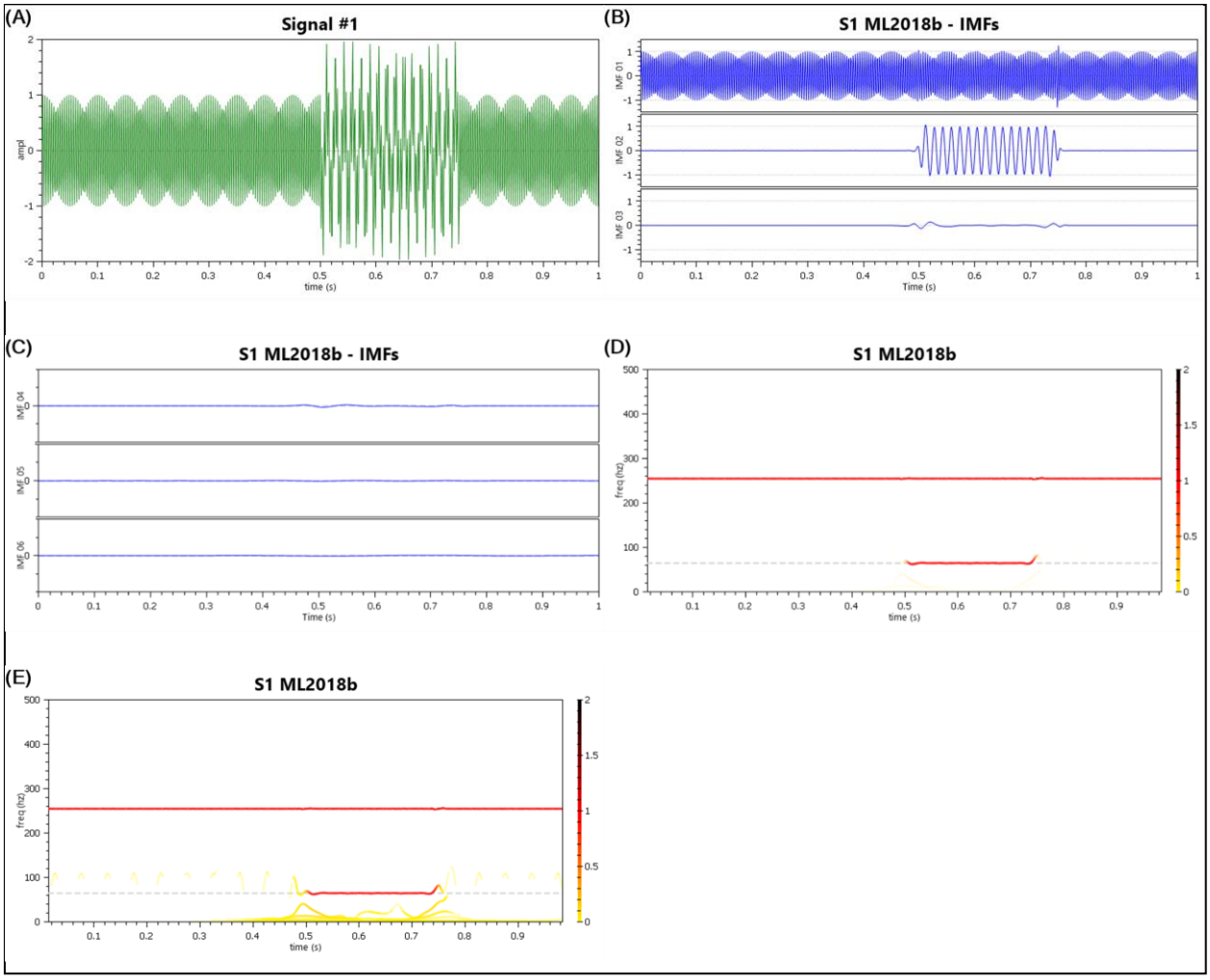


***Figure 1-2 Simple Signal Decomposed by EMD. A) Signal, B) First 3 IMFs of the Decomposition, C) Next 3 IMFs of the Decomposition, D) Hilbert Transform of All IMFs, E) Hilbert Transform of All IMFs With No Transparency***

Note: The HHT plot in Fig. [1-2.D] uses an opacity-reduction approach to reduce the visibility of very low amplitude lines. If this were not done, the HHT plot would look more like the one seen in Fig. [1-2.E]. In more complicated signals, these transient IMFs would obscure the results we would like to observe. However, in some cases, especially when the information being decomposed has both high and low amplitude signals, the transparency settings are manually adjusted for better appearance. Also, the HHT plots provided in this thesis often include dashed lines representing where components are expected to be found as seen in Figs. [1-2.D & E].

The Hilbert transform applied in this thesis returns amplitude and phase for each time step. However, numerical imprecision leads to a certain amount of instability in deriving $\frac{d\theta_t}{dt}$ (the instantaneous frequency at each time step). Since phase is circular about 2π, phase unwrapping creates additional complication. Thus, it is possible to have error in the derivation and even negative frequencies can result. There is much literature on the topic of phase unwrapping (ex. [10] [11] [12]). For the AHHT System, the algorithm detailed by S. Kay in [13] was implemented. This algorithm has a parameter herein referred to as the Kay window parameter. This window acts much like a frequency smoothing parameter by sampling frequencies forward and backward of the instantaneous frequency being derived. This can create some undesirable artifacts, but also allows the production of cleaner HHT Spectrums. In all of the examples where comparisons are made, the same Kay window parameter is used to ensure results that can be compared fairly. Most Hilbert spectrum plots found in this thesis were generated with a Kay window parameter of, at least, 20, but in some cases, as high as 128. However, all comparison metrics were based on a recalculated Hilbert spectrum with the Kay window parameter set to 4. Experimentally, it appears that the implementation of the *hht()* function in the MATLAB 2018b Signal Processing Toolbox is analogous to a Kay window parameter of ~4.

## 1.2 MODE-MIXING, TRANSIENT IMFs, PHANTOM IMFs, and UPPER FREQUENCY LIMITS

The nature of the EMD is such that higher frequencies tend to be extracted in the first IMFs while lower frequencies are extracted in later IMFs. However, the EMD does not thus discriminate frequencies globally, but rather locally. If the highest frequency component $f_1$ exists for only a subinterval or multiple subintervals of the entire signal, then the same IMF that extracts $f_1$ will also extract the next highest frequency component $f_2$ wherever it exists and $f_1$ does not. This leads to Type-I Mode Mixing, where one IMF may contain wildly varying frequencies. Fig. [1-3] shows this by a simple signal which was generated as the sum of three components of equal amplitude, but at different frequencies and spanning different

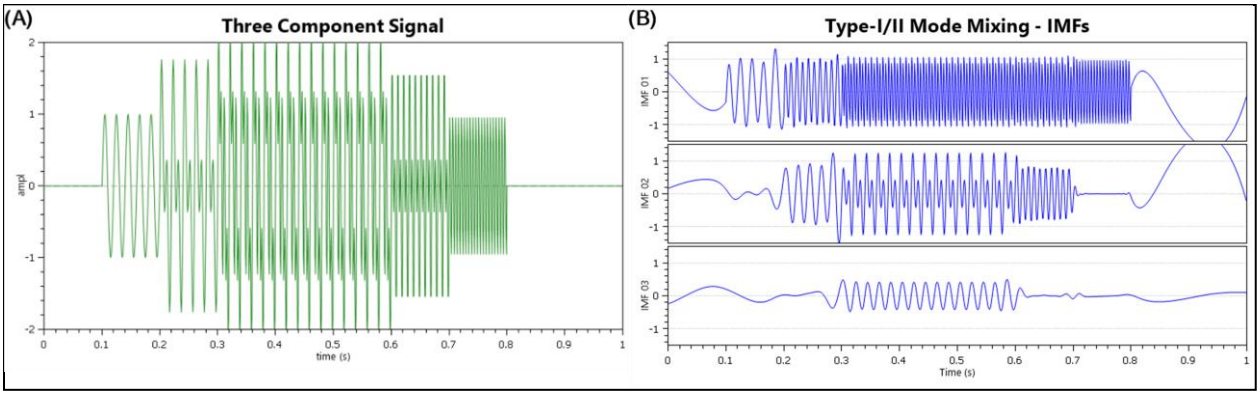


***Figure 1-3 EMD Resulting in Type-I and Type-II Mode Mixing***

but overlapped time intervals. The highest frequency component is a sinusoidal wave that oscillates at 200 Hz on the interval $0.3 < t < 0.8$, the mid-frequency component is sinusoidal at 100 Hz on $0.2 < t < 0.7$, and the low frequency component is 50 Hz on $0.1 < t < 0.6$. Its sum is visible in Fig. [1-3.A].

The EMD was used to decompose this signal and several IMFs were extracted. Only the first three IMFs have any meaningful value and are presented in Fig. [1-3.B] (the remaining were transient IMFs). Looking only at IMF #1, it is easy to see that on $0.1 < t < 0.2$, the EMD has extracted the lowest frequency component. On $0.2 < t < 0.3$, the mid-frequency component was extracted instead of the lowest frequency. Finally, on $0.3 < t < 0.8$, the highest frequency component is fully extracted. This is because the EMD does not globally discriminate per IMF. The lowest frequency component of the signal was the highest frequency component on the interval $0.1 < t < 0.2$ and the mid-frequency component was the highest frequency component on the interval $0.2 < t < 0.3$.

Type II Mode-Mixing problems present themselves as two or more IMFs containing the same time-frequency components, but at reduced amplitude. Fig. [1-3] shows this, as well. It can be seen on the interval $0.3 < t < 0.6$, that IMF #2 contains the mid-frequency component and part of the low-frequency component. The low-frequency component is present in IMF #2 at reduced amplitude. IMF #3 contains what remains of the low-frequency component over that interval. In this case, IMF #2 has failed to fully separate the two components where they both exist at the same time. According to Rilling and Flandrin

in [14], there is an upper limit on the frequency ratio of two components such that they can be separated. According to their research, that limit is ~0.75. Anything higher will result in simultaneous component extraction or Type-II Mode Mixing. The bottom two components in the signal of Fig. [1-3] are indeed separated by exactly a ratio of 0.75. This signal is examined in more detail in Example 3.4 as Signal #3.

Transient IMFs are those IMFs that result from anomalies such as numerical imprecision, incomplete sifting, signal boundary effects, and component boundary effects. They typically show little meaningful information or information at extremely low amplitude and can usually be ignored. The problem with transient IMFs is that they may conceal very low amplitude meaningful information. The transient IMFs and residual from the decomposition of the signal depicted in Fig. [1-3] are shown in Fig. [1-4].

Not often found in the literature is a discussion on the existence of Phantom IMFs. Liu *et al.* refers to these as false components [4]. Phantom IMFs and transient IMFs are very similar, except that Phantom IMFs often have significant amplitude and contain misleading frequency information; Phantom IMFs are transient IMFs that can't be safely ignored. Consider a signal which is zero everywhere. If this null signal were sifted (not actually possible without extrema) and somehow two IMFs were produced such that each IMF were sinusoids of equal amplitude (e.g. 1) and equal frequency (e.g. 50 Hz), but maintaining a 180° phase shift with respect to each other everywhere, then that would be a valid decomposition in

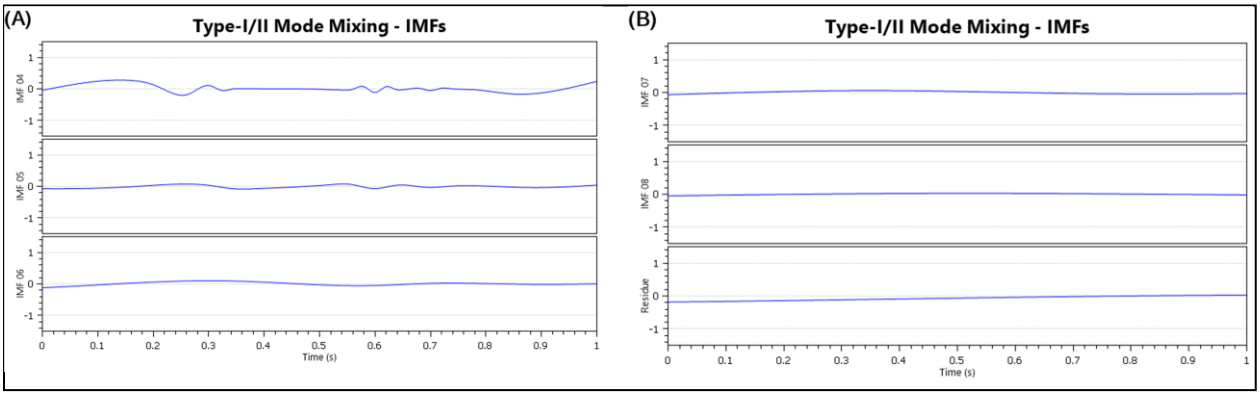


***Figure 1-4 Transient IMFs and Residual from Type-I/II Mode Mixing Example***

that the completeness property is satisfied. Adding these two IMFs together would indeed result in the original null signal, and both IMFs would satisfy the definition of an IMF. But worse than the decomposition not producing meaningful results, it will have produced false results. If these signals are transformed into instantaneous amplitude and frequency, the phase offset information would be lost. The resulting HHT would appear as a Type-II Mode Mixing problem (two IMFs containing same-frequency information) and could lead to the misinterpretation that there exists a component in the signal at 50 Hz of amplitude 2 (the sum of the two combined). Phantom IMFs seem to be generated for various reasons such as: the nearness of the frequency components to Nyquist (see Example 3.12), the closeness of frequency components (see Example 3.7) to each other, and propagation error from signal or component boundary effects; all dependent on the EMD technique being used.

An example Phantom IMF can be seen in the HHT plot in Fig. [1-5] where the decomposition is of a simple two-tone signal. The yellow colored IMF is not a real component of the signal, but rather an artifact of the decomposition process. The actual, original signal decomposed and represented here consisted of the sum of two constant-frequency, constant-amplitude components at 400 Hz and 300 Hz with sampling frequency at 1000 Hz. In this case, the 400 Hz signal was not extracted, the 300 Hz signal was extracted with incorrect and oscillating amplitude, and the 100 Hz yellow-orange (partially transparent) line is a Phantom IMF. Below that Phantom IMF are faintly represented transient IMFs.

As alluded to in the description of Phantom IMFs and exemplified by the signal decomposed in Fig. [1-5], there are limitations with the Classical EMD as it relates to the Nyquist rate. Signal components separated by significant frequency distance still may not be decomposed successfully if they reside above half the Nyquist rate. The components in the example signal are 300 Hz and 400 Hz, which has a separation ratio of 0.75, yet because the Nyquist rate is only 500 Hz they are not easily extracted. This is examined in greater detail later in this chapter and the signal is revisited in Example 3.12.

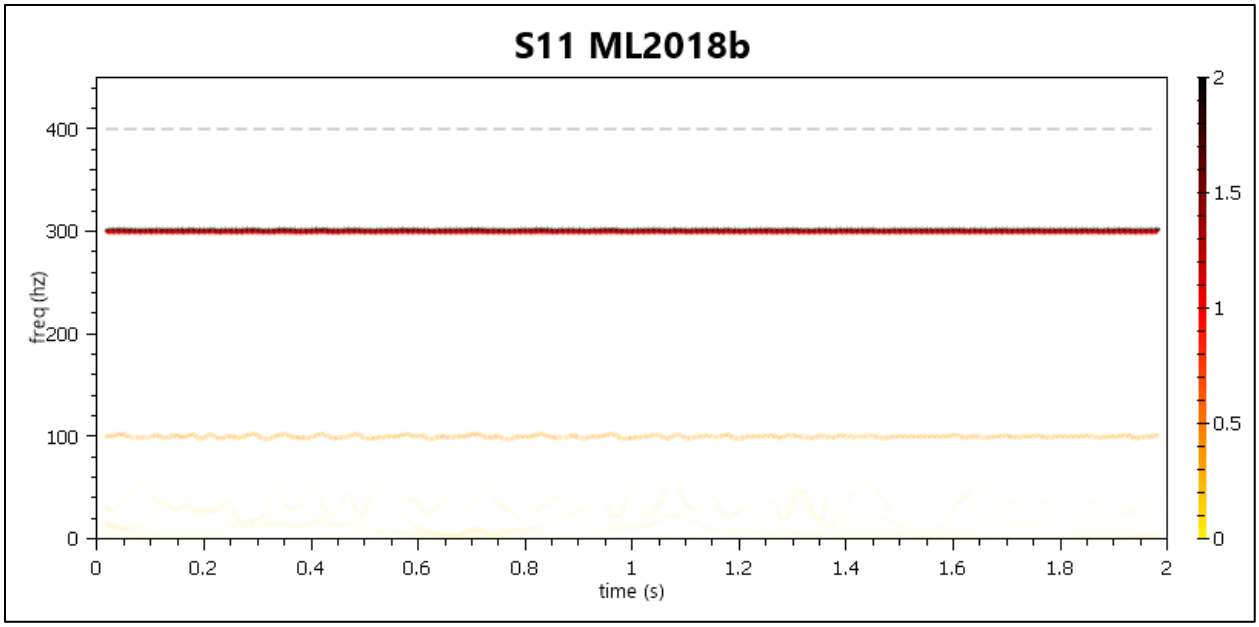


***Figure 1-5 Phantom IMFs Example Drawn From Signal #11***

## 1.3 EMPIRICAL MODE DECOMPOSITION VARIANTS

Various approaches have been taken to address mode-mixing problems, particularly of Type-I. The Ensemble EMD (EEMD) was introduced by Z. Wu and N. E. Huang in [15]. This modification to the algorithm takes *m* copies of the original signal and to each adds randomized Gaussian white noise prior to decomposition. The resulting IMFs of each such decomposition are then averaged together to provide the final decomposition result—simply the summed *associated* IMFs divided by *m*. However, the EEMD introduces new problems. The final extracted IMFs may not be true IMFs—not satisfying the definition of an IMF. Also, as a result of imperfect noise-cancellation through averaging, residual noise may be found in the modes. Thus, the completeness property of the EMD could be violated, since the original signal could not be exactly reconstructed from the IMFs plus residue. Further, depending on the effect of the additive noise, the full decomposition of one ensemble member might return a different number of IMFs than another and the proper handling of these cases in terms of the averaging function is unclear. Also, since the additive noise is generated randomly, no full decomposition of a given signal is guaranteed to be identical to another instance of that decomposition (i.e. non-reproducibility,

indeterminism). Finally, this approach does not eliminate Type-I Mode Mixing but does mitigate the problem.

To address some of the problems associated with EEMD, the Complementary Ensemble EMD (CEEMD) was proposed by J. R. Yeh *et al.* in [16] which adds noise in complementary pairs such that their effects are canceled out in the final averaging. This mitigates the problem of additional residual noise in the IMFs, yet the completeness property could not be proven. The problem of misaligned modes for averaging also remained. Torres et al. proposed an extension to the CEEMD in [17] which they titled Complementary Ensemble EMD with Adaptive Noise (CEEMDAN). The purpose of CEEMDAN was to bring reconstruction error to a minimum and eliminate mode misalignment problems. Continuing that work, Colominas *et al.* proposed a further refinement to CEEMDAN in [18], termed I(mproved)CEEMDAN that could reduce the number of transient IMFs and further reduce the presence of residual noise.

It should be noted here that all of the examples given in this thesis used an ensemble count of 2000 for each of the aforementioned noise-assisted decompositions. Although this took significant time to decompose some signals, it resulted in greatly reduced residual noise. For reference, however, Example 3.11 shows significant residual noise in both the EEMD and CEEMDAN decompositions.

Many other variations of the EMD have been proposed as well, to include bivariate, trivariate, and multivariate algorithms with and without noise; each new version working to improve upon the previous [19] [20] [21] [22] [23] [24] [25] [26] [27] [28]. Notable about multivariate decompositions is that they provide for mode alignment—each IMF from each dimension is sifted out together containing roughly the same frequency bands. However, these algorithms are not easily parallelized by dimension, whereas univariate decompositions of multivariate data can occur in parallel.

Ultimately, the problem of non-reproducibility cannot be fixed with respect to noise-additive solutions unless the same pseudorandom number generator algorithm is always used with a common seed value.

Deering showed that sinusoidal signals may be used instead of noise to assist the decomposition [29]. However, frequency masking has the problem of being asymmetric, thus leading to imbalanced sifting. To address this, Deering's technique uses the average of two sifting operations: the sum of the signal with the frequency mask and again with its complement before taking the average of the two. This complementary frequency-masking provides reproducible decompositions that do not suffer the problem of residual noise in the IMFs. The difficulty with this technique is identifying the optimal frequency masks to apply at each stage of the decomposition (i.e. for each sifting step). Furthermore, the approach taken by Deering does not address the problem of phase offset in the frequency mask which affects the sifting process (noted exception: the natural phase shift entailed by the additional subtractive mask). When a sinusoidal signal is generated as a mask with no phase offset, its additive peaks and troughs affect only specific locations in the signal. A different phase offset could provide a significantly different profile. For the purpose of this thesis, Deering's technique will be referred to as the Frequency-Masked EMD (FM-EMD).

Shen et al. [30] proposed a system to adaptively determine frequencies for the generation of the sinusoidal mask at each decomposition step using an algorithm they title the Sinusoidally-Assisted EMD (SAEMD). This is actually an umbrella term for two sub-algorithms (SAEMD-I and SAEMD-II). Since the SAEMD provides for two approaches to frequency optimization, knowing which approach to use requires an *a priori* understanding of the signal. Also, it does not address the question of optimal or balanced phase offset. Unfortunately, the code for their system was unavailable for deeper analysis at the time the research presented in this thesis was being completed and is left for further investigation by others.

Hu and Mo [31] also proposed a modification to Deering's approach for frequency mask optimization which they title the Improved Masking Signal Method (IMSM). The IMSM is only a slight modification to the FM-EMD, in that it proposes the constant scalar 1.4276 for the optimal mask frequency—ostensibly derived from the FM-EMD's frequency resolution limits and filtering bandwidth.

Sandoval and de Leon propose to further improve frequency masking in [32] with the Hilbert Spectral Analysis which applies sinusoidal signals in ensemble complementary pairs of random phase offsets followed by a final sifting step to force the resulting extracted mode to satisfy the IMF properties. The EMD aspect of their paper has no formal term so it is given here as the HSA-EMD. However, they do not address mask frequency identification in their approach. Further, their approach introduces randomness, which is antithetical to developing an algorithm with deterministic, reproducible results.

Deering suggested two ways that optimal frequency masks could be determined: a) analysis of the Fourier transformation and the use of a threshold value, b) an initial single IMF sifting followed by averaging the frequency of the resulting Hilbert transformation. The former is problematic in that the signal being decomposed by the EMD may not be well-suited to Fourier analysis and, while it has potential, is described by Deering as "discordant" due to the fundamentally different approaches between the way the Fourier transformation works and the way the EMD works. Thus, the FM-EMD takes the latter approach. However, the FM-EMD's use of the mean frequency is not robust to outliers, intermittent signals, skewed populations, nor does it address meaningfulness of existing components, and experimentally has been shown to not work very well. More importantly, it doesn't address the closeness of frequency components and the resulting mode-mixing that results. The IMSM actually improves on this simply by defaulting to a higher frequency at every stage irrespective of its optimality. Neither account for either optimizing the phase offsets or the balancing of phase offsets.

The Uniform Phase EMD (UPEMD) addresses the issue of frequency balancing. In [33] Wang *et al.* use a parameter $n_p$ to specify the number of phases used in ensemble format. However, this is somewhat misleading. Examining the code, it becomes clear that they use $n_p$, not as an ensemble specifier, but rather as an ensemble count upper bound. Consider the ensemble count variable, $cnt_{ens}$. The actual count is defined as: $cnt_{ens} = argmax_n(2^n);\ such\ that\ cnt_{ens} \leq n_p$. Their code then creates an array of phase offsets by dividing the interval [0,2π) into $min(2^{imf_{num}}, cnt_{ens})$ uniformly spaced subdivisions. Finally, they create their ensemble of frequency masks of equal frequency and each offset by a unique phase shift from the array of phase offsets. By dividing the interval [0,2π) by some power of 2, the UPEMD indirectly creates a complementary ensemble, however this does limit the algorithm to a subset of possible ensemble numbers. The ensemble count need not be a power of 2 (i.e. merely be divisible by two). Irrespective of this odd choice, the technique makes no allowance for optimal mask frequencies, merely stepping down from Nyquist by a factor of 2 until *n* IMFs are extracted. The variable *n* represents the number of expected IMFs and has a maximum of $log_2(N)$ where *N* is the length of the signal. They base this latter approach on the property demonstrated by Z. Wu and N. E. Huang in [2] where it was shown that the EMD behaves as a dyadic filter bank in white noise. Thus, the decomposition process in the UPEMD ends when the number of specified IMFs have been extracted (irrespective of the power remaining in the residue after the last IMF has been extracted).

Irrespective of the wisdom to base optimal mask frequencies on the filter bank property of the classic EMD, the system follows a by-rote scheme; it is non-adaptive to the state of the decomposition. Also, this rote approach leads to many transient IMFs between meaningful ones and, conversely, limits the resolution potential. Another problem is that to begin decomposing a signal by the UPEMD, is that the user must specify the amplitude of the mask (which is later normalized and multiplied by the standard deviation of the residual at each stage) as well as the number of sift iterations. So, although the UPEMD

shows better bandwidth resolution than other approaches due to its ensemble-style frequency masking approach, the resolution can be greatly improved, and the number of transient IMFs can be reduced.

## 1.4 FILTERING

Researchers Z. Wu and N.E. Huang [2] and also P. Flandrin *et al.* [3] have noted that the EMD behaves in certain respects as a filter bank—a bank of passband filters with the highest filter behaving as a high-pass filter. Those results were derived from analysis of the EMD in the presence of white noise and fractional Gaussian noise respectively. However, these researchers were attempting to characterize the nature of the results, not necessarily the nuance of the behavior. Indeed, Flandrin takes great pain to point out that the filter bank property is only valid in a local region of a signal. This is because its behavior more similarly imitates overlapped high-pass filters with localized effect, starting with the highest instantaneous frequencies first.

The distinction is important, because if there is incomplete extraction of a high frequency component over some time interval into one IMF, then it will be extracted into a subsequent IMF, and not attenuated as a passband filter would. Further, that higher frequency component remaining will “shield” lower frequency components from being extracted over the same time interval, potentially leading to a series of IMFs with Type-I Mode Mixing. This means that the filtering behavior of the EMD can only be related to a matrix of overlapped high-pass filters for intervals of the signal, not the signal in its entirety. The transition between filtering functions of the same mode has not yet been well analyzed, yet, and would most likely be dependent on the EMD technique being used.

Like most filters, the attenuation at the cutoff frequency is neither sudden nor complete, but rather appears as an attenuation curve. Frequency masking, of the form suggested by Deering *et al.*, provides a method for targeting the cutoff frequency. Consider, for example, a chirp signal as shown in Fig. [1-6.A].

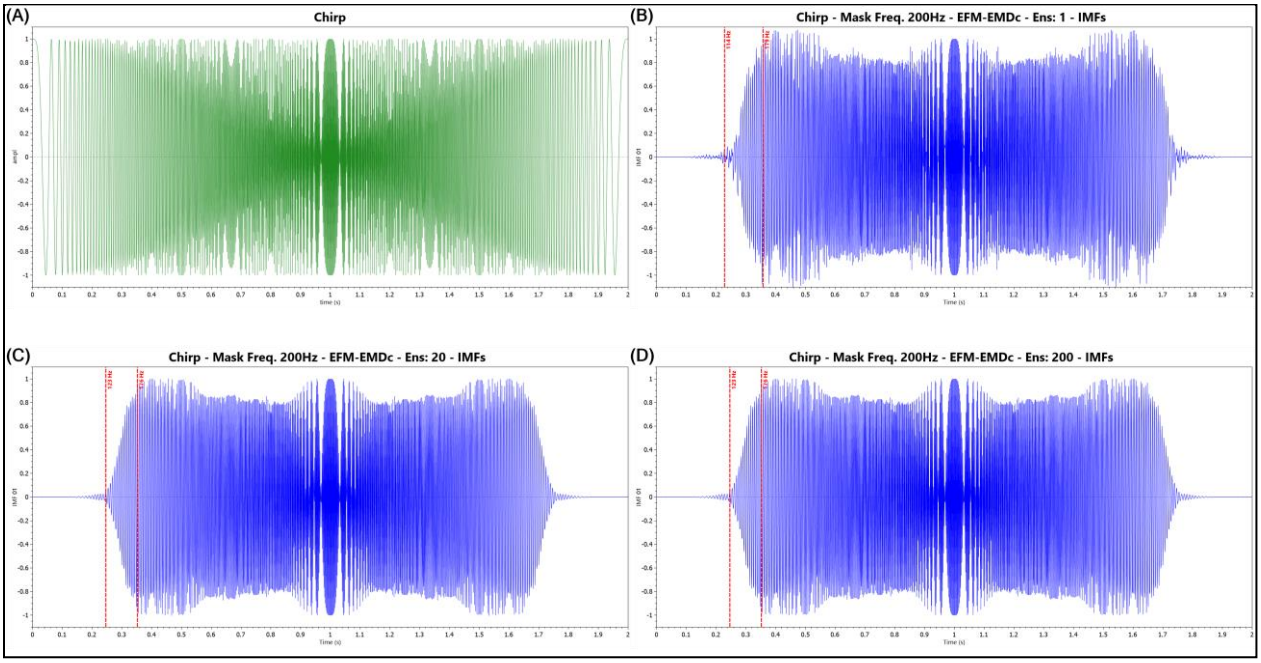


***Figure 1-6 Attenuation Curve Demonstrated on Chirp Decomposition***

The chirp signal maintains constant amplitude throughout but increases the frequency linearly from 0 Hz at time step 0 to 500 Hz at the 1 second mark and then reduces again to 0 Hz at the 2 second mark. The sampling frequency for this signal is 1000 Hz. The chirp signal is itself an IMF exhibiting perfect Type-I Mode-Mixing: a single IMF spanning the entire frequency spectrum from 0 to the Nyquist rate.

This chirp signal is added to each member of an ensemble of frequency masks where each mask was generated using a distinct phase offset following which each was then decomposed by the classical EMD. This is essentially Deering's FM-EMD, but in ensemble. It is referred to here as the EFM-EMDc with the "c" denoting "classical sifting". To generate the IMFs depicted in Fig. [1-6], the first IMFs from the sifting of each ensemble member were summed and averaged. Fig. [1-6.B-D] shows the first resulting average IMF with the masking frequency set to 200 Hz and the ensemble size specification set to 1, 20, and 200 respectively. These are complementary ensembles, thus every mask specified for the ensemble generates two masks, the original with a phase offset in [0, π) and a complementary 180° phase offset counterpart. Ultimately, 2, 40, and 400 masks were used respectively to generate these IMFs .

Without some form of masking, whether frequency-based or noise-based, the Empirical Mode Decomposition should simply return the signal itself as the one and only IMF. However, by using the mask, part of the chirp is not returned in the first IMF. It attenuates below a certain frequency. Since the frequency mask is set to 200 Hz, that equates to the time steps 0.4s and 1.6s in the signal. The vertical red bars indicate the actual cutoff frequency location (on one side) and the subsequent bottom of the attenuation curve. There is little merit to the 200/400 sized ensemble IMF (Fig. [1-6.D]) over the 20/40 sized ensemble IMF (Fig. [1-6.C]). They are virtually identical except marginal differences at high frequencies. However, there is a clear change to the attenuation curve between the 1/2 ensemble IMF (Fig. [1-6.B]) and both of the 20/40+ ensemble IMFs (Fig. [1-6.C-D]). The larger ensemble sizes cause the attenuation to start slightly later and to drop off sharper, but also more smoothly. Studying the behavior of these attenuation curves, dependent on the sifting technique employed, was integral to the development of the AHHT System.

The most important detail about this filtering discussion is noting that the chirp signal has a single frequency component at any given moment. The ability of the frequency mask to *shield* lower frequencies from extraction does not necessarily say anything about the resolution of extracting two closely separated components existing on the same time interval. For example, the attenuation band shown in Fig. [1-6.B] and Fig. [1-6.C] indicates that a component at 100 Hz (@t = 0.2s/1.8s) would not be included in the extraction when a masking frequency of 200 Hz is employed. However, in practice, if a 200 Hz component exists on a time interval *simultaneous* with a 100 Hz component, it is not necessarily the case that the 100 Hz component would be fully excluded in the extraction of the 200 Hz component. All that this attenuation band analysis with a chirp signal indicates is the behavior of the EMD with frequency masking in the presence of multiple components at *different time intervals*—that there is a limit to the amount of Type-I Mode Mixing that would occur.

## 1.5 INTERPOLATION

At the heart of every EMD technique is an interpolation scheme. In an effort to provide a rigorous mathematical underpinning for the EMD, Q. Chen *et al.* used b-spline interpolation for the extrema envelopes. This effort successfully described the resulting IMFs in terms of basis functions [34].

Cubic spline interpolation, on the other hand, which is specified in the classical EMD, can have difficulties with overshooting and undershooting. To address the *misshooting* problem, interpolation by various other techniques have been analyzed and compared to include the rational b-spline interpolation already mentioned and others [34] [35]. Kopsinis and McLaughlin proposed using a genetic algorithm to identify extrema points to exclude select extrema from interpolation in an effort to optimize the decomposition [36]. MATLAB uses a *pchip()* function interpolation algorithm that is shape preserving based on the work in [37] [38]. N. E. Huang reviewed the BS-EMD (B-Spline EMD) in [39] and found rational b-spline interpolation to be slightly superior to cubic spline interpolation, but determining what order of b-spline to use was still an outstanding question.

J. Huang *et al.* presented an alternative to the standard cubic spline envelope mean estimation approach by instead using cubic spline interpolation only on extremum centers [40]. The modification they present is such that linear interpolation is used to derive the upper and lower envelopes. Then the mean is found only for the *extremum centers* at each extremum—simply the midpoint between that extremum and the corresponding envelope interpolation. Finally, the cubic spline interpolation algorithm is applied on these extremum centers (see Fig. [1-7]). This technique replaces one piecewise cubic spline interpolation with two piecewise linear interpolations which reduces the algorithm's computational complexity. Their analysis shows a reduction in *misshooting* in the examples they provide. There are additional benefits and detriments to this technique that will be detailed later. It

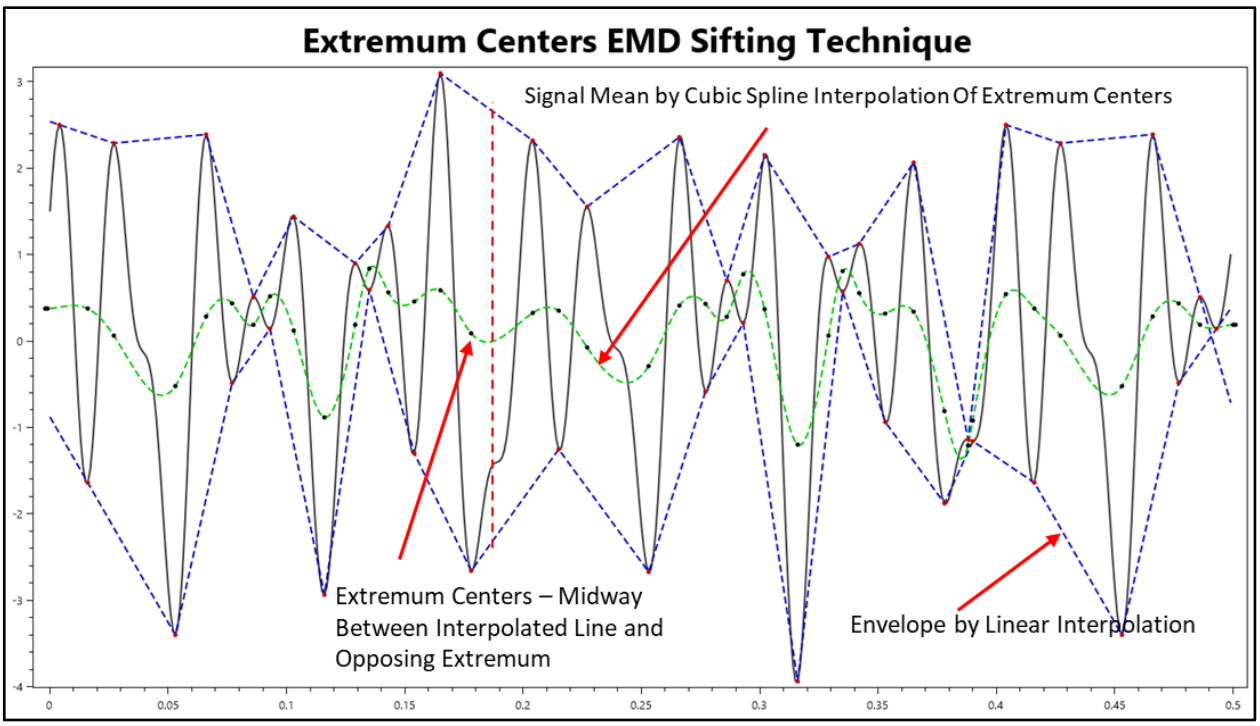


***Figure 1-7 Envelope Mean Developed by Extremum Center Determined by Linear Interpolation of Extrema***

should be noted that the cubic spline interpolation of these centers still has a problem with boundary effect that must be addressed by some scheme (see 1.6).

*Cubic spline interpolation* is not an algorithm in itself, but rather a collection of algorithms which describe piecewise curve fitting using third-degree polynomial functions. The idea is to create a smooth curve between every two contiguous points of a sequence of points and to do so in such a way that the curve is smooth with respect to adjacent curves. Given a N sequence of points $\{pt_0, pt_1, \ldots, pt_N\}$, for each contiguous pair of points, $\{(pt_0, pt_1), (pt_1, pt_2), \ldots, (pt_{N-1}, pt_N)\}$ a smooth curve is generated such that the curve is smooth at the common point between previous and subsequent pair-point curves. So, the curve between $(pt_1, pt_2)$ is smooth at $pt_1$ with respect to the curve on $(pt_0, pt_1)$ and at $pt_2$ with respect to the curve on $(pt_2, pt_3)$. All such curves should be likewise smooth. Many such algorithms exist with differing constraints and assumptions, particularly as they relate to boundary conditions. Of interest in this work are *natural Hermite cubic splines* and *Akima cubic splines* [41]. Both are piecewise cubic polynomial schemes that attempt to provide smooth curvature over an interval between two arbitrary points.

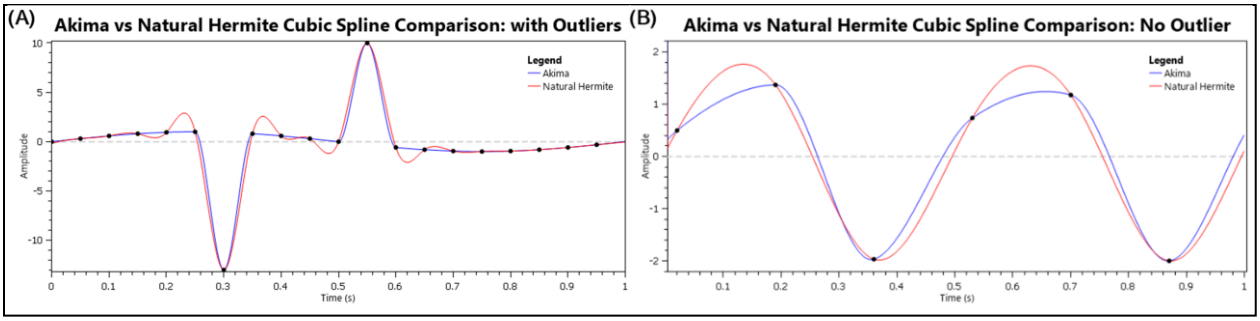


***Figure 1-8 Cubic Spline Interpolation Comparison: Hermite vs. Akima***

The natural Hermite spline algorithm is such that the interpolation is continuous to the second derivative at each point and the second derivative is 0 at the boundaries. The Akima spline interpolation requires only continuity of the first derivative. The net result is that Hermite splines provide smoother, more oscillatory functions, in general, but are also often less robust to outliers. Akima splines tend towards shape-preservation but are not as good for developing oscillatory shapes. See Fig. [1-8] for a comparison of spline interpolation in the presence of outliers and in the presence of sparse data points uniformly sampling a sine wave. In Fig. [1-8.A], the underlying data points describe a 1 Hz signal sampled at 20 Hz, except for the 2 outlying points. The blue line represents how superior the Akima splines handle the outliers on this signal. The Hermite spline interpolation causes oscillation around the advent of these outliers. On the other hand, that oscillatory property also makes the cubic Hermite spline interpolation a better fit for the 2 Hz signal sampled at 5.88 Hz shown in Fig. [1-8.B].

## 1.6 BOUNDARY VALUES

Irrespective of the approach used to generate a decomposition, interpolation of extrema is required. The cubic spline requires four points—the two points bounding the interval of interpolation and two more points—one on each side of the interval—to estimate the derivatives ($1^{st}$ and/or $2^{nd}$ derivate estimates) at the points bounding the interval. Since there are no points outside the known extrema, an extrapolated maximum must be computed to the right of the rightmost maximum and to the left of the leftmost maximum. Likewise, similar points must be extrapolated for the minima. Huang et al. proposed

mirroring the signal to either side of the boundaries to generate these new points [1]. In a 2018 paper, Wu and Riemenschneider proposed using a ratio of the last four extrema and quadratic extrapolation [42]. Z. Qing-jie *et al.* proposed a two-tiered system in [43] where at high frequencies, mirroring is used, and at low frequencies, polynomial regression is used (Least Squares). Jaber *et al.* proposed using local linear quantile regression to correct for boundary effects in [44]. They also survey many other schemes proposed across various disciplines to manage the problem. MATLAB 2018b uses a sinusoidal function estimated based on the two extrema—one maximum and one minimum—at each end to generate new maxima and minima; this approach uses the difference of the amplitude of the signal at each point divided by two to provide an amplitude estimate, and the distance between the two points multiplied by two to provide the period estimate, and then the final values of the signal to help determine the amplitude offset. The noise-assisted variants examined in this work use mirroring. It is unknown how the UPEMD manages the boundary conditions as that source code was unavailable and was not specified in their paper.

Bad boundary extrema extrapolation can lead to significantly degraded results, especially at low frequencies as demonstrated in Chapter 3, and can even lead to decomposition instability as the boundary errors propagate in later IMFs to counterbalance poor extractions in early IMFs.

## 1.7 CLUSTERING

Subtractive Clustering (SC) [45] is an algorithm derived from Mountain Clustering [46] and is often used to estimate clusters when no information is known about the number of clusters represented by a dataset. It's an elegant algorithm that uses existing data points as cluster centers and determines the clustering *potential* of a given multidimensional data point $\boldsymbol{x}_i$ by the following density function:

$$P_i = \sum_{j=1}^{n} e^{-\frac{\|x_i - x_j\|^2}{\left(\frac{r_a}{2}\right)^2}} \quad 1:1$$

where $r_a$ represents a squashing parameter that changes the width of the Gaussian-like density function. This algorithm essentially measures the distance between each point to every other point and calculates a *potential* value for that data point to be a cluster center. Then, until no more acceptable cluster centers are found, the point with the highest potential is selected as a cluster center and its sphere of influence is subtracted from the potential of all the other points. Thus, the computational cost of SC is $O(n^2)$. This algorithm is often used, for instance, in fuzzy classifiers where there is a single pass through the training data to develop fuzzy membership rules for the classifier.

## 1.8 MEASURING DECOMPOSITION PERFORMANCE

There have been many attempts to provide metrics to measure the successfulness of a decomposition. In his initial work, Norden Huang proposed to measure each IMF's orthogonality with respect to each other and to the original signal using the so-called Index of Orthogonality [1]. J. Huang *et al.* showed in [40] why this approach is unsuccessful where they proposed an alternate, but similar strategy. Ultimately, both approaches reduce to correlation measures between a signal and its IMF decompositions, as well as between the IMFs. However, these strategies are best at measuring separation of frequencies over a given interval and for measuring uniqueness of signals over a given interval—they test for Type-II Mode Mixing. They do not test for Type-I Mode Mixing. Two IMFs with equivalent frequencies and amplitudes for alternating intervals will not be directly correlated by these metrics (though, potentially, they would by a similar lag testing scheme).

# Chapter 2

# METHODS

## 2.1 PRELIMINARIES

Instead of presenting a single algorithm to decompose signals, the goal of this thesis is to present a *system* which manages the decomposition by component detection (pattern recognition) and adaptively employing multiple decomposition algorithms. There are five main novel methods presented in this thesis which combine to make this system effective.

The first are slightly altered forms of sifting, both in the form of an alteration to the extremum center technique proposed by J. Huang *et al.* which was described in 1.5 (see 2.2) as well as an alteration to the classic EMD sifting technique described in 1.1 (see SIFT3 below).

The second is the use of order (see 2.3), to force greater attenuation of signal components outside of the frequency bandwidth.

The third is an adaptive mask-frequency shifting scheme for cutoff frequency targeting (see 2.5) which adjusts the target frequency of the mask based upon its associated projected cutoff frequency, as well as an adaptive approach to sifting threshold according to a two-deep decomposition lookahead.

The fourth is the use of subtractive clustering to identify the highest significant frequency component found during a given frequency band test—to drive mask frequency selection.

The fifth is an optimization to subtractive clustering (see 2.7) that reduces its computational burden. The algorithm still maintains a computational complexity of $O(n^2)$, but the cost of each iteration is reduced. Also, subtractive clustering is highly parallelizable, with respect to distance evaluations. If not parallelized, noting the symmetry of the distance measures (the distance from $\mathbf{x_1}$ to $\mathbf{x_2}$ is equivalent to the distance $\mathbf{x_2}$ to $\mathbf{x_1}$) and irrelevance of self-distance measures, the algorithm's complexity may be reduced by an additional factor of > 2. However, for this research, parallelization was adopted.

Additionally, a new approach to measuring the goodness of a decomposition, as it relates to artificial signals is presented (see 2.10).

The ensemble, frequency-mask sifting algorithms are depicted in the flowcharts provided in 2.9. They show that the AHHT System employs three sift techniques.

- SIFT1 uses extremum centers determined by linear interpolation as described in 1.5. The envelope mean is developed with cubic Hermite spline interpolation through these centers.
- SIFT2 uses extremum centers determined by the average of cubic Hermite spline interpolation and Akima spline interpolation as described in 2.2. Then the mean is developed through these centers using cubic Hermite spline interpolation.
- SIFT3 uses the classic approach of deriving the mean by averaging the upper and lower envelopes described in 1.1, but uses the average of cubic Hermite splines and Akima splines to interpolate the upper and lower envelopes as in SIFT2.

These three SIFT techniques are the basis for the three ensemble functions (Ensemble Frequency-Masked EMD or EFM-EMD) which are employed by the AHHT and are defined here as:

- EFM-EMD1: Frequency-mask applied in a complementary ensemble scheme; sifting completed by SIFT1. No mask frequency shifting.

- EFM-EMD2: Frequency-mask applied in a complementary ensemble scheme; sifting completed by SIFT2. Mask frequency shifting as described in 2.5.
- EFM-EMD3: Frequency-mask applied in a complementary ensemble scheme; sifting completed by SIFT3. No mask frequency shifting.

The AHHT System was developed in C# using the open source math libraries Accord.Net [47] and MathNet.Numerics [48]. The cubic Hermite/Akima spline interpolation algorithms are derived from those provided by MathNet.Numerics [48], but have been optimized slightly for increased performance. Plots were generated using the open source OxyPlot library [49] but modified to provide for transparency-capable *heat line plots*. MATLAB 2018b and the Digital Signal Processing Toolkit was used to create the artificial signals and to generate all of the non-AHHT decompositions using code made publicly available by the associated researchers.

## 2.2 SIFT2: Extremum-Center by Spline-Based Interpolation

In their work, J. Huang *et al.*, presented the extremum centers technique where the centers were derived by linear interpolation of the extremum envelopes. Building on that idea, a new algorithm was developed that returns to the use of cubic splines to interpolate the upper and lower extremum as in the classic EMD but using two different interpolation algorithms and then averaging their interpolations. First, the upper and lower envelopes are computed with natural Hermite cubic splines, and then they

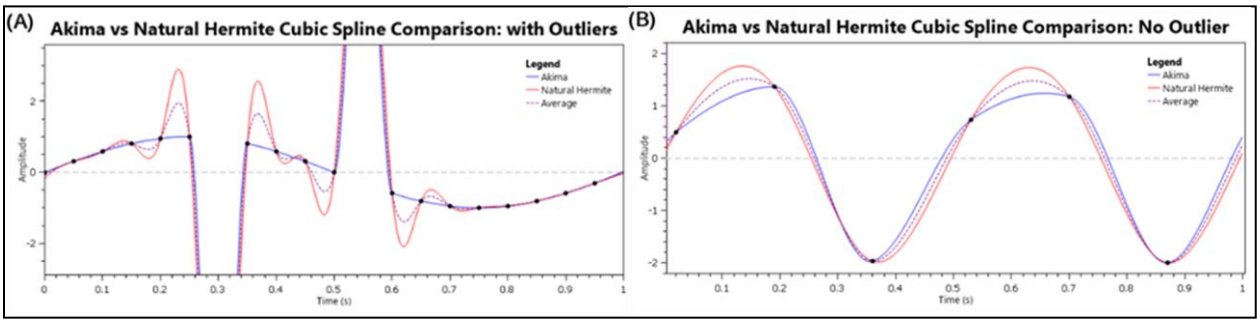


***Figure 2-1 Averaging Hermite and Akima Splines to Capitalize on the Properties of Each***

are recomputed using Akima cubic splines. The two splines for the upper envelope are averaged at the minima locations and the two splines for the lower envelope are averaged for the maxima locations. The midpoints between the extrema and their opposing averaged envelope are then calculated to provide the new centers. Then, as in the work of Huang et al., a natural Hermite cubic spline interpolation is generated with these extremum centers as the knots. The averaging of the spline types helps to reduce the misshooting associated with Hermite splines and reduce the 2$^{nd}$ derivative discontinuity of Akima splines. An example of this is given in Fig. [2-1]. These are the same signals as in Fig. [1-8], however the average of the two spline algorithms is shown (the scale of Fig. [2-1.A] has been adjusted so that the outliers are not visible, but the averaged interpolation is clearer).

Thus, the oscillating tendency of the Hermite splines and the shape-preserving tendency of the Akima splines are both contributing to the final estimated extremum centers.

## 2.3 MASKING ORDER

Regardless of the EMD sifting technique employed as discussed in 1.4, at each decomposition step, the IMF extracted will include the highest frequency component(s) for a given time interval. This means that lower frequency components at that time interval are filtered out. But the IMFs will generally include high frequencies that are close together. For example, assuming a 1000 Hz sampling frequency, a two-tone signal of 200 Hz and 199 Hz will be inseparable by any known EMD technique. Rilling and Flandrin showed that the Classic EMD is unable to separate any components whose frequency ratio is greater 0.75 in [14]. However, w.r.t. the classical EMD, if for some interval of the signal there also exists a 240 Hz signal, then that 240 Hz component will be extracted for that interval, effectively filtering out the 200 Hz and 199 Hz signal over that same interval. This can be seen in Fig. [2-2] where there is a single intermittent component at 255 Hz and a constant component at 65 Hz. The 65 Hz sub-signal is filtered out of the extracted IMF1 on the interval $0.5 < t < 0.75$.

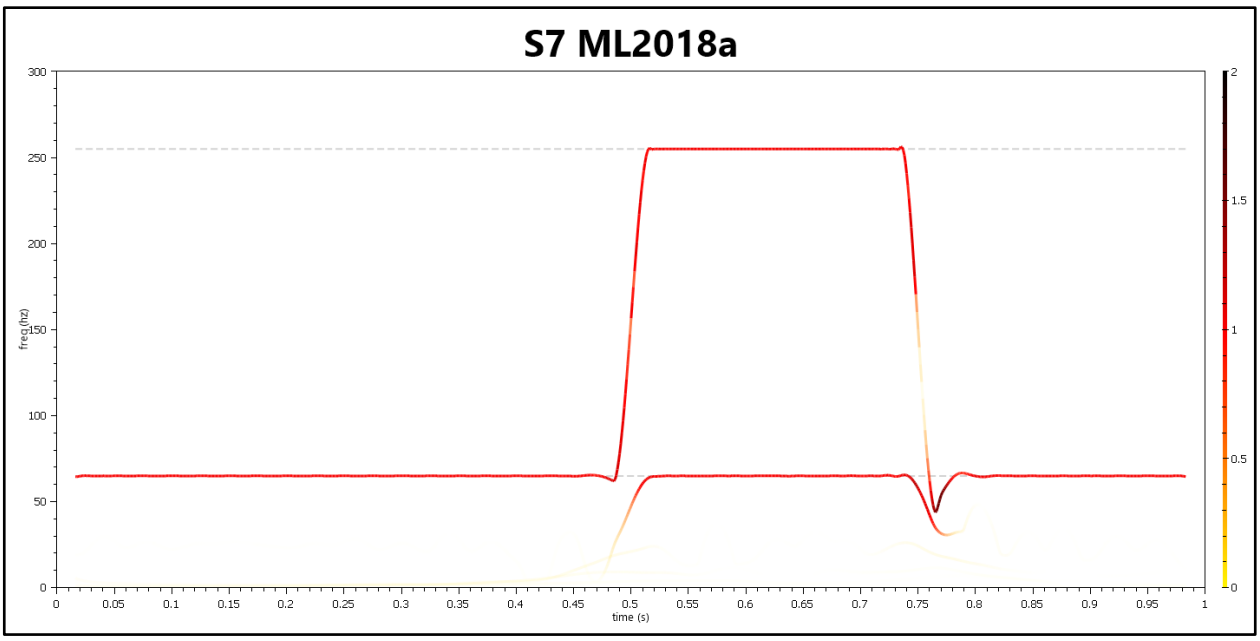


***Figure 2-2 Type-I Mode Mixing Due to Time-Localized High-Pass Filtering***

However, the noise-assisted EMD variants provide high-frequency noise that effectively *shield* lower components from extraction. The noise changes the effective center frequency of the high-pass filter function behavior of the EMD over the intervals where the low frequency component exists alone. This allows the higher frequency component to be extracted with the noise and then the noise is averaged

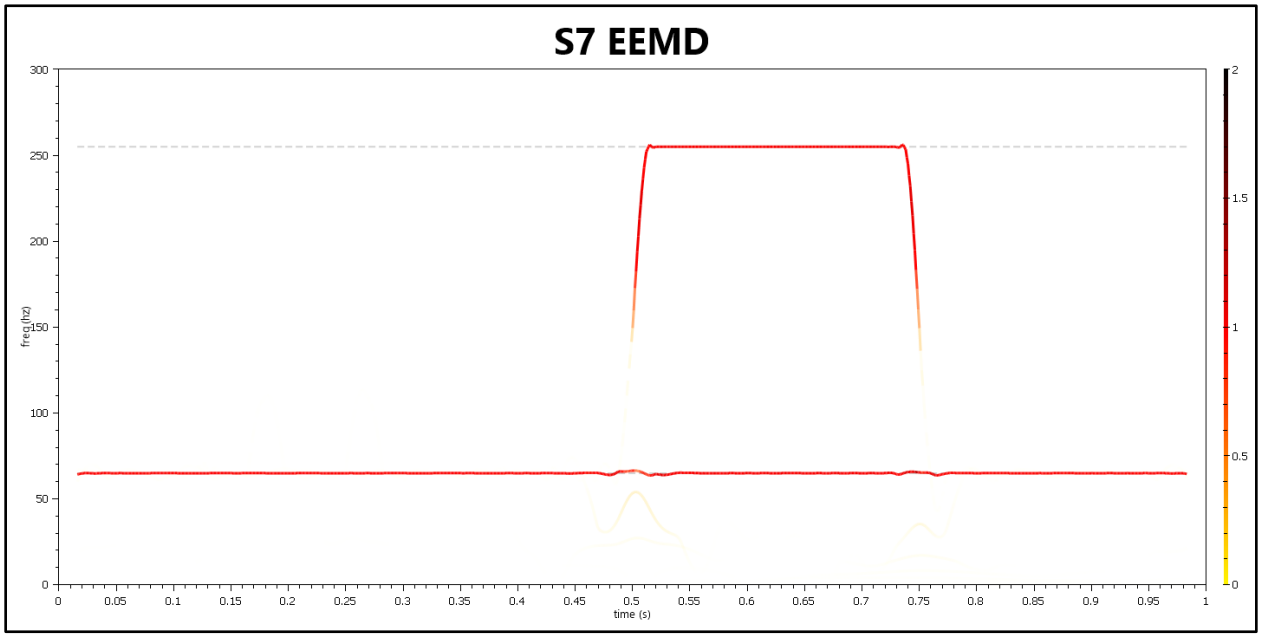


***Figure 2-3 Type-I Mode Mixing Eliminated Due to High-Frequency Noise Masking***

away in the final ensemble merging. The result of this can be seen in Fig. [2-3] where the EEMD has successfully separated the two components without Type-I Mode Mixing. Frequency-masking does this with more intentionality whereas additive noise-averaging seems to provide this benefit as a side-effect. Different noise profiles could easily lead to different results, but with sufficiently large ensembles, should lead to only small differences.

However, for frequency masking, there is a transitionary window for any given targeted mask frequency over which the signal is not entirely attenuated. This was examined initially in 1.4 but is being expanded here. Fig. [2-4] shows the same chirp signal from 1.4 with the first IMF extracted by the MATLAB 2018b EMD implementation. That first IMF is shown in blue underlaying the chirp signal which is plotted in green. As described in 1.4, the signal itself is being considered an IMF by Classical EMD standards because it satisfies the definition of an IMF and is everywhere the highest frequency in the signal. However, the actual decomposition resulted in 9 IMFs! The first IMF produced in this way is almost a perfect replica of the signal. The remaining 8 IMFs exist as a result of Type II Mode-Mixing—a result of boundary effect propagation error. But, as mentioned, it shouldn't be decomposed, since it perfectly

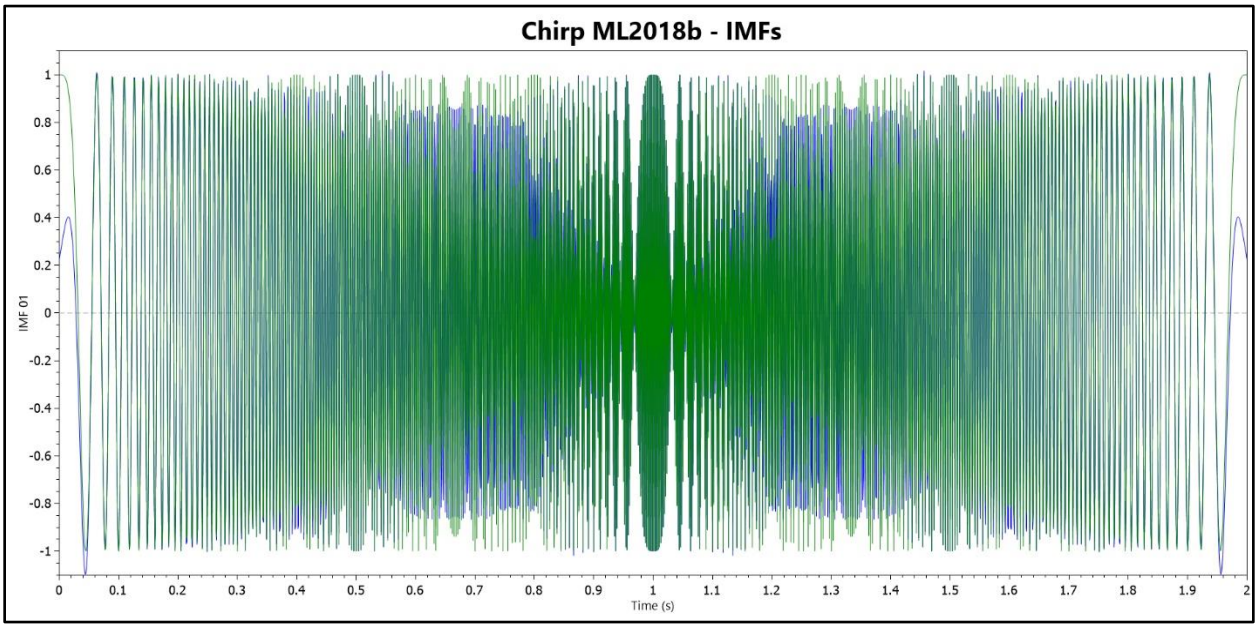


***Figure 2-4 Chirp Signal as Decomposed by MATLAB 2018b, IMF #1 in Blue Underlays Chirp Signal in Green***

fulfills the two properties required of Intrinsic Mode Functions: its mean is 0 and the number of extrema differs from the number of zero-crossings by no more than 1. But as an IMF, the chirp also perfectly demonstrates Type I Mode-Mixing: a single IMF with wildly varying frequencies (i.e. the full spectrum from 0 to the Nyquist rate).

Consider the five time-vs.-amplitude plots produced in Figs. [2-4, 2-5, 2-7, 2-8, 2-9]. The original signal is plotted in green, and the first IMF is underlaid in blue. Only the first IMF is shown from each decomposition. There are several things to note. Firstly, as mentioned, the IMF #1 provided by MATLAB looks very similar to the original signal, but it appears attenuated at higher frequencies—this is probably a combination of poor extraction at high frequencies as well as sampling offsets. Second, IMF #1 provided by each of the noise-assisted variants are very similar: the higher frequencies are captured, and the lower frequencies are filtered out. But of greater importance are both the location of attenuation cutoff and the attenuation curve from unity to 0. The shape of this curve is similar to what might be expected from a first or second order high-pass filter. This, of course, is only true because there are no other frequency components at any time step except for that provided by the chirp. Because the first IMF captures some of the frequency components in this attenuation band, the next IMF will pick up the remainder—which is classic Type-II Mode-Mixing behavior. This can be seen in Fig. [2-6].

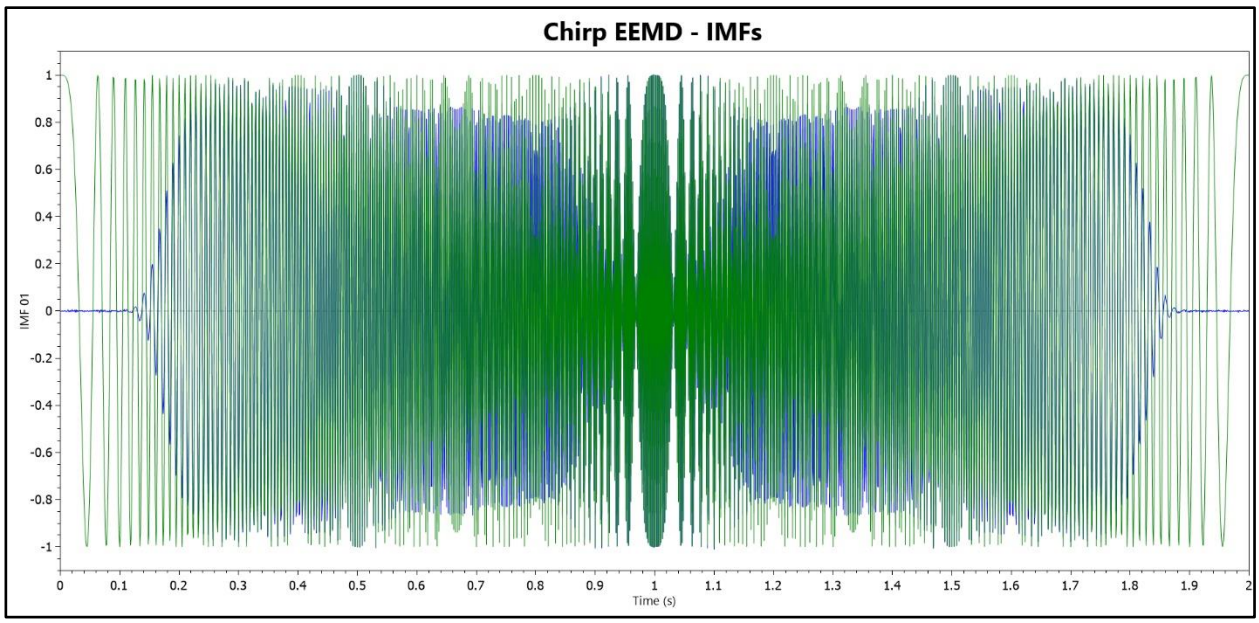


*Figure 2-6 First IMF of Chirp Signal by EEMD - Overlaid on Signal*

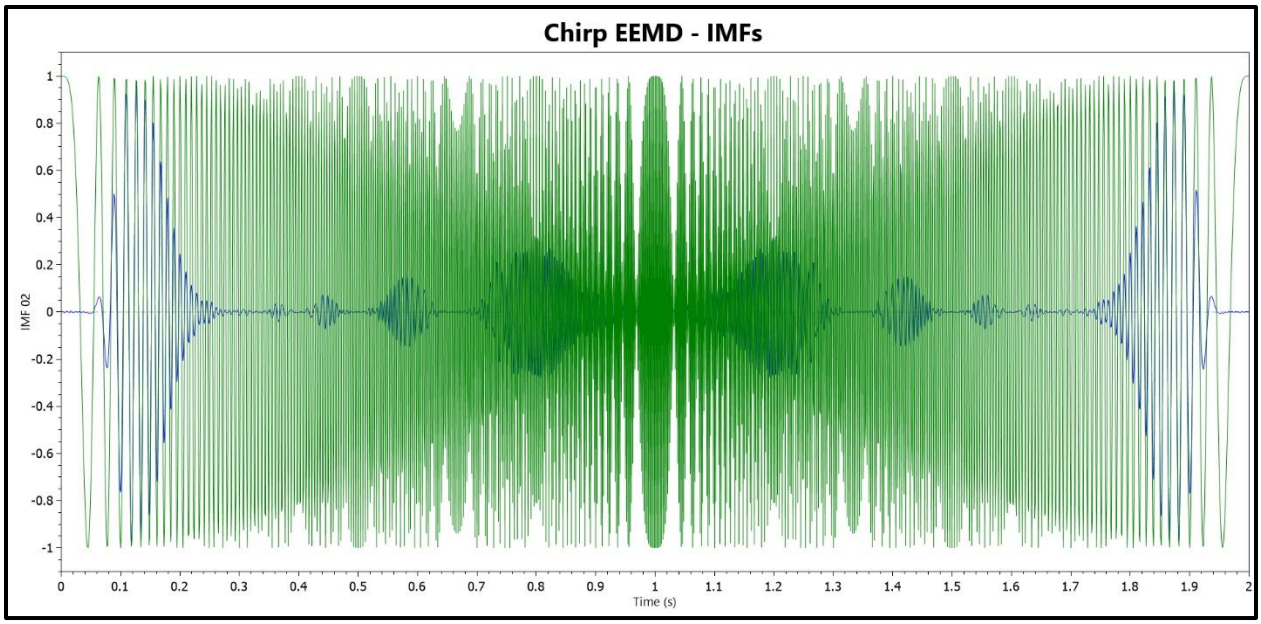


*Figure 2-5 Second IMF of Chirp Signal by EEMD - Overlaid by Signal*

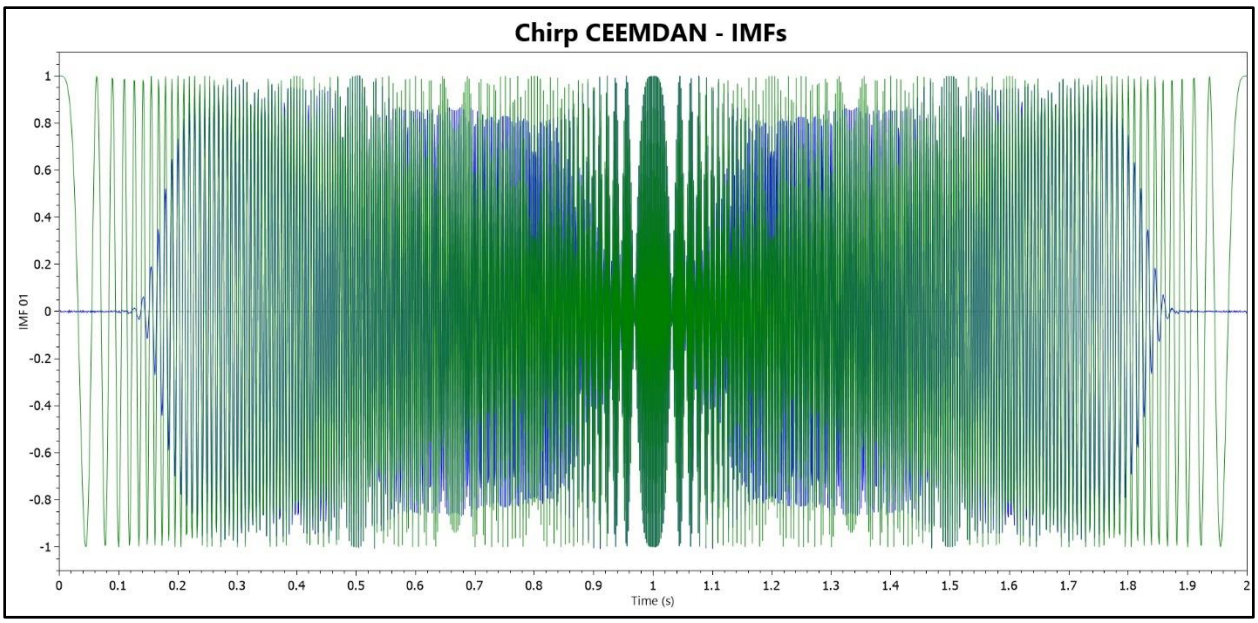


*Figure 2-7 First IMF of Chirp Signal by CEEMDAN - Overlaid on Signal*

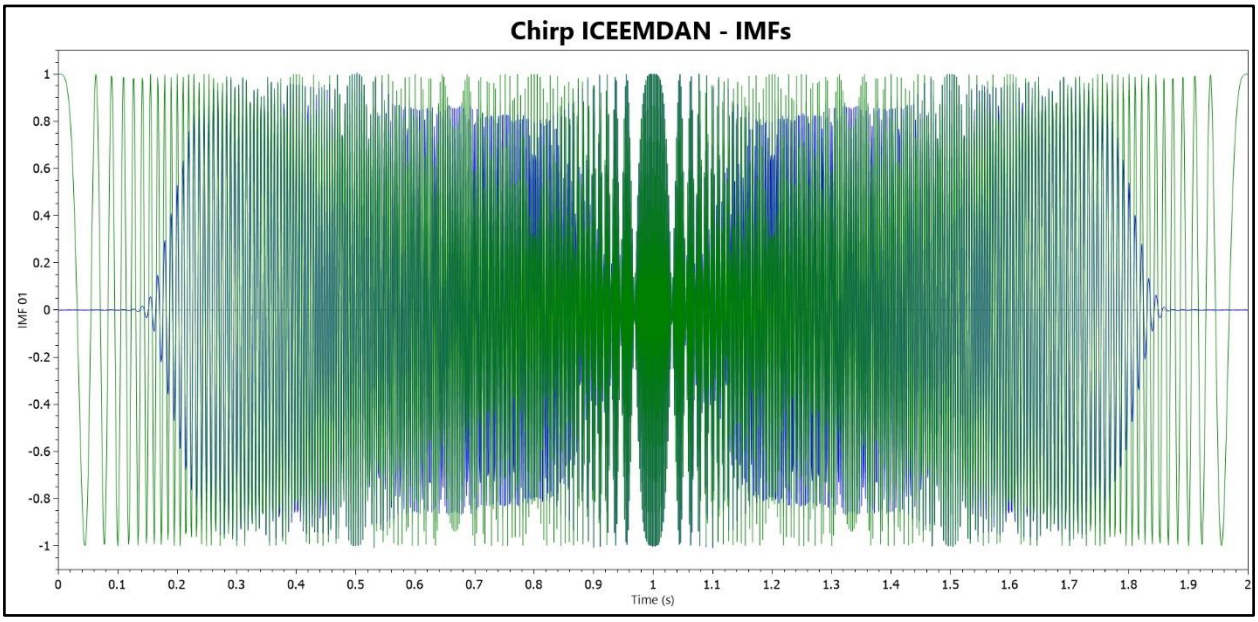


*Figure 2-8 First IMF of Chirp Signal by ICEEMDAN - Overlaid on Signal*

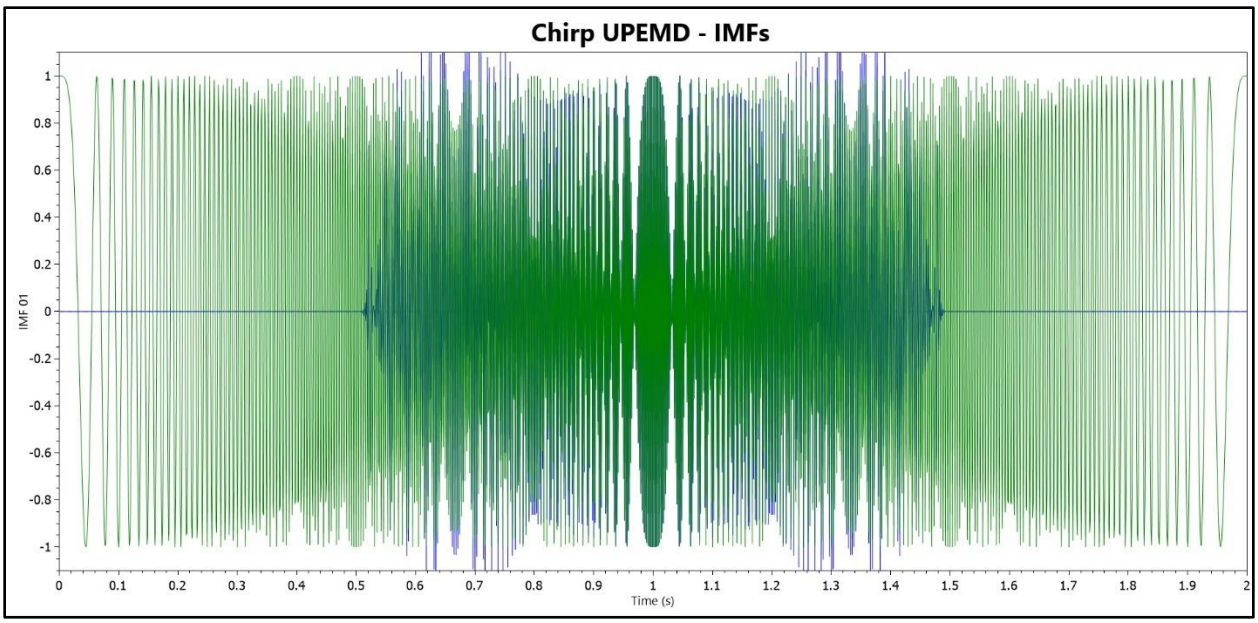


*Figure 2-9 First IMF of Chirp Signal by UPEMD - Overlaid on Signal*

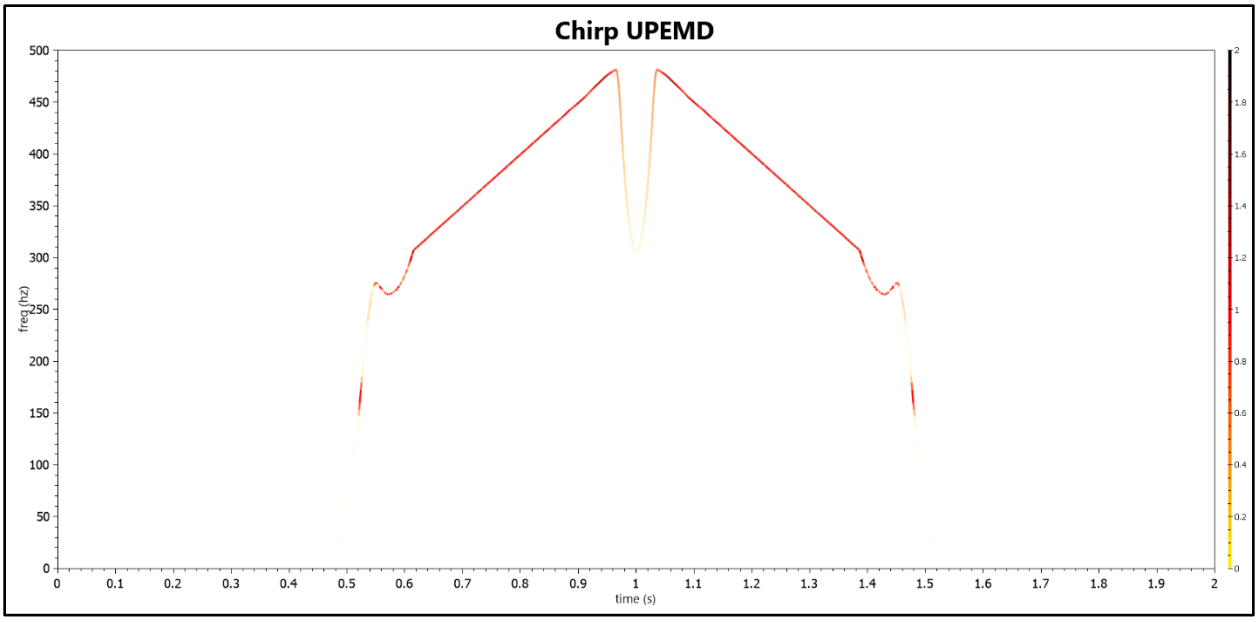


*Figure 2-10 Heat Line Plot of Hilbert Transform of First IMF of Chirp Signal by UPEMD*

Fig. [2-9] represents the first IMF extracted by the UPEMD. It is hard to characterize what is happening here. The HHT of this signal is provided in Fig. [2-10]. The dip present near the Nyquist rate should be ignored as anomalous—the direct result of the EMD having difficulty extracting frequency components very near Nyquist. Of greater interest is what happens between ~0.5s and ~0.62s (corresponding with about ~250 Hz and ~320 Hz in the signal). Also, very importantly, it should be noted that the UPEMD is actually scaling the IMF beyond the original amplitude of the signal. So, not only is the frequency becoming garbled between 250 Hz and 320 Hz, but the amplitudes are not being accurately represented. This leads to other IMFs being generated that offset this phantom amplitude, thus maintaining the completeness property—a combination of both Type II Mode-Mixing and Phantom IMFs.

The chirp signal provides a great analysis tool for assessing the properties of the various EMD techniques when addressing Type-I Mode Mixing. Despite the noise-assisted variants exerting no control over the frequency content of their masks (additive noise), they're suprisingly similar in their extraction. The most likely reason for this is that the large ensemble size of random noise-added masks generates very similar types of content—2000 enemble members were generated for each of algorithms. Regardless, the cutoff frequency for these variants is ~125 Hz, whereas the UPEMD generates it's first frequency mask at 250 Hz. So, for the UPEMD, the first ~70 Hz above it's generated mask is malformed. And then above ~325 Hz, the amplitude is fluctuating oddly. The UPEMD uses its own coded sifting technique that was unavailable for analysis at the time the research for this thesis was completed, so only speculation is possible for this behavior.

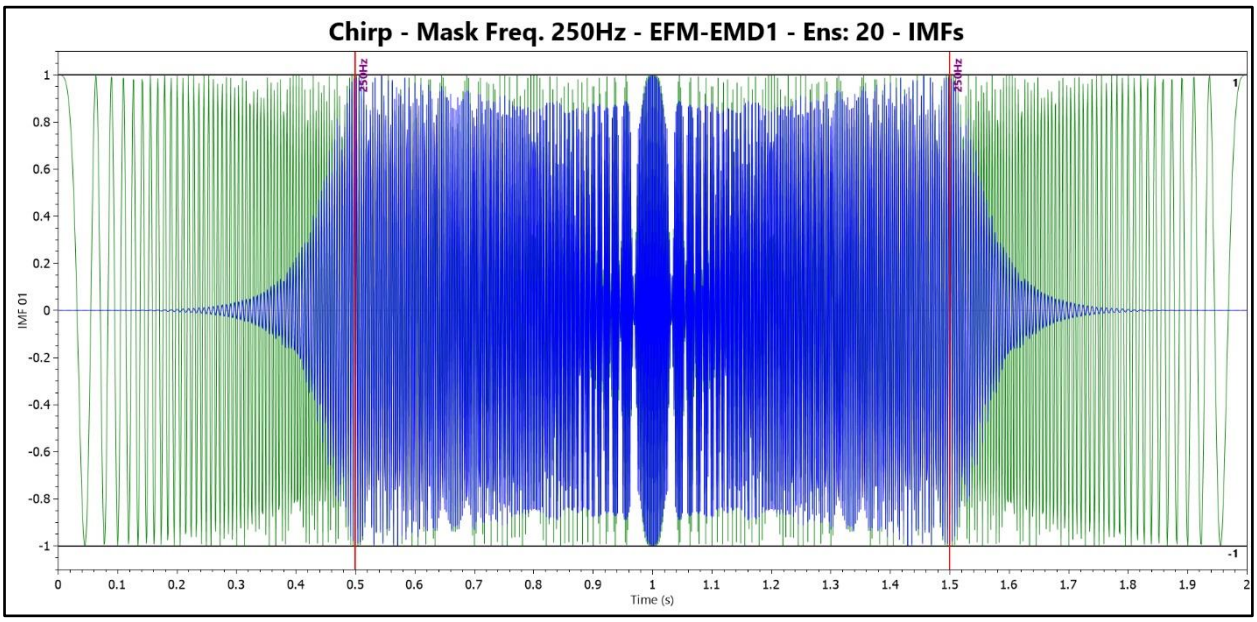


*Figure 2-11 First IMF of Chirp Signal by EFM-EMD1 With Mask Frequency @ 250 Hz - Overlaid on Signal*

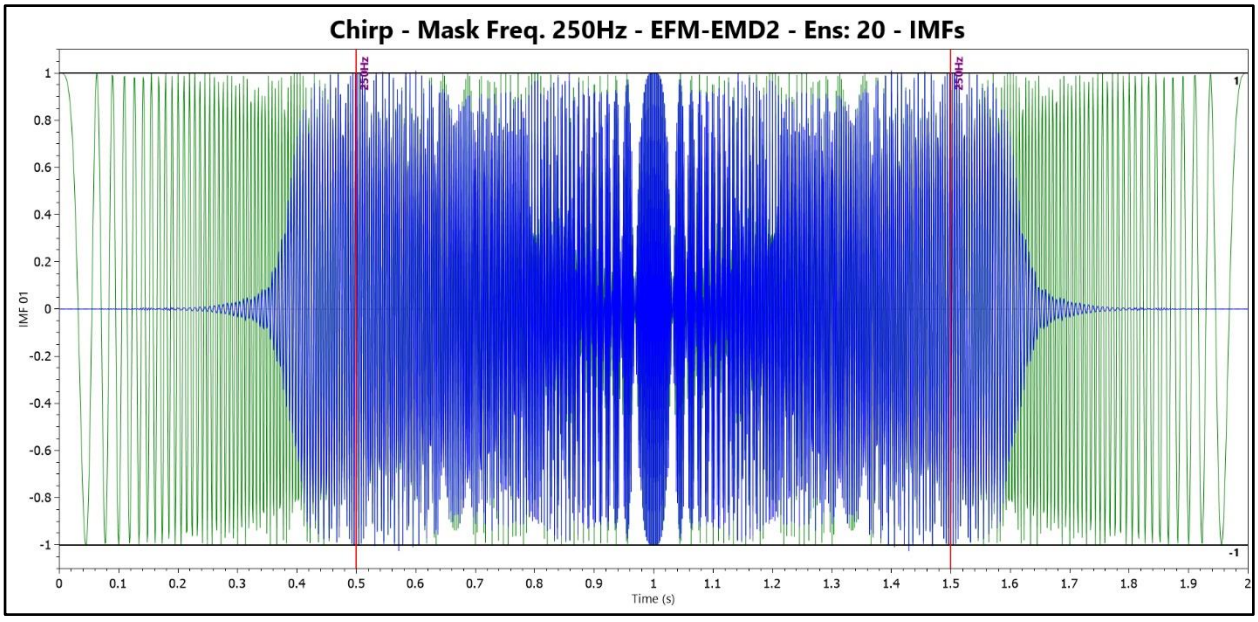


*Figure 2-12 First IMF of Chirp Signal by EFM-EMD2 With Mask Frequency @ 250 Hz - Overlaid on Signal*

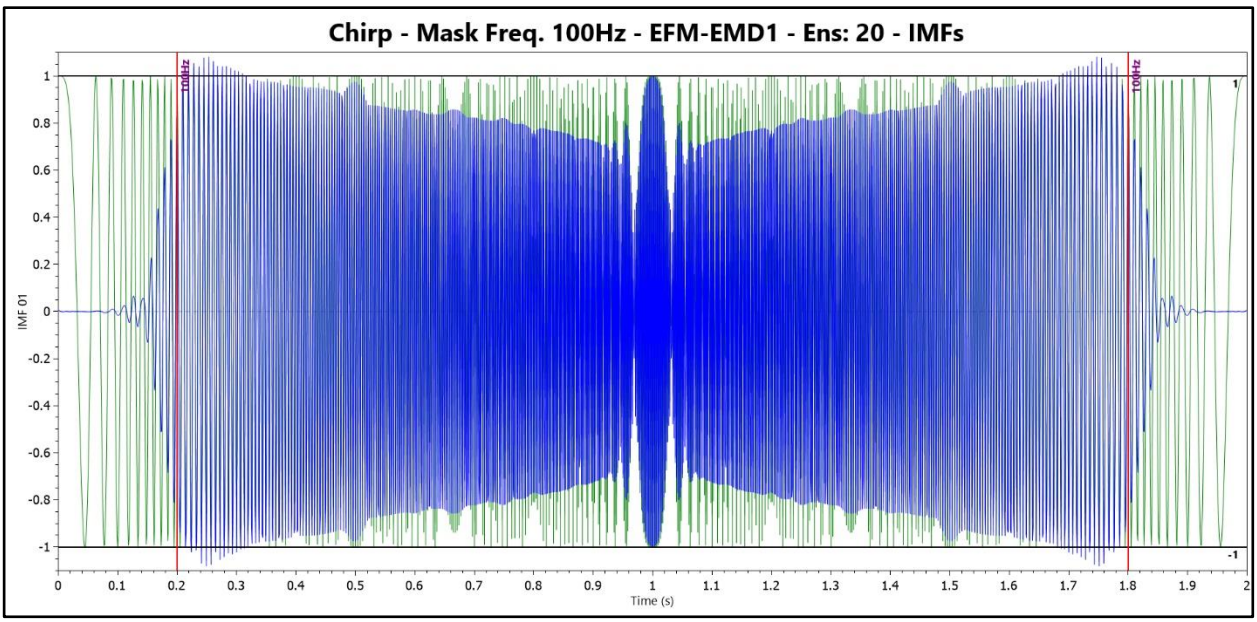


*Figure 2-13 First IMF of Chirp Signal by EFM-EMD1 With Mask Frequency @ 100 Hz - Overlaid on Signal*

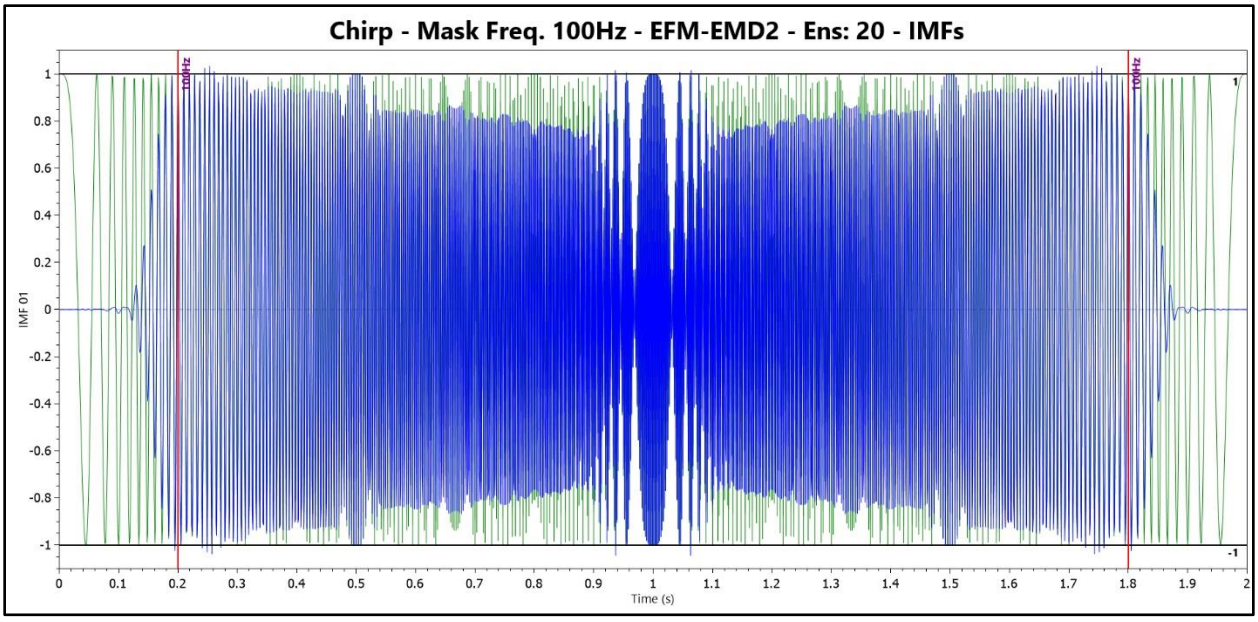


*Figure 2-14 First IMF of Chirp Signal by EFM-EMD2 With Mask Frequency @ 100 Hz - Overlaid on Signal*

But the sifting technique is very important to the behavior of the attenuation transition with respect to the frequency mask. Figure [2-11] shows the first IMF extracted from the same chirp signal using EFM-EMD1 with the frequency mask set at 250 Hz. and ensemble count set to 20. Using the same frequency mask and ensemble count, the EFM-EMD2 produces the IMF shown in Fig. [2-12]. With the EFM-EMD2, the target is 250Hz, but there is no attenuation down as far as 212 Hz, but the slope of the EFM-EMD2 is sharper at its cutoff frequency. The shape and slope of both begin to converge at ~180Hz.

The cutoff is sharper for the EFM-EMD2 than the EFM-EMD1, but both are sharper than noise-assisted variants. If the initial masking frequency is changed to 100 Hz, the two initial IMFs generated are shown in Figs. [2-13 & 2-14]. With the EFM-EMD1, at 100Hz, the amplitude at the mask target is attenuated.

Like filters, the cutoff can be made sharper. Before proceeding to the second IMF, if the decomposition applies the filter mask again, but this time to the first IMF and then re-sifts that IMF, the attenuation of the IMF becomes much sharper. Repeating this process a number of times can lead to very sharp cutoffs that can greatly reduce Type-I and Type-II Mode Mixing. This technique of reapplying the mask and repeating the sifting will be termed *masking order*. Increasing the masking order is not without problems. As shown in Figs. [2-15 & 2-16], when the masking order is 8 and 6 respectively, both the EFM-EMD1 and EFM-EMD2 demonstrate undesirable, anomalous amplitude scaling at low frequencies similar to that seen in the UPEMD. Figs. [2-17 & 2-18] show the resulting first IMFs for the corresponding 250 Hz frequency masks for both techniques.

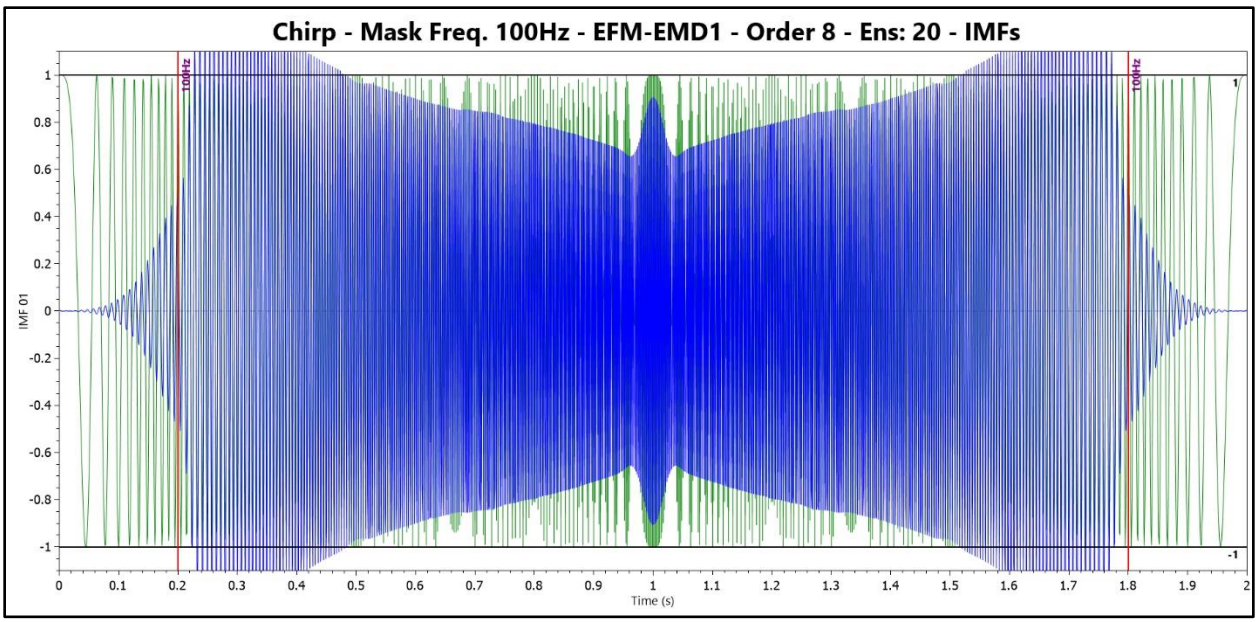


*Figure 2-15 First IMF of Chirp Signal by EFM-EMD1 With Mask Frequency @ 100 Hz - Masking Order 8 - Overlaid on Signal. This Plot Demonstrates the Anomalous Scaling Associated with Masking Order.*

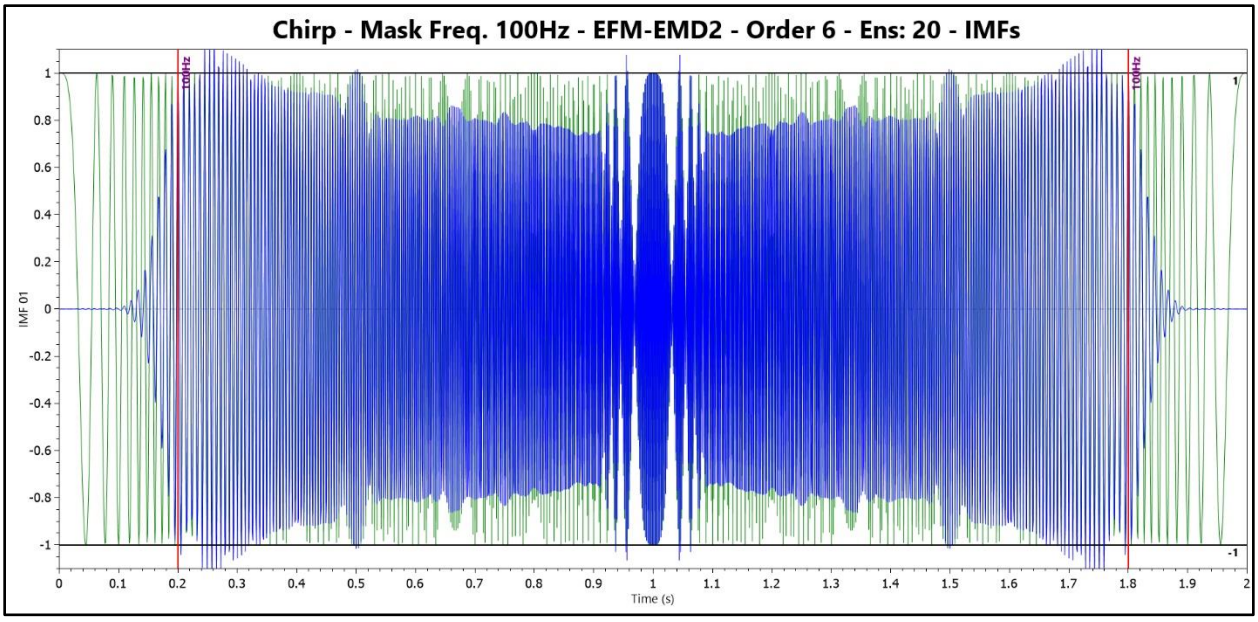


*Figure 2-16 First IMF of Chirp Signal by EFM-EMD2 With Mask Frequency @ 100 Hz - Masking Order 6 - Overlaid on Signal. This Plot Demonstrates the Anomalous Scaling Associated with Masking Order.*

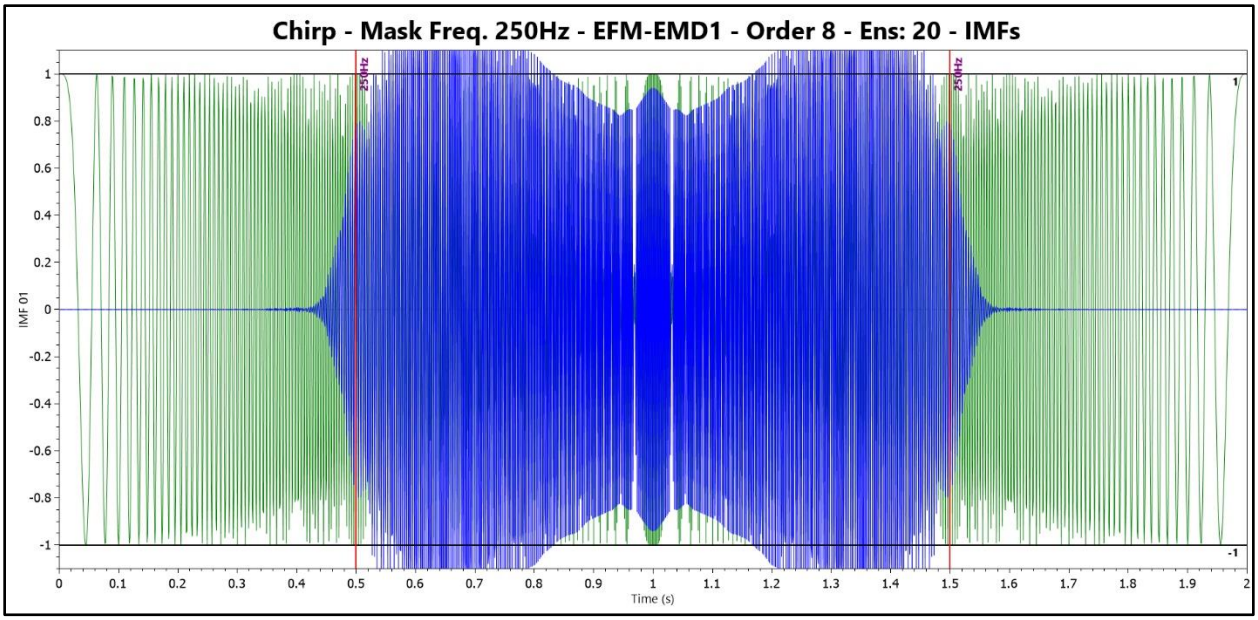


***Figure 2-17 First IMF of Chirp Signal by EFM-EMD1 With Mask Frequency @ 250 Hz - Masking Order 8 - Overlaid on Signal. This Plot Demonstrates the Anomalous Scaling Associated with Masking Order.***

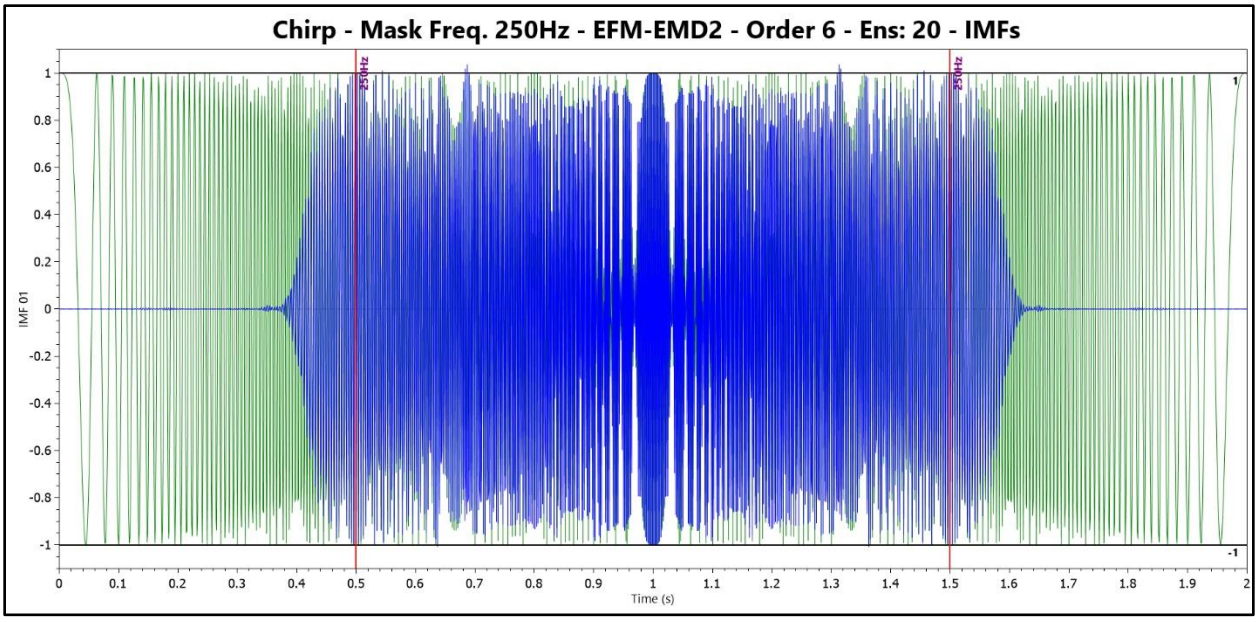


***Figure 2-18 First IMF of Chirp Signal by EFM-EMD2 With Mask Frequency @ 250 Hz - Masking Order 6 - Overlaid on Signal. This Plot Demonstrates the Anomalous Scaling Associated with Masking Order Disappears for EFM-EMD2 at Higher Frequencies Relative to Nyquist.***

As previously stated, when comparing the two techniques, it's clear that the actual cutoff frequency and the masking frequency applied do not align. If the masking frequency is 250 Hz for the EFM-EMD1, then the actual cutoff frequency is ~2.5% higher. Likewise, if the masking frequency is 100 Hz for the EFM-EMD1, then the actual cutoff frequency is ~2.5% higher. For the EFM-EMD2, the difference between the target frequency and the actual cutoff frequency is non-constant, ranging from ~20% lower at high frequencies to ~5% lower at low frequencies. This shift can be accounted for in the decomposition process (see 2.5). The anomalous scaling can be addressed, as well, by addressing the amplitude of the mask (see 2.4).

Most relevant to masking order is the steep slope of the attenuation curve, particularly noticeable in Fig. [2-18]. It is clear, experimentally, that the EFM-EMD2 produces better and more stable decompositions, but at the expense of lower resolution. The EFM-EMD1 is simply capable of much more refined tone separation. As a reminder, the cutoff frequency for Type-I Mode Mixing is not the same as the inclusion bandwidth—or that bandwidth cutoff frequency for separation of components, where Type-II Mode Mixing becomes problematic. For the EFM-EMD1, the cutoff frequency for the inclusion bandwidth is ~10% of the masking frequency and does a fair job to as small as ~7.5%. The EFM-EMD1 is also able to extract components at much higher frequencies relative to the Nyquist rate. Consider Fig. [2-19] where the intermittent two-tone signal has a high component at 80% of the Nyquist rate and a ratio of separation of 0.9 (400 Hz and 360 Hz) between components. No other known EMD technique is capable of decomposing this finely or at this percentage of Nyquist. To achieve this remarkable resolution, the EFM-EMD1 is used with a sifting threshold of $1x10^{7}$, signal prescaling of 100, order 8, and adaptive amplitude. Higher parameter values have little benefit and appear to represent an upper bound on the capability of the EFM-EMD1. Fig. [2-20] shows the same two-tone intermittency, where the frequencies of the two components are 250 Hz and 225 Hz respectively (ratio = 0.9).

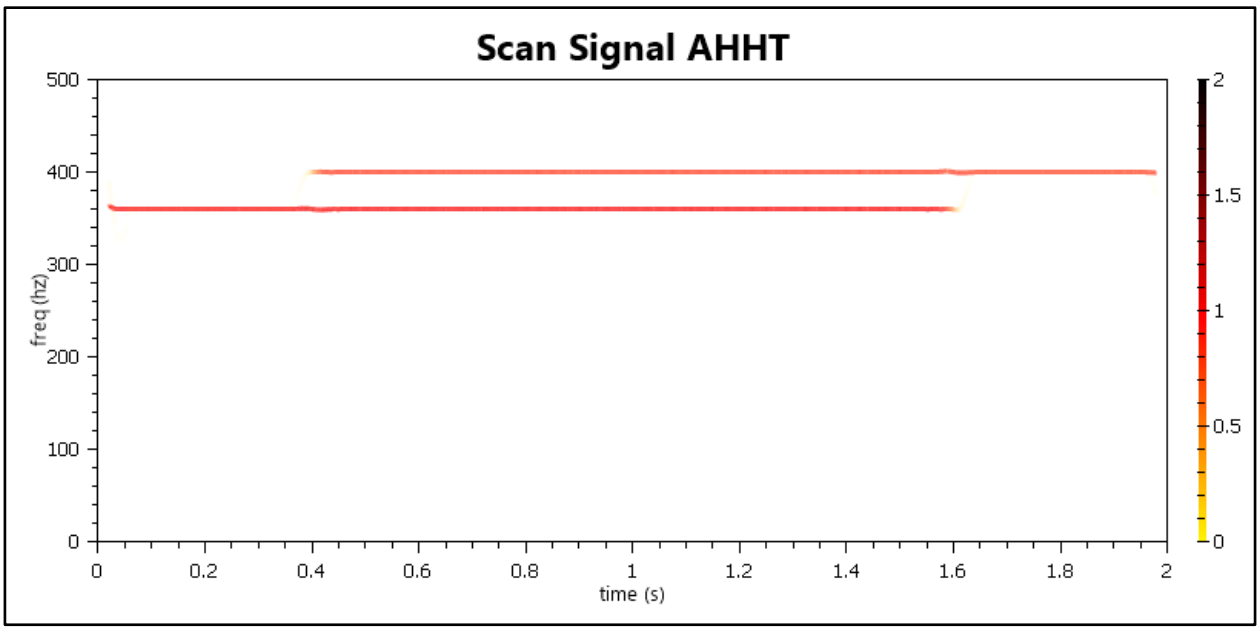


*Figure 2-19 EFM-EMD1 Applied to Non-Constant, Overlapping Two-Tone Signal (400 Hz and 360 Hz) at 80% of the Nyquist Rate With Frequency Ratio 0.9. Anomalous Scaling Has Been Reduced for This Order 8 Decomposition.*

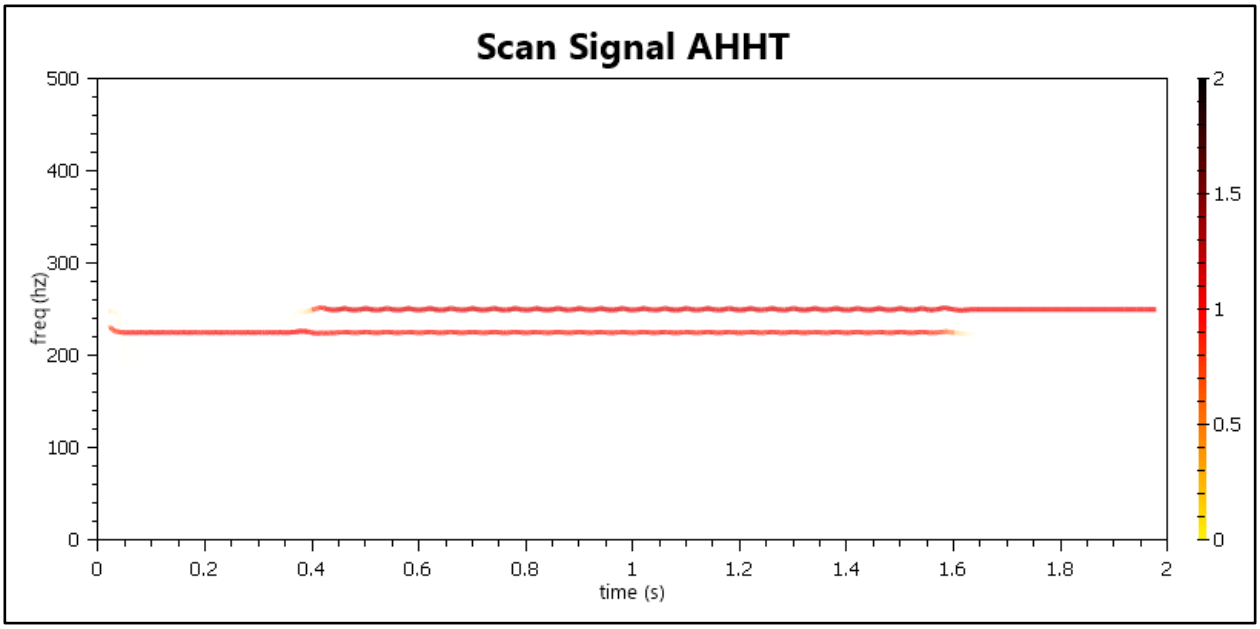


*Figure 2-20 EFM-EMD1 Applied to Non-Constant, Overlapping Two-Tone Signal (250 Hz and 225 Hz) at 50% of the Nyquist Rate With Frequency Ratio 0.9. Anomalous Scaling Has Been Reduced for This Order 8 Decomposition.*

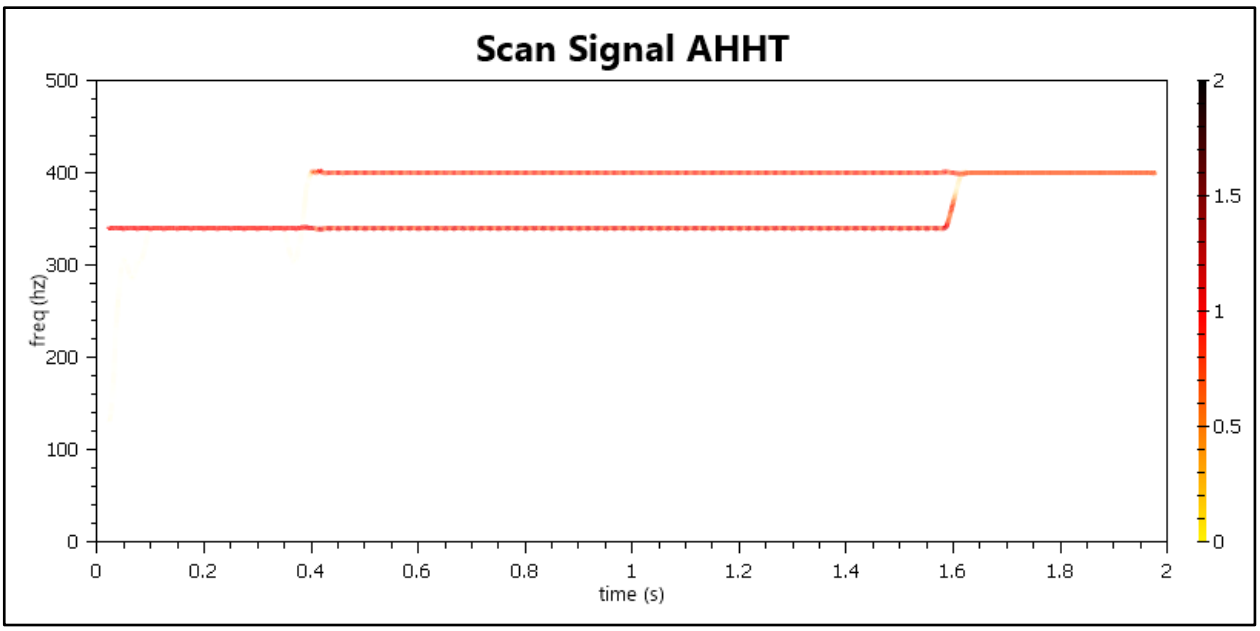


***Figure 2-21 EFM-EMD2 Applied to Non-Constant, Overlapping Two-Tone Signal (400 Hz and 340 Hz) at 80% of the Nyquist Rate With Frequency Ratio 0.9. Anomalous Scaling Has Been Reduced for This Order 6 Decomposition.***

By contrast, the EFM-EMD2 only has ~15% target frequency separation ability, but is also able to achieve this separation at ~80% of the Nyquist rate as shown in Fig. [2-21] (order: 6, threshold: $1x10^7$, frequency shifted, adaptive amplitude).

## 2.4 MASKING AMPLITUDE

The AHHT, through experimentation, has settled on the approach of using an initial mask amplitude equal to the max absolute value of the signal to be decomposed excluding the top 1% of absolute values (to exclude outliers). The amplitude is adjusted after each IMF has been extracted to account for the changing max amplitude in the signal.

As noted in 2.3, there is a large concern that anomalous scaling caused by increased masking order will trigger the generation of Phantom IMFs and/or Type-II Mode-Mixing. A small amount of anomalous scaling was seen in Fig. [2-13] where the masking frequency was 100 Hz and the masking order was 1 using EFM-EMD1. There it was seen that the amplitude at ~125 Hz (coinciding with timestep ~.125) was

maximum and slightly overscaled by ~5% more than the underlying signal. It is worse still in Fig. [2-15] where the order has been increased to 8 and the scaling has grown substantially worse.

However, by reducing the mask amplitude for the iterations of masking order > 1, the anomalous scaling can be greatly reduced, and in the case of the EFM-EMD2, virtually disappears. This can be seen in Figs. [2-22 & 2-23] which are the mask amplitude reduction plots for the same masking frequencies as shown in Figs. [2-15 & 2-16]. The initial mask amplitude is scaled down by the ratio of the masking frequency relative to the Nyquist rate. Then the higher orders of decomposition proceed. So, two remedies can be taken to manage the anomalous scaling. Firstly, when implementing a >1 masking order ensemble sift, the amplitude of the mask can be reduced. Secondly, and for greater stability, using the EFM-EMD2 algorithm in addition to a reduced mask amplitude can provide great attenuation curves for eliminating Type-I Mode Mixing and greatly reduced Type-II Mode Mixing. Of greatest importance is the sharper cutoff provided by the EFM-EMD2 at lower frequencies. The AHHT System hands off from EFM-EMD1 to EFM-EMD2 for masking frequencies below ~0.65 of the Nyquist rate.

However, at very low frequencies, below 1% to 5% of the Nyquist rate, it is nearly impossible to eliminate Mode-Mixing Type I. There are simply too few extrema for the timesteps to generate meaningful masks.

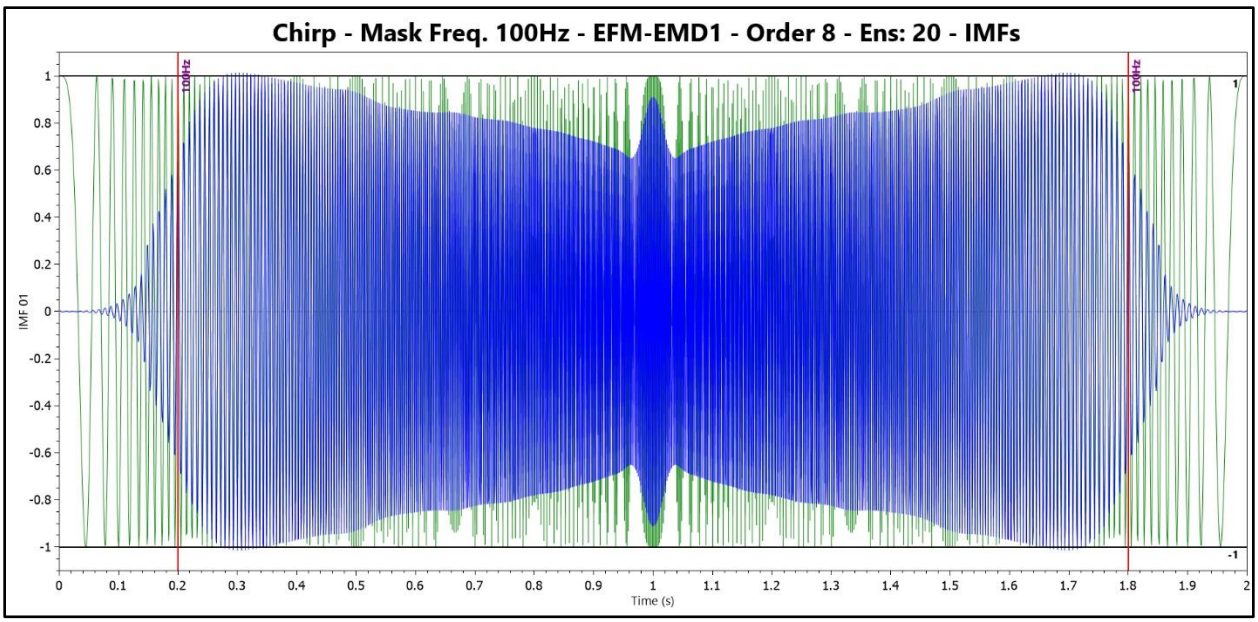


*Figure 2-22 First IMF of Chirp Signal by EFM-EMD1 With Mask Frequency @ 100 Hz - Masking Order 8 - Overlaid on Signal. This Plot Demonstrates the Anomalous Scaling Associated with Masking Order Reduced by Mask Amplitude Reduction.*

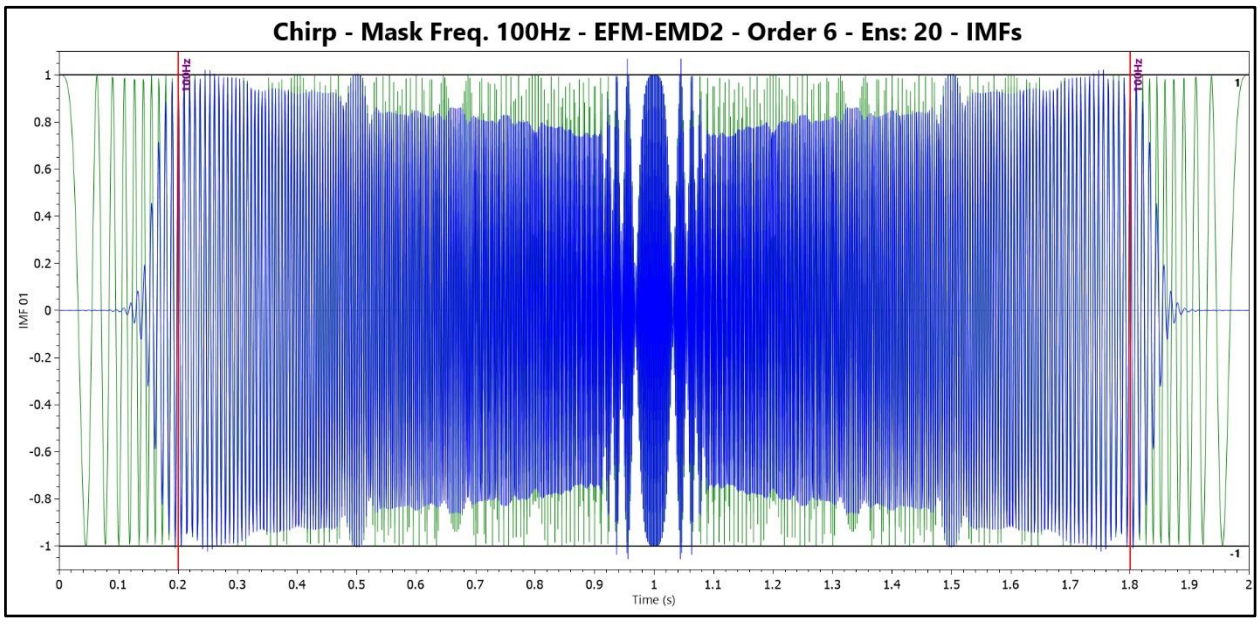


*Figure 2-23 First IMF of Chirp Signal by EFM-EMD2 With Mask Frequency @ 100 Hz - Masking Order 6 - Overlaid on Signal. This Plot Demonstrates the Anomalous Scaling Associated with Masking Order Reduced by Mask Amplitude Reduction.*

## 2.5 MASK FREQUENCY SHIFTING

It is unclear what Hu and Mo [31] were intending to accomplish with their idea of mask frequency shifting. It does not seem to be in anyway related to the attenuation transition analysis described in 2.4. However, as can be seen in the chirp signals of 2.3 and 2.4, the ratio of the cutoff frequency relative to the mask frequency ranges from ~-0.025 to ~+0.2. That frequency distance appears to be dependent on the mask frequency relative to Nyquist and the EFM-EMD technique being used. To increase the resolution of the EFM-EMDs, the AHHT employs an adjustment to the masking frequency prior to generating the ensemble of phase-offset masks:

$$actual\_freq = target\_freq * \left(shift - shift_{offset} * \left(1 - pct_{of_{nyq}}\right)\right) \quad 2:1$$

Knowing that the cutoff frequency will still be below the target frequency, the component of interest can be extracted with minimal impact on lower frequency components. This must be balanced with the notion that the cutoff frequency for Type-I Mode-Mixing concerns differs from the cutoff frequency for Type-II Mode-Mixing concerns.

Little effort was given to finding optimal shift values for EFM-EMD1 or EFM-EMD3 as the majority of the components in the tested signals were between 0.015 and 0.65 of Nyquist, but not much shifting is expected for EFM-EMD1 for the range it is used. Experimentally, it was determined that the following values worked well with all of the tested example signals:

EFM-EMD1: shift = 1, shift_offset = 0

EFM-EMD2: shift = 1.15, shift_offset = 0.14

EFM-EMD3: shift = 1, shift_offset = 0

## 2.6 SIFT STOPPING CRITERION

As noted in 1.1, there are several sifting stop criterion options available. The sifting stop criterion adopted here is to use the ratio between the variance of the original signal and the variance of the current envelope mean. Sifting stops when this threshold is exceeded. While this does not guarantee modes will satisfy the two IMF properties and may not be perfectly orthogonal, it provides good results nevertheless and allows for a relationship between the signal power, frequency-mask/signal-frequency correlation, and the sifting threshold. Further, conforming to IMF properties is highly likely with sufficient threshold levels. Formally, sifting stops once the following condition is satisfied:

$$\frac{var[r(t)]}{var[env_{mean}(t)]} > sift_{threshold} \qquad 2:2$$

For the decomposition stopping criterion, the simple ratio of the variance in the original signal vs. the variance in the residual is compared to a threshold value: 15 DB in all the example cases works well, or if there are no more than 2 extrema remaining in the residual. The negative to this approach is that decomposition might stop early with further low-amplitude, yet meaningful, IMFs potentially able to be extracted. Formally, decomposition stops once the following condition is satisfied:

$$\frac{var[x(t)]}{var[r(t)]} > decomp_{threshold} \qquad 2:3$$

## 2.7 CLUSTERING DENSITY FUNCTION

The clustering density function in subtractive clustering was given in equation 2.1 as:

$$P_i = \sum_{j=1}^{n} e^{-\frac{\|x_i - x_j\|^2}{\left(\frac{r_a}{2}\right)^2}} \quad 2:4$$

But fundamental to that equation is the Gaussian form in 2:5.

$$f(\boldsymbol{x_i}, \boldsymbol{x_j}) = e^{-\frac{\|x_i - x_j\|^2}{\left(\frac{r_a}{2}\right)^2}} \quad 2:5$$

$$Let\ \boldsymbol{y_{ij}} = \|\boldsymbol{x_i} - \boldsymbol{x_j}\|, then$$

$$f(y_{ij}) = e^{-\frac{4}{r_a^2} * y_{ij}^2} \quad 2:6$$

But the density kernel in 2:6 is somewhat arbitrary. It is primarily meant to monotonically decrease the value of *f()* as the distances between points increase with a sharp early drop in value for distances that are still relatively close. While it may have some relationship to the Central Limit Theorem and probability of closeness to a mean value, in reality, since there's no statistical test for variance in the algorithm and $r_a$ is subject to experimental testing on any given dataset, there's no reason to draw that connection. It should be equally correct to use any other shape that is monotonically descreasing from 1 at 0 and approaches 0 as distance approaches infinity—any other bell-like curve with a modifiable width could suffice. And in fact, if one exists that avoids powers, exponentials, and other computationally costly operations such as tanh() or log(), it should be adopted instead. The following equation is able to be implemented simply.

$$f(x) = 1 - \frac{x^2}{1 + x^2} \qquad 2{:}7$$

Equation 2:7 produces similarly shaped bell curves which work well for the purposes of subtractive clustering, provided the correct $r_a$ values. But, this equation is reducible.

$$f(x) = \frac{1}{1 + x^2} \qquad 2{:}8$$

And since *x*, in 2:8, is really $y_{ij}$ in 2:6, the equation becomes:

$$f(y_{ij}) = \frac{1}{1 + {y_{ij}}^2} \qquad 2{:}9$$

But $y_{ij}$ is itself a magnitude—the result of the Euclidean norm—so the term becomes simpler still:

$$f(\boldsymbol{x_i}, \boldsymbol{x_j}) = \frac{1}{1 + \left\|\boldsymbol{x_i} - \boldsymbol{x_j}\right\|^2} = \frac{1}{1 + (x_{i1} - x_{j1})^2 + (x_{i2} - x_{j2})^2 + \cdots + (x_{in} - x_{jn})^2} \qquad 2{:}10$$

However, since, for the purposes of the AHHT, there are only two elements in $\boldsymbol{x}$ (frequency/amplitude), it simplifies to:

$$f(\boldsymbol{x_i}, \boldsymbol{x_j}) = \frac{1}{1 + (x_{i1} - x_{j1}) * (x_{i1} - x_{j1}) + (x_{i2} - x_{j2}) * (x_{i2} - x_{j2})} \qquad 2{:}11$$

This reduces to one divide, two multiplies, and four add/subtracts (since the two differences can be pre-calculated into a single variable prior to multiplication). Putting this back into the density function of subtractive clustering, the final equation used to generate the potential for a given point to be a cluster is simply:

$$P_i = \frac{r_a^2}{4} * \sum_{j=1}^{n} \frac{1}{\frac{r_a^2}{4} + (x_{i1} - x_{j1}) * (x_{i1} - x_{j1}) + (x_{i2} - x_{j2}) * (x_{i2} - x_{j2})} \quad 2:12$$

The scalars can be precomputed, as well, so those operations are one-time costs. The original term was equivalent to:

$$P_i = \sum_{j=1}^{n} e^{\frac{-\left(\sqrt{(x_{i1}-x_{j1})*(x_{i1}-x_{j1})+(x_{i2}-x_{j2})*(x_{i2}-x_{j2})}\right)^2}{\left(\frac{r_a}{2}\right)^2}} \quad 2:13$$

By eliminating the exponential and the wasted square/square-root operations, the computational cost of a given measurement is significantly reduced. And, experimentally, the results are equally good. For an algorithm that is $O(N^2)$, every computational expense eliminated also provides $O(N^2)$ savings.

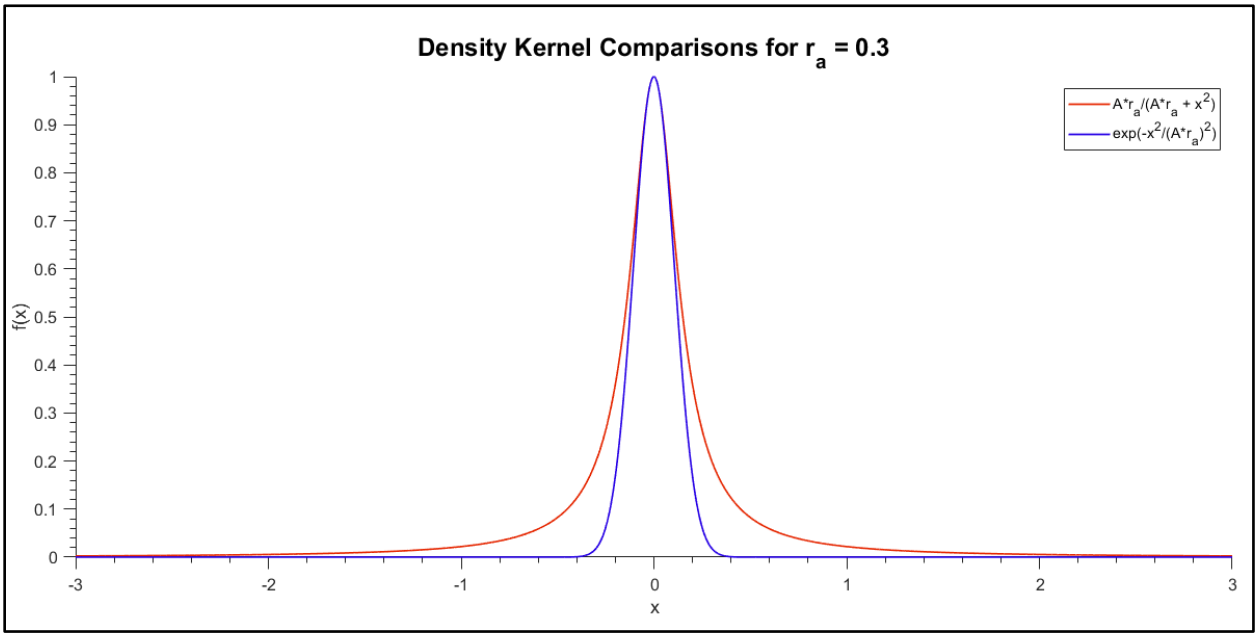


***Figure 2-24 Comparison of Standard Density Kernel for Subtractive Clustering vs. the Modified Version Used in AHHT***

For all of the examples provided in Chapter 3, an $r_a$ value of 0.3 was used. Comparing the graphs for the original density kernel to the new density kernel in Fig. [2-24], it is clear they are similar, but the original density kernel has a narrower base, decaying to near zero much faster.

## 2.8 SYSTEM DECISIONS

To incorporate the analysis presented in 2.2 -> 2.7, the AHHT System uses the masking frequency, as a percentage of Nyquist, to determine which algorithm is to be used in ensemble. If the masking frequency is within 65% of the Nyquist rate, then the EFM-EMD1 is selected. When the masking frequency is between 1.5% and 65% of the Nyquist rate, the EFM-EMD2 is chosen. Below this, the EFM-EMD3 is chosen.

Although a series of merit-based tests are done to determine order and sifting threshold at each decomposition step, when the EFM-EMD1 is chosen, the sifting threshold is reduced by a factor of 100, its masking order is doubled to a maximum of 8, and prior to the first order sift, the mask amplitude is reduced by the ratio of the mask frequency and the Nyquist rate. When the EFM-EMD3 is used, the sifting threshold is set to $1x10^7$ (base threshold) to account for the slow convergence at lower frequencies. The EFM-EMD2 always uses order 6, except in the case where there is no component near the target frequency other than that which was discovered, in which case it is set to 1.

As previously mentioned, the mask amplitude is updated for each residual to be sifted. After trimming the top 1% of absolute values to eliminate outliers, the max absolute value of the signal is chosen for the mask amplitude.

To make these values work, all signals prior to decomposition are prescaled to a common amplitude of 100. The purpose of upscaling smaller signals is to separate meaningful components from the natural noise variability introduced due to numerical imprecision and numerical methods. Extrema found at

very small levels due to imperfections in IMF extraction are ignored, yet small perturbations as might be seen due to vibrational/fault defects will have been amplified in the original signal and are able to be extracted.

The AHHT System uses mirroring as the extrapolation scheme for envelope boundary extrapolation since in testing this led to more generally stable decompositions. For interpolating extremum centers, the boundary values are merely repeated to the left and right of the signal boundary. This approach sets three new center points on each end of the signal at time steps -5, -4, and -3 using the value of the first extremum center, and at n + 2, n + 3, and n + 4 using the value of the last extremum center.

The SIFT2 and SIFT3 algorithms both use mirroring for the upper and lower envelopes. SIFT1 and SIFT2 both use the simple extension described above for the extremum center boundary extrapolation.

## 2.9 SYSTEM OVERVIEW

In short, the system follows these steps:

1. Using a single IMF decomposition step with the frequency mask near to the Nyquist rate, the highest frequency existing within the signal is estimated: *freq_test*.
2. Beginning with *freq_test* as the frequency mask, an “estimation” process (detailed later) is executed on the signal to derive ***mask1***.
3. If a valid frequency is found, then the estimated frequency derived from that process is perturbed down by a very small percentage of bandwidth (dependent on a bandwidth resolution parameter), and the next estimation is made on the remainder from the first estimation to derive ***mask2***. The resolution parameter is 10% for all frequencies above 65% of Nyquist (since EFM-EMD1 will be used), 15% for all frequencies between 65% and 1.5% of

Nyquist (since EFM-EMD2 will be used), and 25% for all frequencies below 1.5% of Nyquist (since EFM-EMD3 will be used).

4. Step 3 provides for potentially two estimates of upcoming IMFs to be sifted out.
    a. Based on these one or two estimates, a further estimate is made for both the sifting threshold and for the masking order. The masking frequency is set to the first estimate.
    b. If a valid frequency is not found, then *freq_test* is reduced by half the resolution bandwidth percentage and **2** Is repeated.
5. A suitable EFM-EMD is chosen and the IMF is extracted.
6. If decomposition is incomplete, return to **2** with the remainder of the signal after subtracting the most recent IMF.

Frequency estimation, provided by a ***MaskEstimation()*** function, proceeds by extracting the first IMF of the signal in its current state (initial or after some IMFs have already been extracted). Then the Hilbert

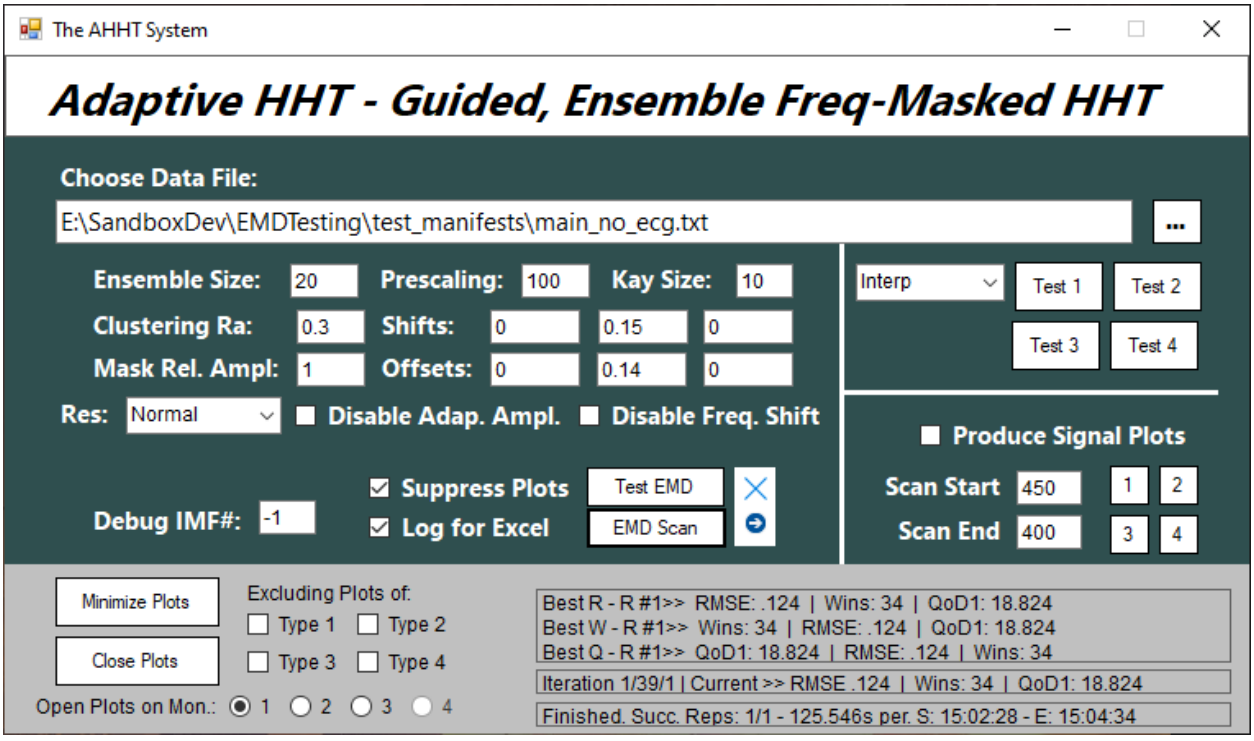


***Figure 2-25 The AHHT System User Interface***

Transform is applied to the temporary IMF from which the instantaneous frequency and amplitude is derived. Using that two-dimensional information, the time steps of the IMF are clustered by fast subtractive clustering (see 2.7). Using simple sufficiency thresholds, the highest significant frequency component in the signal is found. Additional safeguards to avoid spurious IMFs (such as minimum amplitudes relative to the maximum amplitude of the signal, boundary margins to reduce boundary anomalies, and other regulations) are implemented here. In order to be more performant, the AHHT uses a greatly reduced ensemble, Kay window, and in some cases, sift threshold for the HHT test. It then generates the estimate amidst high frequency/amplitude volatility.

Sandoval and de Leon suggested in [32] that for every ensemble sift procedure, one additional sift is performed after the ensemble sifts are completed and averaged. The goal of this is to ensure that the averaged result conforms to IMF properties, which is not guaranteed after the averaging operation. However, in practice, this repeatedly produced poor decompositions for any EFM-EMD technique and was thus not implemented. As a result, the AHHT shares the same flaw as the noise-assisted variants.

Also, of interest, is a variable known as *leakage bias*. During the mask estimation algorithm, an IMF is extracted. The remainder is then passed into the mask estimation algorithm again with a slightly lower test frequency. If that second mask estimation procedure returns a frequency recommendation that is very near the first one, it is considered a leakage event. The remainder is continuously passed through until no leakage event occurs. The number of leakage events that occur at a given IMF extraction step is used to reduce the sifting threshold by factors of 10 to reduce the likelihood of *oversifting* during that step. The $leakage_{bias}$ variable holds a count of such events for a given IMF extraction step.

$$sift_{threshold} = \frac{sift_{threshold}}{10^{leakage_{bias}}} \quad 2:14$$

A complete overview of the AHHT system is provided in Figs. [2-26 → 2-32].

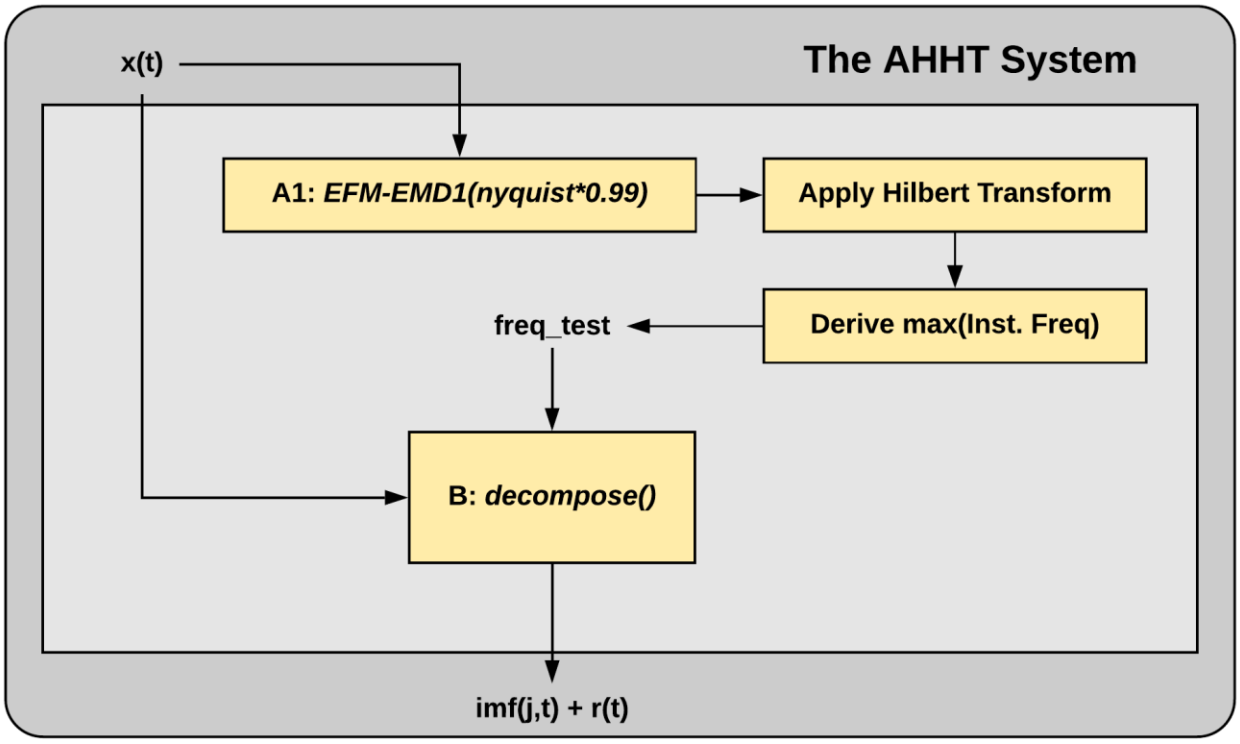


*Figure 2-26 AHHT: System Start*

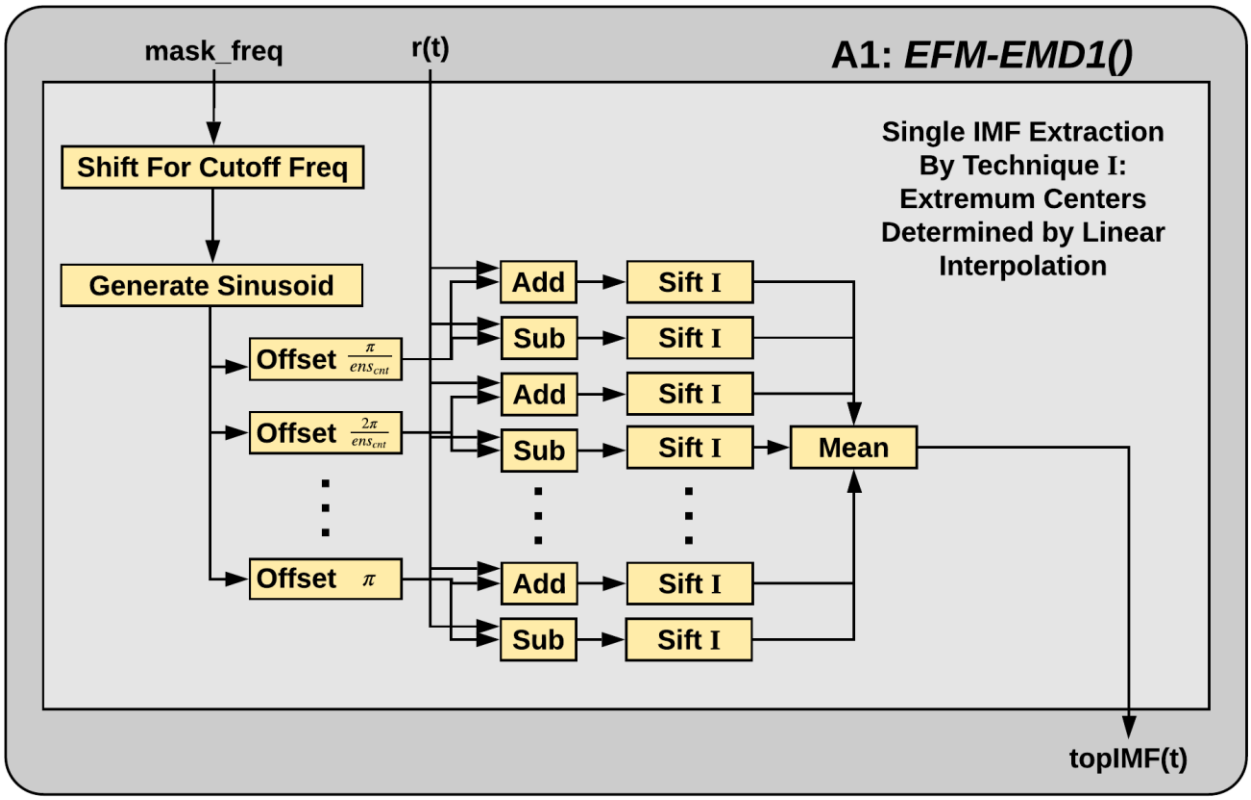


*Figure 2-27 EFM-EMD1() Function Overview*

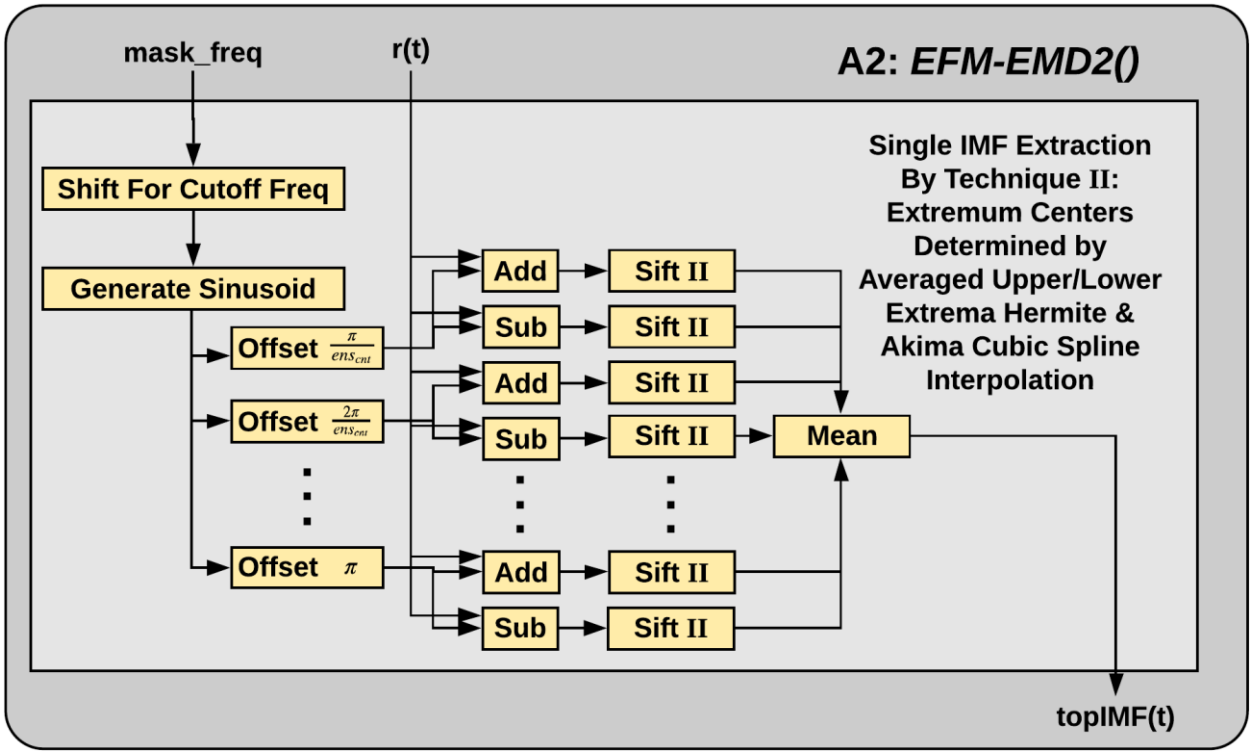


*Figure 2-28 EFM-EMD2() Function Overview*

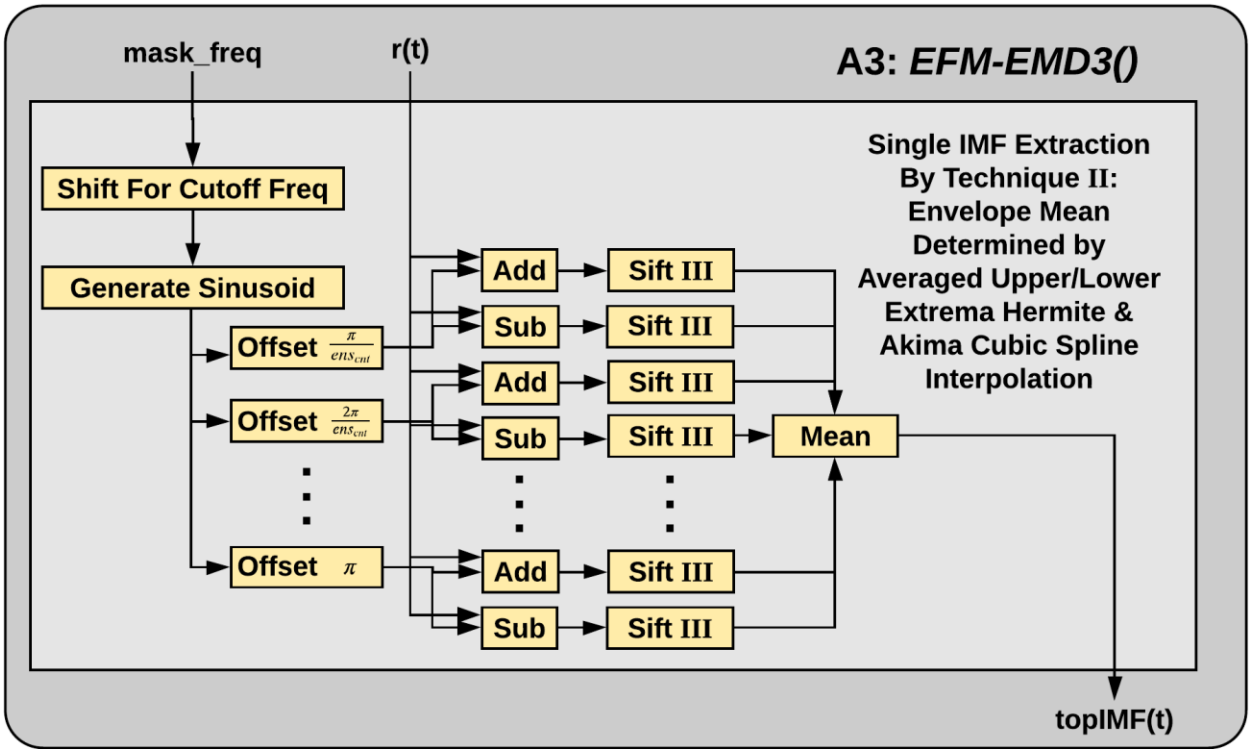


*Figure 2-29 EFM-EMD3() Function Overview*

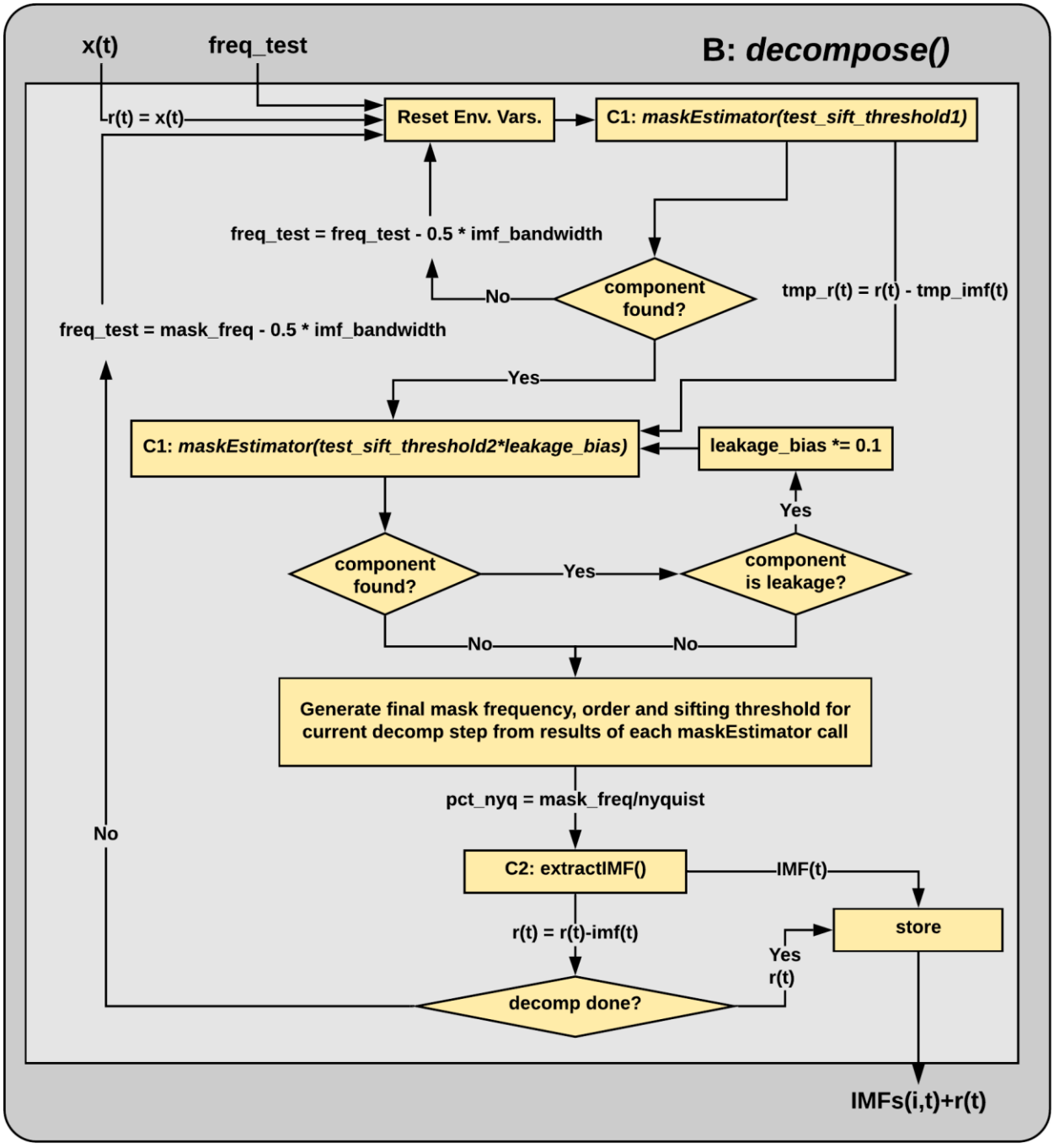


*Figure 2-30 decompose() Function Overview*

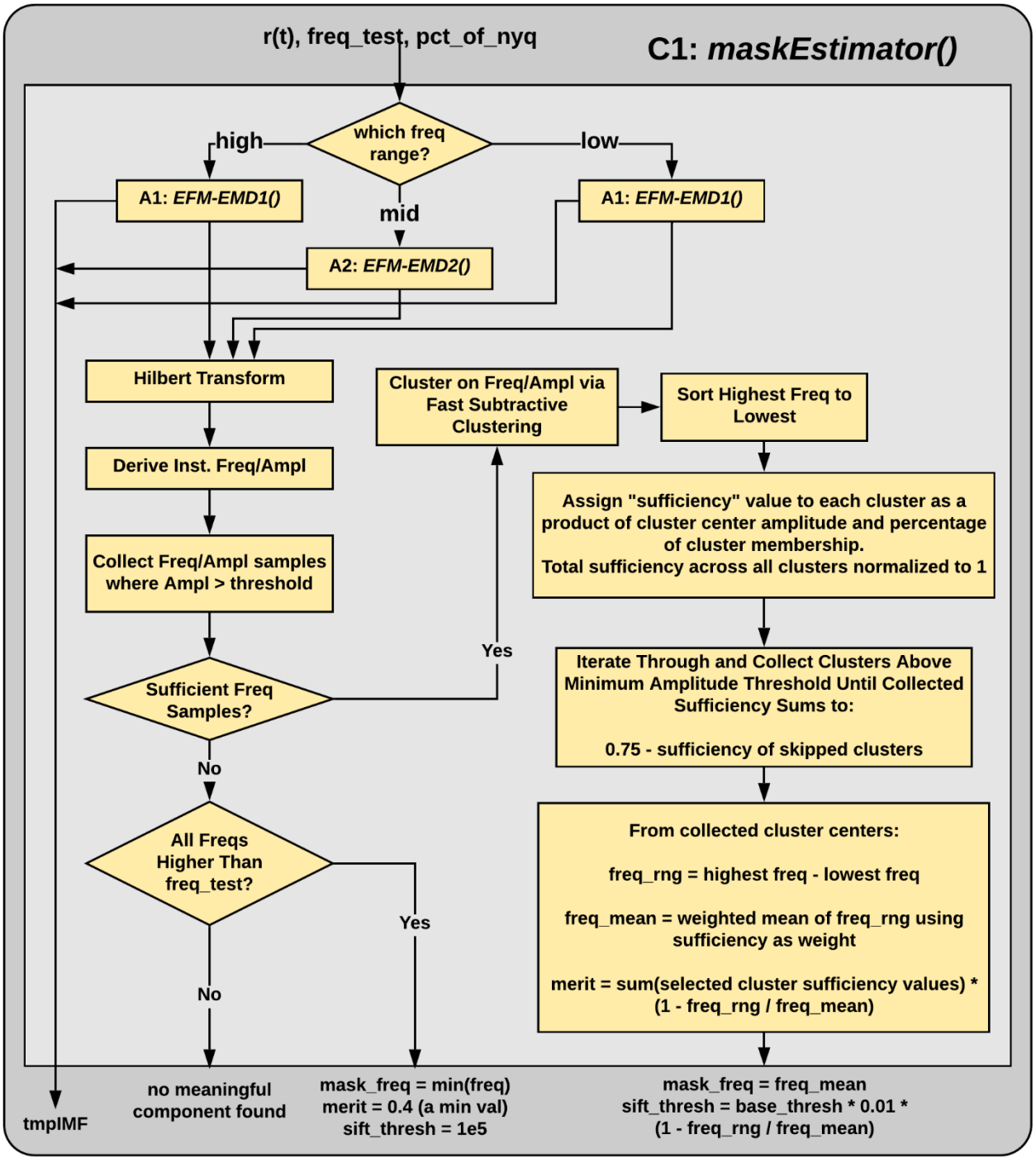


*Figure 2-31 maskEstimator() Function Overview*

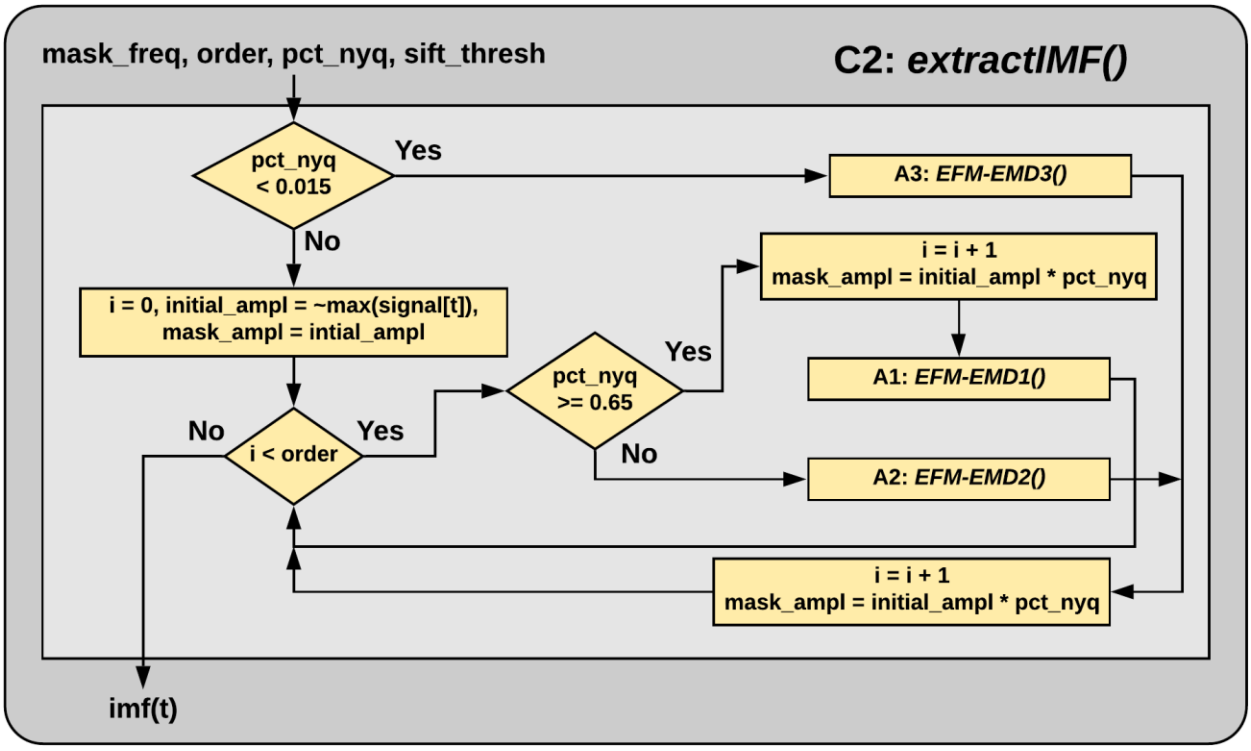


***Figure 2-32 extractIMF() Function Overview***

## 2.10 QUALITY OF DECOMPOSITION (QoD)

N.E. Huang provides a metric called the Index of Orthogonality (IO) in [1] [39] that is given as a suggested measurement of the goodness of decomposition. The idea is that a signal can and should be decomposed into a series of basis functions which, by definition, are orthogonal to each other. However, as shown by J. Huang *et al.* in [40], this measure is critically lacking for discriminating a good decomposition from a bad one. The problem is that if one algorithm's decomposition results in an IMF that is very much like the original signal without separation of components and another algorithm decomposes the signal into almost perfectly formed and separate components, the first might measure better by the IO due to its lack of correlation between IMFs while the latter could score worse, due to some correlation, albeit small, between the IMFs.

J. Huang *et al.* propose two new measures which are similar to the IO. The first calculation, a Type-I Mode-Mixing Error, is a measure of correlation between IMFs and the residuals they would produce—indicative of a component existing within two IMFs. Their second calculation provides a measure of the correlation between the IMFs and the original signal, a Type-II Mode-Mixing Error—indicative of potentially more than one component existing within a single IMF.

However, these metrices are also poor. The divisor in their equations clearly must be a non-zero value at all *t* which is not guaranteed. Second and related, at near zero values of x(t), small perturbations can generate very large error. Further, the second metric is performed per IMF extracted. But each algorithm (EMD, EEMD, CEEMDAN, UPEMD, etc.) provides a different IMF profile as one might generate 5 IMFs and another 7 IMFs. With each IMF potentially containing wildly different components from anything in the corresponding profiles, making comparisons is difficult. Ideally, finding single metrics to evaluate the goodness of decomposition is to be preferred. Finally, correlation does not account very well for matching frequency/amplitude plus phase shift. So, while they may adequately suggest whether a given IMF suffices as a basis function, they do not express anything about the quality of the IMF in terms of meaning. But the first two complaints also plague the IO, which leads the author to wonder whether something else is meant. Perhaps the numerator and denominator should be summed separately, thus only a null signal would generate a zero denominator.

Regardless, while measuring the goodness of a decomposition is a difficult proposition, when the underlying signal is known—as with ideal, artificial signals—it can be assessed in another way beyond the orthogonality tests previously proposed. By taking the Hilbert transform of the IMFs, each of the IMFs can be evaluated for how well their frequency and amplitude match the underlying constituent signals. Those sub-signals are known since they were the initial basis for the development of the very artificial signals being decomposed. This approach essentially represents a limited form of lag

correlation—limited by the length of oscillation periods. Thus, two metrics are being proposed which suffice both intuitionally and experimentally in measuring the quality of the decomposition. These two Quality of Decomposition values, $QoD_1$ and $QoD_2$, are essentially match and mismatch measures respectively.

Let $HHT_i$ represent the Hilbert transform of the *i*-th IMF. Let $SS_j$ represent the Hilbert transform of the *j*-th source sub-signal. Further, let $\alpha HHT_i$ and $\beta HHT_i$ represent the amplitude and frequency of the *i*-th IMF HT respectively, and likewise let $\alpha SS_i$ and $\beta SS_i$ represent the amplitude and frequency of the *j*-th sub-signal HT. When calculating error for frequency and amplitude, the former is a percentage error and the latter an absolute difference (2:17, 2:18). This addresses the issue that small absolute differences at high frequencies are negligible yet are magnified at low frequencies (400 Hz | 402 Hz vs. 1Hz | 3Hz).

Then, the Density Factor, $DF_{ijt}$—the density value an $HHT_i$ has in relationship to a $SS_j$ at a given time step:

$$DF_{ijt} = \frac{0.0001}{0.0001 + dist_{ijt}^4} \qquad 2:15$$

$$dist_{ijt} = \begin{cases} \sqrt{1 + \left(\alpha HHT_{it} - \alpha SS_{jt}\right)^2}, & when\ \beta HHT_{it} + \beta SS_{jt} \approx 0 \\ \sqrt{\left(\alpha HHT_{it} - \alpha SS_{jt}\right)^2}, & when\ \beta HHT_{it}\ xor\ \beta SS_{jt} \approx 0 \\ \sqrt{(1 - \%\beta_e)^2 + {\Delta\alpha_e}^2}, & otherwise \end{cases} \qquad 2:16$$

$$\%\beta_{et} = \min\left(\frac{\beta HHT_{it}}{\beta SS_{jt}}, \frac{\beta SS_{jt}}{\beta HHT_{it}}\right), \Delta\alpha_{et} = \alpha HHT_{it} - \alpha SS_{jt} \qquad 2:17,\ 2:18$$

$$\rho_{ijt} = \frac{1 \times 10^{-18}}{1 \times 10^{-18} + \left({\alpha HHT_{it}}^2 + {\alpha SS_{jt}}^2\right)^5} \qquad 2:19$$

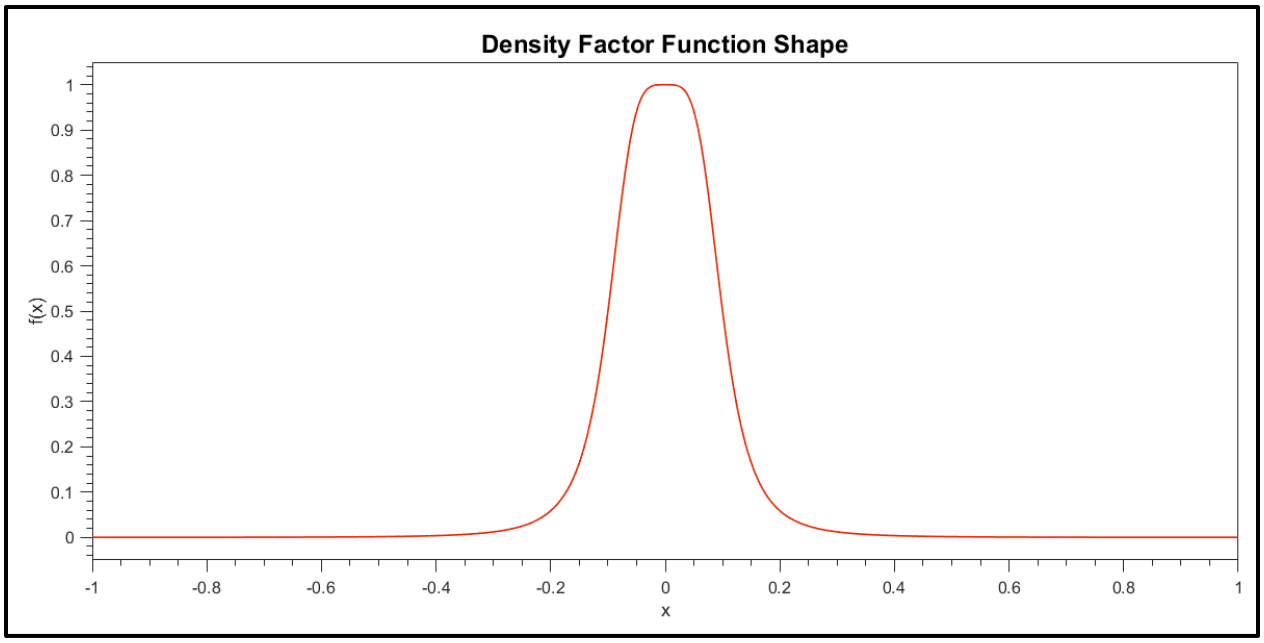


***Figure 2-33 Density Value Provided Per Time Step Between Source Sub-Signal and IMF***

The Density Factor equation in 2:15 is a bell-shaped curve where distances decay very quickly to zero. This piecewise function provides for a minimum of 0 for $\%\beta_{et}$ when both $\beta HHT_{it}$ and $\beta SS_{jt}$ are sufficiently close to zero. If either one is not sufficiently close to zero but the other is, then a maximum of 1 is used to signify maximum distance separation of frequency—this prevents runaway results in the case both frequencies are near zero but precision provides for large percentage differences (such as $5 \times 10^{-10}$ and $5 \times 10^{-8}$—this level of precision is unsupported by the Hilbert Transform, yet would yield a $\%\beta_{et}$ of near 1 instead of 0) . The value 0.0001 constant is a squashing factor that provides for a narrow density band and shows good results, while the fourth power provides for a less-peaked apex. The graph of this function is provided in Fig. [2-33]. While a exponential function would be equally capable of providing this type of shape, the actual shape is somewhat arbitrary—the main goal is to generate a small window over which the distance is considered good and rapidly decay to 0 as the distance increases. The density band given is based on the resolution generally available in an AHHT decomposition.

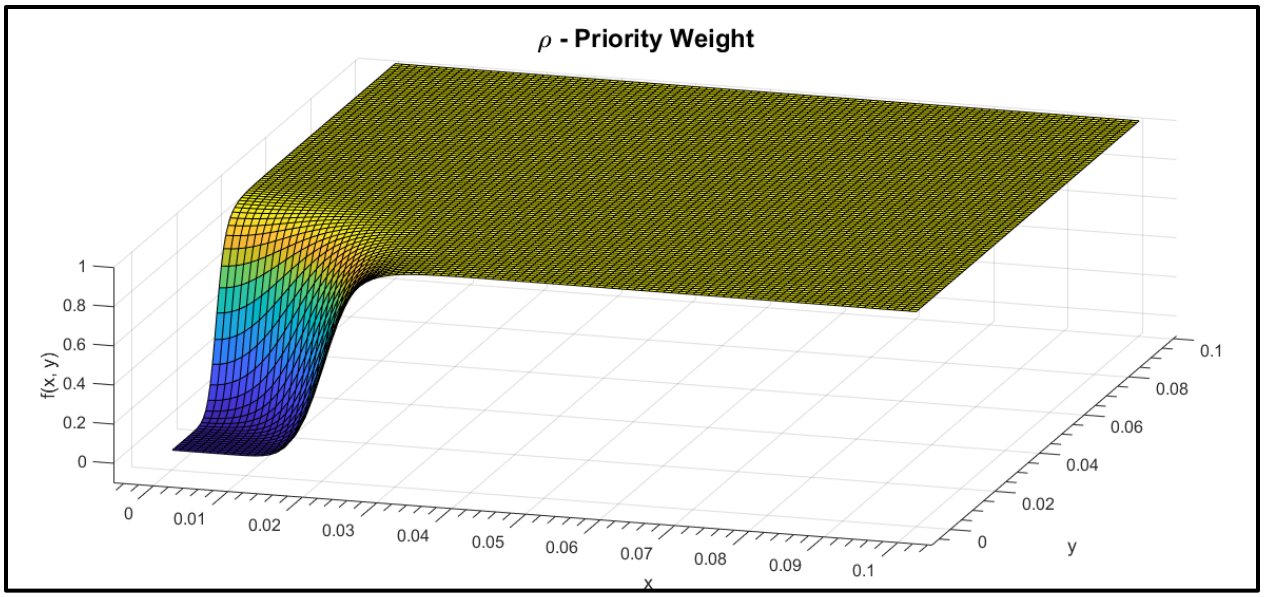


***Figure 2-34 Function Shape for Priority Weight $\rho$***

$\rho_{ijt}$ is a priority factor for the density function that recognizes the higher importance of amplitude over frequency. The value of the Density Factor is of little importance, for instance, when the source sub-signal is non-existent on an interval and the matched IMF is likewise very near zero—even for large variation in frequency. If both amplitudes are within some epsilon of zero at a given timestep, the density factor should be ignored. Otherwise it should be given unity weight. Since $\rho_{ijt}$ is dependent on both $\alpha HHT_{it}$ and $\alpha SS_{jt}$, it is a surface in 3-dimensional space. Again, as with the DF equation, the term $1 \times 10^{-17}$ is a squashing factor that provides for the narrowness of the hole, while the 10$^{th}$ power of the Euclidean norm provides for a flatter bottom. Its graph is provided in Fig. [2-34].

The final Density Function, $DF_{ij}$, is given in the form of a weighted mean:

$$DF_{ij} = \frac{\sum_{t=0}^{T} \rho_{ijt} * DF_{ijt}}{\sum_{t=0}^{T} \rho_{ijt}} \qquad 2:20$$

The DF provides a single value to describe how well one source sub-signal matches against one IMF. A DF is computed between each source-sub-signal/IMF pairing. Finally, $QoD_1$ is the sum of those DF that maximizes the QoD for each $SS_j$ divided by $J$ (i.e. the # of source sub-signals).

Further, it is useful to define a thresholded DF such that any IMF/SS pairing measuring very far apart should be considered identically zero.

$$tDF_{ij} = \begin{cases} DF_{ij}, & for\ DF_{ij} > 0.001 \\ 0, & otherwise \end{cases} \quad 2{:}21$$

The importance of the thresholded DF value of 2:21 is evident in equation 2:24, where blindly matching on highest value can lead to erroneous matches. However, the 0.001 constant is arbitrary and a more rigorous statistical analysis concerning that value would be highly useful to making these QoD values more meaningful.

$$uQoD_1 = (2 * argmax_{j\in\{1,..,J\},i\in\ {}_IP_J} \left( \sum_{j=1}^{J} tDF_{ij} \right) - \sum_{j=1,i=1}^{J,I} DF_{ij} \quad 2{:}22$$

$$QoD_1 = \frac{uQoD_1}{J} \quad 2{:}23$$

2:22 represents the unnormalized $QoD_1$ values, while 2:23 represents the normalized values. Only one DF should add to the QoD for each sub-signal, which is indicated by the first term in 2:22, the remaining are subtracted. This total additive value represents that set of IMFs which generally best matches the set of sub-signals. The possibility for individual ties or a combination of sub-maximum values that combine for a larger summation creates a complication. It is thus an optimization problem in two-dimensional space. Fortunately, it's a discrete problem. Therefore algorithmically, the $QoD_1$ can certainly be generated, but perhaps not most efficiently, by permuting all of the indexes of *I* vs *J* and testing their associated summed thresholded DFs for maximum: ${}_IP_J$ permutations where *I* represents the number and upper bound on indices of IMFs and *J* represents the number and upper bound on indices of sub-signals (1-based indexing).

Thus, the summation in the first term of 2:22 is that unique combination of thresholded DFs related to each *j* such that the whole term is maximized. Unfortunately, using the whole permutation space is only computationally feasible for a small number of source signals and IMFs. In the examples of Chapter 3, one source signal consists of 8 constituent components (see 3.5). When that signal is under noise, a given decomposition may easily generate ~20 IMFs. This leads to greater than 5 billion possible permutations, assuming each DF pairing is greater than 0.001. Finding the global maximum in this case is computationally infeasible. Thus, a recursive algorithm was implemented that chooses the maximum DFs (branching and testing only on ties) for each IMF/sub-signal pair, leading to a good-enough local maximum for this term and does so in a tiny fraction of the time that evaluating all permutations would take. This is particularly relevant, because ties are exceedingly rare and, in most cases, each IMF will be far from all source sub-signals but one—leading to the local maximum thus derived usually being the global maximum, as well. Testing against a permutation-based approach, where possible, this algorithm never produced a value less than the global maximum, though a sample case could be created that proves it does not necessarily do so.

The second term of the $uQoD_1$ subtracts out the remaining IMF DFs that have no match to any source sub-signal, and thus are considered a detraction from the overall decomposition quality (as might happen in Type-II Mode Mixing). Since, mathematically, the DFs of the first term are included in the second term of 2:22, it is necessary to double the first term to compensate. The final $QoD_1$ value is a value normalized against an idealistic decomposition value of 1 (i.e. where the subtracted term of 2:22 vanishes for all IMFs not matching the source sub-signals). It is possible to get $QoD_1$ values that are negative but should not be possible to obtain values greater than 1.

$QoD_2$ is simpler to describe. Excluding all those $HHT_i$'s that were matched to a $SS_j$ (those chosen in the first term of the 2:22) but including those that were matched with a tDF equal to 0, the remaining $HHT_i$'s are addressed again. Let $E_t$ represent the mean operator or *expected value* over time:

$$QoD_2 = \sum_{i=0}^{I-1} E_t[\alpha\mathrm{HHT}_i(\mathrm{t})]\,, where\ i \notin QoD_1(\ {}_IP_J) \qquad 2{:}24$$

This measure addresses the potential existence of transient IMFs, Phantom IMFs, and again Type-II Mode Mixing. Transient and Phantom IMFs may exist far away from any source signal such that it would have very little impact on the $QoD_1$ calculation, even with very large amplitudes. The $QoD_2$ measures them for their impact on the overall quality of decomposition. The mean is used because, in this case, the $QoD_2$ value should *not* be robust to outliers as would be the case in the use, say, of the median.

Clearly, these decomposition metrics are only valid where the source sub-signals can be described by a linear equation, since sub-signals are treated as though they combine linearly and decompose linearly. Fortunately, even though an analytic solution to this problem cannot be found for all of the example artificial signals described in this thesis, extremely close numerical approximations of a linear summation for all of the examined signals can be (as in 3.5 and 3.9).

An important note respecting the Kay window size for the HHT (discussed in 1.1) is that too wide a Kay window will obfuscate variability. For all computed $QoD_1$ values in this thesis, the Kay window was set to 4. This mostly eliminates artificial smoothing and provides for a more accurate comparison. For example, in 3.2. Signal #1, using a Kay window of 20 (as the plot does) for the noiseless signal, the $QoD_1$ value was higher for AHHT than the other decomposition techniques. Reducing the Kay window to 4 showed that the MATLAB EMD algorithm performed better. Thus, a large Kay window may be important for pattern recognition engines or human interpretation but are not great for QoD computations.

# Chapter 3

# EXAMPLES

## 3.1 OVERVIEW

In the following examples, many different signals were evaluated. Before examining the nature of those signals, it should be noted that the artificially generated signals #1 through #5 and the to-be-described ECG signal were generated with noisy variants. These 6 signals were examined with no additive noise as well as with 5 levels of additive Gaussian noise such that the signal-to-noise ratio (SNR) was calculated to be 20 dB SNR, 10 dB SNR, 5 dB SNR, 0 dB SNR, and -5 dB SNR for each. Thus, these 6 signals and their noise variants comprise 36 separate tests. 8 additional signals were examined (signals #6 through #12 plus Signal X). Those 8 signals, as well as an alternate formulation of Signal #8 and a noisy variant of Signal #10, gives a total of 46 test signal decompositions.

Finally, SEMG data was obtained and analyzed in comparison with the frequency shifting found in [50] between the time range of unfatigued and fatigued muscular contractions.

In addition to these evaluations, the AHHT System was tested against varying two-tone signal compositions and analyzed with various frequency masks against chirps as demonstrated in 2.3, 2.4, and 2.5. The two-tone intermittent signals were examined over a large portion of the frequency range. The results show a significant decomposition capability well above 0.8 * Nyquist with decomposition possible where component frequency ratios were as high as 0.9. While the quality of the decomposition at frequencies above 0.8 * Nyquist is not of good quality, the results are still meaningful, and no other current EMD-based technique is able to accomplish this. For example, with a component as high as 0.95 * Nyquist (ex. component #1 at 475 Hz and component #2 at 427.5 Hz where the Nyquist rate is 500 Hz),

both components are separated, but with reduced amplitude and the creation of Phantom IMFs. Reducing the upper component to ~0.9 * Nyquist and maintaining frequency ratio of the two components of 0.9 (450 Hz|405 Hz), the results of the decomposition no longer include Phantom IMFs, but Type-II Mode Mixing is present with the extraction of the upper component. At slightly more than 0.8 * Nyquist where the 0.9 ratio between component frequencies is maintained (400 Hz|360 Hz), even the Type-II Mode Mixing disappears.

As mentioned, there were 12 fundamental simulated signals examined, one real-world signal referenced by existing code and literature, and a real-world data set referenced in literature (the sources and explanation for each of these may be found in their associated Chapter section). It should be noted that in most cases, the frequency vs. time vs. amplitude plots from the Hilbert transform will be used to substitute for multiple IMFs in subplots as they're often far more clarifying, excepting only where IMF plots may demonstrate point(s) of interest. These frequency vs. time vs. amplitude *heat line* plots will be referred to throughout this chapter as Hilbert spectrum plots.

Although the AHHT shows generally superior results in the presence of noise, discussion regarding noise-added signals will primarily be limited to just the 10dB examples. The reader is referred to Appendix A for other noise-added signal decomposition results.

QoD values are only supplied for artificial signals. $QoD_2$ values for decompositions of signals under noisy conditions will show inflation as noise-only IMFs are calculated as non-source-component-matching IMFs—when compared against the ideal signal, they appear exactly like Phantom or transient IMFs. They are included in these cases because they show a relationship to the amount of denoising provided by a given decomposition. For example, if a noisy signal is perfectly decomposed such that $QoD_1$ is nearly equal to 1, then the $QoD_2$ would represent the cost of the noise. But, since Phantom IMFs or

Type-II Mode Mixing may actually exist in the decomposition, the cost of all these complications are conflated.

As previously mentioned, a problem with the UPEMD is that it requires the user to provide a predetermined number of IMFs to be extracted. However, if this parameter is set to a very large number, then the UPEMD will terminate by a different stopping criterion. For the purposes of these tests, that parameter was set to 30 for all UPEMD decompositions, however it should be understood that the UPEMD has an upper limit of $log_2(signal\_length)$ for the number of IMFs it will actually extract. The UPEMD was executed with a *max_size = 64* ensemble. The AHHT System was executed with a size 20 ensemble (for a total of 40 actual frequency masks at each sifting step). In all cases, the EEMD, CEEMDAN, and ICEEMDAN were executed with 2000 noise realizations. Although the MATLAB 2018b ***emd()*** function has various tuning parameters for changing the sifting and decomposition stopping criteria—it was executed with each signal using the default parameters. The AHHT System uses an aggressive decomposition stopping criterion to reduce relatively meaningless IMFs and to increase computational efficiency.

The full results of the EMD/HHT comparisons and QoD tables may be found in Appendix I.

In the Hilbert spectrum plots provided, the residuals of the various decompositions are included, but this is not strictly correct since the residuals are not necessarily IMFs. Regardless, the Hilbert transform has been applied to these residuals and they are included in the Hilbert spectrum plots in the hope that they are able to demonstrate what remains after decomposition. The only exception to this is when the residuals are trendlines, which is common, since they display instability in their instantaneous frequency derivations. In such cases, when the residual is almost perfectly linear, they are excluded. Also, included with the QoD values, there will be found a recording of the number of IMFs generated by each algorithm. These IMF counts include the residual.

According to Rilling and Flandrin [51] and Stevenson *et al.* [52] there is a minimum sampling rate necessary for the EMD to adequately sift components into meaningful IMFs. While Rilling suggests looking at parameters within the signal itself to derive this upper bound. Stevenson *et al.* however provide some statistical guidance where their analysis shows a reduction in amplitude recovery error below 5% as the sampling rate is greater than 10 times the highest component frequency. To this end, although many of the signals presented here in Chapter 3 have a sampling rate below the 0.1 ratio, decompositions of high-sampling-rate versions of the ideal and noisy alternates of Signal #1, Signal #3, and Signal #5, along with Signal #6, Signal 7, and Signal 9 have been provided in Appendix B with their associated QoD calculations.

## 3.2 SIGNAL #1 – DEMONSTRATION OF FUNCTIONALITY

Signal #1 is a signal that demonstrates the EMD technique and provides a simple comparison of the various algorithms used in this research. It was first introduced in this thesis in 1.1 and Fig. [1-2]. Provided by Liu *et al.* in [4]—a comparative study of various decomposition algorithms including the EMD and some of its variants, the Empirical Wavelet Transform (EWT), and others—it is included here for its illustrative value. The signal that is plotted in Fig. [3-1] is defined as:

$$f_{sig_1}(t) = s_1(t) + s_2(t), \qquad (sampled\ at\ 1\ kHz) \tag{3:1:1}$$

$$s_1(t) = sin(65 * 2\pi t), \qquad 0.5 \leq t \leq 0.75 \tag{3:1:2}$$

$$s_2(t) = sin(255 * 2\pi t), \qquad 0 \leq t \leq 1 \tag{3:1:3}$$

A hypothetically ideal decomposition of this signal is shown in Fig. [3-2] with its associated Hilbert spectrum depicted in Fig. [3-3]. The signals in Fig. [3-2] are not the result of a decomposition, but rather represent the source sub-signals that are defined in 3:1:2 and 3:1:3. The heat line plot in Fig. [3-3] represented by the straight red line in the Hilbert spectrum. The color bar indicates the amplitude of

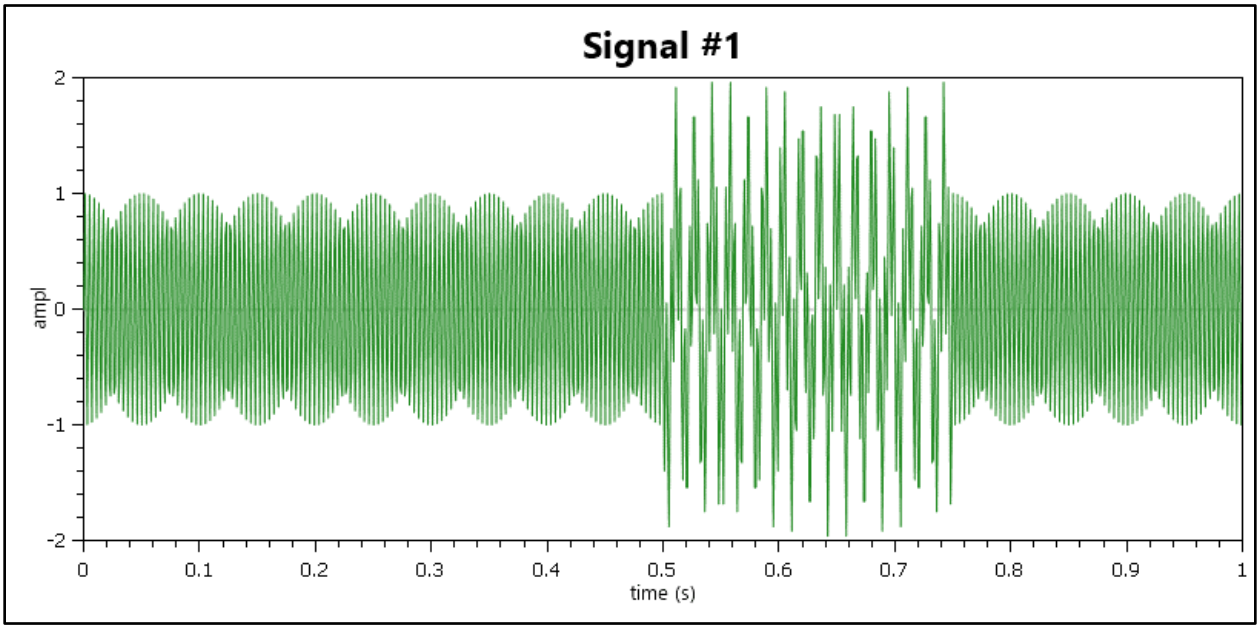


***Figure 3-1 Signal #1 Plot - Time vs. Amplitude***

that component over time. The second IMF is represented by the red line at 65 Hz from between time steps 0.5 and 0.75. At the ends of that interval are artifacts associated with deriving instantaneous frequency from instantaneous phase information. reproduces the information in Fig. [3-2], where the 255 Hz frequency component in the first IMF is  The technique to derive the frequency is detailed in the paper by Kay [13].

This is an easy signal for the EMD to decompose. The highest frequency component at every time step is extracted first, leaving behind only the lowest frequency component. The components are both around or well below 25% of the sampling frequency, and the components are spaced far apart. As such, most EMD algorithms or techniques should adequately decompose these signals.

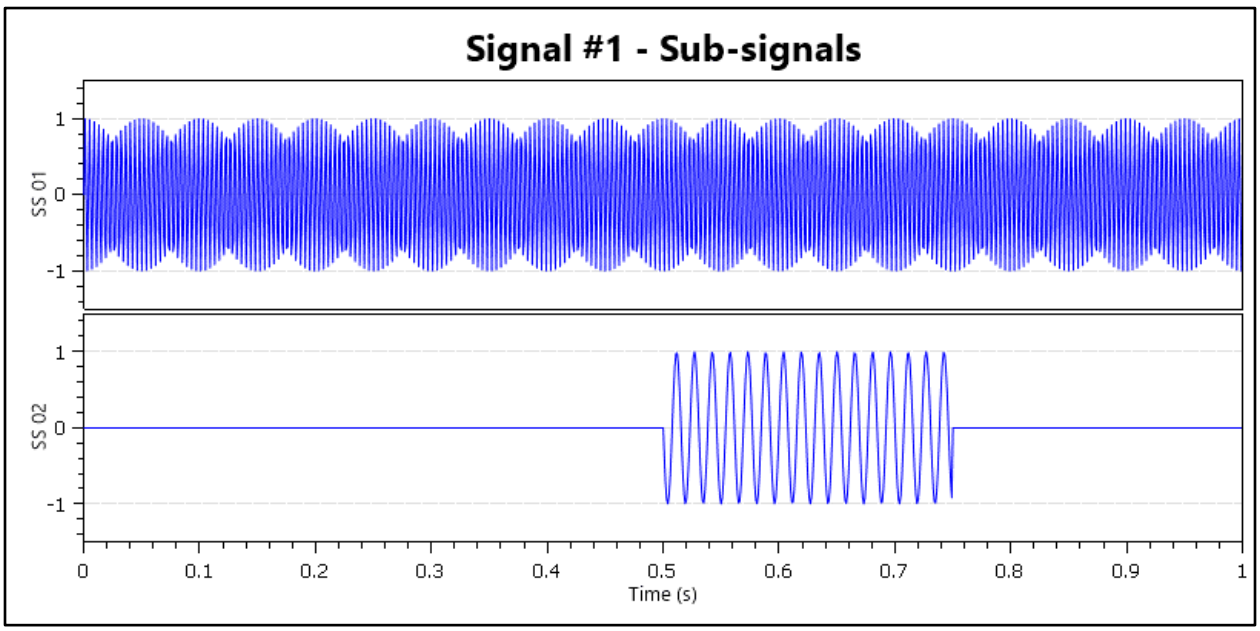


***Figure 3-2  Signal #1 Source Sub-Signal Plots - Time vs. Amplitude***

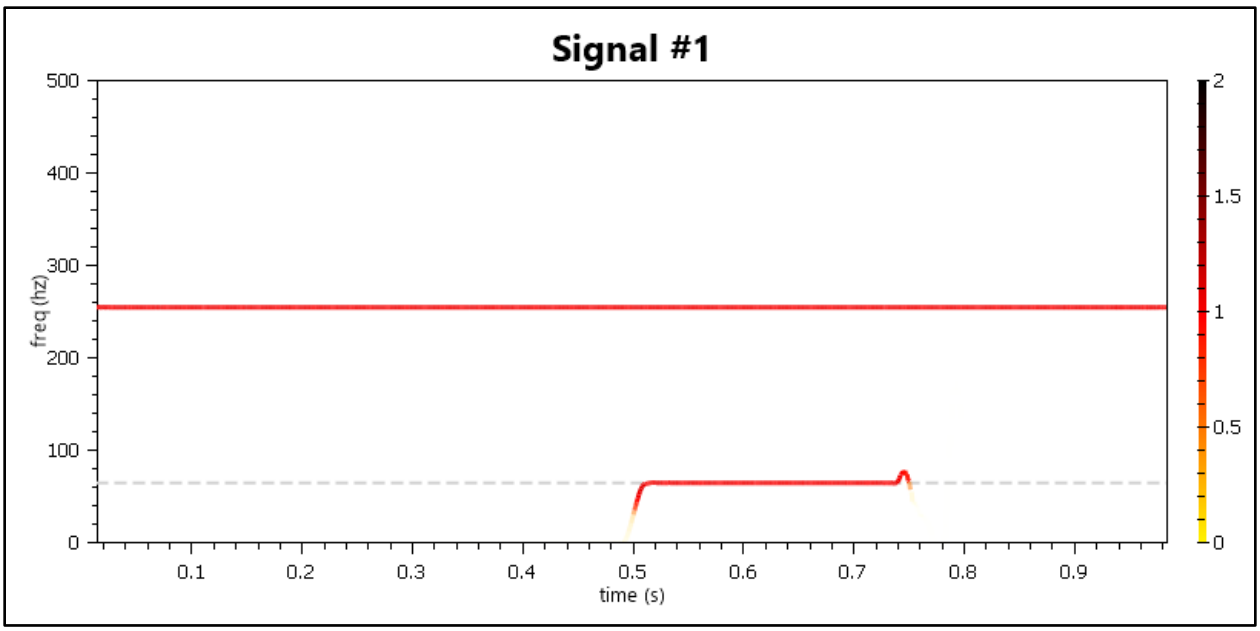


***Figure 3-3 Signal #1 Hilbert Spectrum of Source Sub-Signals***

These figures are, however, the ideal case. As mentioned, the individual signals in Fig. [3-2] were not the result of decomposition rather they are the original signals that were summed together to produce the plot in Fig. [3-1]. It is that summed signal that is compared in the following decompositions.

Fig. [3-4] shows the Hilbert spectrum of six EMD decompositions of Signal #1. Fig. [3-4.A] depicts the result of the MATLAB 2018b implementation. Fig. [3-4.B], Fig. [3-4.C], and Fig. [3-4.D] show the result of the EEMD, CEEMDAN, and ICEEMDAN respectively as supplied by Flandrin [53]. Fig. [3-4.E] displays the output of the UPEMD as provided by [33]. Finally, Fig. [3-4.F] depicts the results of the AHHT System. This signal is simplistic enough that the added complications in all of the algorithms other than the barebones, elegant EMD provided by MATLAB actually detracted from its decomposition. This is not often the case and only relevant for specific artificial signals without noise.

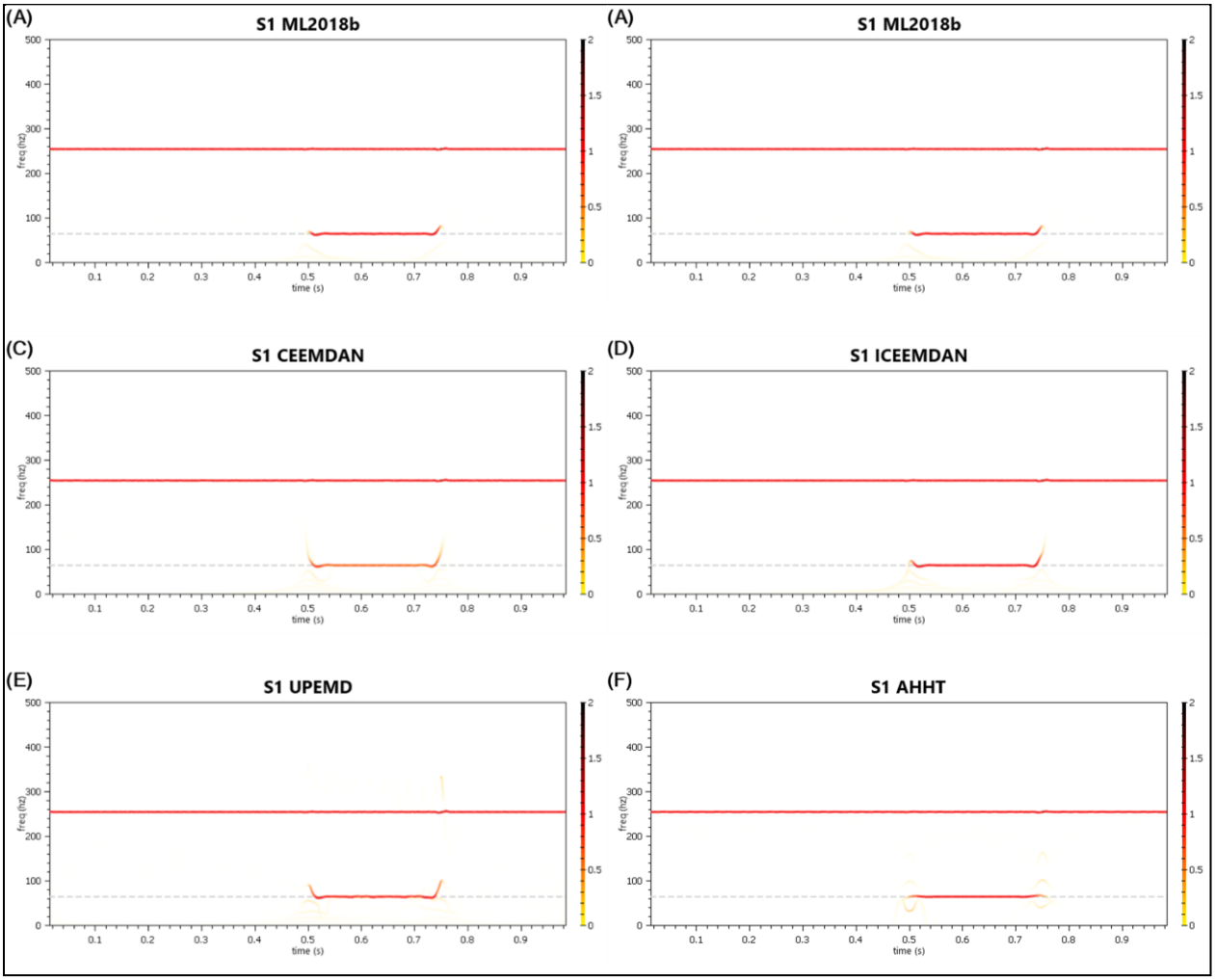


*Figure 3-4 Signal #1 - Decomposition Comparisons in the Hilbert Spectrum*

*Table A-1 IMF Count and QoD Values Associated with Signal #1 EMD Results*

| | MATLAB EMD | EEMD | CEEMDAN | ICEEMDAN | UPEMD | AHHT |
|---|---|---|---|---|---|---|
| **Signal #1 – 2 Component Signals** | | | | | | |
| # of IMFs + Res | 7 | 10 | 10 | 10 | 9 | 5 |
| $QoD_1$ | **0.869198** | 0.838344 | 0.51749 | 0.857836 | 0.715352 | 0.834439 |
| $QoD_2$ | 0.053421 | 0.060249 | 0.133395 | 0.102525 | 0.10824 | **0.042053** |

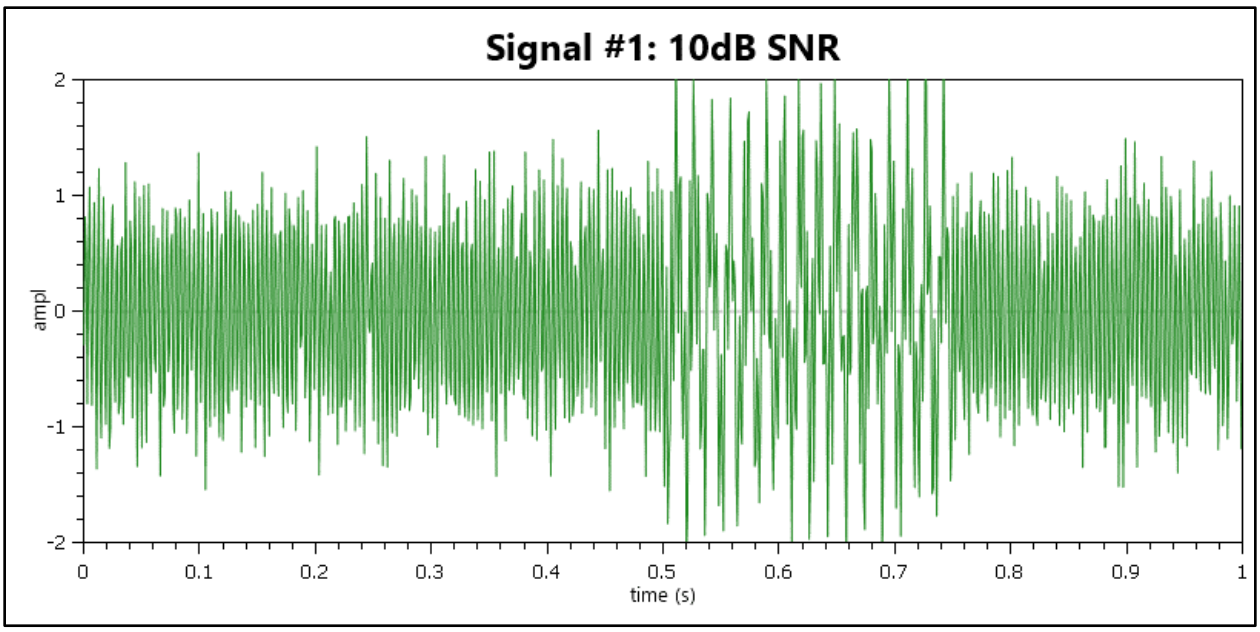


***Figure 3-5 Signal #1 with Additive Gaussian Noise to 10dB SNR Plot - Time vs. Amplitude***

For example, after sufficient white noise was added to this signal such that 10 dB SNR was achieved, as shown in Fig. [3-5], it was again decomposed, and Hilbert spectrum comparisons are given in Fig. [3-6].

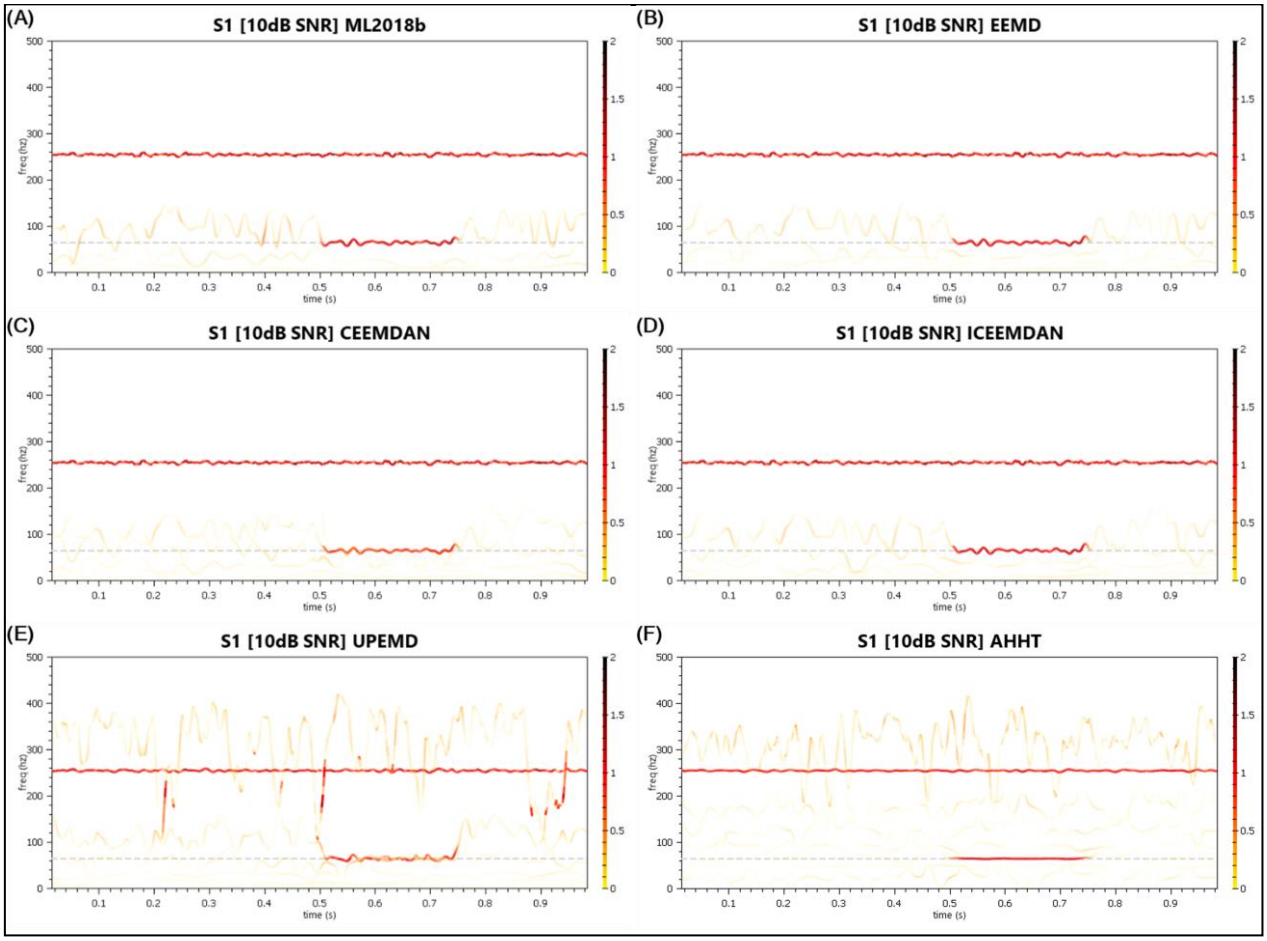


***Figure 3-6 Signal #1 (10dB SNR) - Decomposition Comparisons in the Hilbert Spectrum***

***Table A-2 IMF Count and QoD Values Associated with Signal #1 (10dB SNR) EMD Results***

| | MATLAB EMD | EEMD | CEEMDAN | ICEEMDAN | UPEMD | AHHT |
|---|---|---|---|---|---|---|
| # of IMFs + Res | 7 | 10 | 10 | 9 | 9 | 8 |
| $QoD_1$ | 0.171113 | 0.175995 | 0.168175 | 0.183722 | 0.286008 | **0.454064** |
| $QoD_2$* | 0.230235 | 0.246248 | 0.349367 | 0.314387 | 0.555411 | 0.603517 |

** - $QoD_2$ values for all noise-added signals will be inflated and unreliable due to the mismatch associated with noise-only IMFs.*

The UPEMD and AHHT both did a better job of stripping out the high frequency noise, whereas the other decompositions conflated that noise with the 255 Hz component which contributed more energy to that component. It should be noted that the Kay instantaneous frequency derivation technique effectively smooths out anomalies in the frequency derivation. The Hilbert spectrum plots in Fig. [3-6] were generated with a Kay window of 20 samples. If this window were reduced to 4, fluctuations in the frequency spectrum would be sharper, as shown in Fig. [3-7]. The QoD values would remain unchanged, however, since as noted in Section 2.10 they are already calculated assuming a Kay window of 4.

In Fig. [3-7] it seems that the UPEMD does a similar job of stripping out the high frequency noise as does the AHHT. However, it does a significantly poorer job stripping out the mid-range noise leading to a

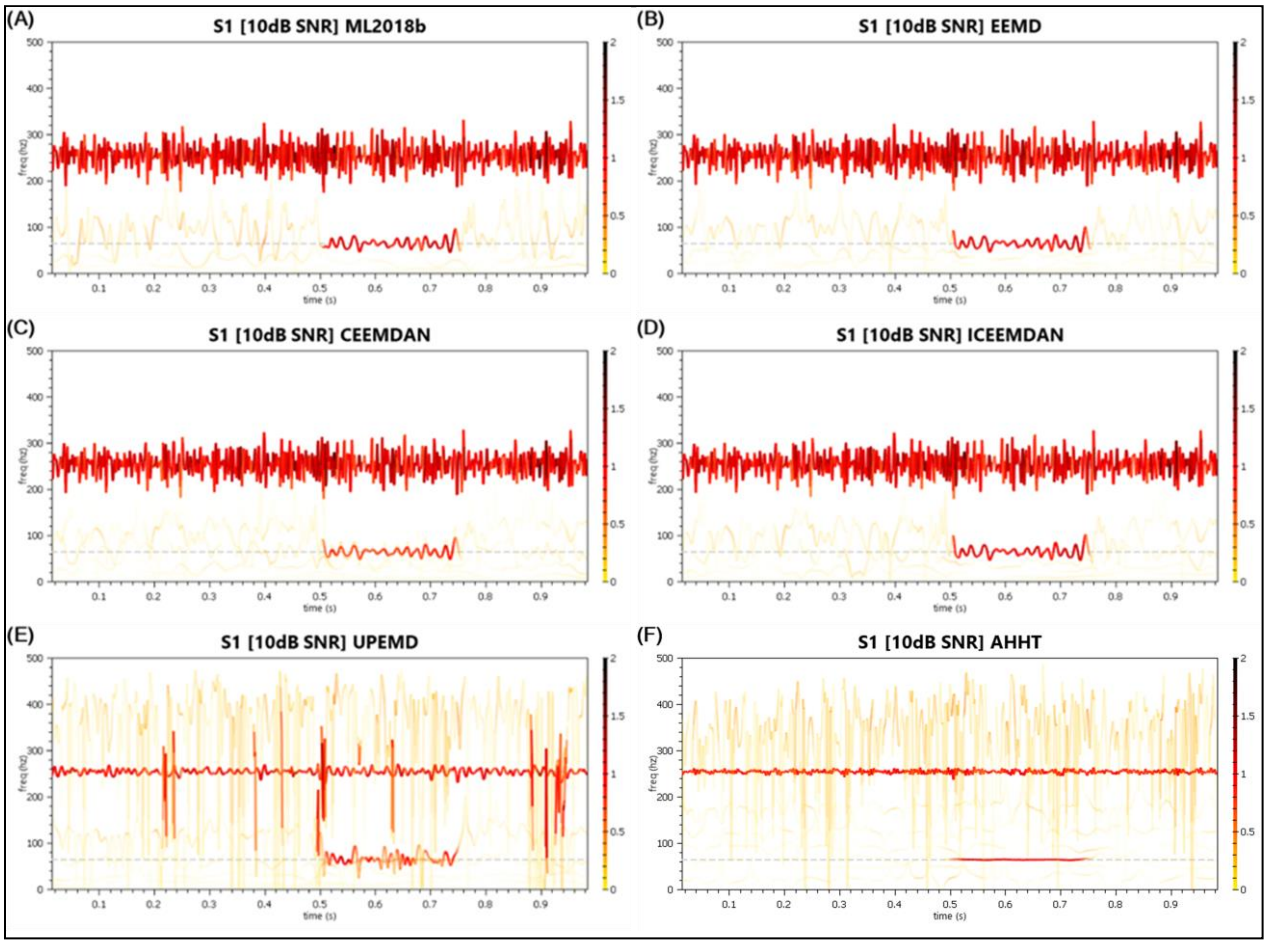


***Figure 3-7 Signal #1 (10dB SNR) - Hilbert Spectrum Comparisons with Kay Frequency Window Set to 4***

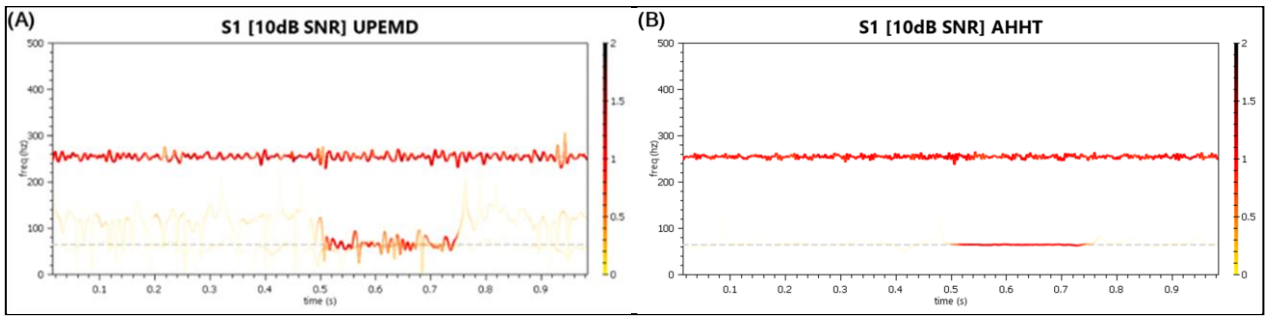


***Figure 3-8 Signal #1 (10dB SNR) - UPEMD & AHHT Hilbert Spectrum Comparisons with Noise-Only IMFs Removed***

much poorer extraction of the lower frequency component: the $DF_{ij}$ [see 2.10] for the best matching UPEMD-derived IMF to the 65 Hz component was 0.513, whereas for AHHT it was 0.710. Additionally, the low frequency component is being extracted in two IMFs (minor Type-II Mode Mixing). Looking at just the UPEMD and AHHT and removing all of the IMFs that contain only noise, the two can be more closely evaluated, as in Fig. [3-7].

Of course, Signal #1 is the easiest signal being evaluated and all of the algorithms did an acceptable job extracting the important components, even in light to moderate noise (though not in the presence of heavy noise—only the UPEMD and AHHT manage well under 0 dB and -5 dB SNR—see Appendix A).

## 3.3 SIGNAL #2 – DECOMPOSING SUM OF DISTINCT-AMPLITUDE, LOW-FREQUENCY COMPONENTS

Signal #2 is provided by J. Huang *et al.* in [27], which cites a source that could not be resolved. Nevertheless, the signal is worthy of study for the difficulty in decomposing its closely spaced components with few extrema. The ideal case—no noise—is simulated as being sampled at 2 kHz for arbitrary testing reasons, the noisy versions were all simulated as being sampled at 1 kHz.

$$f_{sig_2}(t) = s_1(t) + s_2(t) + s_3(t), \qquad (sampled\ at\ 2\ kHz) \tag{3:2:1}$$

$$s_1(t) = 0.6 * sin(4 * 2\pi t), \qquad 0 \leq t \leq 1.35 \tag{3:2:2}$$

$$s_2(t) = cos(2 * 2\pi t), \qquad 0 \leq t \leq 1.35 \tag{3:2:3}$$

$$s_3(t) = 0.5 * sin(0.5 * 2\pi t), \qquad 0 \leq t \leq 1.35 \tag{3:2:4}$$

The plot of $f_{sig_2}(t)$ is given in Fig. [3-9]. The Hilbert spectrum of the various decompositions is then provided in Fig. [3-10].

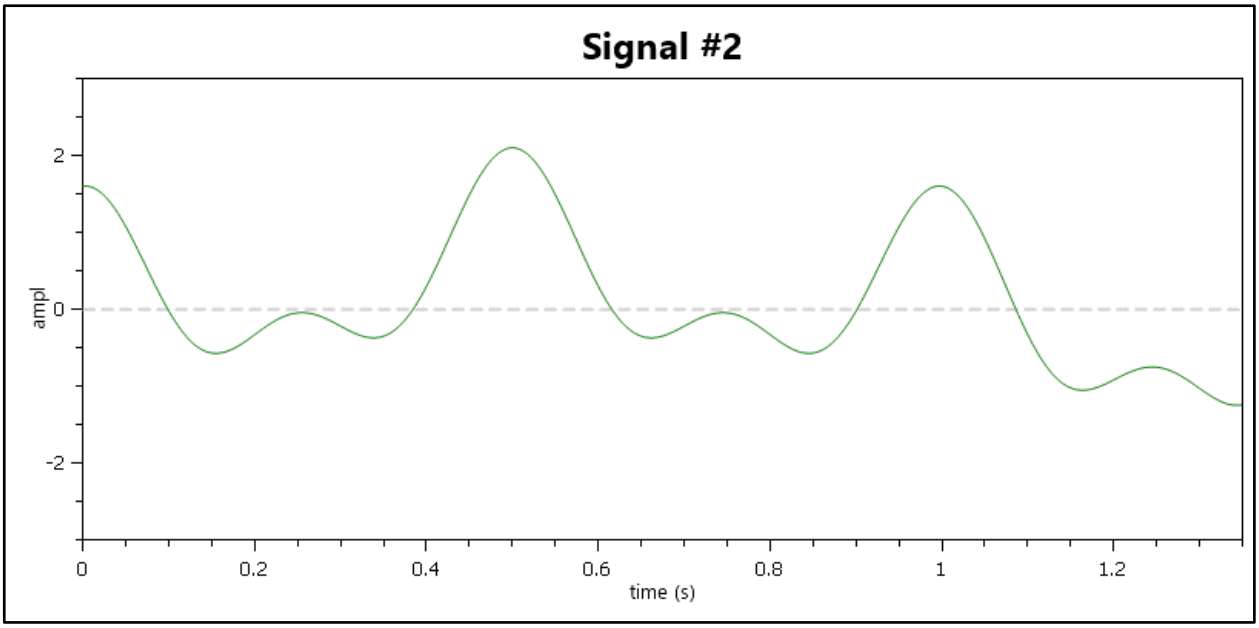


***Figure 3-9 Signal #2 Plot - Time vs. Amplitude***

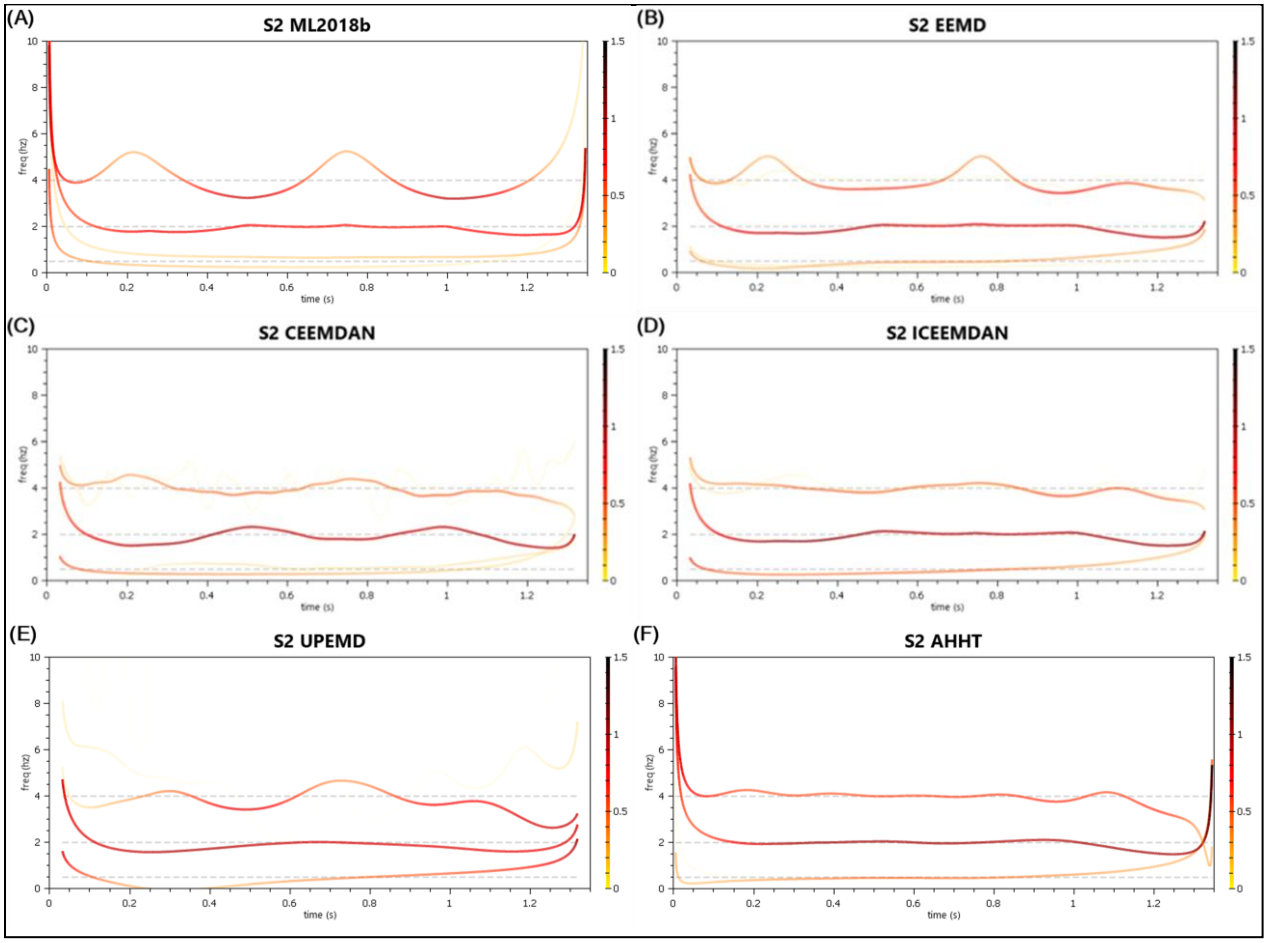


*Figure 3-10 Signal #2 - Decomposition Comparison in the Hilbert Spectrum*

*Table A-1 IMF Count and QoD Values Associated with Signal #2 EMD Results*

| | MATLAB EMD | EEMD | CEEMDAN | ICEEMDAN | UPEMD | AHHT |
|---|---|---|---|---|---|---|
| **Signal #2 – 3 Component Signals** | | | | | | |
| # of IMFs + Res | 4 | 11 | 12 | 9 | 11 | 4 |
| $QoD_1$ | 0.076892 | 0.267081 | 0.168238 | 0.438313 | 0.194584 | **0.747296** |
| $QoD_2$ | 0.25541 | 0.177857 | 0.250678 | 0.083441 | 0.057665 | **0.0218** |

Most of the IMFs for these decompositions are above the frequency scale limit of the plot (10 Hz) or are very small amplitude and are therefore reduced in visibility. Note, only the AHHT actually gets something like the ideal decomposition, the others have multiple transient IMFs.

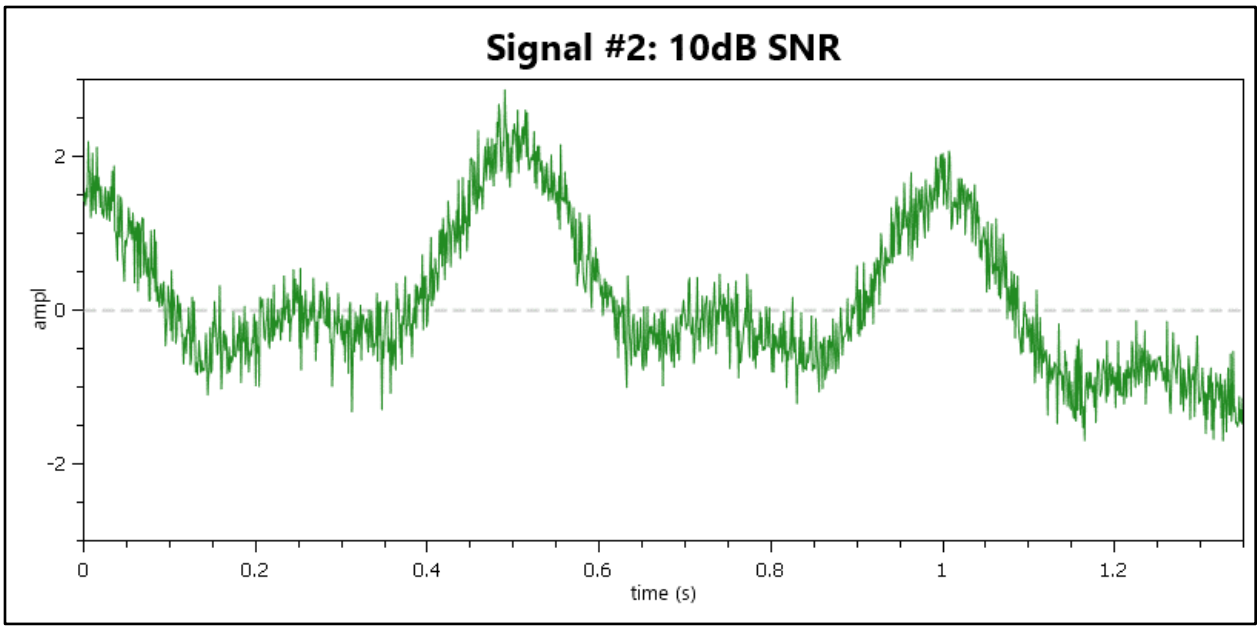


*Figure 3-11 Signal #2 (10dB SNR) Plot - Time vs. Amplitude*

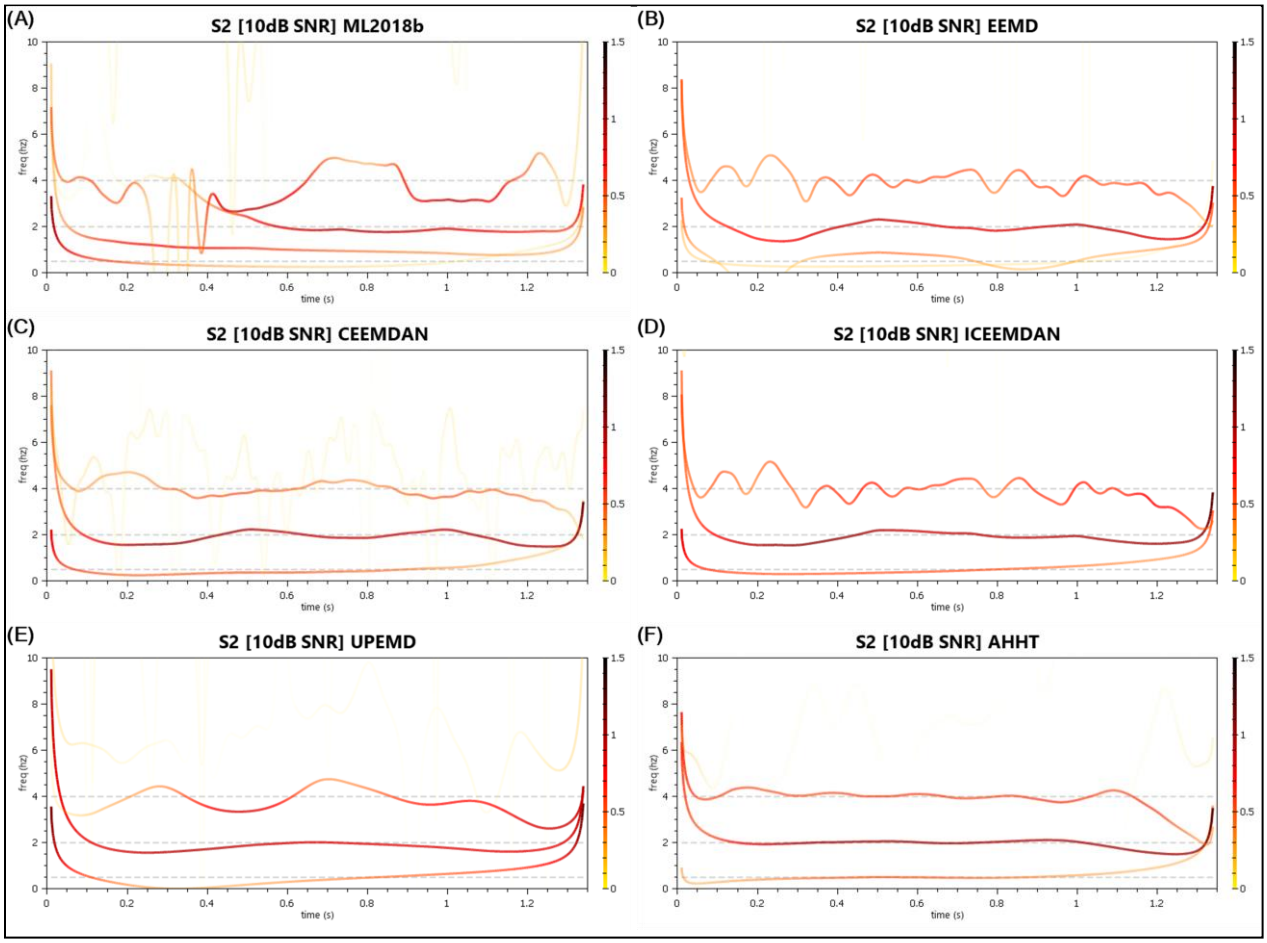


*Figure 3-12 Signal #2 (10dB SNR) - Decomposition Comparison in the Hilbert Spectrum*

The 10 dB SNR version of this signal shows that noise, typically being higher frequency, is stripped out prior to the extraction of these three low-frequency components. Its plot is produced in Fig. [3-11] and the Hilbert spectrum comparison plots are in Fig. [3-12].

***Table A-2 IMF Count and QoD Values Associated with Signal #2 (10dB SNR) EMD Results***

| | MATLAB EMD | EEMD | CEEMDAN | ICEEMDAN | UPEMD | AHHT |
|---|---|---|---|---|---|---|
| **Signal #2 (10dB SNR) – 3 Component Signals** | | | | | | |
| # of IMFs + Res | 8 | 10 | 10 | 8 | 10 | 14 |
| $QoD_1$ | 0.100569 | 0.269905 | 0.300698 | 0.371098 | 0.182505 | **0.691487** |
| $QoD_2$* | 0.839138 | 0.639777 | 0.57363 | 0.491614 | 0.615343 | 0.781927 |

** - $QoD_2$ values for all noise-added signals will be inflated and unreliable due to the mismatch associated with noise-only IMFs.*

The other AHHT decompositions of the noise-added versions of Signal #2 are given in Fig. [3-13]. As expected, the noise is stripped out before the components of interest are encountered in the decomposition steps.

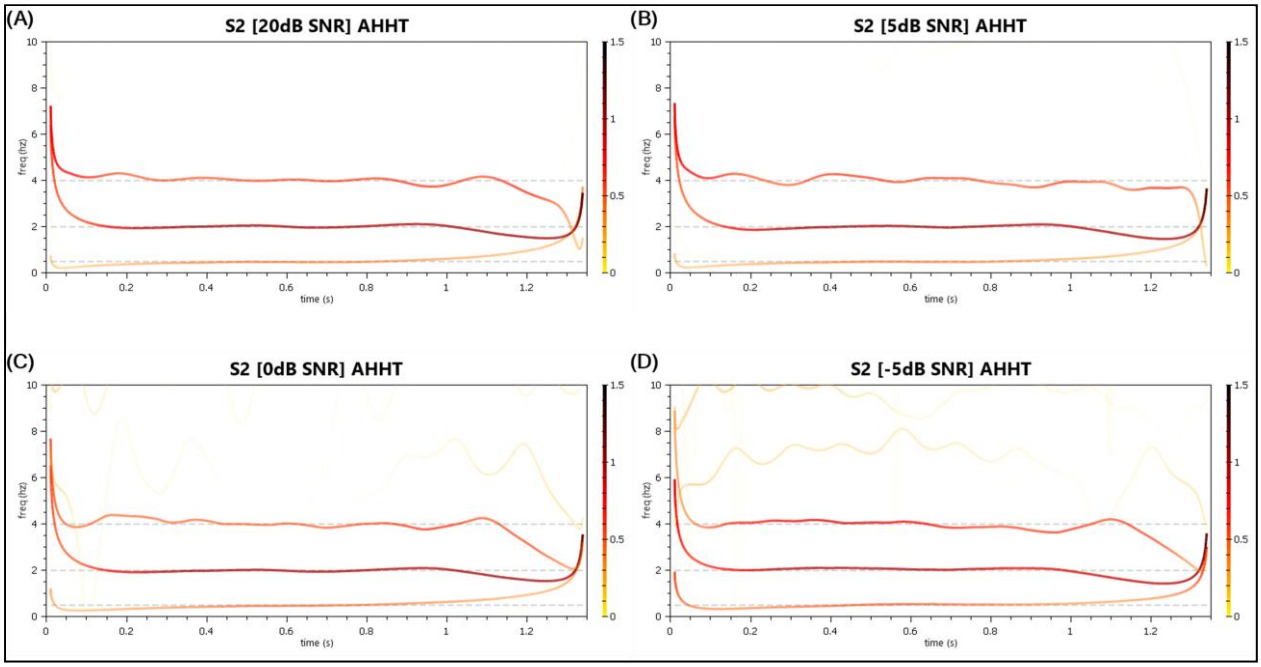


***Figure 3-13 Signal #2 - Remaining AHHT Decompositions in the Hilbert Spectrum for 20dB, 5dB, 0dB, and -5dB SNR Respectively***

## 3.4 SIGNAL #3 – DECOMPOSING OVERLAPPING, INTERMITTENT COMPONENTS

Signal #3 is given by Liu *et al.* in [24] as a simple demonstration of mode mixing resulting from the onset of intermittency in the constituent signals. The EEMD method was proposed to reduce just this sort of mixing, and perhaps, with enough noise realizations, it would. In fact, Liu *et al.* demonstrate just such a result with the EEMD, though they did not give an indication of how many noise realizations were required to be successful. However, for this signal alone and with no additive noise on an Intel Core i7-7820HK CPU with 64 GB of memory, and 2000 noise realizations, EEMD took ~50s to complete, CEEMDAN took ~145s, and ICEEMDAN took ~145s. Yet, that was insufficient to eliminate mode mixing. AHHT, by comparison, took ~0.85s and the UPEMD was blazingly fast at 0.021s.

$$f_{sig_3}(t) = s_1(t) + s_2(t) + s_3(t), \qquad (sampled\ at\ 1\ kHz) \tag{3:3:1}$$

$$s_1(t) = sin(50 * 2\pi t), \qquad 0.1 \leq t \leq 0.6 \tag{3:3:2}$$

$$s_2(t) = sin(100 * 2\pi t), \qquad 0.2 \leq t \leq 0.7 \tag{3:3:3}$$

$$s_3(t) = sin(200 * 2\pi t), \qquad 0.3 \leq t \leq 0.8 \tag{3:3:4}$$

The plot of $f_{sig_3}(t)$ is given in Fig. [3-14] and the subsequent Hilbert spectrum decompositions are depicted in Fig. [3-15].

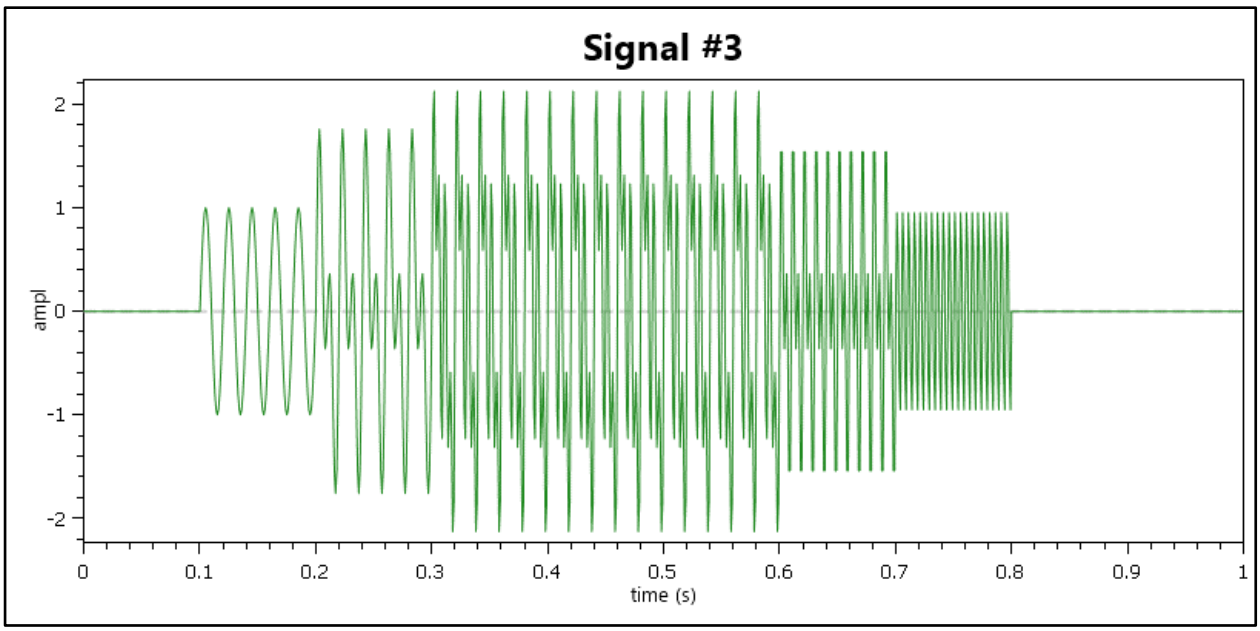


*Figure 3-14 Signal #3 Plot - Time vs. Amplitude*

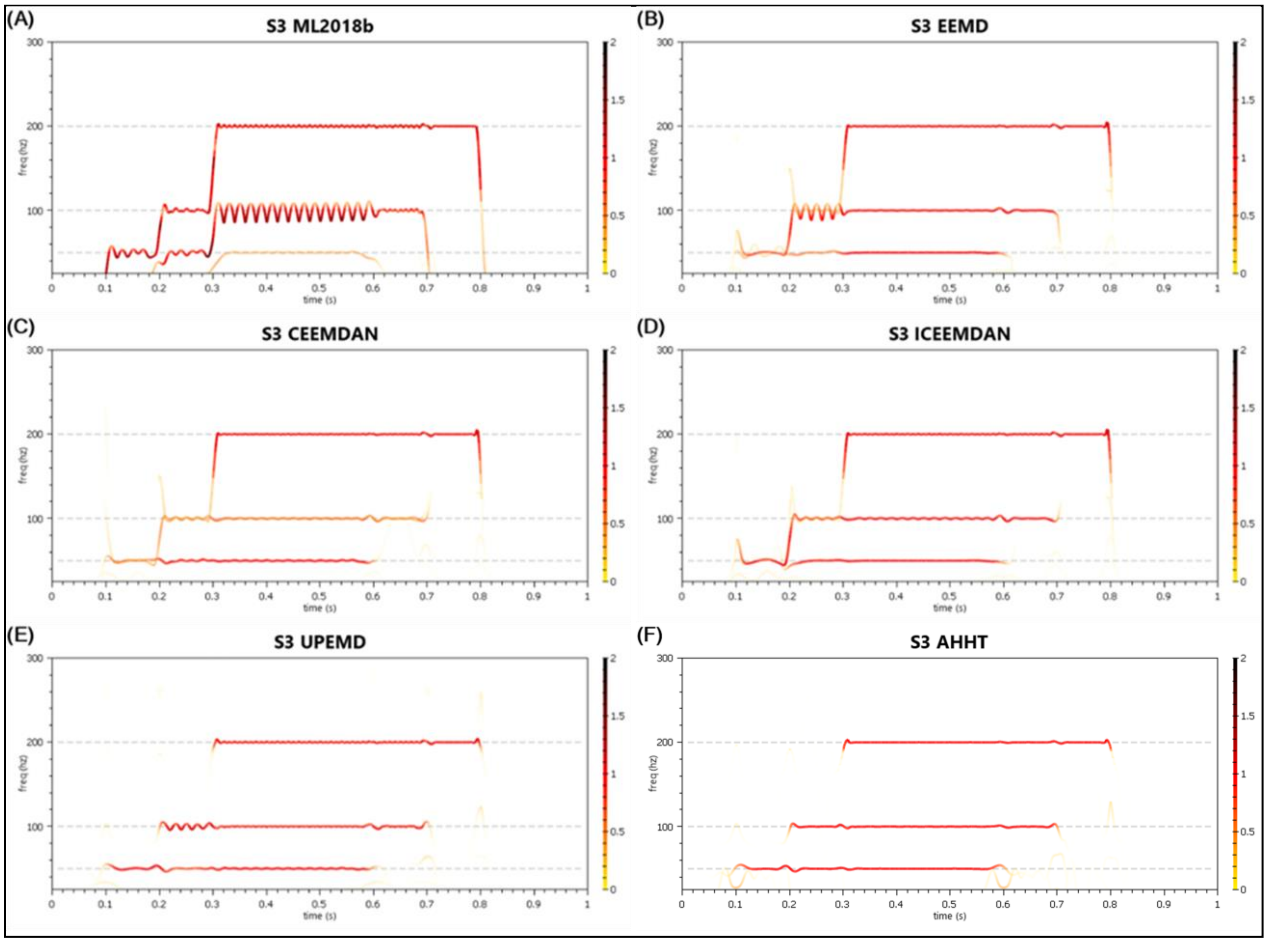


*Figure 3-15 Signal #3 - Decomposition Comparison in the Hilbert Spectrum*

***Table A-1 IMF Count and QoD Values Associated with Signal #3 EMD Results***

| | MATLAB EMD | EEMD | CEEMDAN | ICEEMDAN | UPEMD | AHHT |
|---|---|---|---|---|---|---|
| **Signal #3 – 3 Component Signals** | | | | | | |
| # of IMFs + Res | 9 | 10 | 11 | 10 | 9 | 4 |
| $QoD_1$ | 0.020886 | 0.557792 | 0.37078 | 0.544032 | 0.529846 | **0.753141** |
| $QoD_2$ | 0.613839 | 0.10765 | 0.253335 | 0.174159 | 0.12163 | **0.051944** |

The UPEMD and the AHHT are the only techniques that eliminate Type-I Mode Mixing for this signal. The UPEMD is a slightly inferior decomposition in that the second component on the interval between timestep 0.2 and 0.3 has frequency fluctuations not found in the original signal nor in the decomposition provided by AHHT, there are also slight frequency fluctuations found throughout all of the components which do not exist in the AHHT results.

The same signal with AGWN such that the SNR is 10 dB is depicted in Fig. [3-16] and the subsequent decompositions in Fig. [3-17].

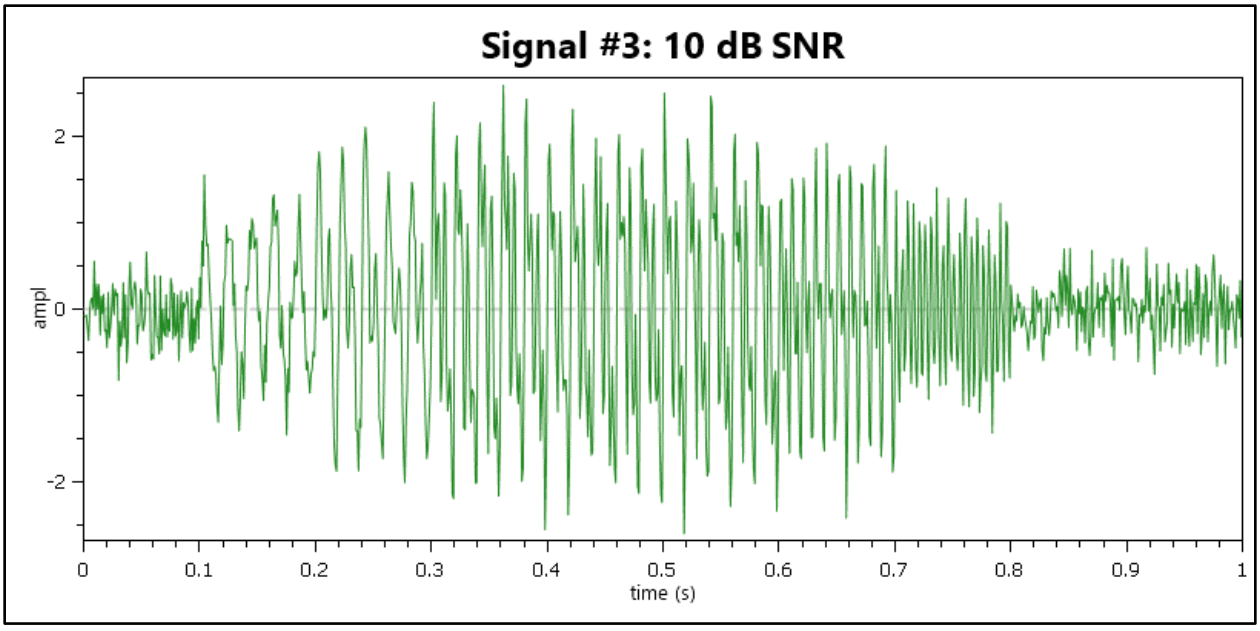


***Figure 3-16 Signal #3 (10dB SNR) Plot - Time vs. Amplitude***

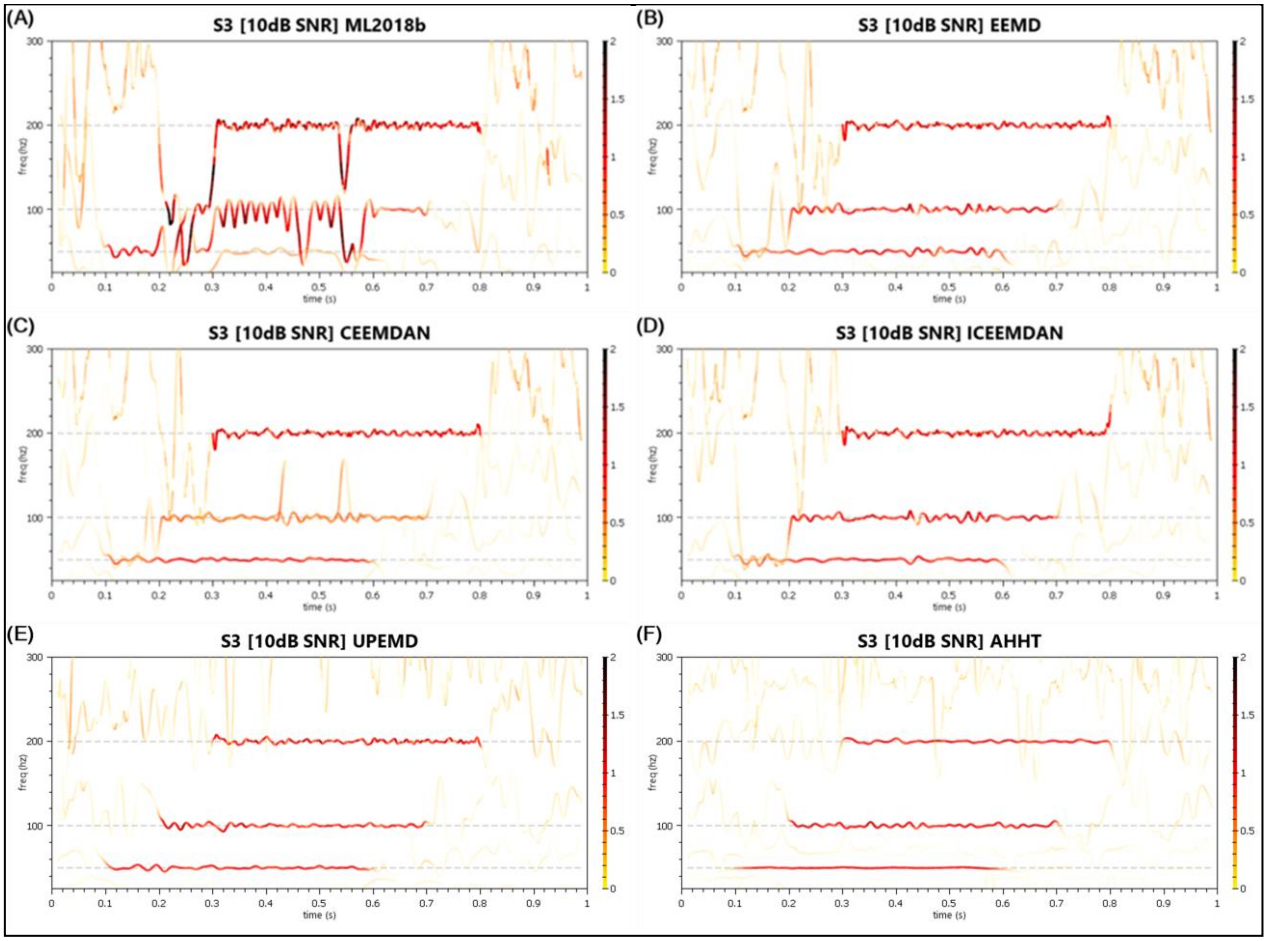


***Figure 3-17 Signal #3 (10dB SNR) - Decomposition Comparison in the Hilbert Spectrum***

***Table A-2 IMF Count and QoD Values Associated with Signal #3 (10dB SNR) EMD Results***

| | MATLAB EMD | EEMD | CEEMDAN | ICEEMDAN | UPEMD | AHHT |
|---|---|---|---|---|---|---|
| **Signal #3 (10dB SNR) – 3 Component Signals** | | | | | | |
| # of IMFs + Res | 8 | 11 | 10 | 8 | 9 | 8 |
| $QoD_1$ | -0.00556 | 0.106585 | 0.097331 | 0.151765 | 0.18288 | **0.385018** |
| $QoD_2$* | 0.401339 | 0.24 | 0.807162 | 0.30251 | 0.433253 | 0.527114 |

** - $QoD_2$ values for all noise-added signals will be inflated and unreliable due to the mismatch associated with noise-only IMFs.*

Noise added to the signal, as it tends to be higher frequency, should aid in the separation of the components. And that is, indeed, what occurs with the noise-assisted decomposition algorithms. The UPEMD and the AHHT still show better decompositions since they have reduced Type II Mode-Mixing. In both cases, the results for these latter two approaches are similar, which is unsurprising since they share similar decomposition mechanisms. AHHT has impressively better denoising characteristics.

## 3.5 SIGNAL #4 – DECOMPOSING AN AMPLITUDE MODULATED SIGNAL

J. Huang *et al.* gives signal #4 in [27] as a comparison for the extremum centers method versus the classical dual cubic spline method. This signal was chosen for its likelihood to generate *misshooting* and difficulty in properly decomposing by EMD.

$$f_{sig_4}(t) = s_1(t) * \big(s_2(t) + s_3(t) + s_4(t)\big), \qquad (sampled\ at\ 1\ kHz) \tag{3:4:1}$$

$$s_1(t) = 1 + 0.2 * sin(7.5 * 2\pi t), \qquad 0 \le t \le 0.5 \tag{3:4:2}$$

$$s_2(t) = sin(15 * 2\pi t), \qquad 0 \le t \le 0.5 \tag{3:4:3}$$

$$s_3(t) = 1.5 * sin(30 * 2\pi t), \qquad 0 \le t \le 0.5 \tag{3:4:4}$$

$$s_4(t) = sin(50 * 2\pi t), \qquad 0 \le t \le 0.5 \tag{3:4:5}$$

This signal is plotted in Fig. [3-18] and the decomposition comparison is depicted in Fig. [3-19]

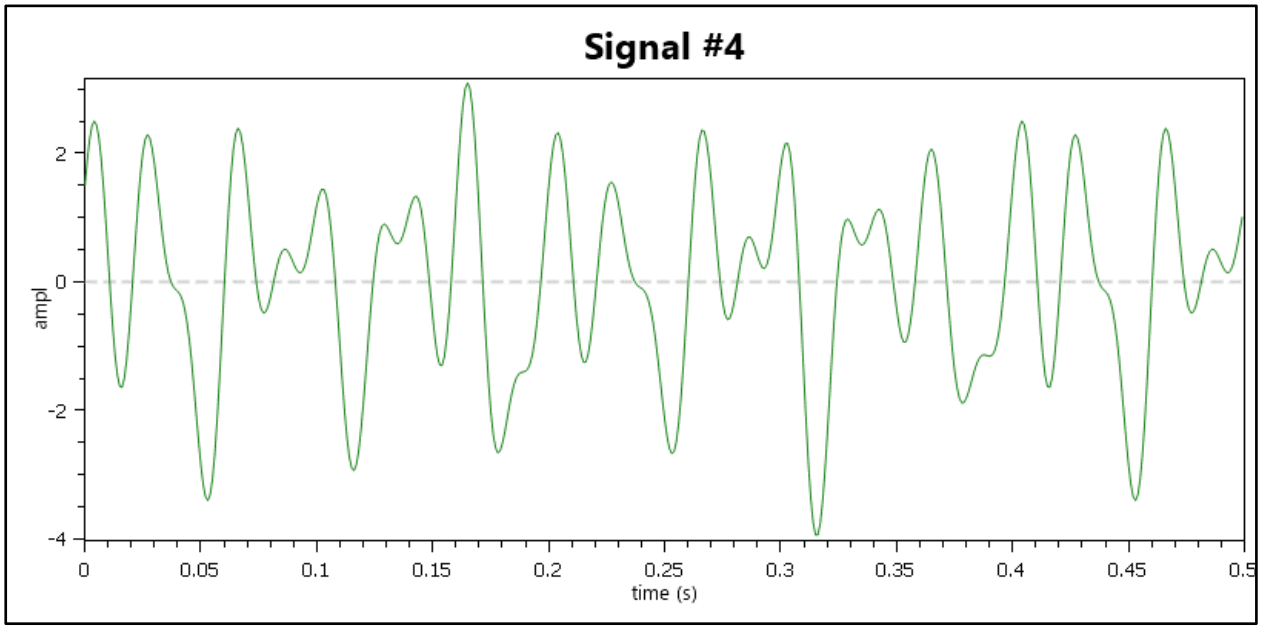


***Figure 3-18 Signal #4 Plot - Time vs. Amplitude***

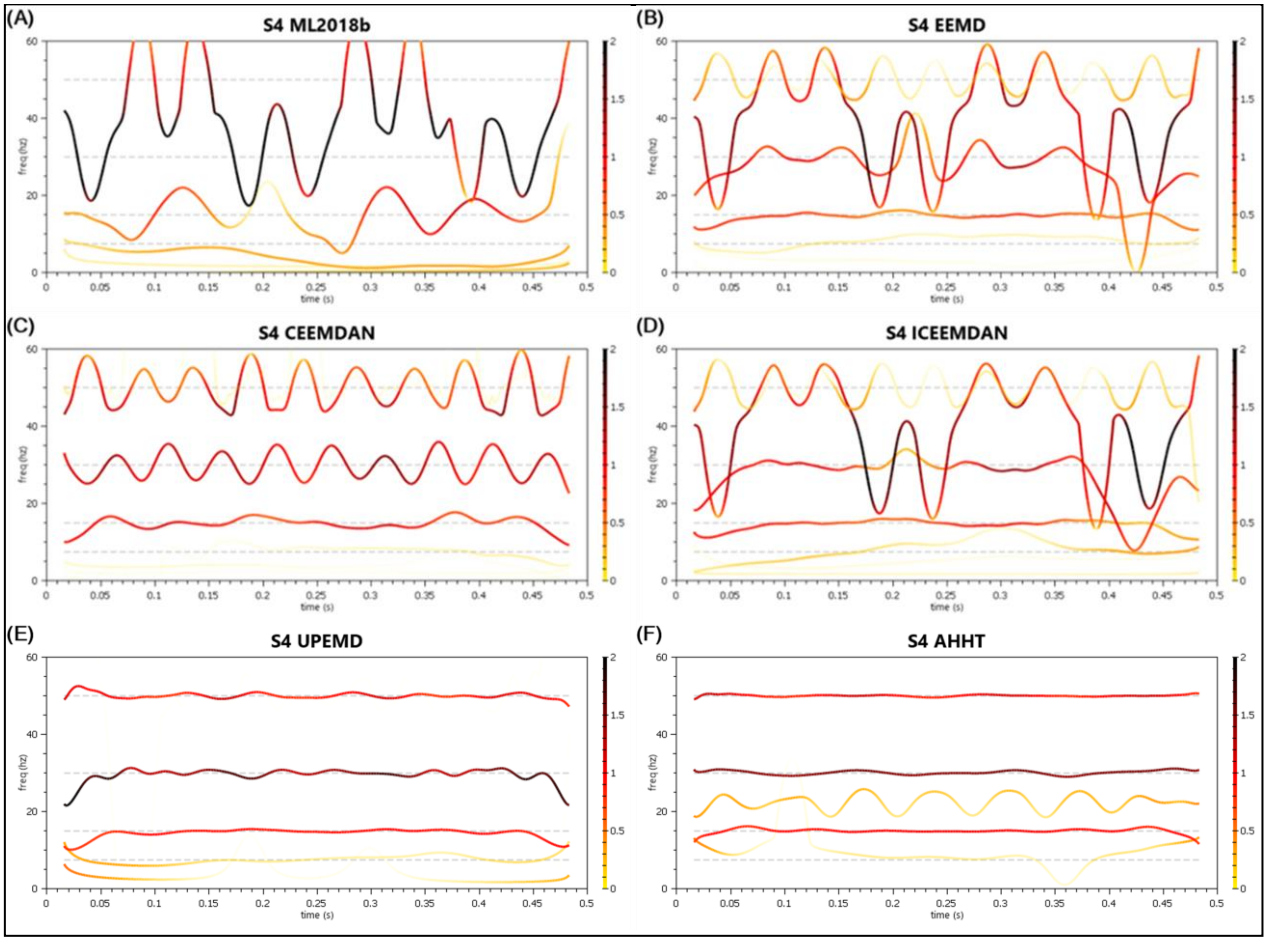


***Figure 3-19 Signal #4 - Decomposition Comparison in the Hilbert Spectrum***

***Table A-1 IMF Count and QoD Values Associated with Signal #4 EMD Results***

| | MATLAB EMD | EEMD | CEEMDAN | ICEEMDAN | UPEMD | AHHT |
|---|---|---|---|---|---|---|
| **Signal #4 – 8 Component Signals** | | | | | | |
| # of IMFs + Res | 5 | 10 | 10 | 8 | 8 | 5 |
| $QoD_1$ | 0.005595 | 0.024312 | 0.060725 | 0.030793 | 0.198268 | **0.295797** |
| $QoD_2$* | 0.493316 | 0.04983 | 0.090839 | 0.113139 | 0.155964 | 0 |

** - $QoD_2$ values are 0 for any decomposition with equal or fewer IMFs than sub-signals in the source.*

It is clear that the two frequency masked decompositions are much better than the noise-assisted decompositions and unmasked decomposition. The AHHT generated only 4 IMFs plus residual, while the UPEMD was tasked with an arbitrary number and produced a number of IMFs consistent with that specification. Of interest, however, is the component obtaining between the 15 Hz and 30 Hz components in the AHHT plot.

The cause of this component stems from the trigonometric combination of the linear and non-linear parts. Using trigonometric identities and a close approximation for the sum of two terms with equal frequency, there is another purely linear way to generate this signal.

$$f_{sig_4}(t) = s_2(t) + s_3(t) + s_4(t) + s_5(t) + s_6(t) + s_7(t) + s_8(t) + s_9(t) \quad \text{3:4:1b}$$

$$s_5 = -0.1 * \cos(57.5 * 2\pi t) \quad \text{3:4:6}$$

$$s_6 = 0.1 * \cos(42.5 * 2\pi t) \quad \text{3:4:7}$$

$$s_7 = 0.15 * \sin(37.5 * 2\pi t) \quad \text{3:4:8}$$

$$s_8 = -0.15 * \sin(22.5 * 2 * pi * x) - 0.1 * \cos(22.5 * 2 * pi * x) \cong 0.18028 * \cos(22.5x + 2.158) \quad \text{3:4:9}$$

$$s_9 = 0.1 * \cos(7.5 * 2\pi t) \quad \text{3:4:10}$$

This alternative formulation for $f_{sig_4}(t)$ produces an almost perfect replica of the plot shown in Fig. [3-18]. Its transform is given in Fig. [3-20]. However, now it is clear that there are multiple components that are not being extracted between the three major components in any of the decompositions, except for

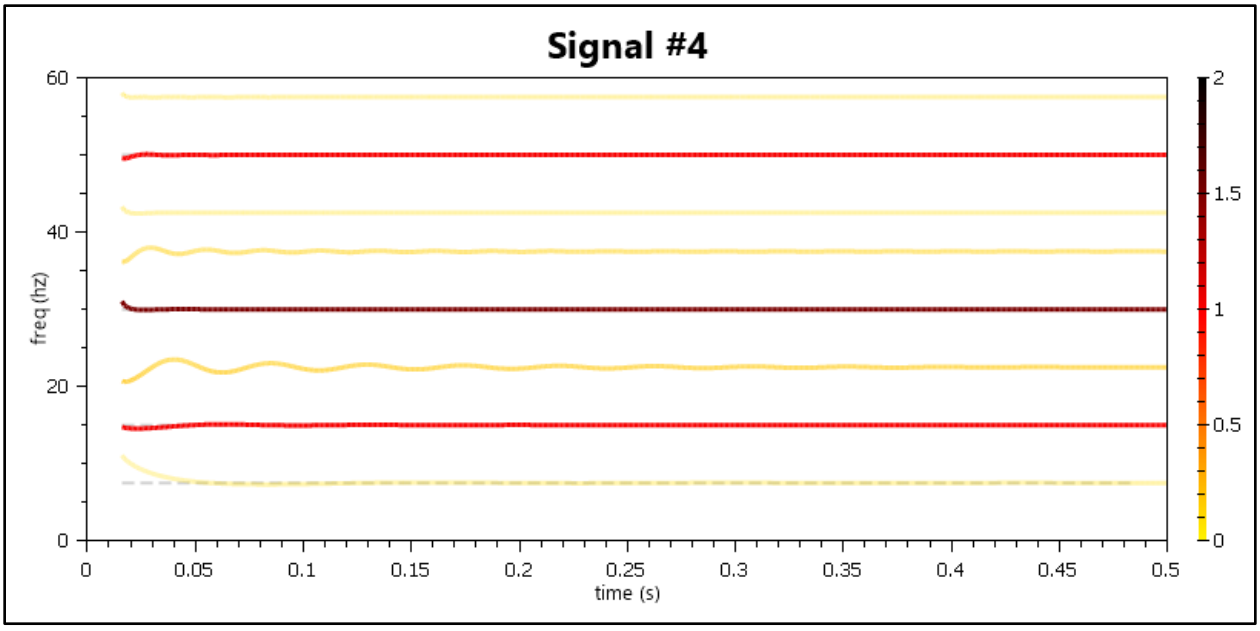


***Figure 3-20 Signal #4 - Source Sub-Signals - Hilbert Spectrum***

the component described by 3:4:9 by the AHHT. It's the combination of both low amplitude and proximity causing the components given in equations 3:4:6 through 3:4:8 to not be extracted. Looking at the IMFs generated by the AHHT given in Fig. [3-21], it's possible to see the oscillating amplitude modulation of the first IMF. The cause of this is unclear. However, IMF #3 has enough amplitude and/or separation from the other components that it is possible to extract by the AHHT.

Adding noise does little to help the decompositions of the other algorithms as demonstrated by the 10 dB SNR. The AHHT still extracts the $s_8$ component given in 3:4:9. The $s_1$ term is poorly represented by the UPEMD, but it provides the next best results . The decomposition comparison for this noise-added signal is given in Fig. [3-22].

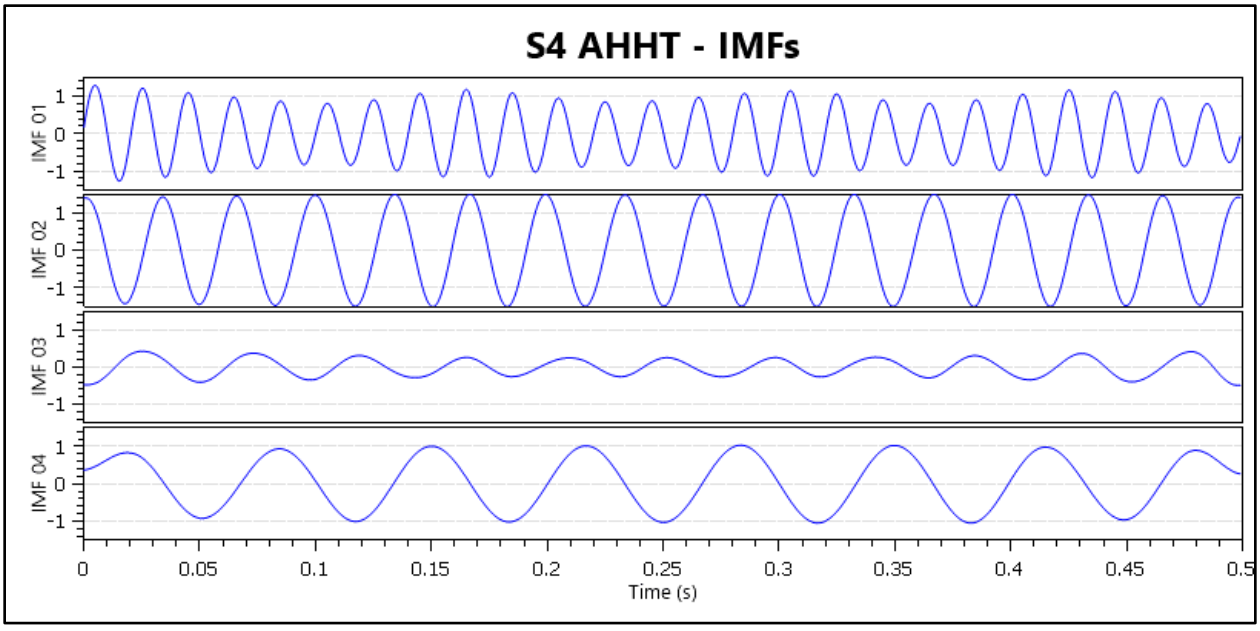


***Figure 3-21 Signal #4 - IMF Plots - First 4 IMFs by AHHT Decomposition***

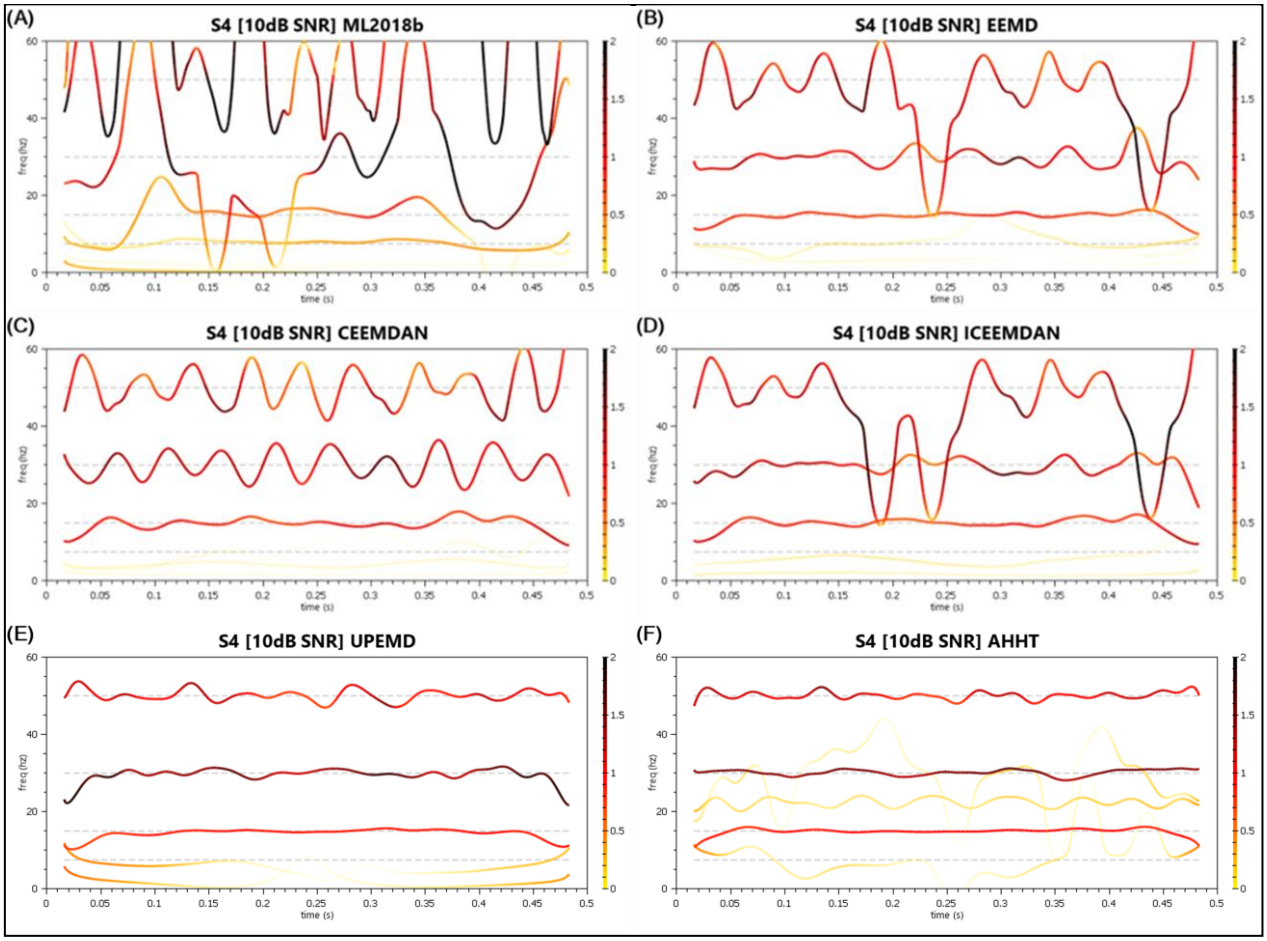


***Figure 3-22 Signal #4 (10dB SNR) - Decomposition Comparison in the Hilbert Spectrum***

***Table A-2 IMF Count and QoD Values Associated with Signal #4 (10dB SNR) EMD Results***

| | MATLAB EMD | EEMD | CEEMDAN | ICEEMDAN | UPEMD | AHHT |
|---|---|---|---|---|---|---|
| # of IMFs + Res | 7 | 10 | 9 | 7 | 8 | 11 |
| $QoD_1$ | 0.005865 | 0.052937 | 0.060017 | 0.05125 | 0.15364 | **0.274203** |
| $QoD_2$* | 0.672487 | 0.048135 | 0.125739 | 0.073667 | 0.504773 | 0.812328 |

** - $QoD_2$ values are 0 for any decomposition with equal or fewer IMFs than sub-signals in the source. $QoD_2$ values for all noise-added signals will be inflated and unreliable due to the mismatch associated with noise-only IMFs.*

## 3.6 SIGNAL #5 – DECOMPOSING CLOSELY SPACED COMPONENTS

Signal #5 is given to demonstrate a deficiency of EMD algorithms in general. Liu *et al.* describe this signal in [24] as one such that "…for a reasonable number of iterations… the components cannot be separated." Using analyses provided by Rilling and Flandrin in [14], Liu *et al.* suggest the components at 75 Hz and 100 Hz are expected to be inseparable. Even using the EFM-EMD2, this is easy to disprove.

$$f_{sig_5}(t) = s_1(t) + s_2(t) + s_3(t), \qquad (sampled\ at\ 2kHz) \tag{3:5:1}$$

$$s_1(t) = sin(75 * 2\pi t), \qquad 0 \leq t \leq 1 \tag{3:5:2}$$

$$s_2(t) = sin(100 * 2\pi t), \qquad 0 \leq t \leq 1 \tag{3:5:3}$$

$$s_3(t) = sin(200 * 2\pi t), \qquad 0 \leq t \leq 1 \tag{3:5:4}$$

This signal is plotted in Fig. [3-23] and the decomposition comparison is depicted in Fig. [3-24].

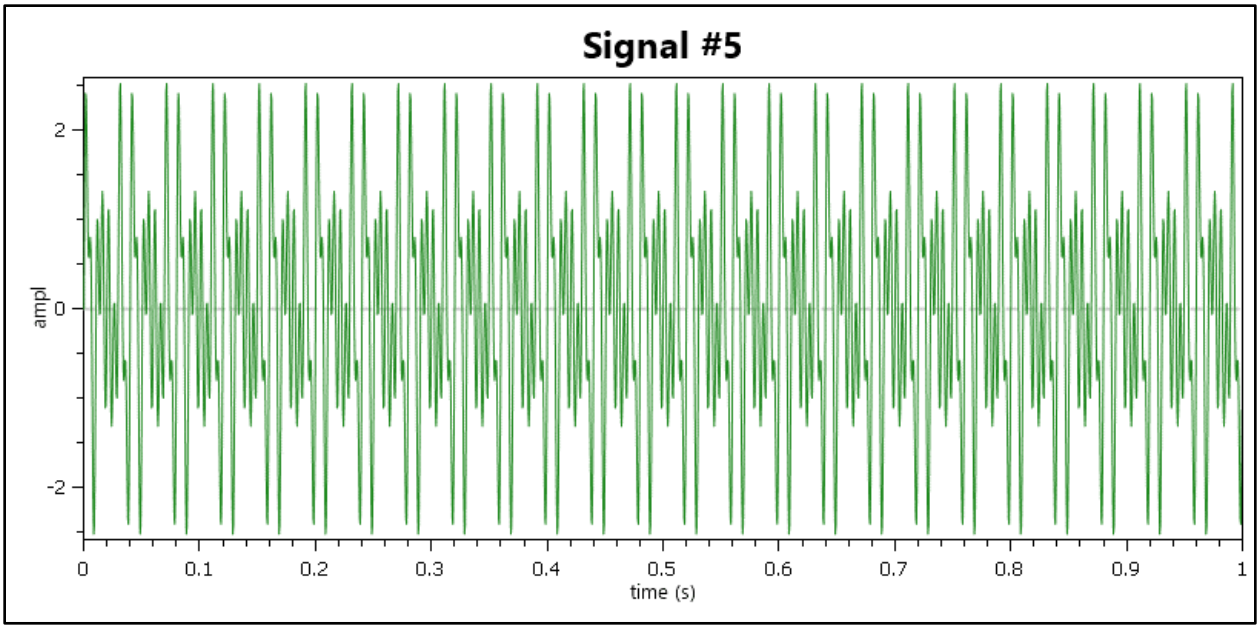


***Figure 3-23 Signal #5 Plot - Time vs. Amplitude***

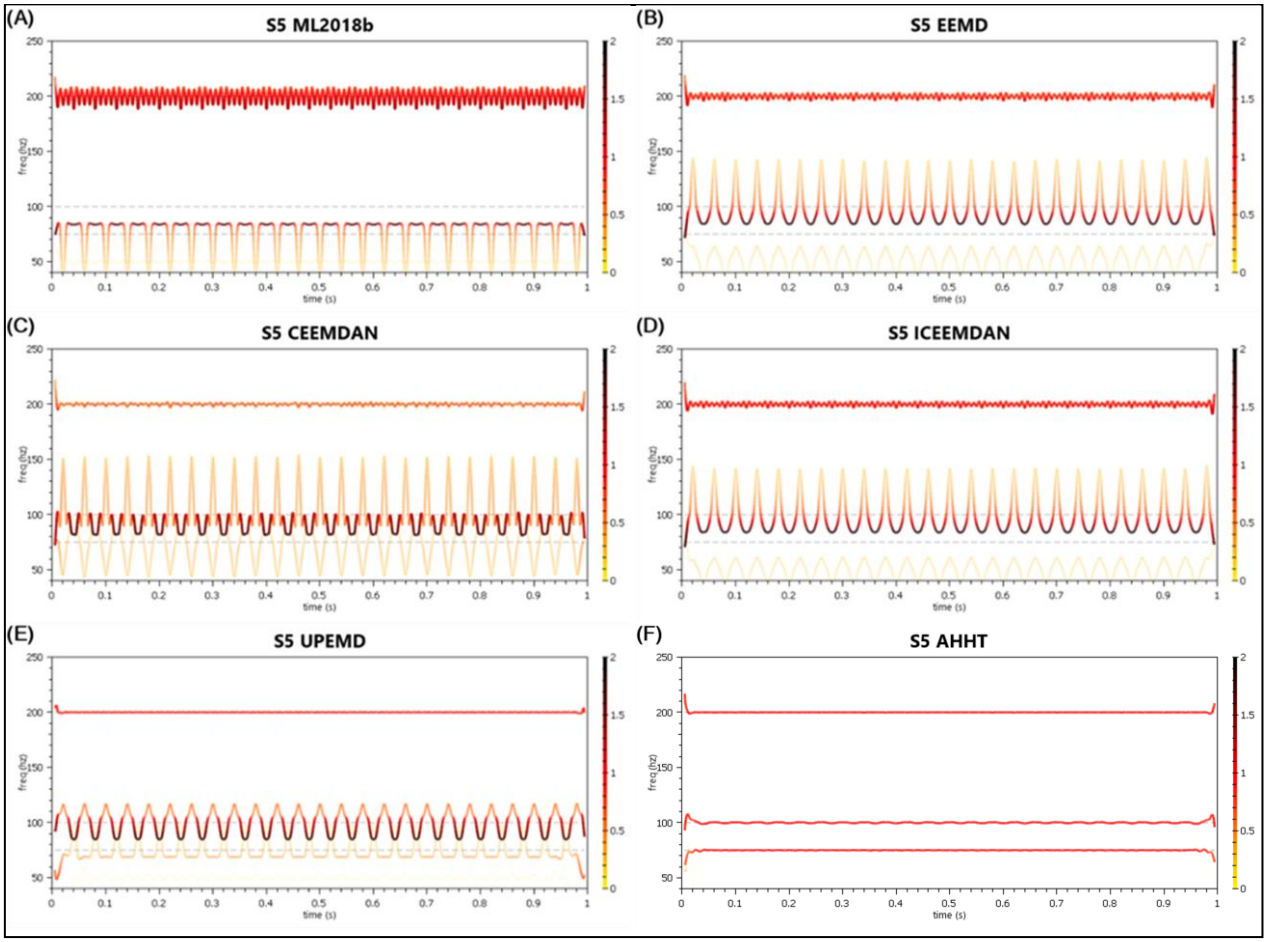


*Figure 3-24 Signal #5 - Decomposition Comparison in the Hilbert Spectrum*

*Table A-1 IMF Count and QoD Values Associated with Signal #5 EMD Results*

| | MATLAB EMD | EEMD | CEEMDAN | ICEEMDAN | UPEMD | AHHT |
|---|---|---|---|---|---|---|
| **Signal #5 – 3 Component Signals** | | | | | | |
| # of IMFs + Res | 5 | 12 | 11 | 10 | 10 | 4 |
| $QoD_1$ | 0.10039 | 0.230145 | 0.021741 | 0.304136 | 0.320848 | **0.950357** |
| $QoD_2$ | 0.132166 | 0.289157 | 0.539182 | 0.272371 | 0.191616 | **0.007954** |

The AHHT is clearly the superior decomposition in this case. Noisy versions of this signal are no better for the other algorithms. Fig. [3-25] depicts the decomposition comparison of the 10 dB SNR version of this signal.

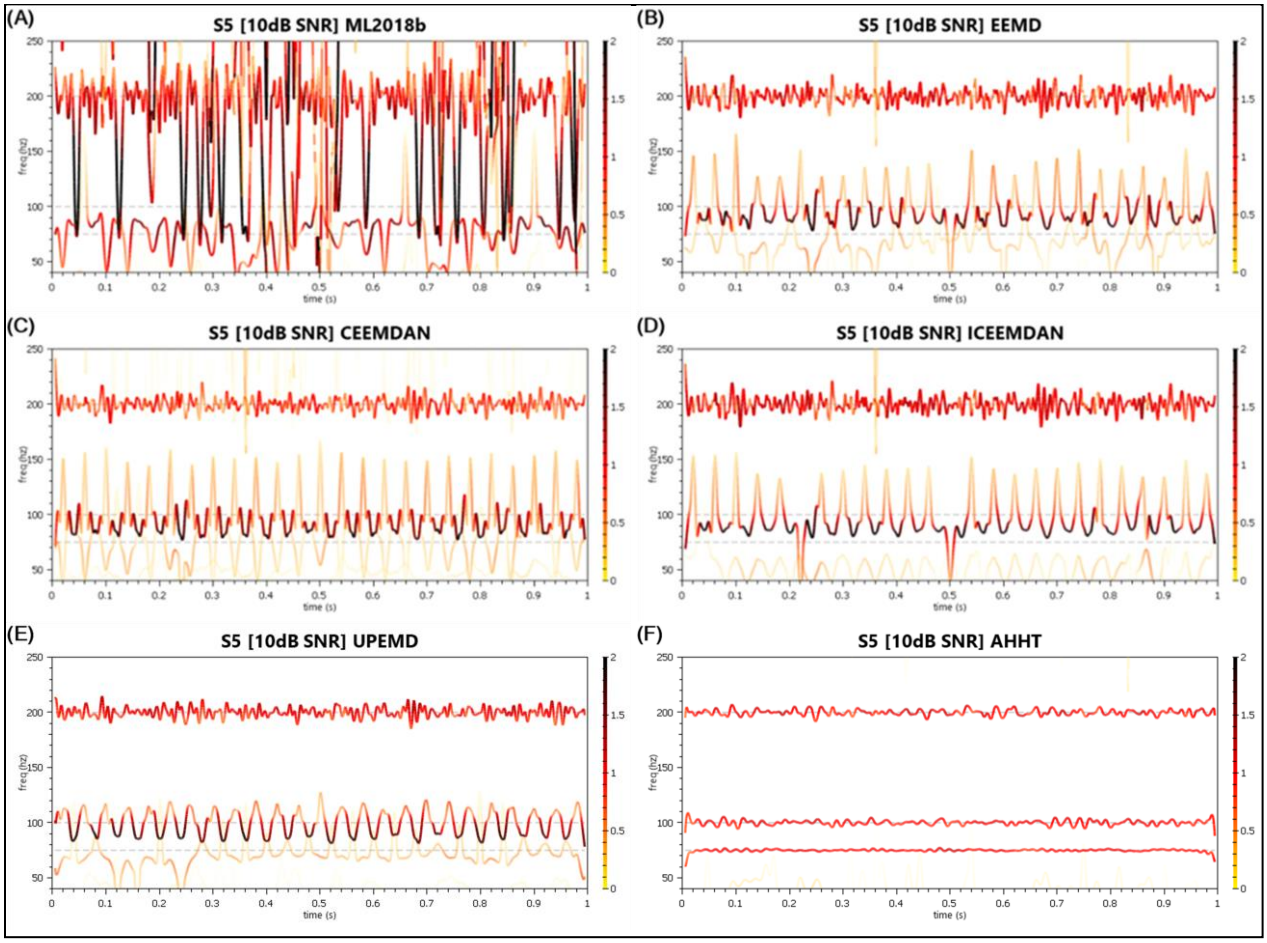


***Figure 3-25 Signal #5 (10dB SNR) - Decomposition Comparison in the Hilbert Spectrum***

***Table A-2 IMF Count and QoD Values Associated with Signal #5 (10dB SNR) EMD Results***

| | MATLAB EMD | EEMD | CEEMDAN | ICEEMDAN | UPEMD | AHHT |
|---|---|---|---|---|---|---|
| **Signal #5 – 3 Component Signals** | | | | | | |
| # of IMFs + Res | 8 | 12 | 12 | 9 | 10 | 8 |
| $QoD_1$ | 0.033308 | 0.091251 | 0.091839 | 0.09175 | 0.190836 | **0.714732** |
| $QoD_2$* | 0.521943 | 0.799889 | 1.0263 | 0.738757 | 0.778061 | 0.774399 |

** - $QoD_2$ values for all noise-added signals will be inflated and unreliable due to the mismatch associated with noise-only IMFs.*

In certain instances, adding small amounts of noise can aid the decomposition as was seen in Signal #1—which forms the basis for the noise-assisted EMD variants. Here it does little to aid the algorithms and instead makes the basic non-ensemble implementation remarkably worse. No decomposition at any level of noise added to Signal #5 is better, relative, to the AHHT (see Appendix A).

## 3.7 SIGNAL #6 – DECOMPOSING MORE-CLOSELY SPACED COMPONENTS

Signal #6 is given to demonstrate resolution limitations of the EMD algorithm. This two-tone signal has closely spaced components that are difficult to separate, but the spacing is far enough apart that it presents further problems. There exists a range where the tones can be spaced that not only presents separation challenges but attempting to do so may lead to phantom signals.

$$f_{sig_6}(t) = s_1(t) + s_2(t), \qquad (sampled\ at\ 1\ kHz) \tag{3:6:1}$$

$$s_1(t) = sin(100 * 2\pi t), \qquad 0 \leq t \leq 10 \tag{3:6:2}$$

$$s_2(t) = sin(80 * 2\pi t), \qquad 0 \leq t \leq 10 \tag{3:6:3}$$

While Signal #5 had two components at 100 Hz and 75 Hz, Signal #6 brings them closer together with separation of the lower frequency from the higher frequency at 20% rather than 25%. The plot of the first 10% of Signal #6 is given in Fig. [3-26] and the full decomposition comparison in Fig. [3-27].

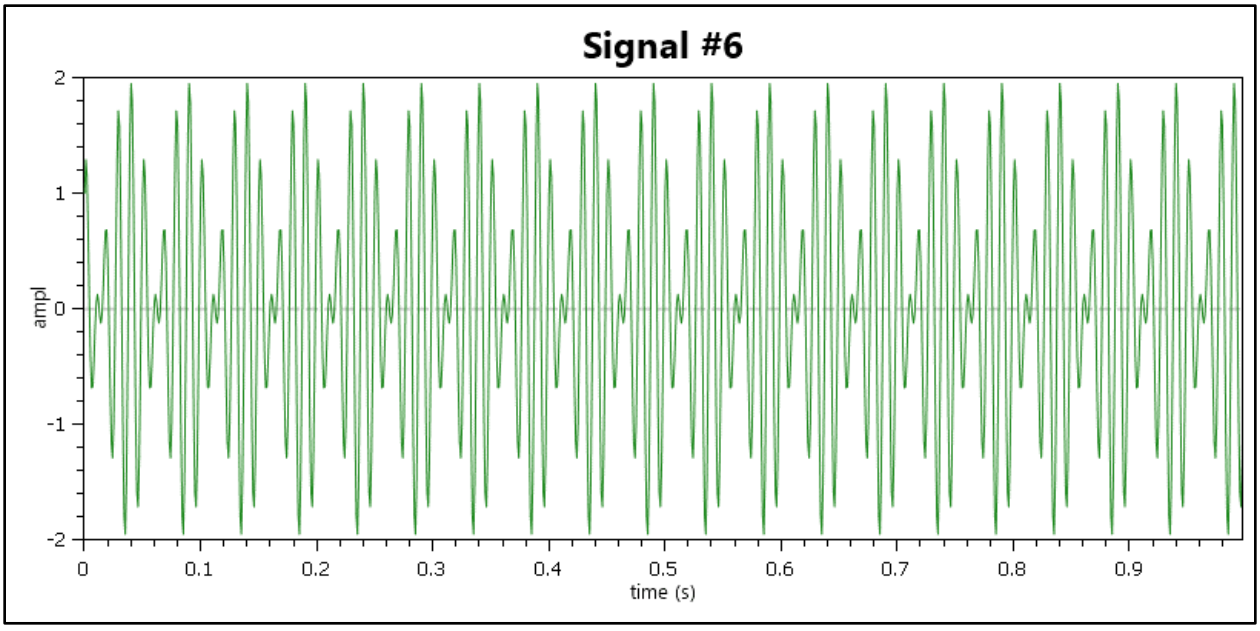


***Figure 3-26 Signal #6 Plot – 10% of Time vs. Amplitude***

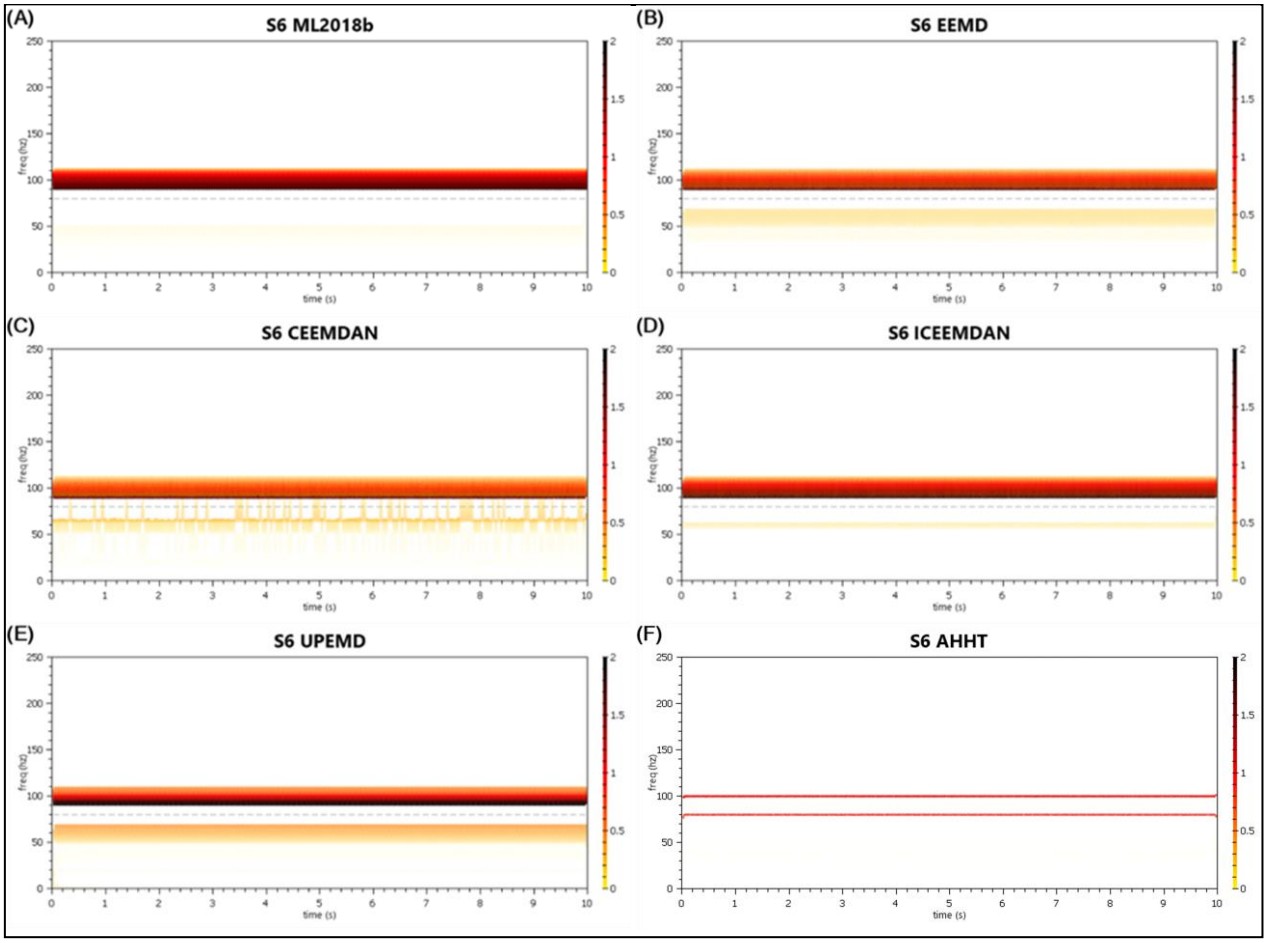


*Figure 3-27 Signal #6 - Decomposition Comparison in the Hilbert Spectrum*

*Table A-1 IMF Count and QoD Values Associated with Signal #6 EMD Results*

| | MATLAB EMD | EEMD | CEEMDAN | ICEEMDAN | UPEMD | AHHT |
|---|---|---|---|---|---|---|
| **Signal #6 – 2 Component Signals** | | | | | | |
| # of IMFs + Res | 3 | 15 | 16 | 14 | 13 | 5 |
| $QoD_1$ | 0.006497 | 0.023184 | 0.011612 | 0.017926 | 0.028354 | **0.89535** |
| $QoD_2$ | 0.03871 | 0.340859 | 0.423141 | 0.227672 | 0.428347 | **0.018928** |

The base EMD implementation provided by MATLAB 2018b and AHHT generate a small number of IMFs, though clearly only the AHHT is providing an adequate decomposition. What is seen in the poor decompositions is the Hilbert transform of essentially deformed versions of the original signal (as represented in IMF 1) generating high frequency-oscillations between the 100 Hz and 80 Hz levels. Then, the next component is a frequency-oscillating Phantom IMF.

## 3.8 SIGNAL #7 – DECOMPOSING INTERMITTENT HIGH FREQ. COMPONENTS OVER CONSTANT LOW FREQ. COMPONENTS

Signal #7 is given as contrast to Signal #1. The higher frequency component is pulsed on for a bounded time interval instead of the lower frequency component. Despite the frequency spacing being larger than in the case with Signal #3, the classical EMD still exhibits Type I Mode-Mixing.

$$f_{sig_7}(t) = s_1(t) + s_2(t), \qquad (sampled\ at\ 1\ kHz) \tag{3:7:1}$$

$$s_1(t) = sin(65 * 2\pi t), \qquad 0 \leq t \leq 1 \tag{3:7:2}$$

$$s_2(t) = sin(255 * 2\pi t), \qquad 0.5 \leq t \leq 0.75 \tag{3:7:3}$$

The plot for this signal is given in Fig. [3-28] and the subsequent decomposition comparison is given in Fig. [3-29].

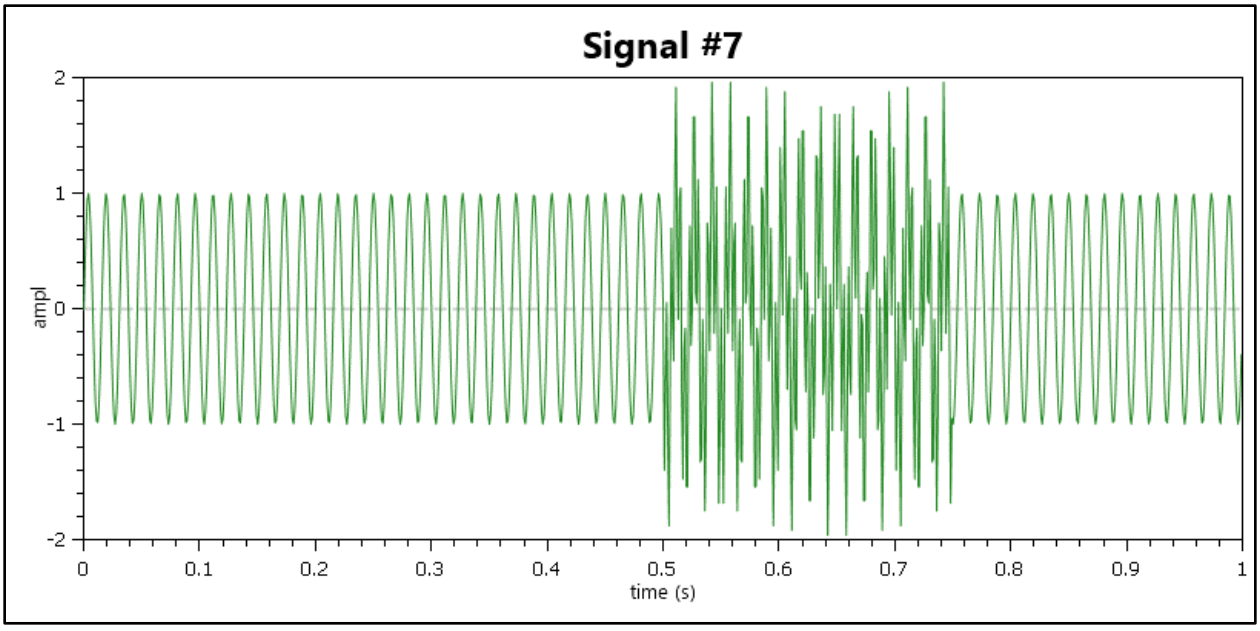


***Figure 3-28 Signal #7 Plot - Time vs. Amplitude***

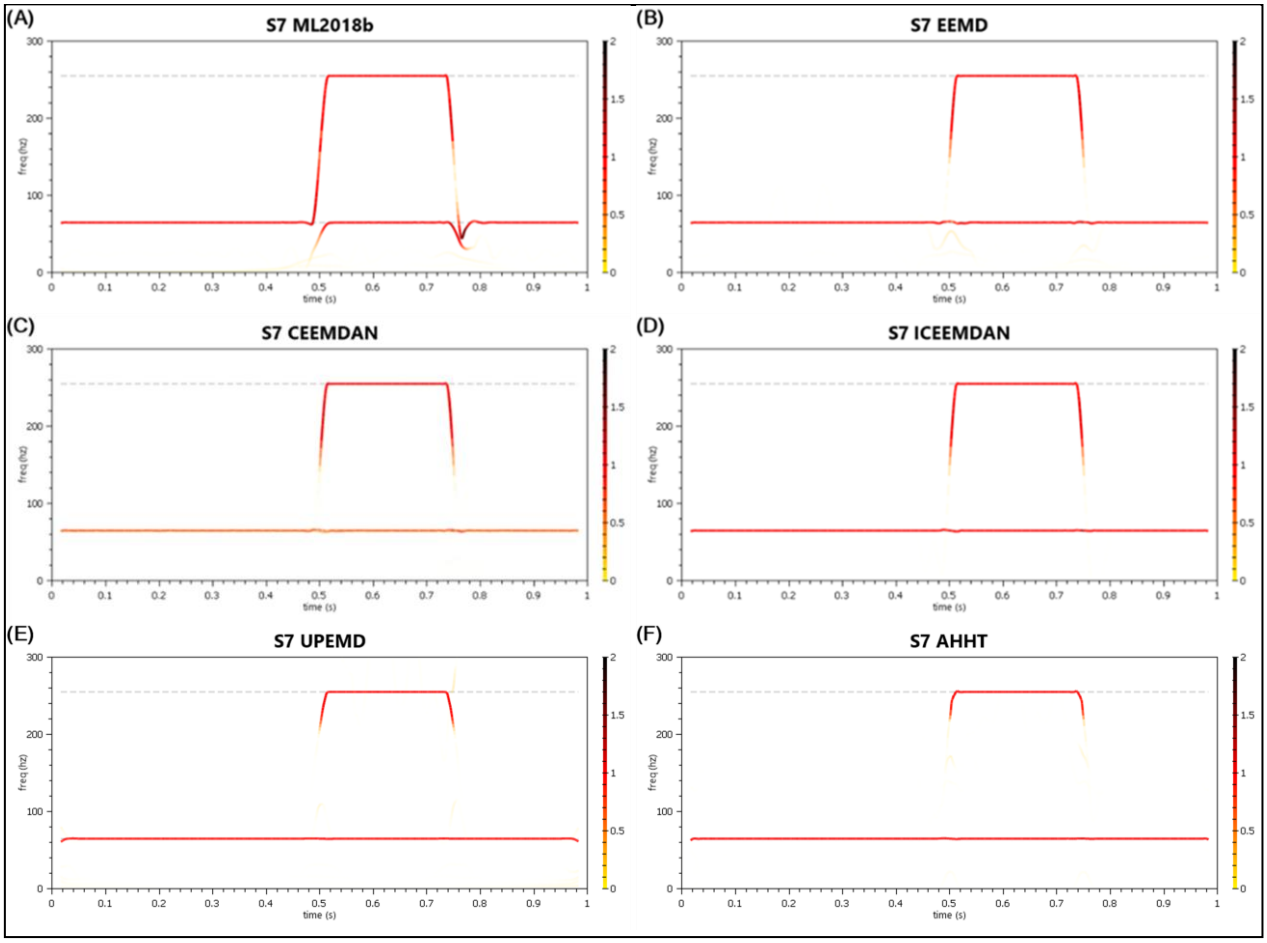


*Figure 3-29 Signal #7 - Decomposition Comparison in the Hilbert Spectrum*

*Table A-1 IMF Count and QoD Values Associated with Signal #7 EMD Results*

| | MATLAB EMD | EEMD | CEEMDAN | ICEEMDAN | UPEMD | AHHT |
|---|---|---|---|---|---|---|
| **Signal #7 – 2 Component Signals** | | | | | | |
| # of IMFs + Res | 8 | 10 | 11 | 2 | 9 | 5 |
| $QoD_1$ | 0.115095 | 0.863624 | 0.41947 | 0.923283 | 0.904884 | **0.924295** |
| $QoD_2$ | 0.128662 | 0.053114 | 0.313989 | **0** | 0.094126 | 0.016248 |

The main result from this decomposition is that masking is necessary to eliminate Type I Mode-Mixing. The secondary result is that masking may lead to many transient IMFs despite good extraction of the primary components. Four of the five masking algorithms worked very well, with ICEEMDAN, UPEMD, and AHHT having trivial differences.

## 3.9 SIGNAL #8 – DECOMPOSING NON-STATIONARY SIGNALS

Signal #8 is was created mistakenly, but serves as an interesting example, nevertheless. In [30], Shen *et al.* used the equations in 3:8:2 through 3:8:4 separately to demonstrate their approaching to finding the minimum period of a signal with which to derive a mask frequency. They were combined in linear summation in this thesis to form Signal #8.

$$f_{sig_8}(t) = s_1(t) + s_2(t) + s_3(t), \qquad (sampled\ at\ 1\ kHz) \tag{3:8:1}$$

$$s_1(t) = sin(7.8125 * 2\pi t), \qquad 0 \leq t \leq 1 \tag{3:8:2}$$

$$s_2(t) = 3 * cos(1.953125 * 2\pi t), \qquad 0 \leq t \leq 1 \tag{3:8:3}$$

$$s_3(t) = -6 * sin(1.953125 * 2\pi t) + \frac{2}{75}t, \qquad 0 \leq t \leq 1 \tag{3:8:4}$$

The second term in equation 3:8:4 is merely a linear term that provides non-stationarity. However, the sum of the sinusoidal terms in $s_2 + s_3$ is itself sinusoidal, roughly conforming to: $s_2(t) + s_3(t) = 6.7081 * cos\left(1.953125 * 2\pi t + \frac{1}{\sqrt{2}} * \frac{\pi}{2}\right)$. The values 7.8125 and 1.953125 are derived from 500/64 and 500/264 respectively. The ideal decomposition would thus provide just two IMFs plus residual: one containing the $s_1$ component, one containing the frequency component of $s_2 + s_3$, and the residual would hold the linear term of $s_3$.

Signal #8 is depicted in Fig. [3-30] and its subsequent decomposition comparison is given in Fig. [3-31]. Note, since there is both a low amplitude component and a high amplitude component, the transparency of low amplitude signals has been adjusted for better visibility in the Hilbert spectrum plots.

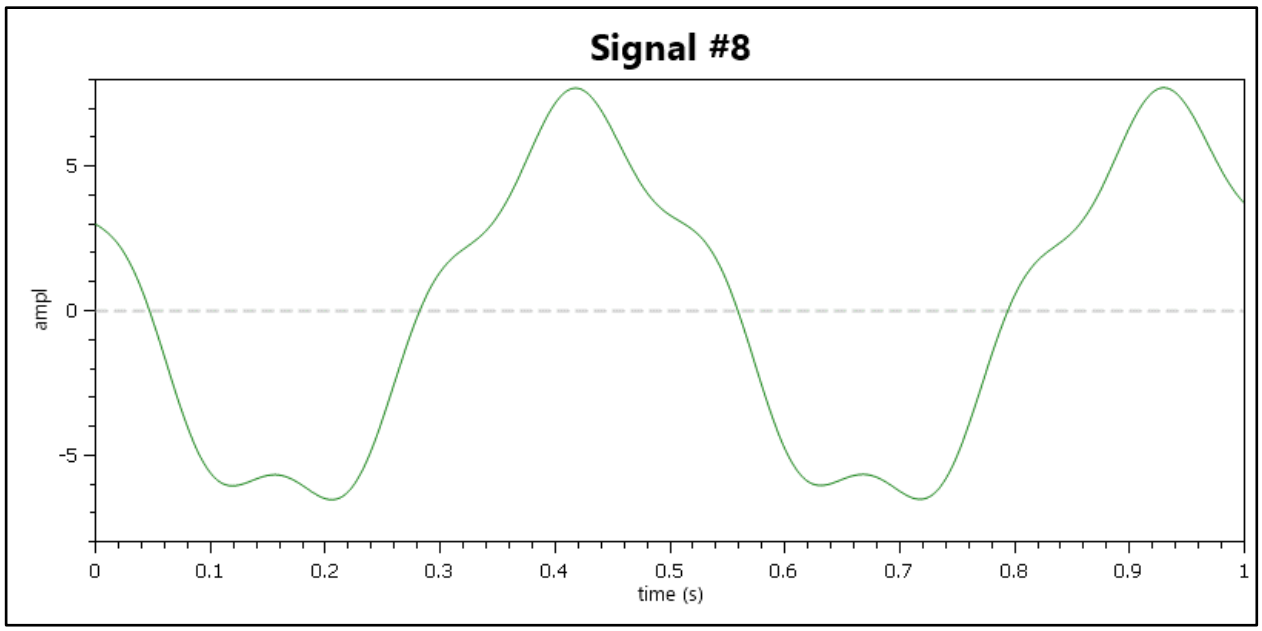


*Figure 3-30 Signal #8 Plot - Time vs. Amplitude*

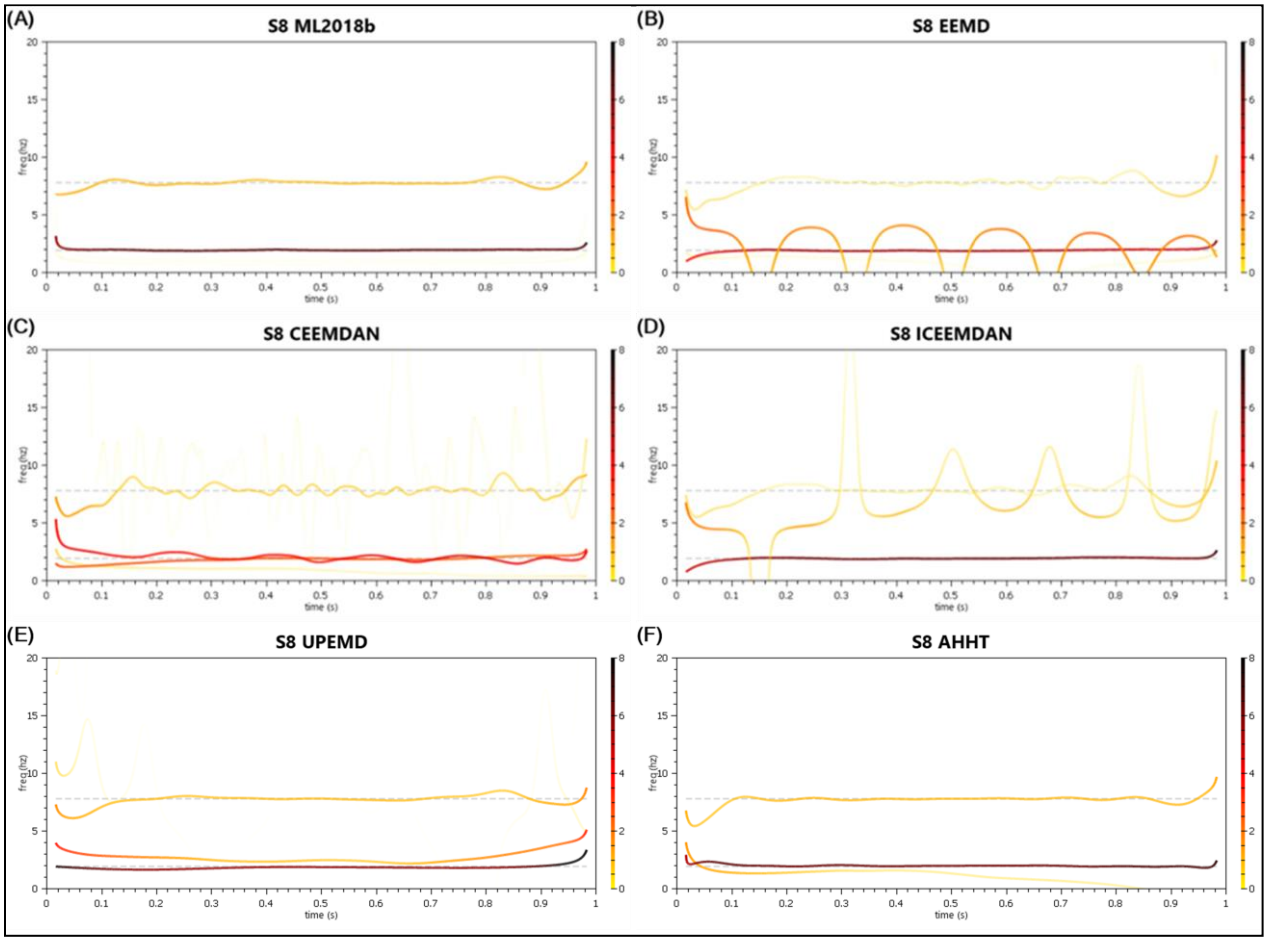


*Figure 3-31 Signal #8 - Decomposition Comparison in the Hilbert Spectrum*

***Table A-1 IMF Count and QoD Values Associated with Signal #8 EMD Results***

| | MATLAB EMD | EEMD | CEEMDAN | ICEEMDAN | UPEMD | AHHT |
|---|---|---|---|---|---|---|
| **Signal #8 – 2 Component Signals** | | | | | | |
| # of IMFs + Res | 4 | 9 | 10 | 7 | 9 | 3 |
| $QoD_1$ | **0.612176** | 0.047074 | 0.024415 | 0.275469 | 0.329786 | 0.569422 |
| $QoD_2$ | **0.159315** | 1.801686 | 3.219262 | 0.813113 | 1.717778 | 0.606953 |

Clearly, the best decomposition is provided by baseline EMD in MATLAB 2018b—this decomposition is near perfect. The second-best decomposition was provided by AHHT and is only slightly inferior, since the residual and IMF#2 demonstrate a small amount of Type-II Mode Mixing. The main reason this signal is difficult to decompose is the location of the lower frequency extrema. The boundary extension method of MATLAB 2018b is perfect for managing this component, since it extrapolates new extended extrema by sinusoidal extension—whereas, heretofore, this boundary extension scheme has been inferior in other decompositions, it is clearly superior to the mirroring scheme in this case. The most interesting result here is that masking provided no obvious benefit. It's also unclear why the other decompositions are poor.

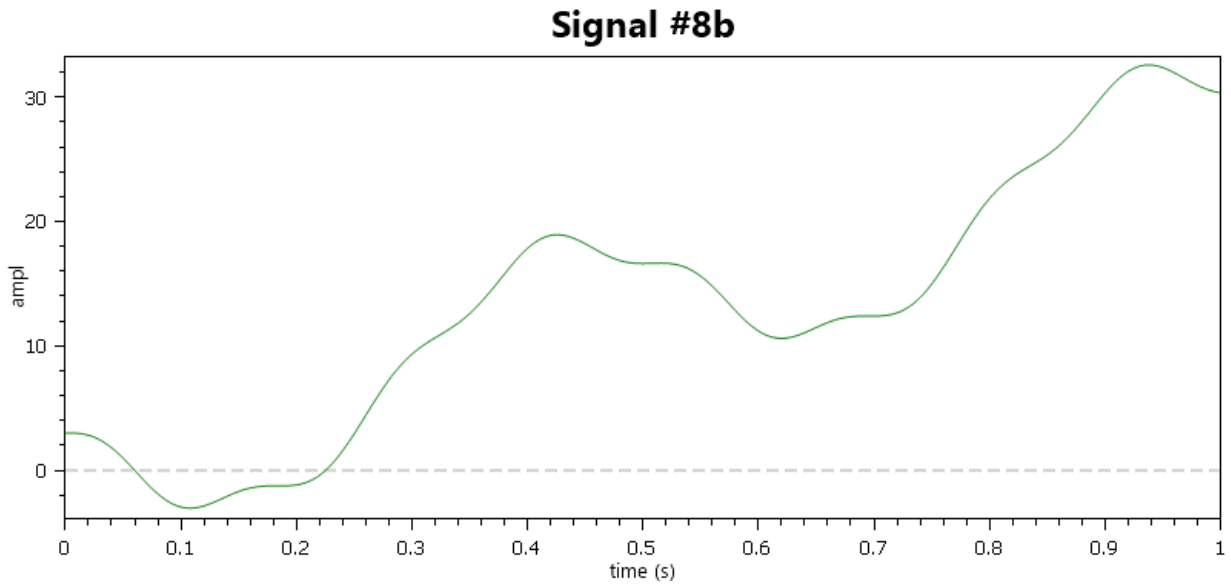


***Figure 3-32 Signal #8b Plot - Time vs. Amplitude***

For additional comparison, a second version of Signal #8 (referred to as Signal #8b) replaces the non-stationarity term of 13.4 with a much larger slope.

$$f_{sig_{8b}}(t) = s_1(t) + s_2(t) + s_{3b}(t), \qquad (sampled\ at\ 1\ kHz) \tag{3:8:1b}$$

$$s_{3b}(t) = -6 * sin(1.953125 * 2\pi t) + \frac{160}{3}t, \qquad 0 \leq t \leq 1 \tag{3:8:4b}$$

The plot of Signal #8b is given in Fig. [3-32] and the comparison of its decompositions is given in Fig. [3-33].

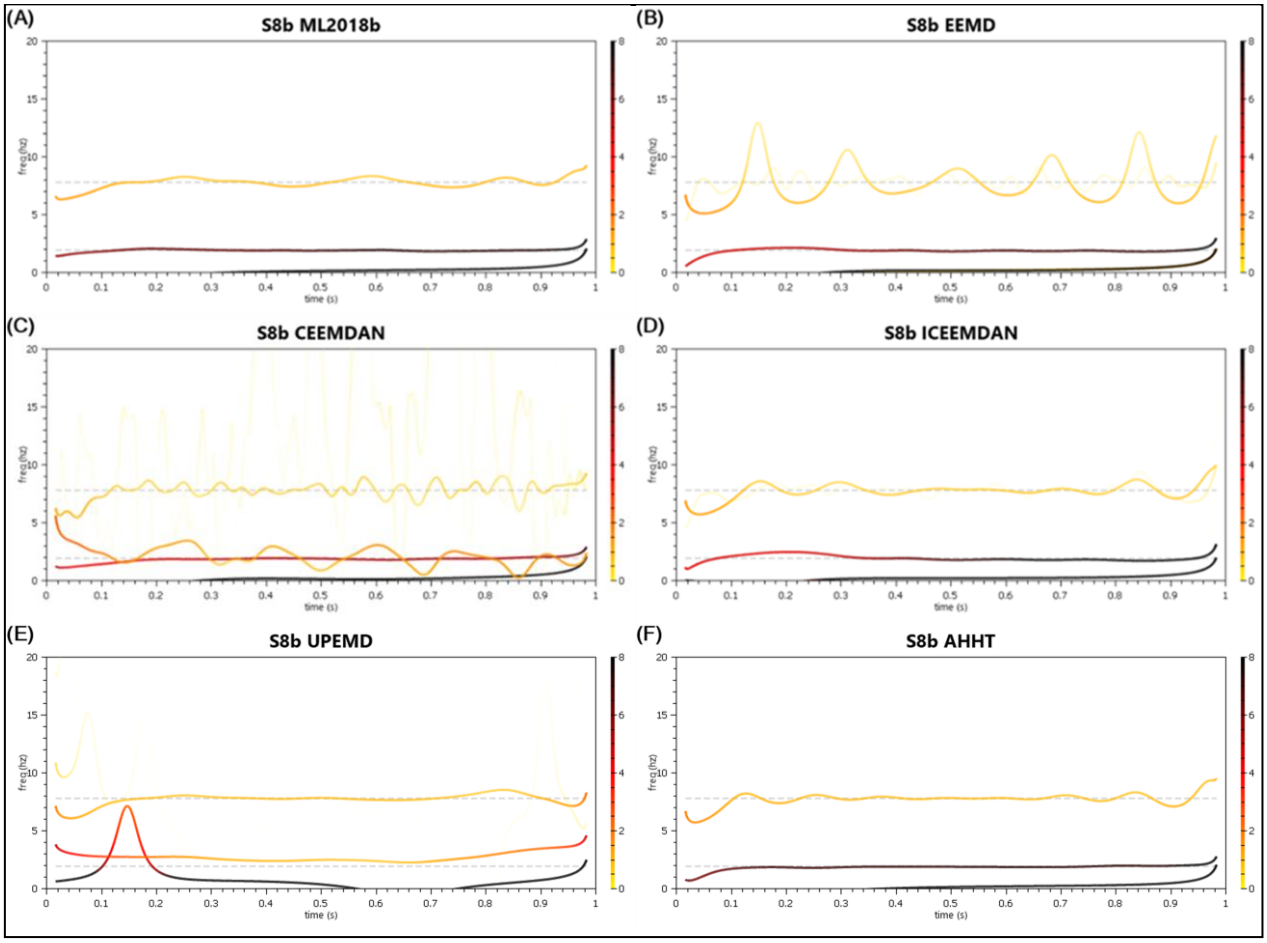


*Figure 3-33 Signal #8b - Decomposition Comparison in the Hilbert Spectrum*

*Table A-2 IMF Count and QoD Values Associated with Signal #8b EMD Results*

| | MATLAB EMD | EEMD | CEEMDAN | ICEEMDAN | UPEMD | AHHT |
|---|---|---|---|---|---|---|
| **Signal #8b – 2 Component Signals** | | | | | | |
| # of IMFs + Res | 3 | 9 | 10 | 8 | 9 | 3 |
| $QoD_1$ | 0.636169 | 0.346151 | 0.26351 | 0.298206 | 0.199724 | **0.654943** |
| $QoD_2$ | **0** | 0.997061 | 1.873362 | 0.149712 | 1.96271 | **0** |

Both the MATLAB 2018b implementation and the AHHT are near perfect when the linear trend is much more pronounced, but the advantage is now with AHHT, since there is no Phantom IMF generated.

## 3.10 SIGNAL #9 – DECOMPOSING WITH LARGE AMPLITUDE DISPARITY

Signal #9 is similar to Signal #7, only with the lower frequency component scaled down by 0.25:

$$f_{sig_9}(t) = s_1(t) + s_2(t), \qquad (sampled\ at\ 1\ kHz) \tag{3:9:1}$$

$$s_1(t) = 0.25 * sin(65 * 2\pi t), \qquad 0 \leq t \leq 1 \tag{3:9:2}$$

$$s_2(t) = sin(255 * 2\pi t), \qquad 0.5 \leq t \leq 0.75 \tag{3:9:3}$$

The purpose of this signal is to test how the decompositions manage amplitude during IMF extraction. The end result is that 3 of the 6 do very well. The UPEMD, like with Signal #7, edges out AHHT by a trivial amount. The plot of this signal is given in Fig. [3-35] and its decomposition comparison is given in Fig. [3-36]. Note: the transparency settings were adjusted to allow the low amplitude component to be clearly visible.

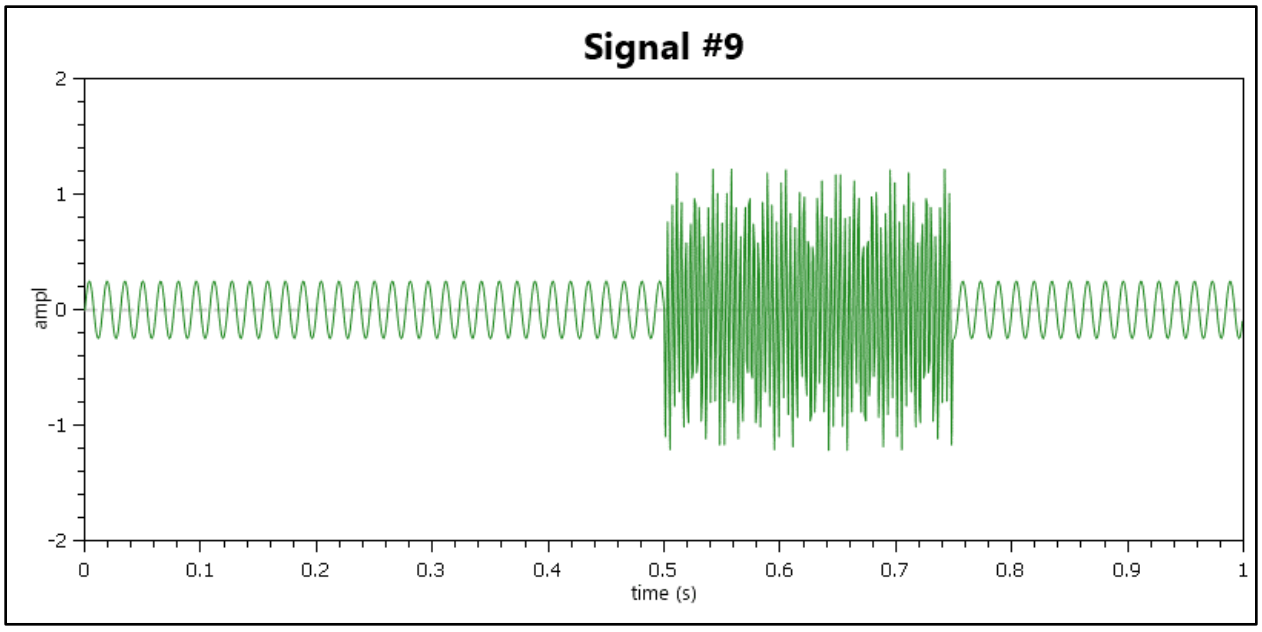


***Figure 3-34 Signal #9 Plot - Time vs. Amplitude***

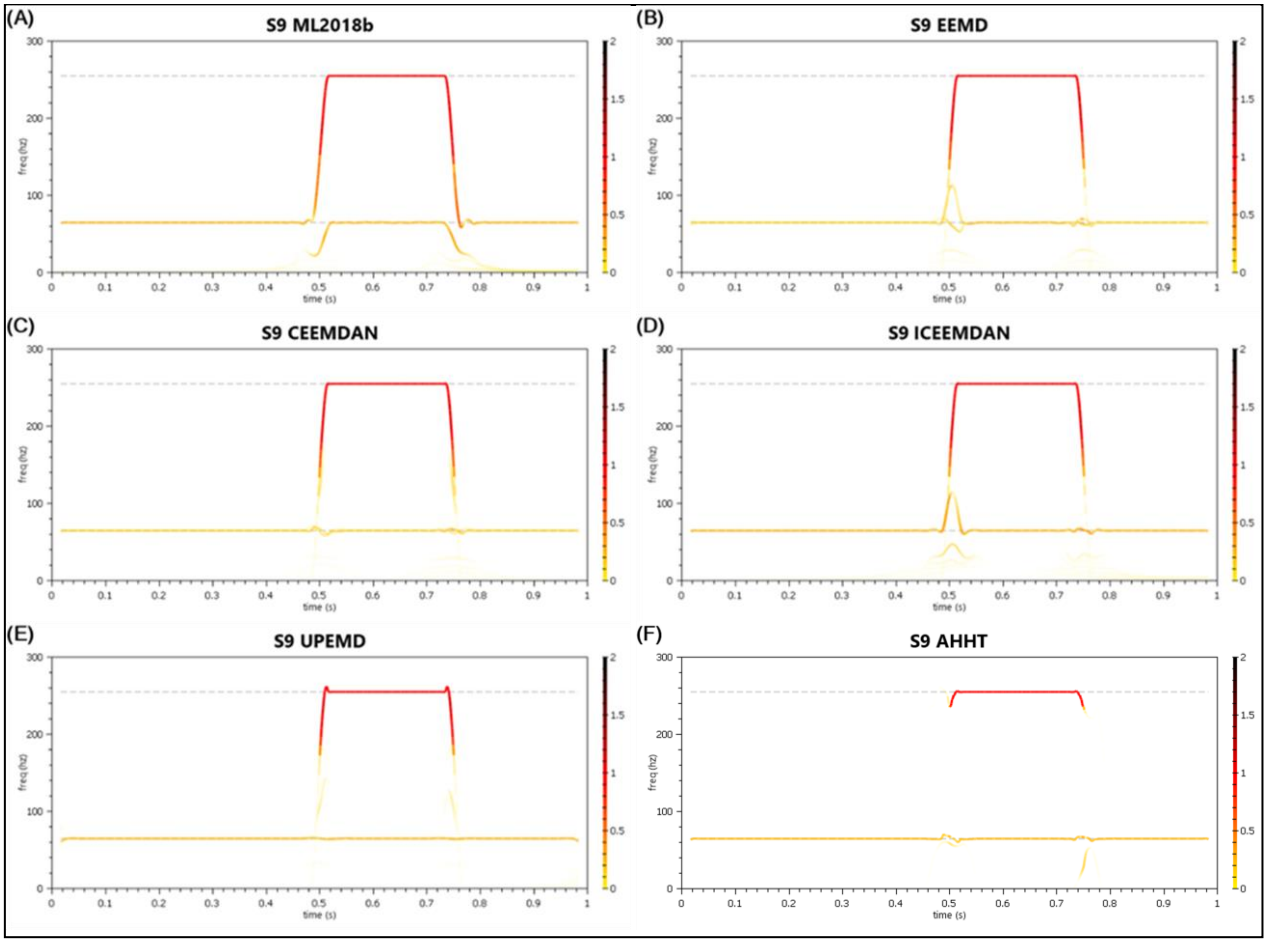


*Figure 3-35 Signal #9 - Decomposition Comparison in the Hilbert Spectrum*

*Table A-1 IMF Count and QoD Values Associated with Signal #9 EMD Results*

| | MATLAB EMD | EEMD | CEEMDAN | ICEEMDAN | UPEMD | AHHT |
|---|---|---|---|---|---|---|
| **Signal #9 – 2 Component Signals** | | | | | | |
| # of IMFs + Res | 7 | 11 | 10 | 11 | 9 | 3 |
| $QoD_1$ | 0.102185 | 0.46892 | 0.420989 | 0.874851 | **0.942162** | 0.902378 |
| $QoD_2$ | 0.07751 | 0.106619 | 0.11403 | 0.086259 | 0.032487 | **0.008494** |

## 3.11 SIGNAL #10 – FAULT DETECTION – DECOMPOSING VERY LOW AMPLITUDE RIDING WAVES RELATIVE TO A CARRIER SIGNAL

Signal #10 represents a carrier/rider wave scenario as might be seen in defect detection. In this case, the amplitude of the carrier wave is much larger than that of the rider.

$$f_{sig_{10}}(t) = s_1(t) + s_2(t), \qquad (sampled\ at\ 1\ kHz) \tag{3:10:1}$$

$$s_1(t) = 0.08 * cos(100 * 2\pi t)$$
$$on\ .316 \le t \le .355, \qquad .581 \le t \le .62, \qquad .848 \le t \le .887 \tag{3:10:2}$$

$$s_2(t) = sin(3.75 * 2\pi t), \qquad 0 \le t \le 1.2 \tag{3:10:3}$$

Signal #10 has a special-case noise-added variant that was tested. Heavy noise was added to the signal such that a SNR of -9.2 dB was achieved against the riding wave only. The actual SNR is much higher at 22.75 dB, but the carrier wave is inconsequential to this analysis. The plot of both signals is given in Figs. [3-37 & 3-39] and their decompositions given respectively in Figs. [3-38] and [3-40]. Again, since the amplitudes are so disparate, transparency settings have been adjusted accordingly.

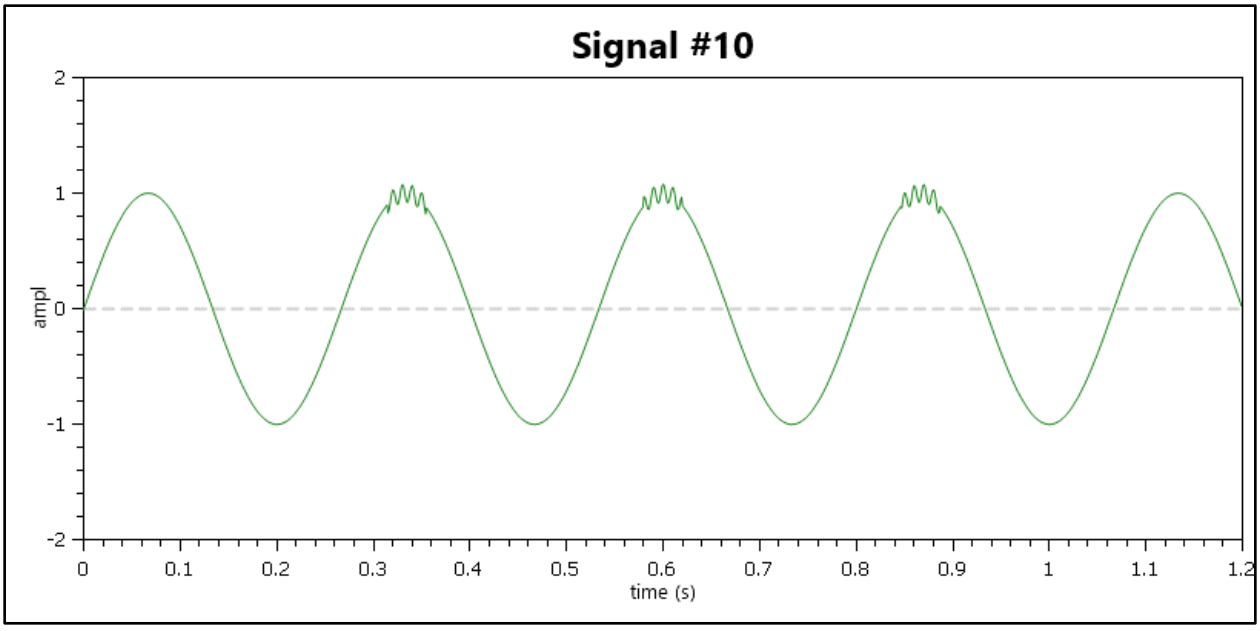


***Figure 3-36 Signal #10 Plot - Time vs. Amplitude***

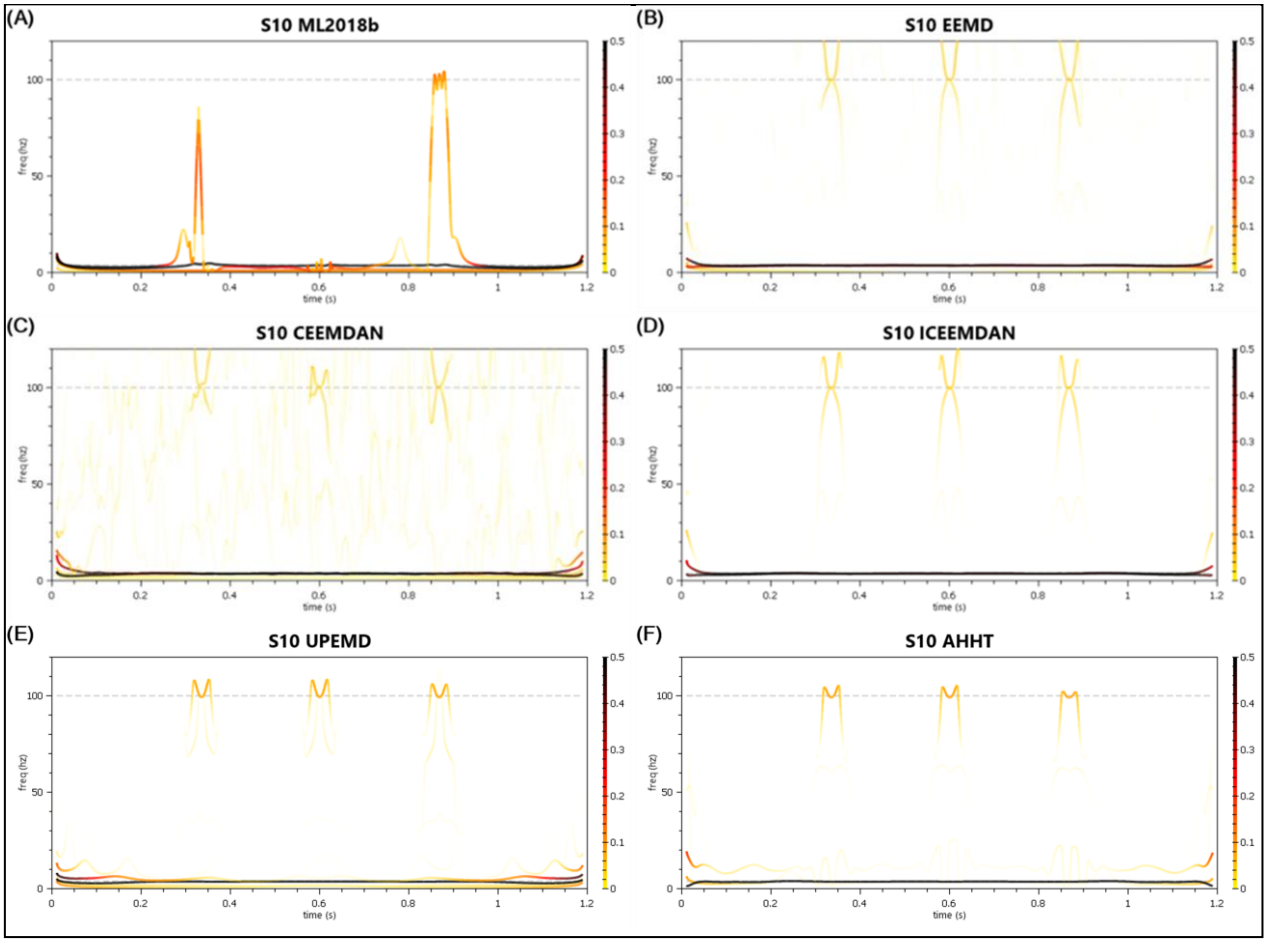


*Figure 3-37 Signal #10 - Decomposition Comparison in the Hilbert Spectrum*

*Table A-1 IMF Count and QoD Values Associated with Signal #10 EMD Results*

| | MATLAB EMD | EEMD | CEEMDAN | ICEEMDAN | UPEMD | AHHT |
|---|---|---|---|---|---|---|
| **Signal #10 – 2 Component Signals** | | | | | | |
| # of IMFs + Res | 5 | 10 | 11 | 6 | 10 | 6 |
| $QoD_1$ | 0.1037 | 0.037899 | 0.016519 | 0.038398 | 0.406582 | **0.591427** |
| $QoD_2$ | 0.228057 | 0.407359 | 0.576082 | 0.487356 | 0.204101 | **0.03929** |

For fault detection, all but the non-masked EMD do an adequate job, though even the MATLAB 2018b implementation does detect one clearly, a second one indicated, and misses on one. The AHHT is showing more artifacts in the decomposition than the UPEMD. Boundary extension is the primary culprit for the very low frequency component generating multiple IMFs—the wave-extension scheme used by MATLAB 2018b is well-suited to this signal.

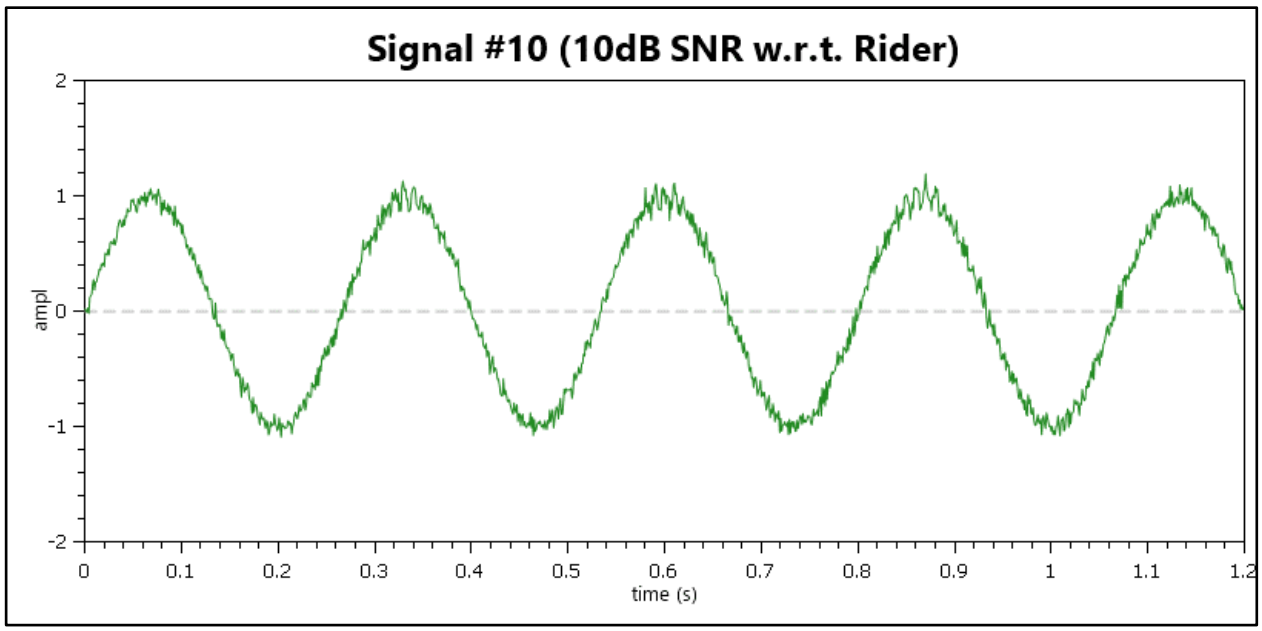


*Figure 3-38 Signal #10 (-9.2dB w.r.t Rider) Plot - Time vs. Amplitude*

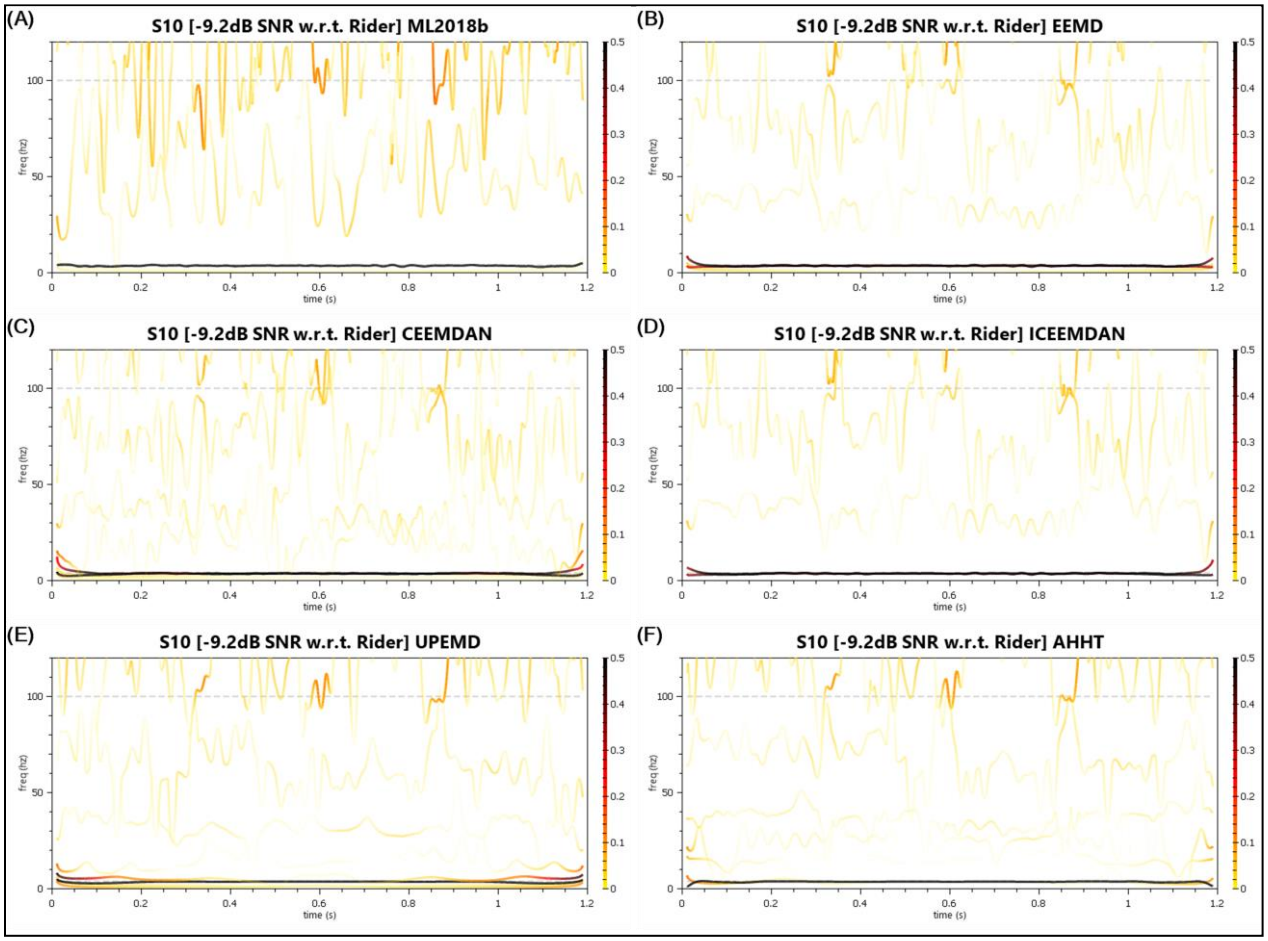


*Figure 3-39 Signal #10 (-9.2dB w.r.t Rider) - Decomposition Comparison in the Hilbert Spectrum*

***Table A-2 IMF Count and QoD Values Associated with Signal #10 (-9.2dB w.r.t Rider) EMD Results***

| | MATLAB EMD | EEMD | CEEMDAN | ICEEMDAN | UPEMD | AHHT |
|---|---|---|---|---|---|---|
| **Signal #10 (-9.2 dB SNR w.r.t. Riding Signal)** | | | | | | |
| # of IMFs + Res | 7 | 10 | 12 | 6 | 10 | 9 |
| $QoD_1$ | 0.453868 | -0.00497 | -0.01244 | 0.011398 | **0.460711** | 0.452966 |
| $QoD_2$* | 0.083734 | 0.535078 | 0.586462 | 0.52819 | 0.289933 | 0.126818 |

** - $QoD_2$ values for all noise-added signals will be inflated and unreliable due to the mismatch associated with noise-only IMFs.*

In noise, even the MATLAB 2018b implementation is able to generate reasonable detection signals, but its high $QoD_1$ comes from the very clear extraction of the carrier signal. The UPEMD and AHHT have a remarkably similar appearance and their QoD values are accordingly very similar. Very low frequency signals often result in poor extraction with AHHT primarily due to its boundary extension techniques. However, from a pattern recognition perspective, it's hard to select one as clearly superior to other. Fig. [3-41] shows the similarity of these two decompositions with noise-only IMFs removed.

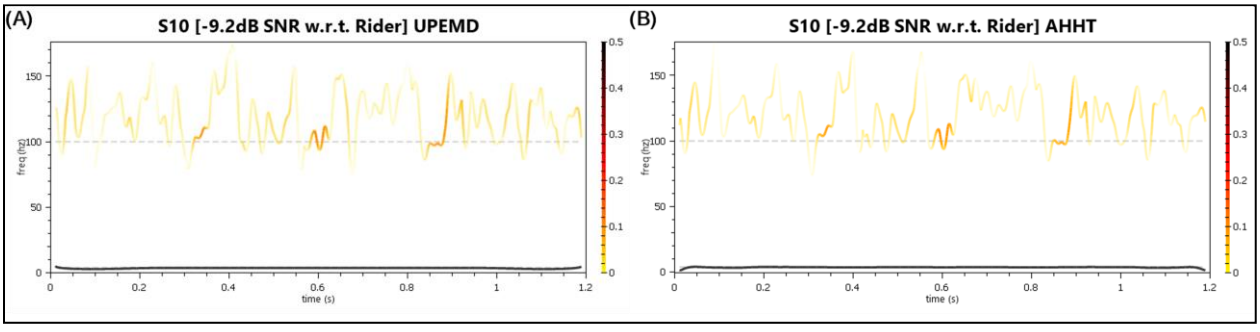


***Figure 3-40 Signal #10 (-9.2dB w.r.t Rider) - UPEMD & AHHT Hilbert Spectrum Comparison – Noise-Only IMFs Removed***

## 3.12 SIGNAL #11 – DECOMPOSING WELL-SPACED, HIGH-FREQUENCY COMPONENTS

Signal #11 is a constant two-tone signal well above the half-Nyquist rate. It is included to demonstrate the limitations of the EMD in decomposing even well-spaced components above 25% of the sampling frequency. It is defined as:

$$f_{sig_{11}}(t) = s_1(t) + s_2(t), \qquad (sampled\ at\ 1\ kHz) \tag{3:11:1}$$

$$s_1(t) = sin(400 * 2\pi t), \qquad 0 \leq t \leq 1 \tag{3:11:2}$$

$$s_2(t) = sin(300 * 2\pi t), \qquad 0 \leq t \leq 1 \tag{3:11:3}$$

The plot of the first 10% of the signal is shown in Fig. [3-42]. The Hilbert spectrum decomposition comparisons for the full signal are depicted in Fig. [3-43].

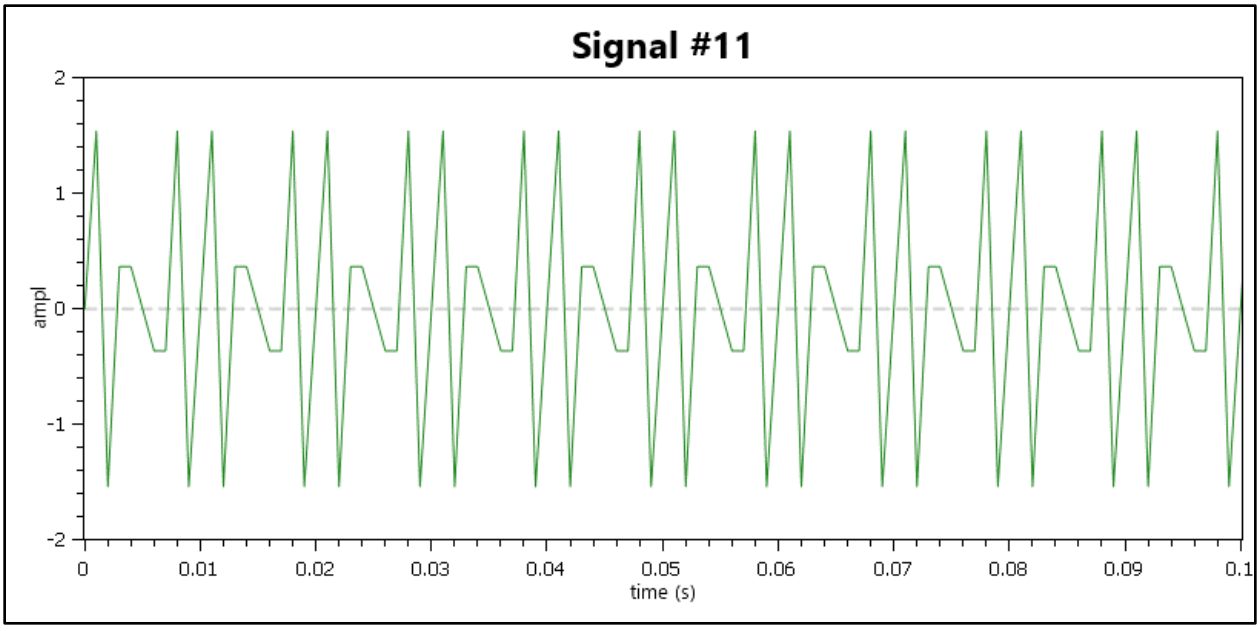


***Figure 3-41 Signal #11 Plot - Time vs. Amplitude***

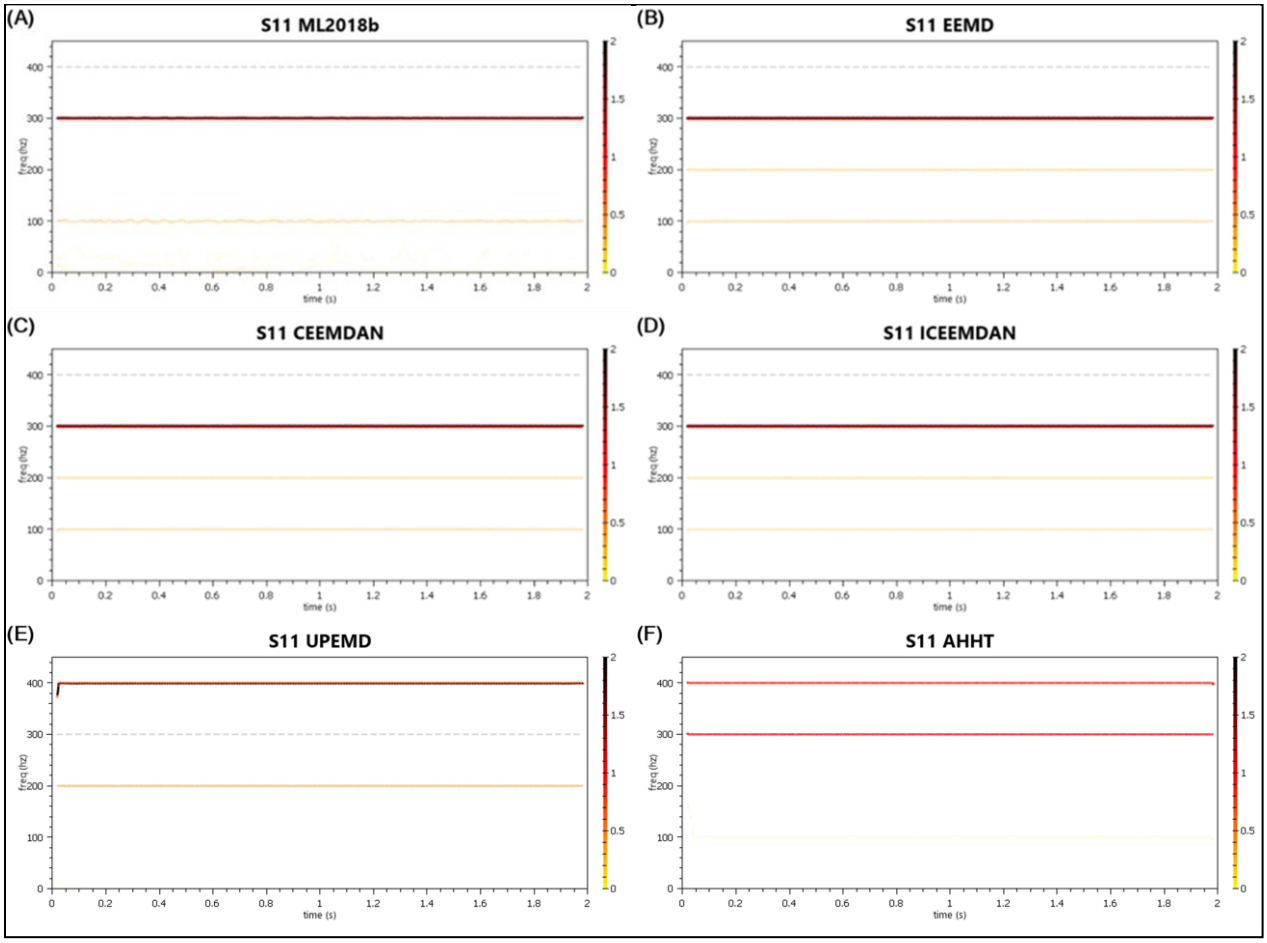


*Figure 3-42 Signal #11 - Decomposition Comparison in the Hilbert Spectrum*

*Table A-1 IMF Count and QoD Values Associated with Signal #11 EMD Results*

| | MATLAB EMD | EEMD | CEEMDAN | ICEEMDAN | UPEMD | AHHT |
|---|---|---|---|---|---|---|
| **Signal #11 – 2 Component Signals** | | | | | | |
| # of IMFs + Res | 9 | 12 | 13 | 3 | 10 | 3 |
| $QoD_1$ | 0.013308 | 0.000238 | 0.000113 | 0.004813 | 0.000559 | **0.576315** |
| $QoD_2$ | 0.526655 | 0.61775 | 0.618331 | 0.494555 | 0.456143 | **0.055918** |

The AHHT system is the only one able to decompose this signal well.

## 3.13 SIGNAL #12 – DECOMPOSING MULTIPLE, INTERMITTENT RIDING WAVES

Signal #12 is similar to Signal #10 except that the low frequency component is lower by a third, there are two different riding waves at different frequencies and amplitudes, appearing only once, and not necessarily at the extrema. It is defined:

$$f_{sig_{12}}(t) = s_1(t) + s_2(t) + s_3(t), \quad (sampled\ at\ 1\ kHz) \qquad 3:12:1$$

$$s_1(t) = 0.1 * sin(40 * 2\pi t), \quad 0.5 \leq t \leq 0.6 \qquad 3:12:2$$

$$s_2(t) = 0.35 * sin(5 * 2\pi t), \quad 1.2 \leq t \leq 1.4 \qquad 3:12:3$$

$$s_3(t) = sin(1.75 * 2\pi t), \quad 0 \leq t \leq 2.4 \qquad 3:12:4$$

The plot of this signal is depicted in Fig. [3-44]. The Hilbert spectrum of the decompositions of this signal are given in Fig. [3-55]. Note, transparency has been turned off for these depictions.

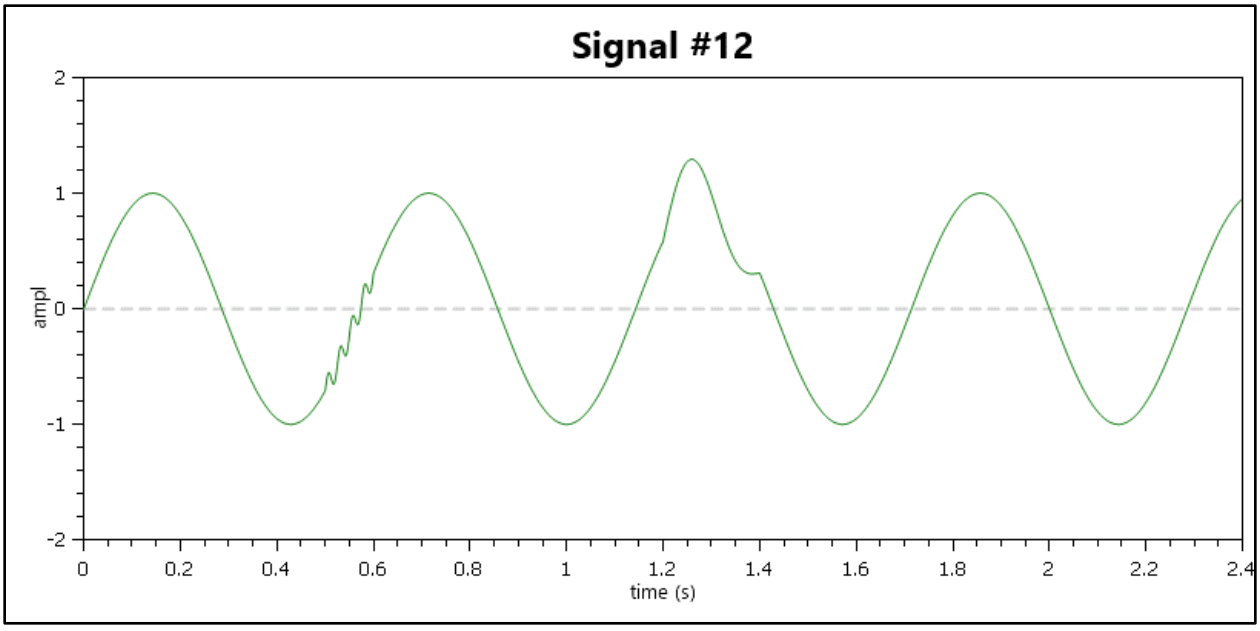


***Figure 3-43 Signal #12 Plot - Time vs. Amplitude***

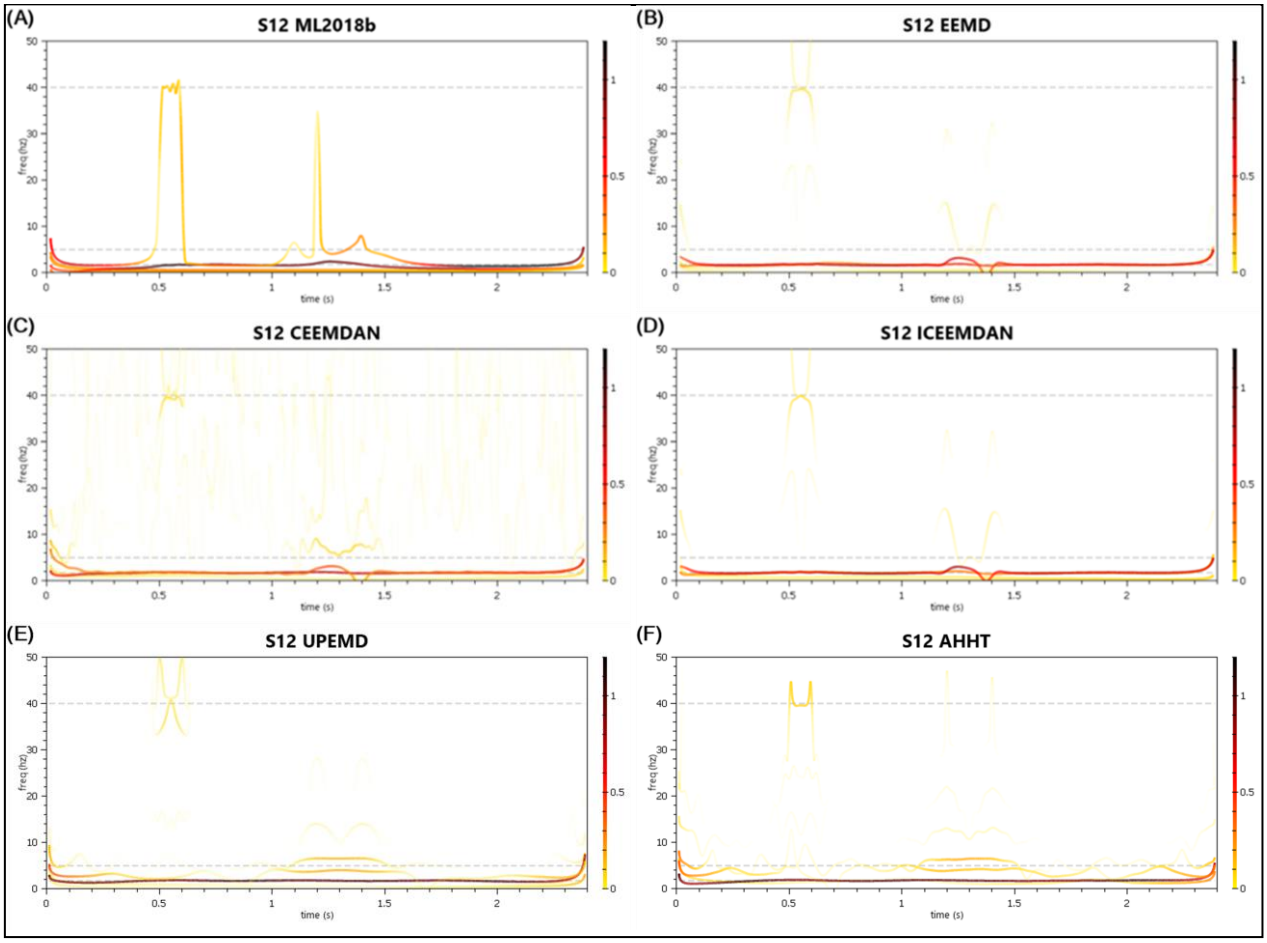


*Figure 3-44 Signal #12 - Decomposition Comparison in the Hilbert Spectrum*

*Table A-1 IMF Count and QoD Values Associated with Signal #12 EMD Results*

| | MATLAB EMD | EEMD | CEEMDAN | ICEEMDAN | UPEMD | AHHT |
|---|---|---|---|---|---|---|
| **Signal #12 – 3 Component Signals** | | | | | | |
| # of IMFs + Res | 5 | 11 | 11 | 9 | 11 | 7 |
| $QoD_1$ | 0.033761 | 0.021324 | -0.02086 | -0.0067 | **0.272741** | 0.263005 |
| $QoD_2$ | 0.578082 | 0.435397 | 0.424518 | 0.404332 | 0.203293 | **0.120043** |

It's hard to qualify these results. The Fourier transform of this signal shows no presence of the 40 Hz signal and little evidence of the 5 Hz signal. However, all seem adequate to the task of detection. The UPEMD has better QoD scores, but AHHT more clearly identifies the 40 Hz signal. Both the UPEMD and AHHT are the only ones that correctly extract the carrier wave ($S_3$) from the riding components with fidelity to amplitude and without significant mode-mixing. The major culprit of the poor extraction of the 5 Hz component lies in AHHT's pattern recognition. The peak at time step 1.4s appears as a higher

frequency component and is removed in a series of transient IMFs (~20 Hz and ~13 Hz), transforming the extrema.

## 3.14 ECG SIGNAL– DECOMPOSING A REAL-WORLD SIGNAL

The ECG signal, plotted in Fig. [3-46], is from the MIT-BIH Normal Sinus Rhythm Database—specifically the first 10 seconds of the first channel of record 16265 sampled at 128 Hz. This signal was chosen as it has been commonly used for assessing the potential for EEMD-based variants to act on real-world data and is referenced and provided in the ICEEMDAN code base [53].

According to a review of literature provided by Elgendi *et al.* in [54], the ECG QRS complex is typically found in the 8-20 Hz band. Since the QRS complex in this signal was, by manual measurement, appearing every ~0.08 seconds, an arbitrary line was added to the HHT plots at that frequency (12 Hz). Stress should be placed on the fact that this is indicative only of the actual frequency of the entire spike, not that of which it is composed. In fact, spikes like this will be composed of multiple sub-signals, since it

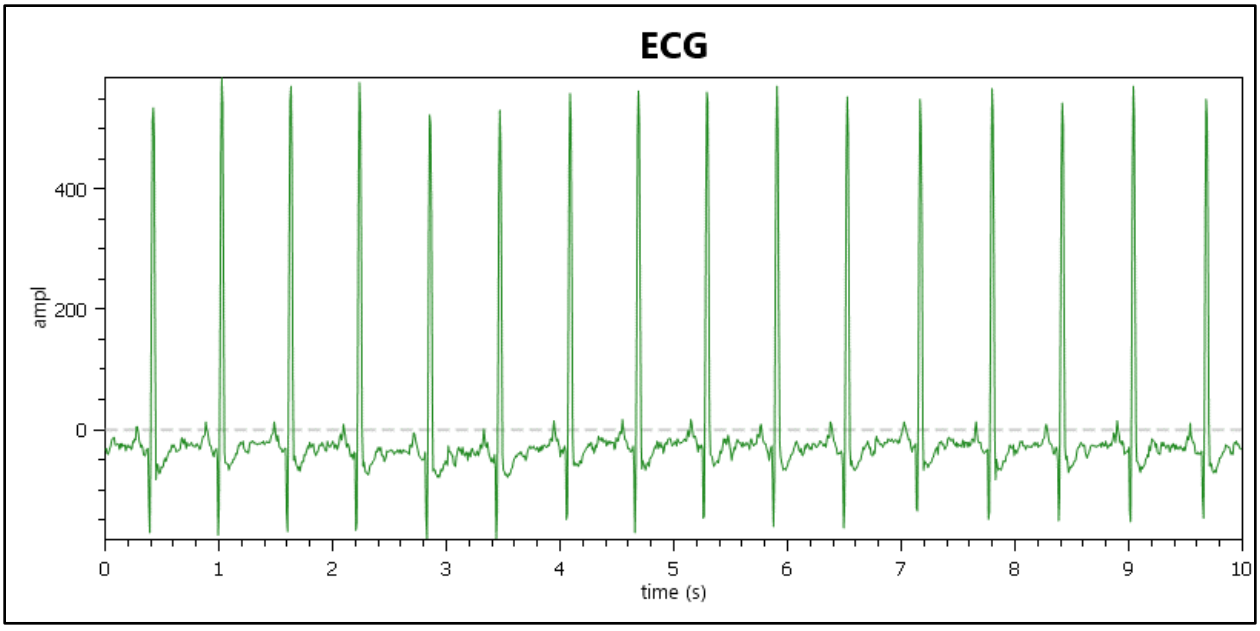


***Figure 3-45 ECG Signal Plot - Time vs. Amplitude***

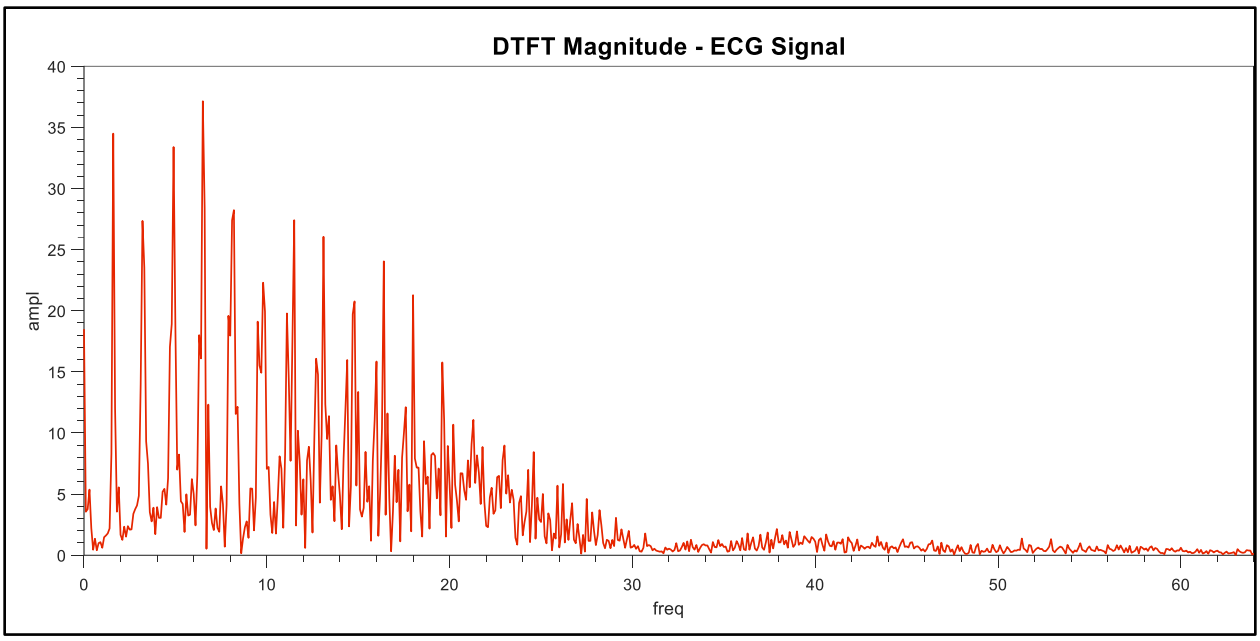


***Figure 3-46 ECG Signal - FFT Magnitude Plot***

is not a well-formed IMF (violates the 2nd property: mean equal to zero). However, as additional validation, the DTFT was applied to this signal and the amplitude of the results are plotted in Fig. [3-47].

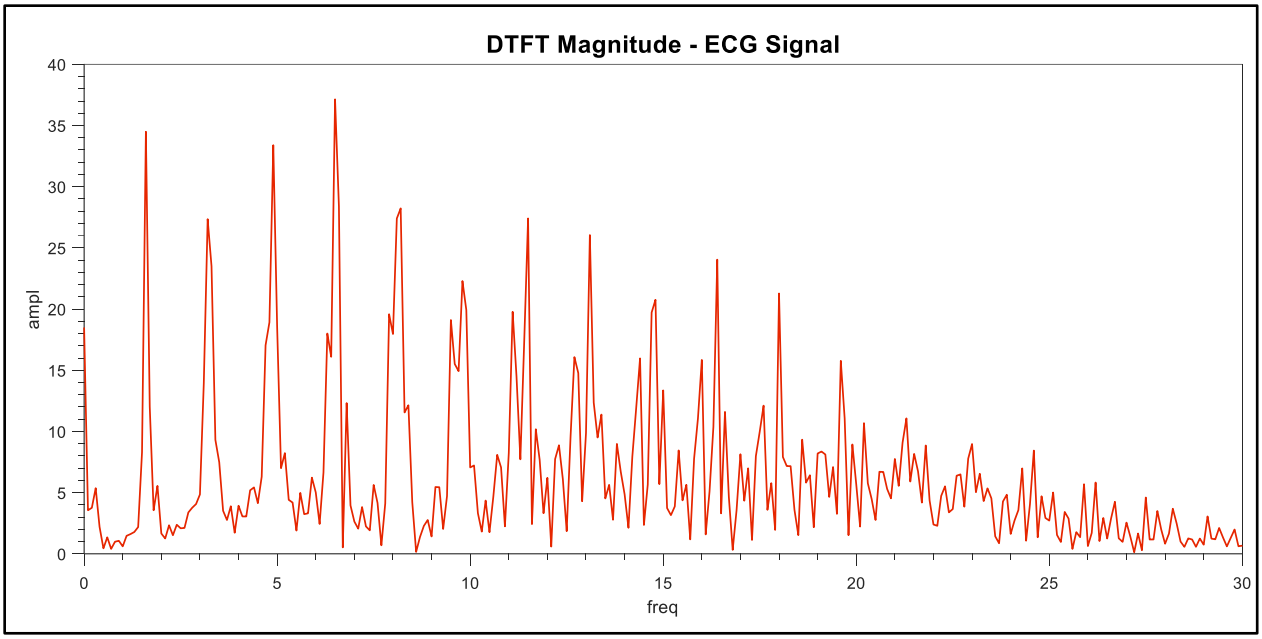


***Figure 3-47 ECG Signal - FFT Magnitude Plot - Narrowed Focus***

Clearly, there is little meaningful to be found above 30 Hz except for low-level noise. What *is* noteworthy are the almost-uniformly-spaced modes clearly visible in the spectrum. A closer inspection is given in Fig. [3-48].

According to this FFT result, we would expect to find meaningful modes at or near the Hertzian frequencies 1.6, 3.2, 4.9, 6.5, 8.3, 9.7, 11.3, 12.9, 14.6, 16.2, 17.8, and 19.6. Like Signals #1 -> #5, this ECG signal has been examined in its ideal state (as found in the database), and subsequently with Gaussian additive noise at SNR levels: 20dB, 10dB, 5dB, 0dB, and -5dB. The Hilbert spectrums of the decompositions of the original signal are shown in Fig. [3-49].

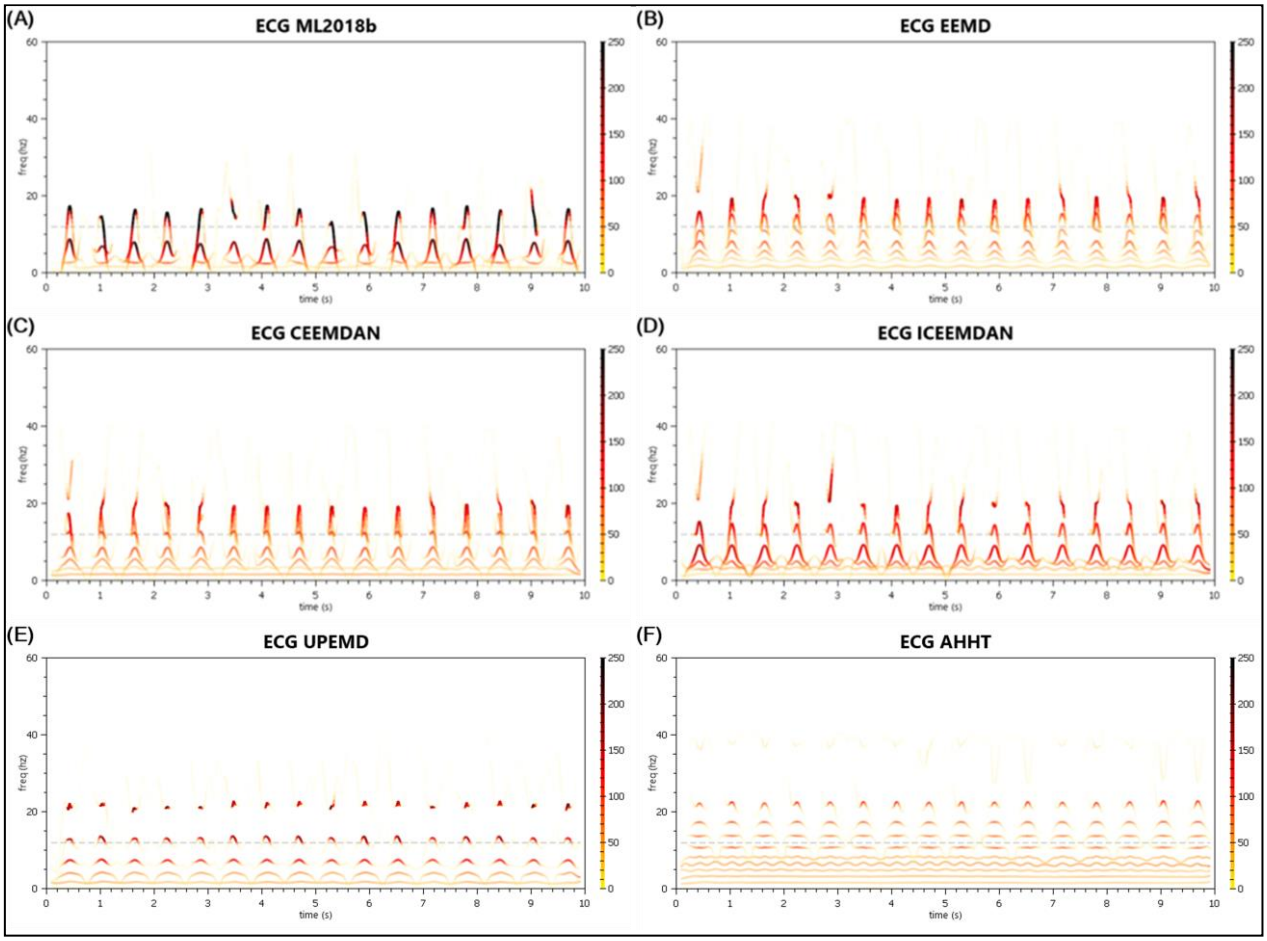


***Figure 3-48 ECG Signal - Decomposition Comparison in the Hilbert Spectrum***

***Table A-1 IMF Counts Associated with ECG Signal EMD Results***

| | MATLAB EMD | EEMD | CEEMDAN | ICEEMDAN | UPEMD | AHHT |
|---|---|---|---|---|---|---|
| # of IMFs + Residual | 7 | 12 | 10 | 8 | 10 | 10 |

The amplitude of the modes depicted in each of these signal decompositions are dramatic. The AHHT has the most reduced amplitudes due to the greater separation of modes. Relative to the AHHT, the colors in the upper spectrum of the other decompositions indicates a great deal more energy. This is because many of the modes of the signal are being conflated in those decompositions, which causes an increase in the amplitude discovered there. After the AHHT results, the next best results seem to be those provided by the EEMD which starts to find many of the lower modes in the signal. The AHHT decomposition, however, is evidently superior for at the lower end of the spectrum, the resolution of the AHHT is sufficient to realize the first six modes which no other decomposition is doing.

When considering the DTFT magnitude plot of Fig. [3-48], it can be seen that above the 8.3 Hz mode, the other modes in the signal are still separated by a near constant distance, yet at a decreasing ratio of frequency from each other. For example, while the difference between the $8^{th}$ and $7^{th}$ modes is 1.6 Hz (12.9 - 11.3 = 1.6 Hz of separation), likewise the distance between the $2^{nd}$ and $3^{rd}$ modes is 1.6 Hz (3.2 - 1.6 = 1.6 Hz of separation). Comparatively, it is also true that 1.6 is half the frequency of 3.2, but 11.3 is 87.6% of 12.9. So, the higher modes begin to resolve together in the AHHT decomposition above 8.3 Hz. In fact, this is the problem with all of the other decompositions, they simply have much coarser resolution than the AHHT. The AHHT extracts the 9.7 Hz & 11.3 Hz modes together, the 12.9 Hz & 14.6 Hz modes together, and the 16.2 & 17.8 Hz & (maybe) the 19.6 modes together.

All of the AHHT plots generated in this thesis, to this point, have used a decrease in the frequency spectrum testing of 0.5 * *bw*, where *bw* represents a bandwidth variable associated with the EFM-EMD technique being employed. So, for example, above 65% of the Nyquist rate, *bw* takes on the value of

0.1. Between 1.5% and 65% of the Nyquist rate, when the EFM-EMD2 takes over the decomposition duties, *bw* becomes 0.15 to account for the lower resolution capabilities of the EFM-EMD2. So, as the AHHT System steps down through the frequency spectrum searching for meaningful components to mask against, it does so in increments of 0.5 * *bw*. The exception to this rule is that while it steps down from the last unsuccessful test in this way, in the case of a successful test, it steps down from the associated mask frequency. By way of example, if a test at 200 Hz (with Nyquist at 500 Hz) fails to find a meaningful component, the next test would occur at 185 Hz. $(200 - 0.5 * bw * 200)$. On the other hand, assuming a component was estimated at 195 Hz after the 200 Hz frequency was tested, then the next test would occur at 180.375 Hz $(195 - 0.5 * bw * 195)$. But this half bandwidth stepping is somewhat arbitrary. It is a compromise between the need for performance and for high resolution. The AHHT System provides for an experimental high-resolution switch that reduces the fraction of the bandwidth to: 0.25 * *bw*. The switch also reduces the handover threshold between EFM-EMD1 and EFM-EMD2 from 65% of the Nyquist rate to 55% of the Nyquist rate. When engaging the high-resolution switch, the decomposition is compelling, as seen in Fig. [3-49].

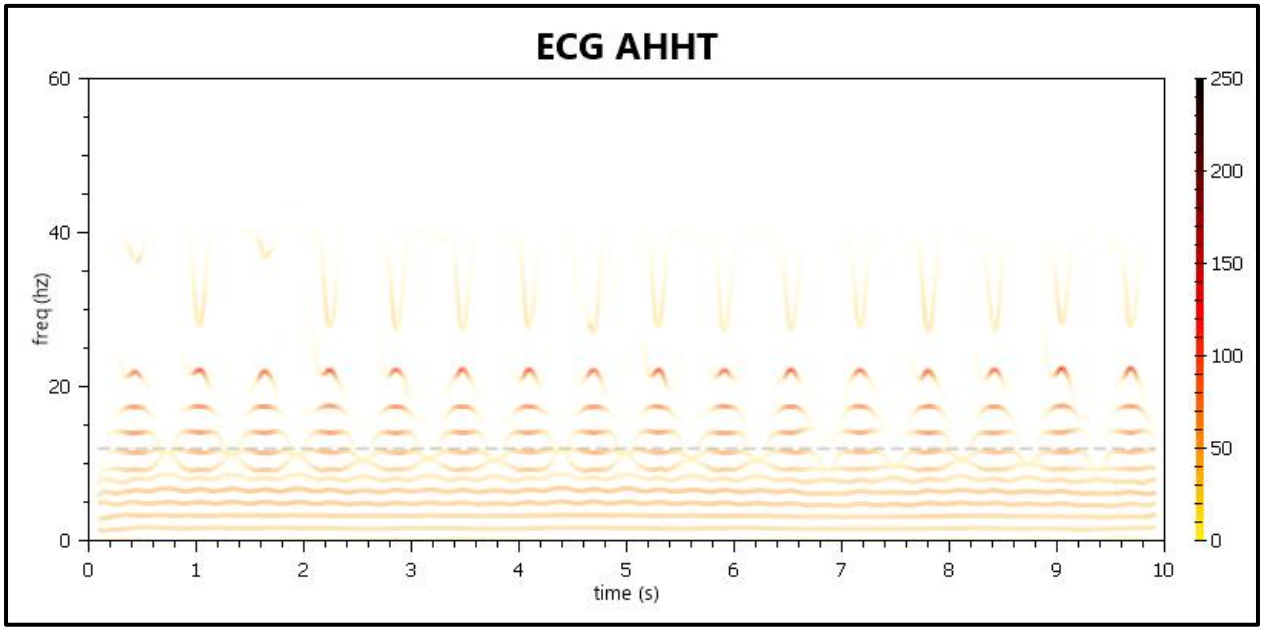


***Figure 3-49 Changed resolution testing parameters to demonstrate resolution capability***

Now the first 7 modes are clearly extracted, modes 8 & 9 are extracted in one IMF, and modes 10, 11, & 12 are extracted in one IMF. This high resolution switch, however, while good for this real world signal where frequency is continous across the spectrum, was often inferior on certain artificial signals and also exhibited slower execution speed.

Again, noise was added such that the signal's SNR is 10 dB and subsequently decomposed. The Hilbert spectrums of those decompositions are given in Fig. [3-50]. Obviously, 10 dB of noise is significant in this signal, since the signal has very large intermittent components. The high-resolution switch was turned off to preserve consistency with the other demonstrated examples in this thesis. More work needs to be done to stabilize the process at these resolutions. Still, for real-world signals, it is worth considering higher resolution decompositions.

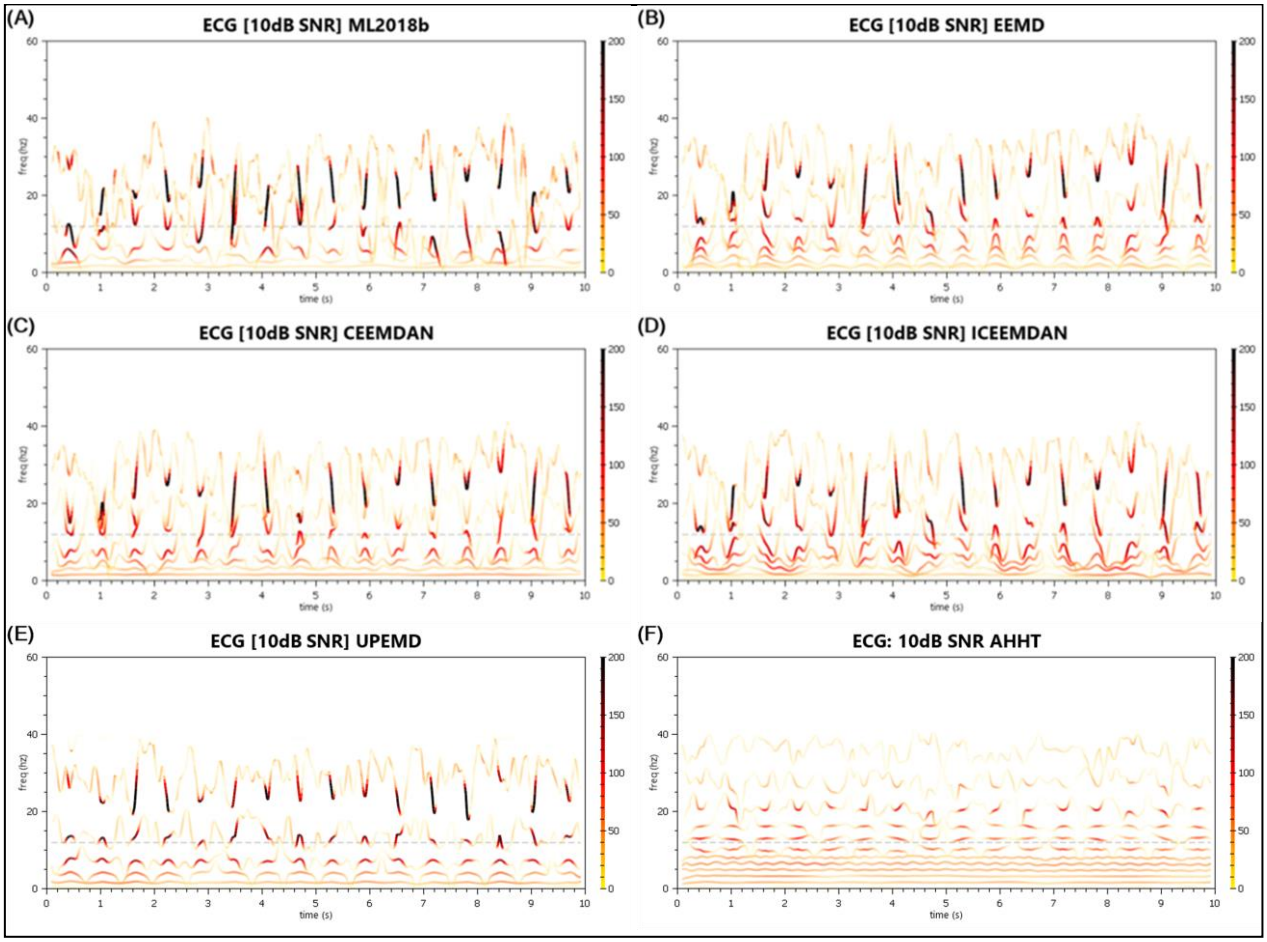


***Figure 3-50 ECG Signal (10dB SNR) - Decomposition Comparison in the Hilbert Spectrum***

In noise, the AHHT performs very well at extracting the relevant modes in the signal. After the AHHT, the next best decompositions have lost almost all of their information on upper frequency modes to the noise.

## 3.15 APPLICATION TO SEMG DATA—FREQUENCY SHIFT DETECTION OVER TIME AND FATIGUE

Using the continuous wavelet transform—Daubechies-4 wavelet—Croce et al. showed in [50] that as muscular fatigue increases, there is an associated decrease in the frequency spectrum of the surface electromyographical (SEMG) recordings of those muscles. The protocol of the given experiment was leg extension trials across 10 subjects where each subject was given the task of maximum-effort, reciprocal flexion-extension movements until volitional muscular exhaustion triggered cessation of movement. During these repetitions, continuous SEMG monitoring recorded data from the rectus femoris, vastus medialis, and vastus lateralis. Note: In this thesis, the focus is entirely on the data produced from the rectus femoris due to its greater reliability (the sensors had greatest stability at this location). According to Croce et al., there was a significant reduction in the frequency content as the subjects began to fatigue. They hypothesized that the cause of this reduction in frequency content is due to the changing nature of muscle recruitment brought about by fatigue—fast-twitch muscles are recruited early and tire quickly, while slow-twitch muscles show greater long-term resiliency.

The results provided by Croce et al. are reproduced in Table [3-21]. The values provided are the mean frequency and standard deviation at various percentages of the complete experiment for each subject and then averaged across subjects. For example, under 15%RC, is seen the values associated with the frequency spectrum averaged across subjects after 15% of the leg-extension repetitions were completed.

***Table A-1 Mean & Std. Deviation Values of Frequency Content Across All Subjects as Published by Croce et al.***

| | 1%RC | 15%RC | 30%RC | 45%RC | 60%RC | 75%RC | 90%RC | 100%RC |
|---|---|---|---|---|---|---|---|---|
| Mean | 71.25 | 58.45 | 52.15 | 50.65 | 50.20 | 48.03 | 46.75 | 46.05 |
| SD | 12.67 | 14.86 | 10.26 | 10.92 | 10.06 | 5.60 | 5.88 | 7.50 |

An alternative—and probably more meaningful—result was given by normalizing against the first percent of repetition completed and generating changing percentage values. Those values are given in Table [3-22].

***Table A-2 Normalized Mean & Std. Deviation Values of Frequency Content Across All Subjects as Published by Croce et al.***

| | 1%RC | 15%RC | 30%RC | 45%RC | 60%RC | 75%RC | 90%RC | 100%RC |
|---|---|---|---|---|---|---|---|---|
| Mean | 1.00 | 1.21 | 1.32 | 1.26 | 1.20 | 1.14 | 1.25 | 0.97 |
| SD | 0.00 | 0.28 | 0.37 | 0.25 | 0.29 | 0.36 | 0.25 | 0.19 |

Unfortunately, the reduction in frequency shifting was not as clearly visible here. Also, there is an apparent error in the data presentation in that the first column likely should have been labeled as being normalized according to the first repetition completed, not the first 1% of repetitions complete (as only equal frequency means throughout the 1% of RC per subject could give a standard deviation of zero).

Signal Pre-Processing:

For the EMD decompositional comparison, only the data from six of the subjects were examined. Since the SEMG data was recording continuously, segmentation was used to isolate repetitions. Each repetition was isolated to just the periods of extension from 180° to 0°—from leg down to leg extended. The first two reps and last two reps for each subject were excluded as potential outliers leaving 90 to 621 reps (depending on the subject) to be decomposed.

Analysis Protocol:

Since each subject has unique SEMG anomalies due to various factors such as skin impedance, sensor placement, and environmental interference, as well as biological differences, it was desirable to look at the percentage of shift rather than raw values. To that end, the protocol adopted was to first project the Hilbert spectrum against frequency bins at half-Hertzian resolution with amplitude summation. For example, the decomposition of an arbitrary repetition as shown in Fig. [3-51] leads to the projection shown in Fig. [3-52]. From this amplitude/frequency plot, a weighted mean and weighted standard deviation (SD) is calculated. In the case given, that weighted mean/SD is 107.929/86.732. Note, the high-resolution switch was enabled for all AHHT decompositions of the SEMG data.

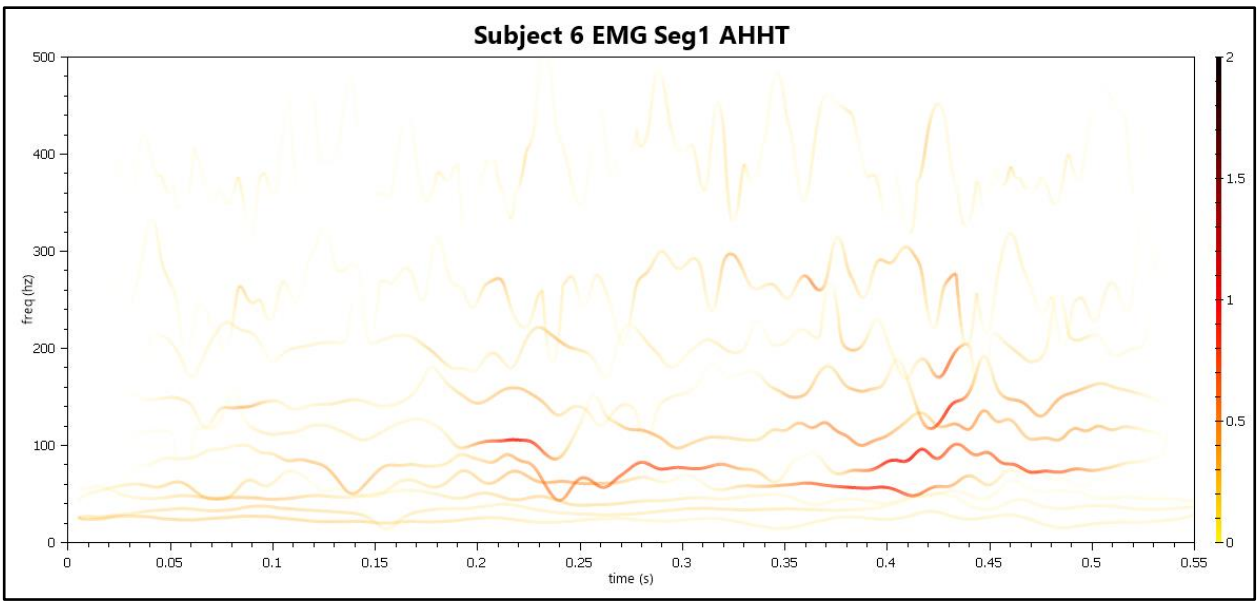


*Figure 3-51 SEMG Hilbert Spectrum - First Decomposed Repetition Complete for Subject 6 by AHHT*

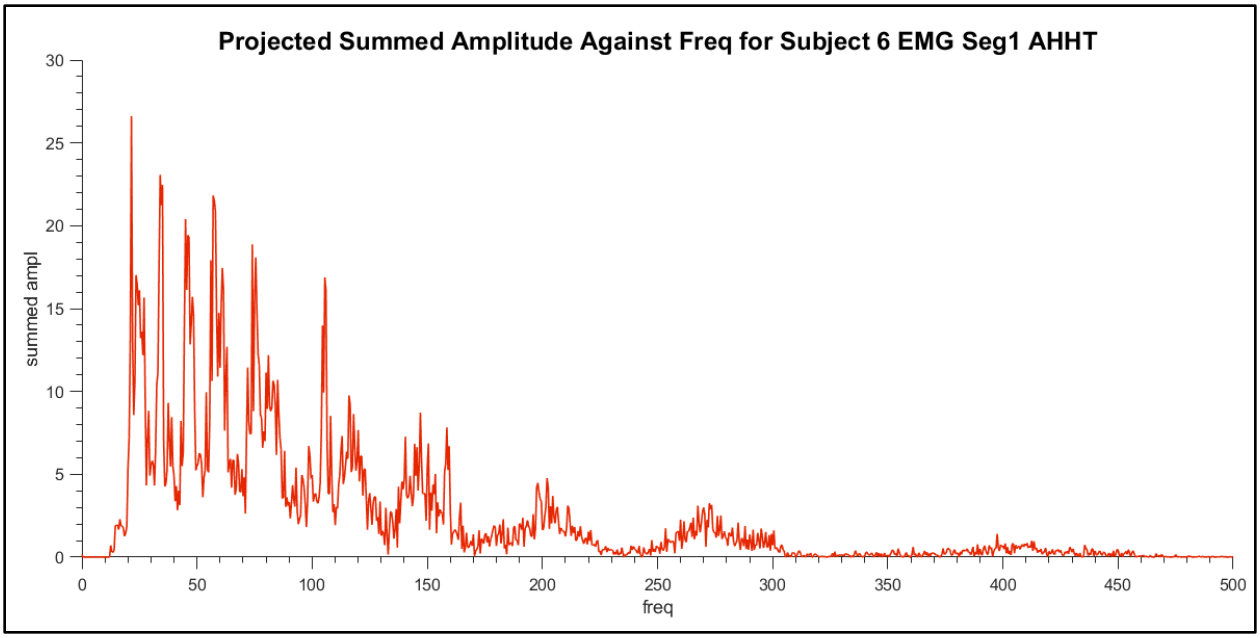


*Figure 3-52 SEMG Hilbert Spectrum Freq./Ampl. Projection - First Decomposed Repetition Complete for Subject 6 by AHHT*

The goal, then, was to normalize the weighted means and weighted standard deviations. The formula for the weighted mean is given in 3:13:1:

$$\widehat{\mu^*} = \frac{\sum_{i=1}^{N} w_i x_i}{\sum_{i=1}^{N} w_i} \qquad 3:13:1$$

In 3:13:1, $w_i$ represents the *i*-th weight and $x_i$ represents the sample. From the plot in Fig. [3-52], the amplitude represents the weights, while frequency represents the sample. From the weighted mean, the weighted standard deviation can be derived. It is given in 3:13:2.

$$\widehat{\sigma^*} = \sqrt{\frac{\sum_{i=1}^{N} w_i (x_i - \overline{x^*})^2}{\frac{M-1}{M} \sum_{i=1}^{N} w_i}} \qquad 3:13:2$$

In 3:13:2, *M* represents the number of non-zero weights. From this it is clear that the weighted standard deviation cannot be normalized without first shifting and rescaling the individual samples that contribute to the normalized weighted means. So, first the maximum and minimum weighted mean was found for each subject. Since summation and scaling are linear operations, the actual frequency bins for each subject were shifted down by the minimum and divided by the difference of the maximum and minimum. The weighted mean and standard deviation were then recalculated.

For a given subject:

1. An array of weighted means $\overline{\widehat{\mu^*}}$ were generated from the array of HHTs generated from the set of individually isolated completed repetitions.
2. Shift factor α and scale factor β were generated by:

$$\alpha = min(\overline{\widehat{\mu^*}}) \qquad 3:13:3$$

$$\beta = max(\overline{\widehat{\mu^*}}) - min(\overline{\widehat{\mu^*}}) \qquad 3:13:4$$

3. Since frequency bins were initially standardized to 0.5Hz, the shifting/scaling value applies equally:

$$x = \beta * (bin_{freq} - \alpha) \qquad 3:13:5$$

4. By equation 3:13:1 and 3:13:2, new weighted means and standard deviations were calculated.

The above procedure produced weighted means that ranged from 0 to 1 for every subject. Then those weighted means were themselves averaged across the same range of repetitions complete as was done in the paper by Croce *et al.* However, it was not clear from the paper whether the values at each percentage RC were instantaneous or cumulative; it was unclear whether the mean values calculated for a given %RC were such that the samples in lower %RC calculations were included or excluded. So, both possibilities were computed, and the results can be found in Tables [3-23] and [3-24] respectively. When looking at the overall mean of mean values—which are analogous values to those found in Table [3-22], it is clear that there is more variance in the results presented in the instantaneous results and more stability in the cumulative results, as would be expected; the latter coincides more with the published data.

*Table A-3 Mean of Instantaneous Normalized Weighted Means/SDs of SEMG Decomposition HHT Projections for All Subjects by Percentage of Repetitions Complete.*

| | | 1%RC | 15%RC | 30%RC | 45%RC | 60%RC | 75%RC | 90%RC | 100%RC |
|---|---|---|---|---|---|---|---|---|---|
| Mean | Subj.1 | 0.712 | 0.862 | 0.673 | 0.518 | 0.381 | 0.413 | 0.381 | 0.245 |
| SD | 90 Reps | 1.611 | 1.606 | 1.475 | 1.361 | 1.273 | 1.321 | 1.270 | 1.273 |
| Mean | Subj.2 | 0.857 | 0.696 | 0.277 | 0.117 | 0.061 | 0.374 | 0.194 | 0.119 |
| SD | 121 Reps | 1.532 | 1.202 | 0.901 | 0.780 | 0.791 | 0.981 | 0.867 | 0.818 |
| Mean | Subj.3 | 0.818 | 0.435 | 0.368 | 0.437 | 0.499 | 0.565 | 0.588 | 0.577 |
| SD | 612 Reps | 1.261 | 0.965 | 0.957 | 1.008 | 1.042 | 1.065 | 1.073 | 1.057 |
| Mean | Subj.4 | 0.753 | 0.775 | 0.435 | 0.230 | 0.141 | 0.347 | 0.196 | 0.156 |
| SD | 207 Reps | 1.716 | 1.629 | 1.318 | 1.259 | 1.184 | 1.360 | 1.274 | 1.232 |
| Mean | Subj.5 | 0.745 | 0.480 | 0.199 | 0.218 | 0.321 | 0.300 | 0.242 | 0.228 |
| SD | 395 Reps | 1.597 | 1.178 | 0.993 | 1.019 | 1.063 | 1.009 | 0.959 | 0.942 |
| Mean | Subj.6 | 0.914 | 0.599 | 0.270 | 0.136 | 0.107 | 0.313 | 0.192 | 0.163 |
| SD | 317 Reps | 1.171 | 0.993 | 0.829 | 0.741 | 0.724 | 0.829 | 0.733 | 0.729 |
| **Mean** | **Overall** | **0.800** | **0.641** | **0.370** | **0.276** | **0.252** | **0.385** | **0.299** | **0.248** |
| SD | **Mean** | 0.070 | 0.153 | 0.155 | 0.150 | 0.159 | 0.089 | 0.145 | 0.153 |
| Means | Overall | 1.481 | 1.262 | 1.079 | 1.028 | 1.013 | 1.094 | 1.029 | 1.009 |
| SDs | Std. Dev | 0.197 | 0.266 | 0.235 | 0.227 | 0.197 | 0.189 | 0.199 | 0.200 |

*Table A-4 Mean of Cumulative Normalized Weighted Means/SDs of SEMG Decomposition HHT Projections for All Subjects by Percentage of Repetitions Complete.*

| | | 1%RC | 15%RC | 30%RC | 45%RC | 60%RC | 75%RC | 90%RC | 100%RC |
|---|---|---|---|---|---|---|---|---|---|
| Mean | Subj.1 | 0.712 | 0.852 | 0.766 | 0.681 | 0.609 | 0.568 | 0.538 | 0.509 |
| SD | 90 Reps | 1.611 | 1.606 | 1.543 | 1.481 | 1.431 | 1.408 | 1.386 | 1.375 |
| Mean | Subj.2 | 0.857 | 0.705 | 0.491 | 0.366 | 0.290 | 0.304 | 0.287 | 0.271 |
| SD | 120 Reps | 1.532 | 1.221 | 1.061 | 0.967 | 0.924 | 0.932 | 0.923 | 0.913 |
| Mean | Subj.3 | 0.818 | 0.460 | 0.414 | 0.422 | 0.441 | 0.466 | 0.486 | 0.495 |
| SD | 612 Reps | 1.261 | 0.984 | 0.971 | 0.983 | 0.998 | 1.011 | 1.022 | 1.025 |
| Mean | Subj.4 | 0.753 | 0.773 | 0.604 | 0.479 | 0.395 | 0.385 | 0.354 | 0.334 |
| SD | 207 Reps | 1.716 | 1.635 | 1.476 | 1.404 | 1.349 | 1.351 | 1.338 | 1.327 |
| Mean | Subj.5 | 0.745 | 0.498 | 0.348 | 0.304 | 0.309 | 0.307 | 0.296 | 0.289 |
| SD | 395 Reps | 1.597 | 1.206 | 1.099 | 1.072 | 1.070 | 1.058 | 1.041 | 1.031 |
| Mean | Subj.6 | 0.914 | 0.618 | 0.446 | 0.342 | 0.284 | 0.290 | 0.274 | 0.263 |
| SD | 317 Reps | 1.171 | 1.004 | 0.917 | 0.858 | 0.825 | 0.826 | 0.810 | 0.802 |
| **Mean** | **Overall** | **0.800** | **0.651** | **0.512** | **0.432** | **0.388** | **0.387** | **0.373** | **0.360** |
| SD | **Mean** | 0.070 | 0.141 | 0.138 | 0.125 | 0.114 | 0.101 | 0.103 | 0.103 |
| Means | Overall | 1.481 | 1.276 | 1.178 | 1.128 | 1.100 | 1.098 | 1.087 | 1.079 |
| SDs | Std. Dev | 0.197 | 0.260 | 0.243 | 0.232 | 0.220 | 0.212 | 0.209 | 0.208 |

These results are quite in-line with the results provided by Croce *et al.*, though perhaps clearer. But there is still a better way to view this data. It turns out that the frequency shift is subject independent. Fig. [3-53] depicts the weighted means plotted against each repetition that gave rise to those means. At a glance, it appears that the majority of frequency downshifting is front loaded. That is, for all subjects, the downshifting in frequency happened early, regardless of the number of repetitions each subject was able to complete.

Fig. [3-54] is another look at this same data using the normalized weighted means. Once the means are normalized to the same range, the shifting pattern looks a great deal more compelling.

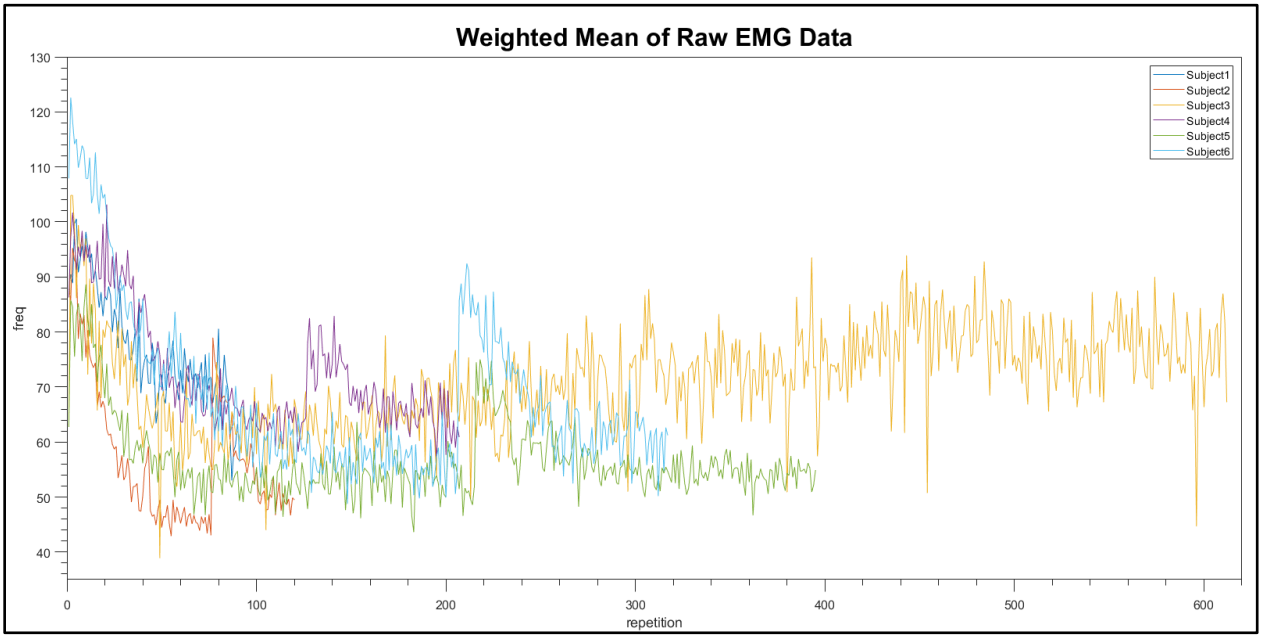


***Figure 3-53 SEMG AHHT-Generated Weighted Means Plot by Subject***

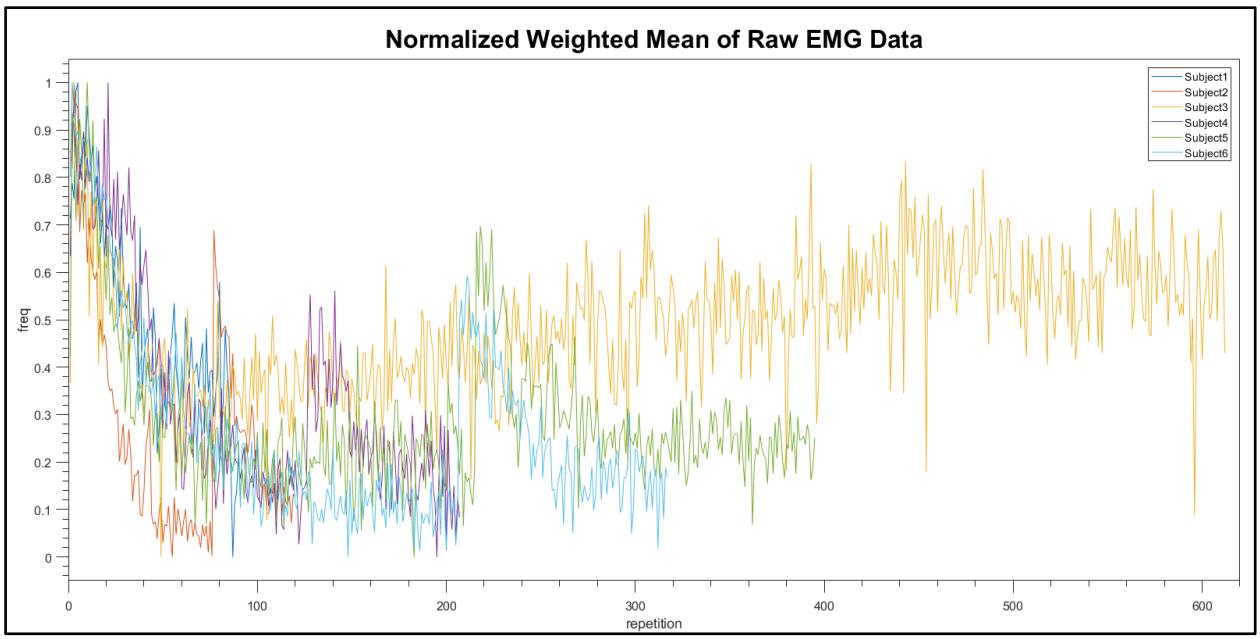


*Figure 3-54 SEMG AHHT-Generated Normalized Weighted Means Plot by Subject*

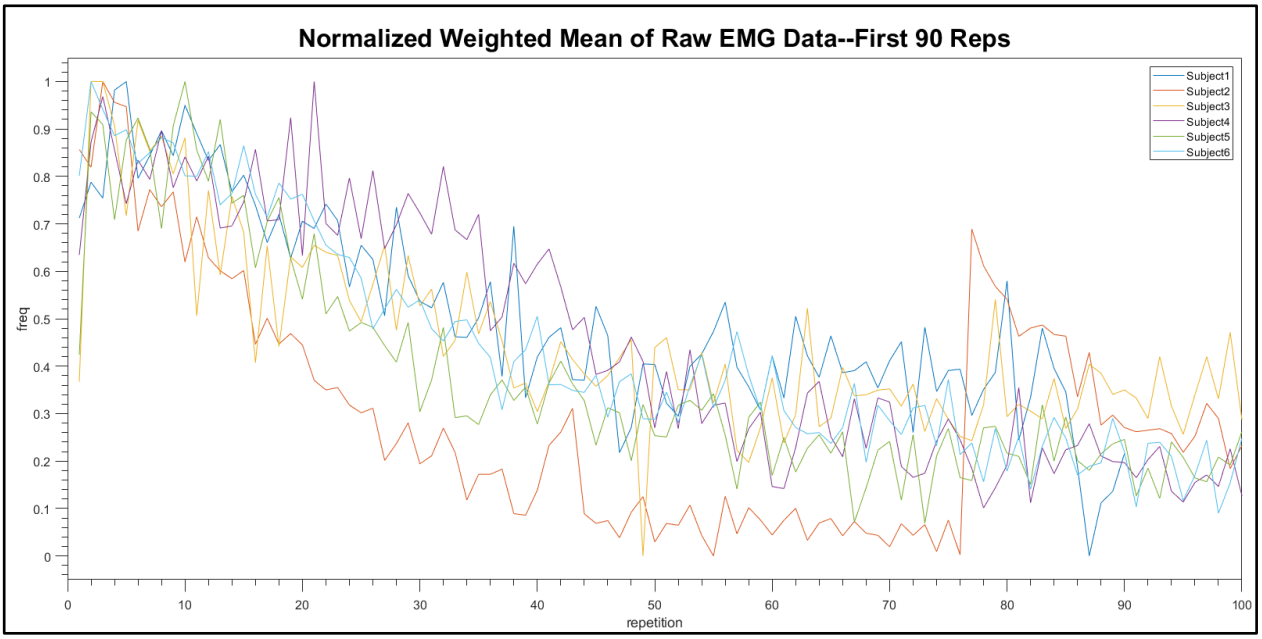


*Figure 3-55 SEMG AHHT-Generated Normalized Weighted Means Plot by Subject - Narrowed*

Fig. [3-55] shows the same normalized data, just narrowed down to just the first 90 repetitions—that is, the number of repetitions for which every subject has a sample.

Applying a 10-sample moving average filter to these signals produces the plot shown in Fig. [3-56].

This clearly lends itself to the proposition that, regardless of subject, frequency shifting is going to occur in roughly the same time frame.

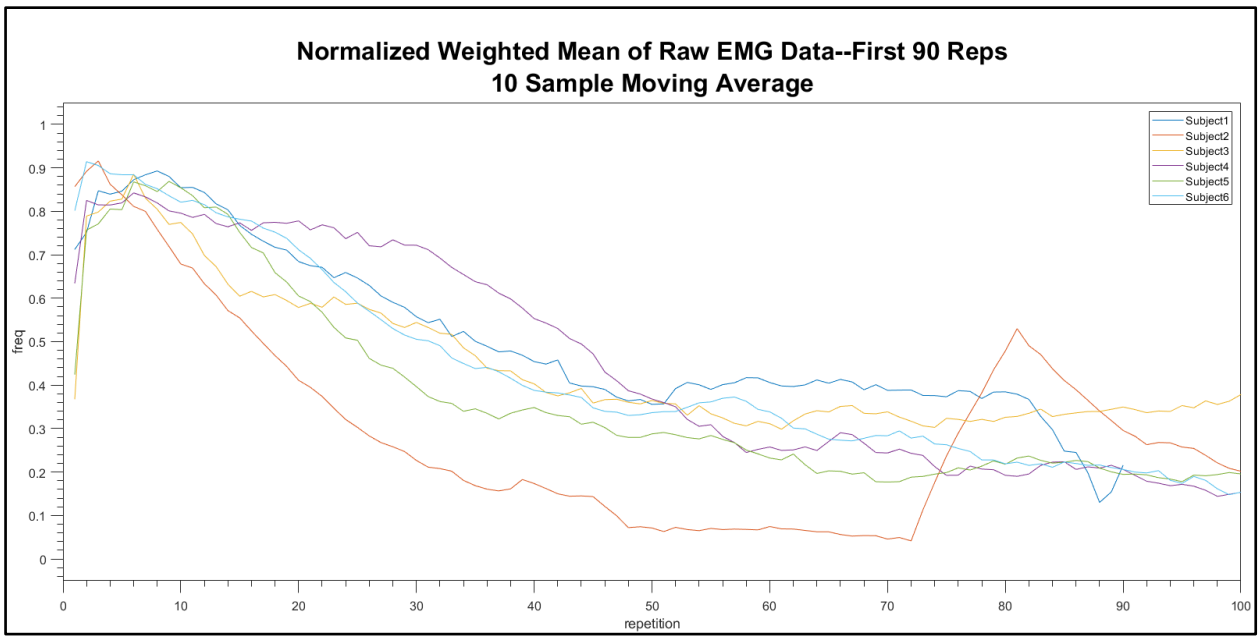


***Figure 3-56 SEMG AHHT-Generated Normalized Weighted Means Plot by Subject - Narrowed - 10 Sample Moving Avg.***

Finally, using the non-averaged data as sample points in the frequency vs. repetition space, a 2nd degree polynomial fit was generated for each subject. The fits were fairly strong with a minimum relative squared residual of 0.691 (Subj. 4) and a maximum of 0.931 (Subj. 6) as shown in Fig. [3-57]. The $R^2$ values here should be not be considered standard correlation metrics, since these data mimic a repeated measures experimental design and as such, each measurement is not independent of prior measurements which is required for accuracy in correlation values as is typical with simple regression. Still, it's clear that despite the anomaly in Subject 2's first 90 repetitions as shown in Fig. [3-56], that there is a similar decay function applicable to each subject that implies frequency shifting is not associated with slow-twitch muscle stamina; that is, the shifting in frequency is not a function of the total number of repetitions able to be completed by a given subject.

Unfortunately, only six of the subjects were examined for this thesis. More subject data might have been able to give greater certainty to these results. This research is fascinating and validates the findings in Croce *et al.* with some caveats.

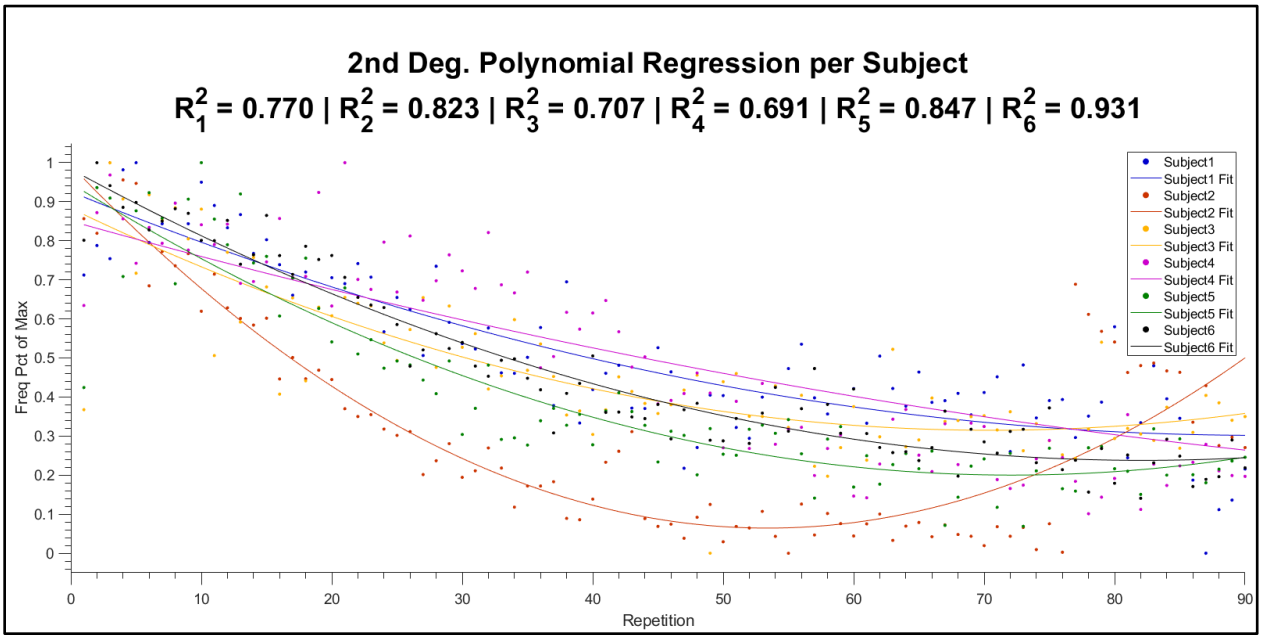


***Figure 3-57 2nd-Degree Polynomial Regression of AHHT-Derived SEMG Normalized Weighted Means***

Though unrelated to that validation, there was an interesting finding that should be reported. The HHT of the first three repetitions examined for a given subject were markedly different than the last three. For example, Subject 6 completed 317 repetitions (after discarding the first two and last two). The plots in Fig. [3-58] represent the Hilbert spectrum of the decomposition of the SEMG recordings of those first and last three repetitions. What is interesting is the obvious volatility in frequency content early in the exercise period vs. the relative stability in the last parts of the exercise. This was visible for all of six of the subjects. As these results are merely produced here for their interest value, they are not also included in Appendix A.

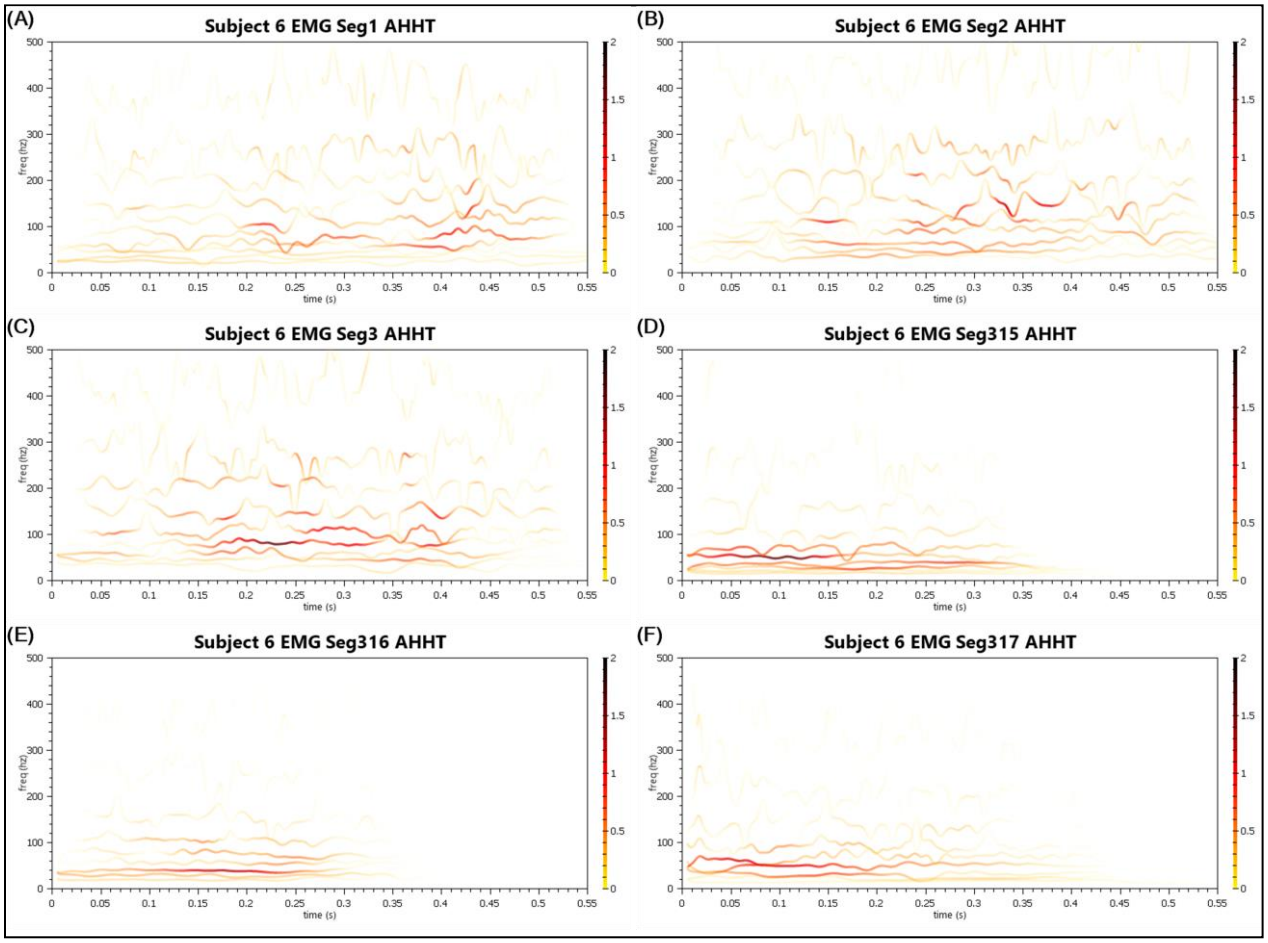


***Figure 3-58 First Three (A, B, C) and Last Three (D, E, F) Hilbert Spectrums of the Rectus Femoris SEMG Decompositions by AHHT of Subject 6 Repetitions***

# Chapter 4

# DISCUSSION

To date, the author knows of no other software tool (system) that has been constructed which allows the management of the HHT in a comprehensive way. This thesis has aimed to provide just that tool. The AHHT System is built to intelligently find the most important components during decomposition and emphasize their extraction. As demonstrated in the background and by the development of the AHHT System, the many different EMD techniques can be viewed as a collection of algorithms that can decompose nonlinear, non-stationary signals. While it is not well-backed by rigorous mathematical explication, comfort should be taken in Heaviside's response to criticisms that his self-derived operational calculus had vague meaning, "Shall I refuse my dinner because I do not fully understand the process of digestion?" The EMD works and can separate frequency and amplitude of signals into meaningful components at each time step. This thesis will hopefully be valuable to anyone who would like to make a more detailed analysis of what needs to be done to improve result on various real-world signals where traditional methods of analysis fail. It is hoped by using this system, better guidance for choice of parameters can be facilitated.

Throughout Chapter 3, the results of the comparisons of prominent algorithms against the AHHT System were provided. With the addition of another artificial signal detailed later in this chapter, there were 40 artificial signals for which meaningful $QoD_1$ values could be calculated. The AHHT System had the best $QoD_1$ values on 36 of them. Of the remaining 4: 2 were competitive with less than 1% difference in $QoD_1$ scores and 2 were competitive with less than 4% difference in $QoD_1$ scores. The UPEMD repeatedly

showed itself to be generally superior to any of the noise-assisted algorithms. Clearly, frequency masking in some form is to be preferred over indeterministic, noise-assisted decompositions.

## 4.1 On Limitations of the AHHT System

Real-world signals are not discrete like the artificial signals presented in the Examples 3.2 - 3.13. Instead, their frequency content is continuous, and meaningfulness becomes a vaguer concept. In the context of the AHHT, it is defined simply as a certain percentage of sufficiently large amplitude components in a given frequency band, or failing that, if there is nothing but higher frequencies evident when testing a band, it takes the lowest of such higher frequencies and uses it as the next mask frequency—a clearing step that often gathers up noise and strips it away for more meaningful component extraction later. Still, information might be in those small samples of high amplitude or large samples of high frequency that are missed. Pattern recognition techniques, optimization techniques, and similar algorithms might be employed to do a better job at pulling out the important components. In fact, the weakest part of the AHHT system is the pattern recognition engine. A more robust approach to the design of such a pattern recognition engine is currently being planned.

There is a resolution limit to the current system. Because there is a small but significant attenuation band at the cutoff frequency created by the frequency mask, any component caught in this band will tend to be split between two frequency bands of IMF extraction. This was evident in the decomposition of the ECG signal (Example 3.14).

Further, the AHHT has difficulty with very low frequency components where the total number of extrema is very small. In these cases, implementing a better boundary extension technique such as the wave extrapolation approach that MATLAB uses might improve the quality of these low frequency IMFs. Also, at very low frequencies, ensemble techniques become much less effective for short signals

because they provide little or no extra extrema to the decomposition step—understanding this and finding a remediation technique would be helpful.

Another significant problem is one that plagues the noise-assisted decomposition algorithms, as well. After the ensemble averaging process is complete, the final mode may not conform well to the required properties of an IMF. Further sifting at this stage would seem to be in order, but in practice seems to degrade the results. More investigation into why this is true would be beneficial and might help answer this important question.

The AHHT System was originally developed as a need to improve the EMD/HHT for use in EEG and BCI work. However, the approach taken to improve the decompositions also led to a very time-consuming process. Although the system was programmed in C#, decomposing a 1280 sample ECG signal under excess noise could still take between 30 seconds and 1 minute. Which is about 1000 times too long for BCI work on similar EEG signals. A much higher performing pattern recognition engine for generating frequency masks would go a long way towards solving this problem.

Also, there are limitations with the QoD values that are explained in 4.3.

## 4.2 On the Quality of Decomposition Metrics

As noted by Zeiler *et al.* in [55]:

> *The most serious drawback of the method* [EMD] *is certainly its* [sic] *lacking any theoretical basis which would allow to evaluate the performance of the algorithm in objective terms. Hence to do so one needs to employ carefully designed toy data to simulate the decomposition process into single modes and the impact of the various*

*parameters and constraints onto the sifting process. Despite all this, EMD has since been applied successfully to solve many practical problems…*

Also, as mentioned in 2.10, J. Huang *et al.* found shortcomings with the Index of Orthogonality proposed by N.E. Huang because it did not show superior values for higher resolution decompositions in all cases. The researchers were displeased that the Index of Orthogonality gave no qualitative measure to the meaningfulness of their decomposition innovations. Their new measures presumably do a better job of measuring the resolution of a decomposition, but still fail to satisfactorily provide meaningful measures. For example, if a decomposition produces perfectly orthogonal IMFs at great resolution, but those IMFs do not match against any of the sub-signals inherent in the signal being decomposed, the measures provided by both N.E. Huang and J.Huang *et al.* become irrelevant. For example, in 3.12, the UPEMD produces two IMFs which should yield high marks by both J. Huang and N.E. Huang measures. But the decomposition is clearly very poor. This would be true of all the 3.12 decompositions; they would have high marks by orthogonality measurements but are all objectively poor decompositions by the eye test, excepting one. That exception being that the AHHT decomposition of that signal is good. Further, neither of these measures would adequately account for Type-I Mode Mixing, since two IMFs might carry similar frequencies, just on different time intervals. By merely testing for correlation at each time step, this type of mode mixing error is missed.

The QoD values seek to solve this by using a source-of-truth as a template against which each decomposition is evaluated. In the spirit of the EMD, this approach does not seek to provide an objective measure of decomposition from inherent properties of the decomposition, but rather is an empirical test. QoD values measure both types of Mode-Mixing, phantom IMFs, transient IMFs, and decomposition resolution. Since the meaningfulness of a decomposition is only quantitatively able to be

evaluated against artificially generated signals, their source components are available to act as that source-of-truth.

For example, when looking at the AHHT decomposition of the ECG signal in its initial state and when under additive Gaussian noise such that the SNR is 20 dB, it is clear there are small differences in how the modes that are shown in the DTFT are extracted by EMD-based techniques around the 12 Hz range. The resolution property of a given decomposition technique causes different modes to take precedence, even though the noise is mostly stripped out of the second signal at this point. The meaningfulness and superiority of the AHHT decompositions in this range is unclear and seems to be the purview of subjective evaluation.

Other improvements to these QoD values can certainly be found, as mentioned in 2.10. Particularly, an algorithm that unfailingly finds the global maximum in the first term of equation 2:22 without being time prohibitive would be useful. Secondly, evaluating the squashing terms more rigorously in equations 2:15 and 2:19 could provide a more (subjectively) useful value. Further consideration should be given to the second term of equation 2:22. Does it actually make sense to subtract the DFs of unmatched IMFs? Also, does the 0.001 constant for thresholding the DFs in 2:21 provide a good boundary for IMF/SS match sufficiency?

# Chapter 5

# Recommendations and Future Investigations

## 5.1 Recommendations

For signals that are not necessary to analyze in real-time or are relatively short with a limited frequency range, AHHT makes a great tool for decomposition and frequency spectrum viewing. The EMD which forms the basis of the AHHT system is suitable for decomposition of signals for which the Fourier transform, the wavelet transform, and the Short-Time Fourier Transform are unsuitable. Firstly, the EMD is applicable to signals that are both nonlinear and nonstationary unlike the aforementioned analysis tools (STFT and wavelets are suitable for nonstationary signals to varying degrees), has excellent temporal resolution at all decomposable frequencies (unlike the STFT which is temporally windowed and wavelets which have variable temporal resolution across the frequency spectrum), and requires no *a priori* knowledge of the signal to begin the decomposition process. Further, unlike with other EMD-based algorithms, with AHHT the components of interest in the signal may be emphasized since pattern recognition is used to prioritize their extraction.

However, for long signals or signals of significant complexity and length that must be analyzed in real-time, a compromise must be made between accuracy and speed. For these kinds of signals, the best technique would probably be that provided by the UPEMD, which still applies frequency masking in ensemble format, but eliminates intelligent mask frequency selection and does not employ considerations such as masking order. The consequence is the loss of resolution and targeted extraction.

One benefit that algorithms such as the UPEMD enjoy is that the IMF profile output is more likely to find a mathematical modeling due to its patterned approach to decomposition. The use of pattern

recognition in AHHT to identify ideal masking frequencies makes the proposition of finding a reasonably simple function to describe its behavior unlikely.

## 5.2 On Further Investigative Directions

There is quite a lot that can still be done.

The AHHT could use with a more rigorous analysis of the nature of the changing attenuation curves and separation resolution with increasing levels of order as the masking frequency progresses through the frequency spectrum starting at the Nyquist rate. The width of the attenuation band, as a percentage of the masking frequency relative to Nyquist was useful in generating a masking frequency shift to improve on decomposition resolution. A rigorous cataloguing of this changing resolution would be highly beneficial to improve upon the accuracy of this system. All these investigations would ideally be done in conjunction with investigating the causes of the anomalous scaling seen with higher order sifting at low frequencies relative to Nyquist.

Additionally, this analysis could be done in conjunction with the investigation into other forms of interpolation. There were two interpolating algorithms employed in the AHHT System (natural cubic Hermite splines and cubic Akima splines), and they were employed in three different schemes. An investigation into additional schemes for interpolation and an analysis of those schemes in practice could possibly lead to better results. The linear-interpolation-based sifting scheme, for example, had the property of being able to separate signals with high resolution well above 50% of the Nyquist rate (25% of the sampling frequency), but also demonstrated odd oscillations in amplitude and anomalous scaling at these frequencies without mask amplitude reduction and had the property of being potentially unstable at low frequencies, especially with order values higher than 1. Might another sifting scheme provide the same benefits, but with reduced anomalous behavior? Different interpolation algorithms,

different boundary extrapolation algorithms, and different ways to combine them should be considered to provide a more accurate, higher resolution system. One algorithm that is also shape-preserving, would potentially be easy to implement, and is often credited with being superior to Akima splines is the Steffen spline interpolation algorithm [56].

As was seen with the decomposition of Signal #10 in 3.11, many transient IMFs were generated between the detected riding wave IMF and the carrier wave IMF. Finding an approach that would minimize the likelihood of the AHHT to extract such transient IMFs would improve the QoD.

To manage the appearance of anomalous scaling with order, the approach was to reduce the amplitude of the frequency mask for all $2^{nd}$-order and higher decompositions. While this approach worked very effectively, it was not perfect. Finding a different management technique would prove very beneficial for QoD.

N.E. Huang in [39] referred to the use of a normalized Hilbert transform to generate a more accurate and meaningful phase function. This was not implemented in AHHT and could potentially provide more accurate QoD values as the frequencies may be more accurate. However, it was given a cursory test and the preliminary results were not promising. This approach was based, in part, on attempting to satisfy the constraint imposed by the Bedrosian Theorem and also to reduce the error described by the Nutall Theorem as they both relate to the Hilbert Transform.

Extracting very high frequency components often leads to the formation of phantom IMFs elsewhere in the spectrum. Typically, when this happens with the AHHT System, they are very low amplitude IMFs, although not so low that they would be dismissed as transient. They imply false information. Understanding the cause of these Phantom IMFs and developing mitigating techniques is an area of interest to this research and would be a good direction for a graduate student to pursue.

Very low frequency components are not well extracted by AHHT; Type-I Mode Mixing is often unavoidable. Realizing that this is partly due to propagation error from boundary effects, it might be prudent to adopt a scheme similar to that proposed in [43] where different boundary extrapolation approaches could be adopted dependent on the ratio of the mask frequency to Nyquist. The wave boundary extension method implemented in MATLAB 2018b appears to be very successful when extracting very low frequency components. More investigation into the nature of these decompositions would be useful.

As mentioned in 4.1, the AHHT is much slower than desirable. It would be highly beneficial to find a more optimized solution. In addition, it would be ideal to incorporate the notion of online, real-time decomposition as proposed by R. Fontugne in [57].

Another area of research is related to the nature of the high-pass filtering functionality of the EMD itself. There has been little to no analysis done to characterize the transition between components and what necessary length of the signal (# of extrema) must exist to properly transition from a local region at one frequency to a different frequency of an adjacent region. Consider the following signal:

$$f_{sig_x}(t) = s_1(t) + s_2(t), \qquad (sampled\ at\ 1\ kHz) \tag{4:1}$$

$$s_1(t) = sin(100 * 2\pi t), \qquad 0 \le t \le 0.1, 0.2 \le t \le 0.3, 0.4 \le t \le 0.5, 0.6 \le t \le 0.7, 0.8 \le t \le 0.9 \tag{4:2}$$

$$s_2(t) = sin(60 * 2\pi t), \qquad 0.1 \le t \le 0.2, 0.3 \le t \le 0.4, 0.5 \le t \le 0.6, 0.7 \le t \le 0.8, 0.9 \le t \le 1 \tag{4:3}$$

This Signal X, which can be seen in Fig. [4-1], when decomposed by the MATLAB 2018b implementation of the EMD, produces a single meaningful IMF—it carries both $s_1$ and $s_2$ as a mode-mixed IMF—which is reasonably expected of an unmasked approach; the signal is IMF-like across every time interval with only a single frequency component anywhere. Note, the Kay window for these Hilbert transforms was set very low (4) to make clear what is happening at a granular level.

How frequency masked EMD behaves as the intervals are decreased, the frequencies are brought closer together, as intervals begin to overlap, and the behavior of ensemble frequency masking with respect to those changes should receive some significant attention.

For example, when looking at the plot from the AHHT decompositions, the artifacts round up or down at the edges of each intermittent pulse. It is noteworthy that the UPEMD and the AHHT System are the

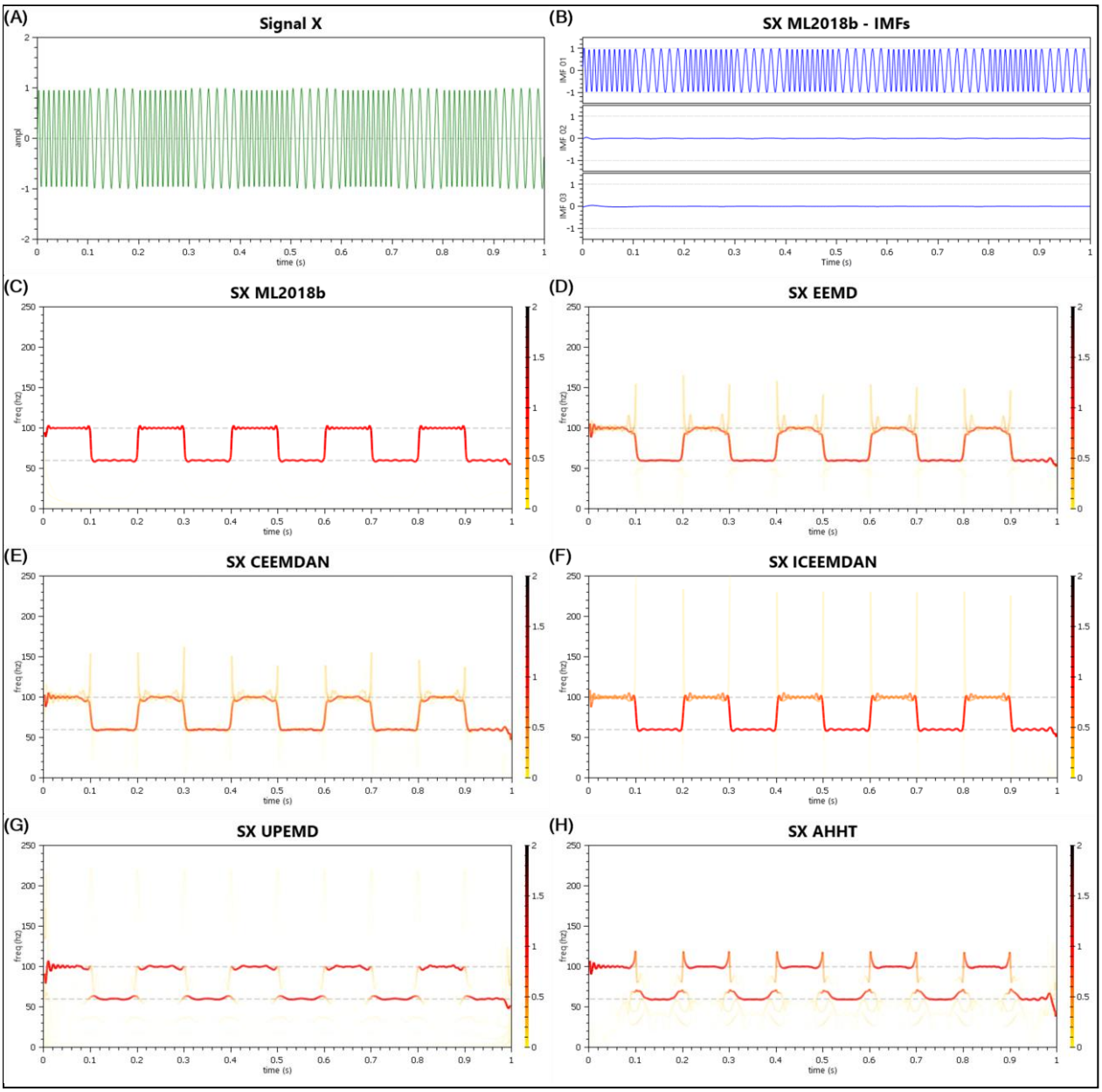


***Figure 5-1 Signal X – Signal, IMFs, and Hilbert Spectrum Decompositions***

only ones that even try to separate these signals. And the UPEMD only does so as if by accident. One of its scheduled frequency stops is at 125 Hz. With its low frequency resolution, this sift captures the 100 Hz component (0.8 frequency ratio), leaving the 62.5 Hz stop to pick up the 60 Hz component. Still, the AHHT results are far from ideal, even though the component frequency ratio is well below the standard upper bound of 0.75. Its less-than-ideal decomposition is primarily due to the boundary effects of intermittency.

Another area of interest is the clustering technique used by the AHHT System which is a parallelized and modified-for-performance version of subtractive clustering. Fundamentally the algorithm is still an $O(N^2)$ procedure. This makes the decomposition time-consuming for very long signals. Finding a more optimized way of performing subtractive clustering would be useful and have wide-reaching impact in the clustering field. One potential research approach would be the use of tiered clustering—there should be no reason why a point $\mathbf{X_1}$ in n-dimensional space that is very near point $\mathbf{X_2}$ should ever be measured against point $\mathbf{X_3}$, if $\mathbf{X_3}$ is known to be far from $\mathbf{X_2}$, much less twice. Using this insight could potentially lead to an algorithm with much-reduced computational cost. As noted in 2.1, blindly measuring every point to every other point, including itself, wastes computational units. By eliminating all self-measurements and all redundant measurements, $O(N^2)$ is no longer the upper bound. While still exponential, the upper-bound is more akin to $O(\sum_{k=1}^{N} k - 1)$. That algorithm could potentially be parallelized, further reducing the time cost, if not the computational cost. But a reduction in the algorithmic cost with a research focus on a notion of "Hypersphere's of Proximity" as a measurement-event regulator where, perhaps, one Mahalanobis distance represents a threshold for proximity would seem to be an interesting research direction.

A preliminary review of Subtractive Clustering suggests that such performance enhancing techniques may already exist. As of 12/1/2019, a search of Google Scholar for "subtractive clustering" turns up over

41,400 results. Many deal with the usage of SC to generate fuzzy classification rules in pattern recognition engines, but many others deal with improving SC (and MC) itself.

Also, with respect to clustering, it would be interesting to find a transformation to the time component of each freq/ampl data point such that contiguous points of similar frequency robust to amplitude differences tend to cluster together. One such approach might be to converge the amplitude values for closely related frequency data points that appear close together in time.

Finally, the issue of component recognition within IMFs is of high importance. Being able to distinguish physically meaningful IMFs from those stemming primarily from noise is critical to future use of EMD techniques. In a paper published this year (2019), J. Smith, M. Al-Badrawi, and N. Kirsch demonstrated that a highly efficient algorithm exists for discriminating between noise-dominant IMFs and signal-dominant IMFs [58]. It would be good to have AHHT IMFs likewise verified against this algorithm, since the AHHT is more likely to separate noise from the signal due to the higher resolution of decomposition.

In his dissertation [59], M. Al-Badrawi provides a statistical analysis of the power distributions of the IMFs produced by the EMD across many different random variable distributions used to generate a signal. This same sort of analysis applied to the IMFs generated across the frequency spectrum produced by AHHT could provide valuable insight into the nature of the outputs of each of the EFM-EMD techniques used by AHHT. Also, with the improved denoising capability demonstrated by AHHT on artificial signals, it could provide insight as to AHHT's ability to denoise real-world signals.

# List of References


[1] N. E. Huang, Z. Shen, R. Long, M. C. Wu, H. H. Shih and Q. Zheng, "The empirical mode decomposition and the Hilbert spectrum for nonlinear and non-stationary time series analysis," *Proc. Roy. Soc. London Ser. A,* vol. 454, no. 1971, pp. 903-995, March 1998.

[2] Z. Wu and N. E. Huang, "A study of the characteristics of white noise using the Empirical Mode Decomposition method," *Proc. Roy. Soc. London Ser. A,* December 2002.

[3] P. Flandrin, G. Rilling and P. Gonçalves, "Empirical mode decomposition as a filter bank," *IEEE Signal Processing Letters,* no. 11, pp. 112-114, 2003.

[4] T. Liu, Z. Luo, J. Huang and S. Yan, "A comparative study of four kinds of adaptive decomposition algorithms and their applications," *Sensors,* vol. 18, no. 2120, pp. 1-51, 2018.

[5] N. E. Huang, M. C. Wu, S. R. Long, S. Shen, W. Qu, P. Gloersen and K. Fan, "The Empirical Mode Decomposition and the Hilbert Spectrum for Nonlinear and Non-Stationary Time Series Analysis," *Proceedings: Mathematical, Physical and Engineering Sciences,,* vol. 459, no. 2037, pp. 2317-2345, 2003.

[6] G. Rilling, P. Flandrin and P. Gonçalves, "On empirical mode decomposition and its algorithms," in *IEEE-EURASIP workshop on nonlinear signal and image processing (NSIP-03)*, Grado, 2003.

[7] M. Peel, G. Amirthanathan, P. G.G.S., T. McMahon and F. Chiew, "Issues with the application of empirical mode decomposition analysis," *Modsim05 - International Congress On Modelling and Simulation: Advances and Applications For Management and Decision Making, Proceedings,* pp. 1681-1687, 2005.

[8] N. E. Huang and Z. Wu, "A review on Hilbert–Huang transform: method and its applications to geophysical studies," *Rev. Geophys.,* vol. 46, no. 2, p. RG2006, 2008.

[9] I. The MathWorks, *MATLAB and Signal Processing Toolbox Release,* 2018b ed., Natick, Massachusetts.

[10] J. Tribolet, "A new phase unwrapping algorithm," *IEEE Transactions on Acoustics, Speech, and Signal Processing,* vol. 25, no. 2, pp. 170-177, 1977.

[11] J. Huntley, "Noise-immune phase unwrapping algorithm," *Applied Optics,* vol. 28, no. 16, pp. 3268-3270, 1989.

[12] M. D. Pritt and J. S. Shipman, "Least-squares two-dimensional phase unwrapping using FFT's," *IEEE Transactions on Geoscience and Remote Sensing,* vol. 32, no. 3, pp. 706-708, May 1994.

[13] S. Kay, "A Fast and Accurate Single Frequency Estimator," *IEEE Transactions on Acoustics, Speech, and Signal Processing,* vol. 37, no. 12, pp. 1987-1989, 1989.

[14] G. Rilling and P. Flandrin, "One or two frequencies? The empirical mode decomposition answers," *IEEE Transactions on Signal Processing,* vol. 56, no. 1, pp. 85-95, 2008.

[15] Z. Wu and N. E. Huang, "Ensemble empirical mode decomposition: a noise-assisted data analysis method," *Adv. Adapt. Data Anal,* vol. 1, no. 1, pp. 1-41, 2009.

[16] J. R. Yeh, J. S. Shieh and N. .. Huang, "Complementary ensemble empirical mode decomposition: a novel noise enhanced data analysis method," *Adv. Adap. Data Anal.,* vol. 2, no. 2, pp. 135-156, 2010.

[17] M. E. Torres, M. A. Colominas, G. Schlotthauer and P. Flandrin, "A complete ensemble empirical mode decomposition with adaptive noise," *Proc. IEEE Int. Conf. Acoust. Speech Signal Process (ICASSP),* pp. 4144-4147, 2011.

[18] M. A. Colominas, G. Schlotthauera and M. E. Torres, "Improved complete ensemble EMD: A suitable tool for biomedical signal processing," *Biomed. Signal. Process. Control,* vol. 14, pp. 19-29, November 2014.

[19] Z. Jinde, C. Junsheng and Y. Yang, "Partly ensemble empirical mode decomposition: An improved noise-assisted method for eliminating mode mixing," *Signal Processing,* vol. 96, pp. 362-374, 2013.

[20] G. Rilling, P. Flandrin, P. Gonçalves and J. Lilly, "Bivariate Empirical Mode Decomposition," *IEEE Signal Processing Letters,* vol. 14, 2008.

[21] C. Damerval, S. Meignen and V. Perrier, "A fast algorithm for bidimensional EMD," *IEEE Signal Processing Letters,* vol. 12, no. 10, pp. 701-704, 2005.

[22] N. u. Rehman and D. P. Mandic, "Empirical Mode Decomposition for Trivariate Signals," *IEEE Transactions on Signal Processing,* vol. 58, no. 3, pp. 1059-1068, 2010.

[23] N. u. Rehman and D. P. Mandic, "Multivariate empirical mode decomposition," *Proc. Math. Phys. Eng. Sci.,* vol. 466, pp. 1291-1302, 2010.

[24] N. u. Rehman, C. Park, N. Huang and D. Mandic, "EMD via MEMD: multivariate noise-aided computation of standard EMD," *Advances in Adaptive Data Analysis,* vol. 5, no. 2, pp. 1350007.1-1350007.25, 2013.

[25] X. Lang, Q. Zheng, Z. Zhang, S. Lu, L. Xie, A. Horch and H. Su, "Fast Multivariate Empirical Mode Decomposition," *IEEE Access,* vol. 6, pp. 65521-65538, 2018.

[26] N. u. Rehman and D. P. Mandic, "Filter Bank Property of Multivariate Empirical Mode Decomposition," *IEEE Transactions on Signal Processing,* vol. 59, no. 5, pp. 2421-2426, 2011.

[27] Y. Zhang, P. Xu, P. Li, K. Duan, Y. Wen, Q. Yang, T. Zhang and D. Yao, "Noise-assisted multivariate empirical mode decomposition for multichannel EMG signals," *BioMedical Engineering OnLine,* vol. 16, 2017.

[28] W. Huang, J. Zeng, Z. Wang and J. Liang, "Partial noise assisted multivariate EMD: An improved noise assisted method for multivariate signals decomposition," *Biomedical Signal Processing and Control,* vol. 36, pp. 205-220, 2017.

[29] R. Deering and J. F. Kaiser, "The use of a masking signal to improve empirical mode decomposition," in *Proceedings of IEEE International Conference on Acoustics, Speech, and Signal Processing (ICASSP '05)*, Philadelphia, 2005.

[30] W. C. Shen, Y. H. Chen and A. Y. Wu, "Low-complexity sinusoidal-assisted EMD (SAEMD) algorithms for solving mode-mixing problems in HHT," *Digital Signal Processing,* vol. 24, pp. 170-186, 2014.

[31] W. Hu and J. Mo, "Improvement of Frequency Resolution of EMD Using an Optimized Masking Signal," in *2010 International Conference on Multimedia Technology*, Ningbo, 2010.

[32] S. Sandoval and P. L. D. Leon, "Advances in empirical mode decomposition for computing instantaneous amplitudes and instantaneous frequencies," *Proc. IEEE Int. Conf. Acoust. Speech Signal Process (ICASSP),* pp. 4311-4315, 2017.

[33] Y. Wang, K. Hu and M. Lo, "Uniform phase empirical mode decomposition: an optimal hybridization of masking signal and ensemble approaches," *IEEE Access,* vol. 6, pp. 34819-34833, 2018.

[34] Q. Chen, N. Huang, S. Riemenschneider and Y. Xu, "A B-spline approach for empirical mode decompositions," *Adv. Comput. Math.,* vol. 24, pp. 171-195, 2006.

[35] M. Peel, G. Pegram and T. Mcmahon, "Empirical mode decomposition: Improvement and application," in *MODSIM07 - Land; Water and Environmental Management: Integrated Systems for Sustainability*, 2007.

[36] Y. Kopsinis and S. McLaughlin, "Investigation and Performance Enhancement of the Empirical Mode Decomposition Method Based on a Heuristic Search Optimization Approach," *IEEE Transactions on Signal Processing,* vol. 56, no. 1, pp. 1-13, 2008.

[37] F. N. Fritsch and R. E. Carlson, "Monotone Piecewise Cubic Interpolation," *SIAM Journal on Numerical Analysis,* vol. 17, no. 2, pp. 238-246, 1980.

[38] D. Kahaner, C. Moler and S. Nash, Numeric Methods and Software, Upper Saddle River, NJ: Prentice Hall, 1988.

[39] N. E. Huang and S. Shen, Hilbert-Huang Transform and Its Applications, 2nd ed., vol. 16, Danvers, MA: World Scientific Publishing Co. Pte. Ltd., 2014.

[40] J. Huang, J. Tang, M. Zhang, X. Zhang and T. Han, "An improved EMD based on cubic spline interpolation of extremum centers," *Journal of Vibroengineering,* vol. 17, pp. 2393-2409, 2015.

[41] C. d. Boor, A practical guide to splines, New York: Springer-Verlag, 2001.

[42] Q. Wu and S. Riemenschneider, "Boundary extension and stop criteria for empirical mode decomposition," *Advances in Adaptive Data Analysis,* vol. 2, pp. 157-169, 2010.

[43] Z. Qingjie, H. Zhu and S. Lincheng, "A new method for mitigation of end effect in empirical mode decomposition," *CAR 2010 - 2010 2nd International Asia Conference on Informatics in Control - Automation and Robotics,* vol. 1, pp. 400-403, 2010.

[44] A. M. Jaber, M. T. Ismail and A. M. Altaher, "Empirical mode decomposition combined with local linear quantile regression for automatic boundary correction," *Abstract and Applied Analysis,* vol. 2014, pp. 731827.1-731827.8, 2014.

[45] S. Chiu, "Fuzzy model identification based on cluster estimation," *Journal of Intelligent and Fuzzy Systems,* vol. 2, no. 3, pp. 267-278, 1994.

[46] R. R. Yager and D. P. Filev, "Approximate clustering via the mountain method," *IEEE Transactions on Systems, Man, and Cybernetics,* vol. 24, no. 8, pp. 1279-1284, Aug. 1994.

[47] Accord.NET. (ver. 3.8.0). C. R. d. Souza. Accessed: Oct. 19, 2019. [Online]. Available: http://accord.net.

[48] Math.NET Numerics. (ver. 4.9.0). C. Rüegg and M. Cuda. Accessed: 13 October 2019. [Online]. Available: https://numerics.mathdotnet.com. [Accessed 2019].

[49] OxyPlot. (ver. 1.0.0). O. Bjorke. Accessed: Jun. 11, 2019. [Online]. Available: https://oxyplot.github.io.

[50] R. Croce, A. Craft, J. Miller, K. Chamberlin and D. Filipovic, "Quadriceps mechano- and electromyographic time-frequency responses during muscular contractions to volitional exhaustion," *Muscle & Nerve,* vol. 53, pp. 452-463, 2016.

[51] G. Rilling and P. Flandrin, "On the Influence of Sampling on the Empirical Mode Decomposition," in *2006 IEEE International Conference on Acoustics Speech and Signal Processing Proceedings*, Toulouse, 2006.

[52] N. Stevenson, M. Mesbah and B. Boashash, "A sampling limit for the empirical mode decomposition," in *Proceedings of the Eighth International Symposium on Signal Processing and Its Applications, 2005*, Sydney, Australia, 2005.

[53] P. Flandrin, "Empirical Mode Decomposition," 25 February 2015. [Online]. Available: http://perso.ens-lyon.fr/patrick.flandrin/emd.html. [Accessed 28 March 2019].

[54] M. Elgendi, M. Jonkman and F. D. Boer, "Frequency Bands Effects on QRS Detection," in *Proceedings of the 3rd International Conference on Bio-inspired Systems and Signal Processing*, Valencia, 2010.

[55] A. Zeiler, R. Faltermeier, I. R. Keck, A. M. Tomé, C. G. Puntonet and E. W. Lang, "Empirical Mode Decomposition - an introduction," in *The 2010 International Joint Conference on Neural Networks (IJCNN)*, Barcelona, 2010.

[56] M. Steffen, "A simple method for monotonic interpolation in one dimension," *Astron. & Astrophys.,* vol. 239, pp. 443-450, 1990.

[57] R. Fontugne, P. Borgnat and P. Flandrin, "Online empirical mode decomposition," in *2017 IEEE International Conference on Acoustics, Speech and Signal Processing (ICASSP*, New Orleans, LA, 2017.

[58] J. Smith, M. Al-Badrawi and N. Kirsch, "An Optimized De-Noising Scheme Based on the Null Hypothesis of Intrinsic Mode Functions," *IEEE Signal Processing Letters,* vol. 26, no. 8, pp. 1232-1236, 2019.

[59] M. Al-Badrawi, "Statistical Properties and Applications of Empirical Mode Decomposition," Durham, NH, 2017.

# List of Abbreviations

**EMD** – Empirical Mode Decomposition

**IMF** – Intrinsic Mode Function

**EEMD** – Ensemble Empirical Mode Decomposition

**CEEMD** – Complementary Ensemble Empirical Mode Decomposition

**CEEMDAN** – Complete Ensemble Empirical Mode Decomposition with Adaptive Noise

**ICEEMDAN** – Improved Complete Ensemble Empirical Mode Decomposition with Adaptive Noise

**SAEMD(I & II)** – Sinusoidally-Assisted Empirical Mode Decomposition

**IMSM** – Improved Masking Signal Method

**HSA-EMD** – Hilbert Spectral Analysis Empirical Mode Decomposition

**UPEMD** – Uniform Phase Empirical Mode Decomposition

**BS-EMD** – B-Spline Empirical Mode Decomposition

**HT** – Hilbert Transform

**HHT** – Hilbert-Huang Transform

**FM-EMD** – Frequency-Masked Empirical Mode Decomposition

**EFM-EMD** – Ensemble Frequency-Masked Empirical Mode Decomposition

**AHHT** – Adaptive Hilbert-Huang Transform System

**SC** – Subtractive Clustering

**EFM-EMDc** – Ensemble Frequency-Masked Empirical Mode Decomposition using Classic Sifting Technique

**EFM-EMD1** – Ensemble Frequency-Masked Empirical Mode Decomposition Technique I used by AHHT

**EFM-EMD2** – Ensemble Frequency-Masked Empirical Mode Decomposition Technique II used by AHHT

**EFM-EMD3** – Ensemble Frequency-Masked Empirical Mode Decomposition Technique III used by AHHT

**QoD** – Quality of Decomposition

**$QoD_1$** – Quality of Decomposition Matching Metric

**$QoD_2$** – Quality of Decomposition Mismatching Metric

**DF** – Density Factor (used in QoD calculations)

**SNR** – Signal-to-Noise Ratio

**EWT** – Empirical Wavelet Transform

**EMG** – Electromyograph

**SEMG** – Surface Electromyograph

# Appendix A

# Fundamental Signal Plots and Hilbert Spectrums of All Signals

Many of the plots in this Appendix are reproductions of plots found throughout the thesis. They are included here for comparison purposes. The same is true with some of the QoD values in the tables.

In many cases, the noise overwhelms the signal. For example, in Signal #3 (-5dB SNR), after some of the high frequency noise-only IMFs have been removed, the highest frequency component is more visible. But whether pattern recognition could detect it is unknown.

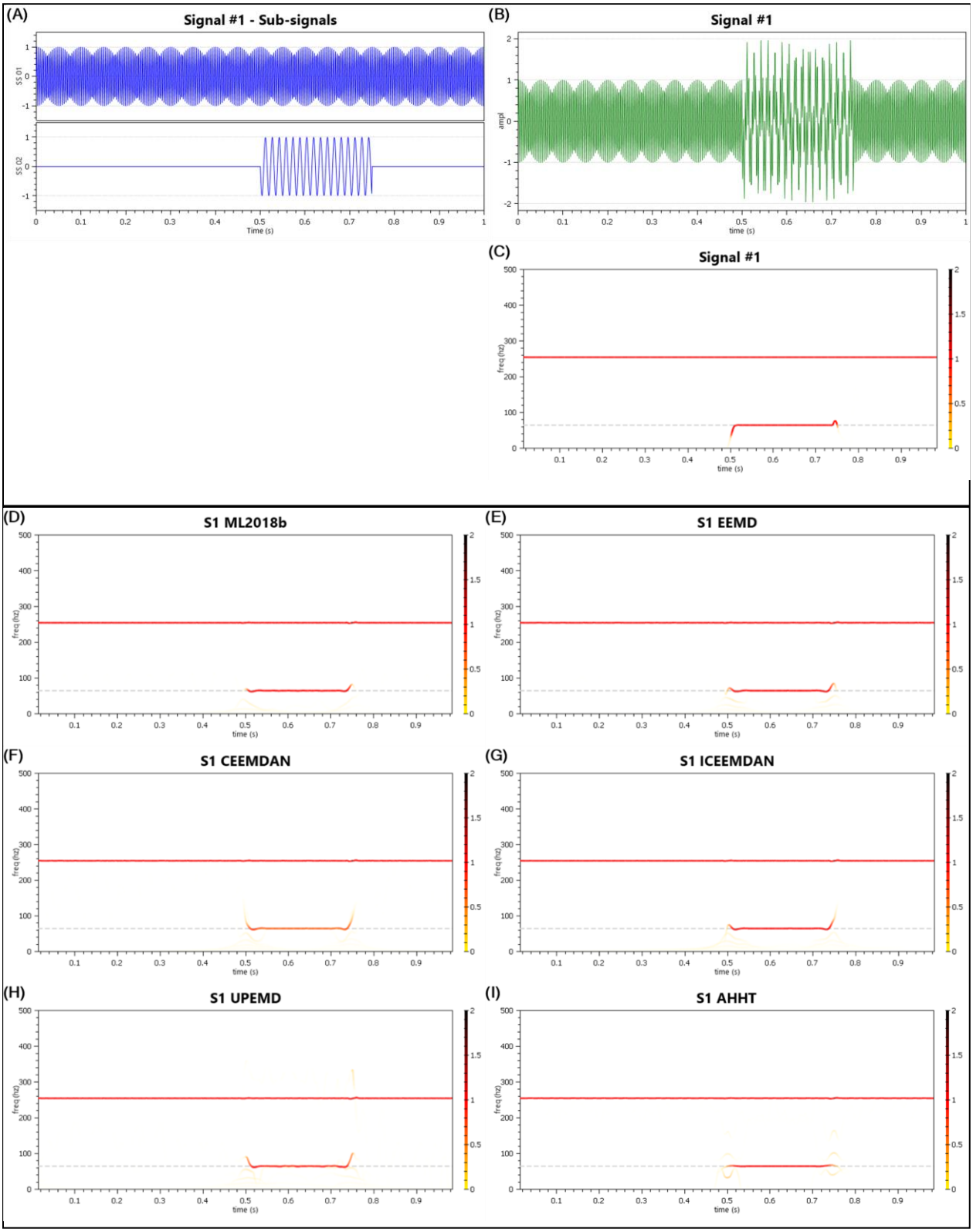


***Figure A-1 Signal 1 - Plot, Source Sub-Signals, Hilbert Spectral Decompositions***

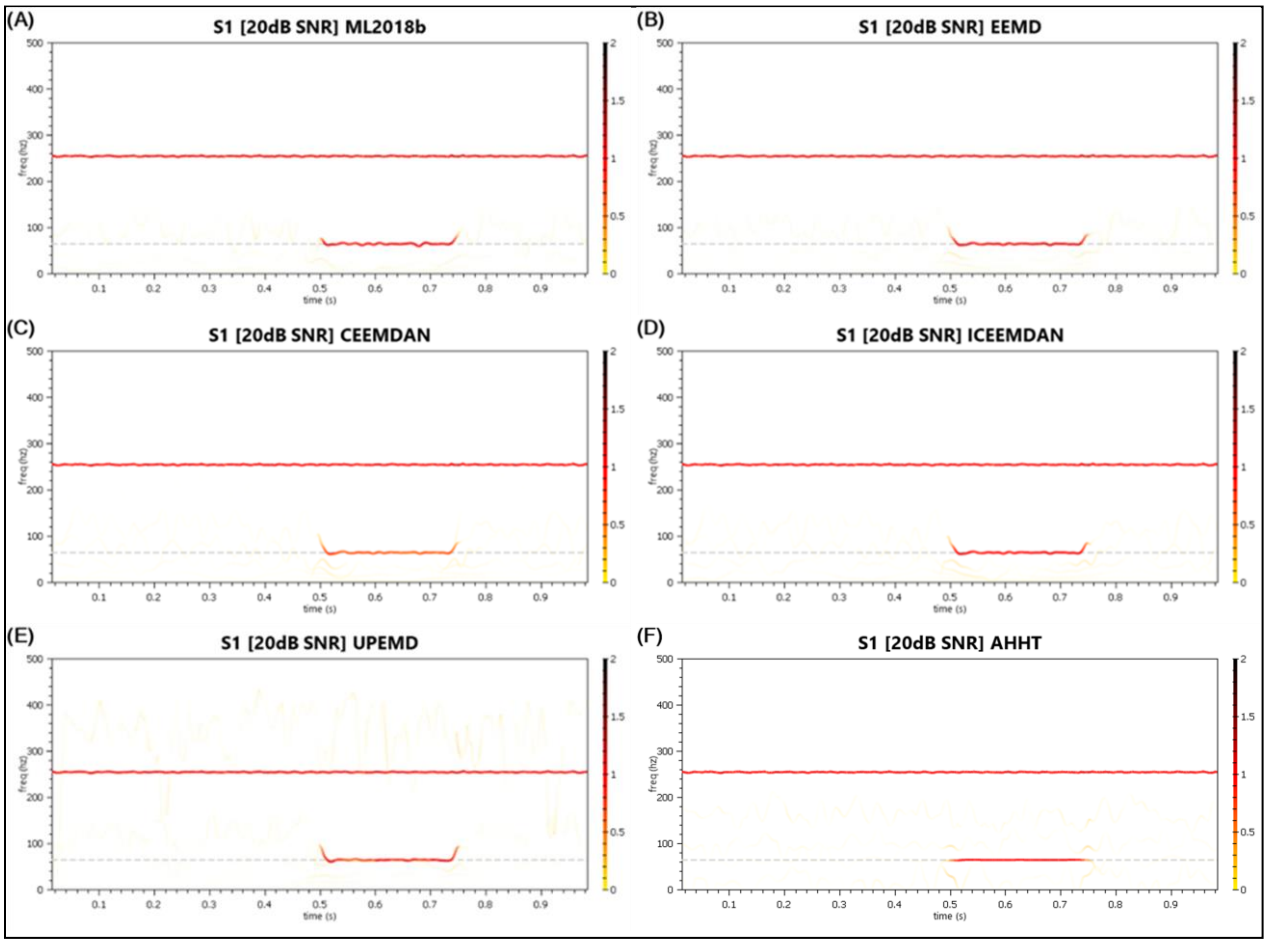


***Figure A-2 Signal 1 (20dB SNR) - Hilbert Spectral Decompositions***

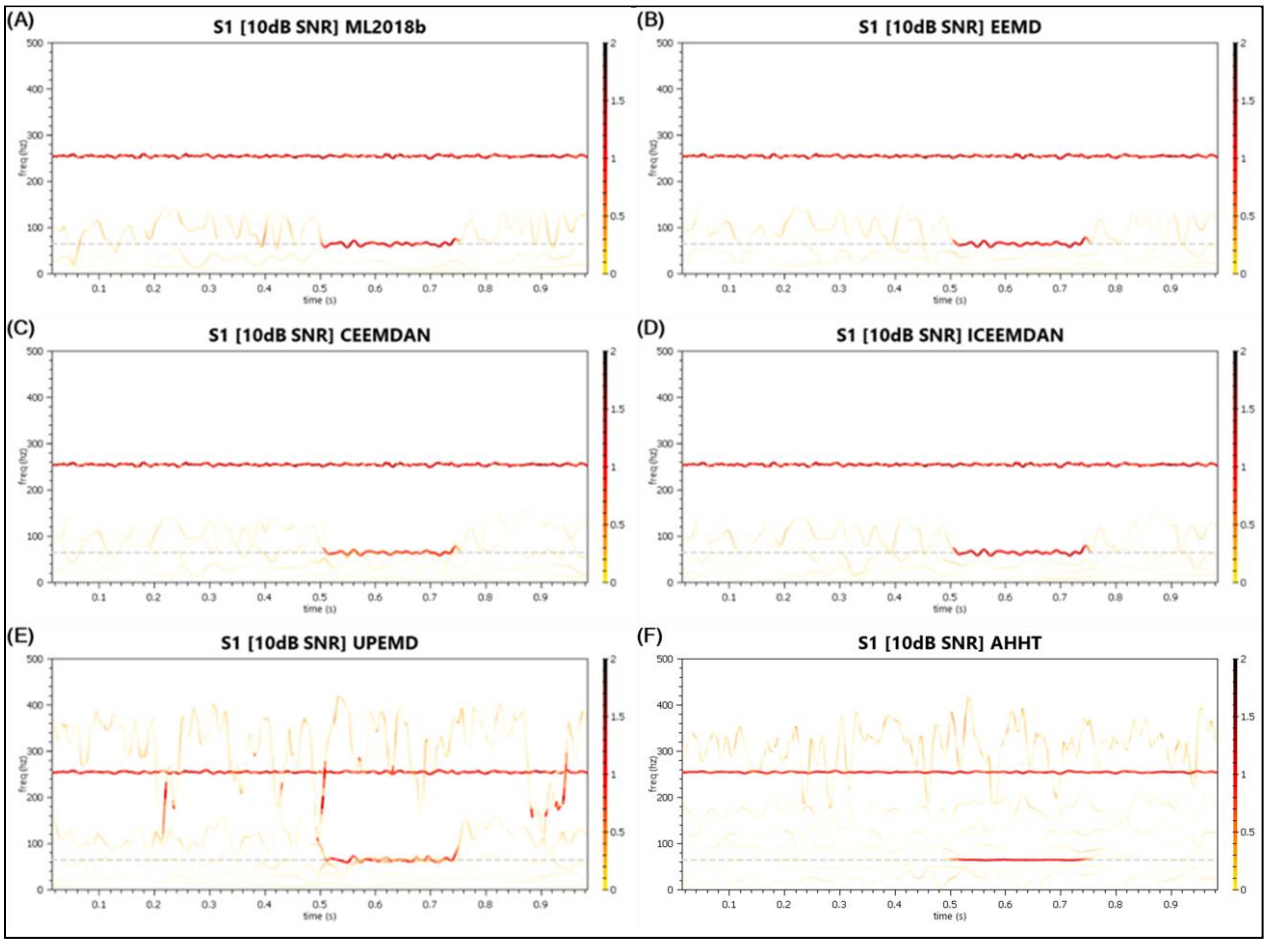


***Figure A-3 Signal 1 (10dB SNR) - Hilbert Spectral Decompositions***

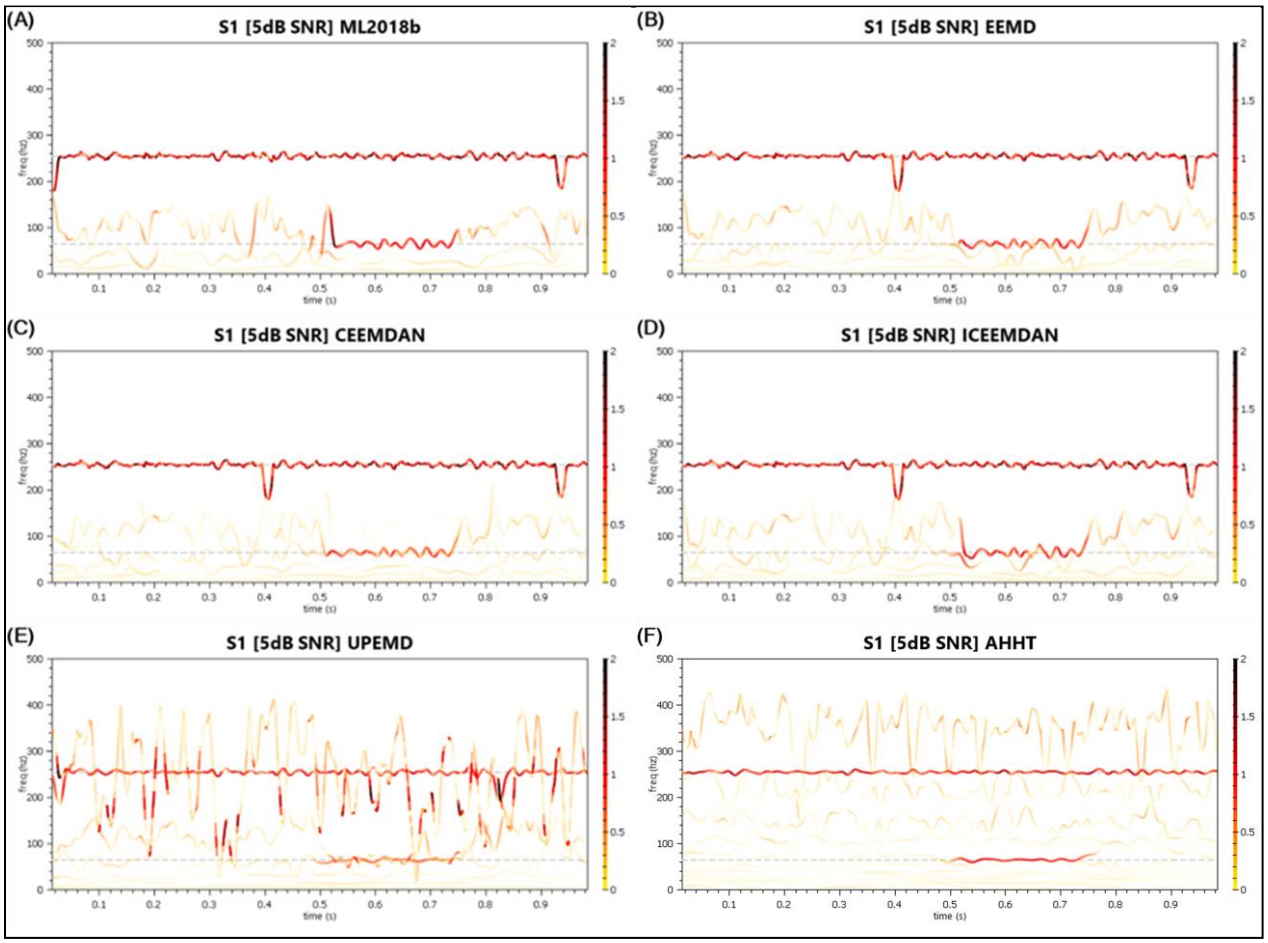


***Figure A-4 Signal 1 (5dB SNR) - Hilbert Spectral Decompositions***

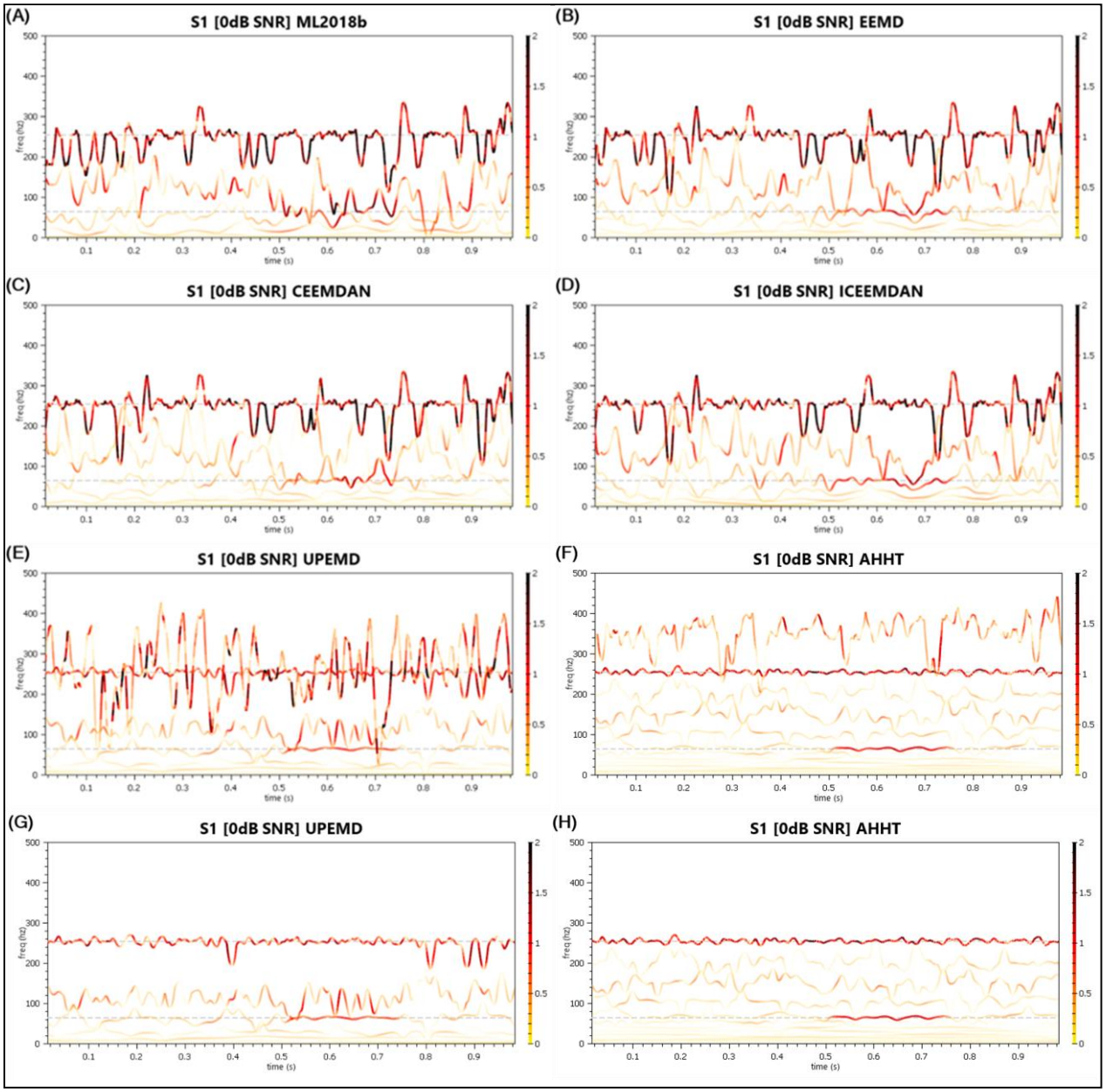


***Figure A-5 Signal 1 (0dB SNR) - Hilbert Spectral Decompositions (G – Top 1 IMF Removed, H – Top 1 IMF Removed)***

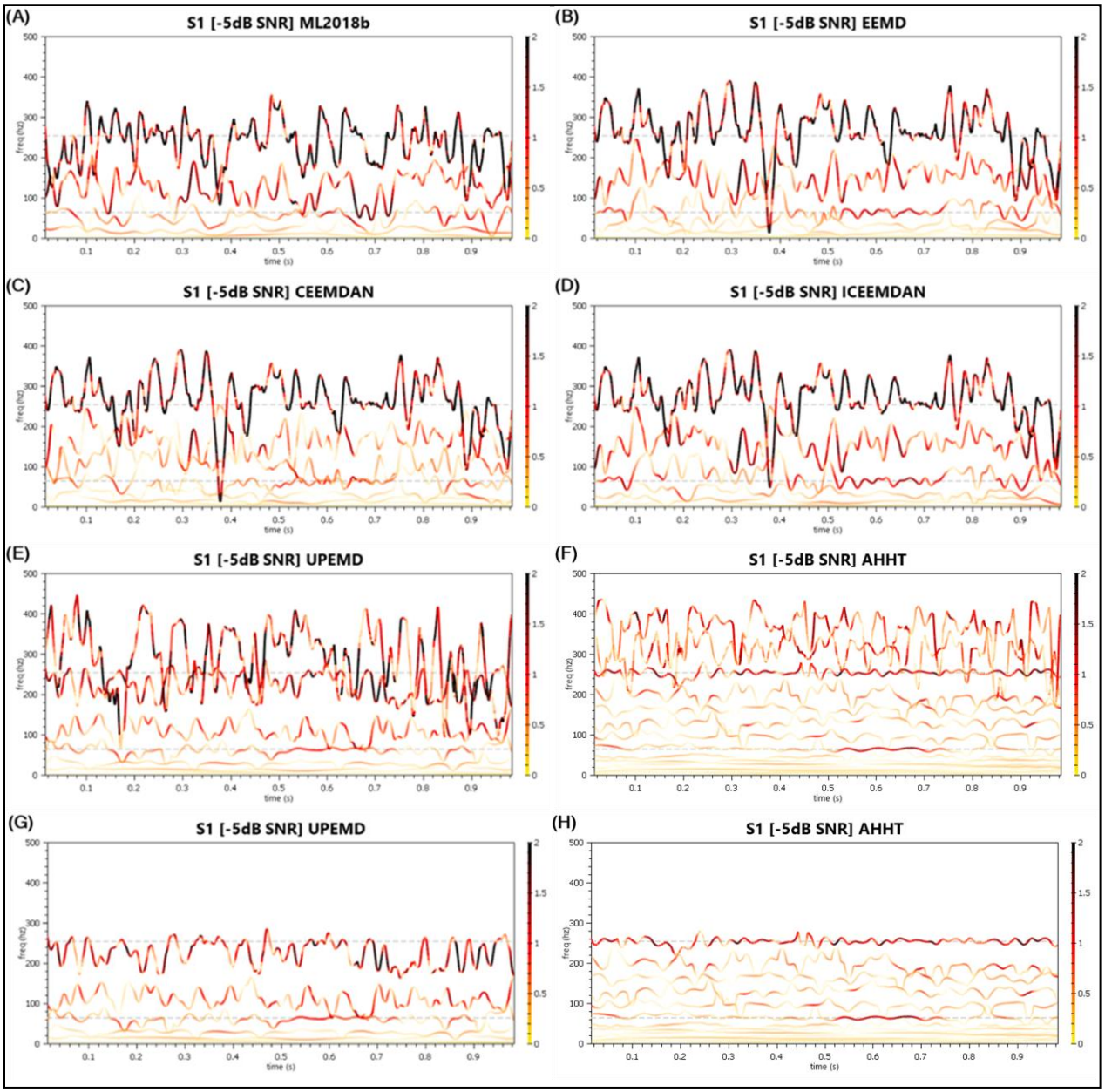


*Figure A-6 Signal 1 (-5dB SNR) - Hilbert Spectral Decompositions (G – Top 1 IMF Removed, H – Top 2 IMFs Removed)*

*Table A-1 Signal 1 (All) - IMF Counts and QoD Values*

| | MATLAB EMD | EEMD | CEEMDAN | ICEEMDAN | UPEMD | AHHT |
|---|---|---|---|---|---|---|
| **Signal #1 – 2 Component Signals** | | | | | | |
| # of IMFs + Res | 7 | 10 | 10 | 10 | 9 | 5 |
| $QoD_1$ | **0.869198** | 0.838344 | 0.51749 | 0.857836 | 0.715352 | 0.834439 |
| $QoD_2$ | 0.053421 | 0.060249 | 0.133395 | 0.102525 | 0.10824 | **0.042053** |
| **Signal #1 (20 dB SNR)** | | | | | | |
| # of IMFs + Res | 8 | 10 | 11 | 10 | 9 | 5 |
| $QoD_1$ | 0.487623 | 0.501189 | 0.421786 | 0.542996 | 0.512891 | **0.606335** |
| $QoD_2$ | 0.110465 | 0.11705 | 0.210101 | 0.174872 | 0.190688 | 0.121002 |
| **Signal #1 (10 dB SNR)** | | | | | | |
| # of IMFs + Res | 7 | 10 | 10 | 9 | 9 | 8 |
| $QoD_1$ | 0.171113 | 0.175995 | 0.168175 | 0.183722 | 0.286008 | **0.454064** |
| $QoD_2$ | 0.230235 | 0.246248 | 0.349367 | 0.314387 | 0.555411 | 0.603517 |
| **Signal #1 (5 dB SNR)** | | | | | | |
| # of IMFs + Res | 8 | 10 | 10 | 9 | 9 | 12 |
| $QoD_1$ | 0.079249 | 0.051696 | 0.051677 | 0.05829 | 0.124063 | **0.242681** |
| $QoD_2$ | 0.417397 | 0.832311 | 0.626395 | 0.635768 | 1.312459 | 1.230345 |
| **Signal #1 (0 dB SNR)** | | | | | | |
| # of IMFs + Res | 8 | 11 | 10 | 10 | 9 | 15 |
| $QoD_1$ | 0.034824 | 0.001193 | 0.002075 | 0.004692 | 0.070668 | **0.151361** |
| $QoD_2$ | 1.555243 | 1.478251 | 1.502957 | 1.323609 | 2.036594 | 2.163717 |
| **Signal #1 (-5 dB SNR)** | | | | | | |
| # of IMFs + Res | 9 | 11 | 10 | 8 | 9 | 16 |
| $QoD_1$ | 0.05929 | 0.003586 | -0.02291 | 0.002839 | 0.081633 | **0.116049** |
| $QoD_2$ | 2.209561 | 1.663627 | 2.176141 | 1.852081 | 2.629585 | 4.192807 |

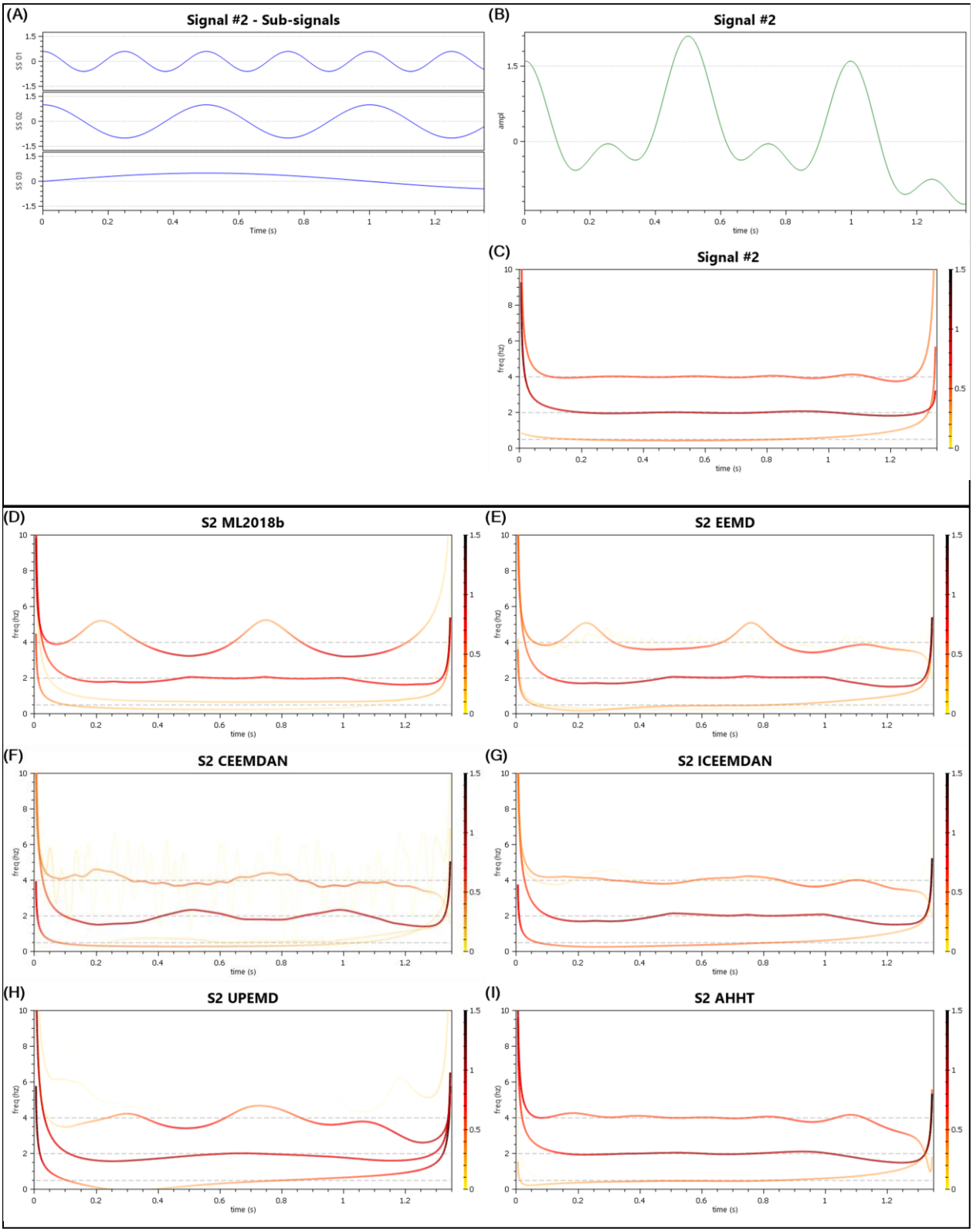


*Figure A-7 Signal 2 - Plot, Source Sub-Signals, Hilbert Spectral Decompositions*

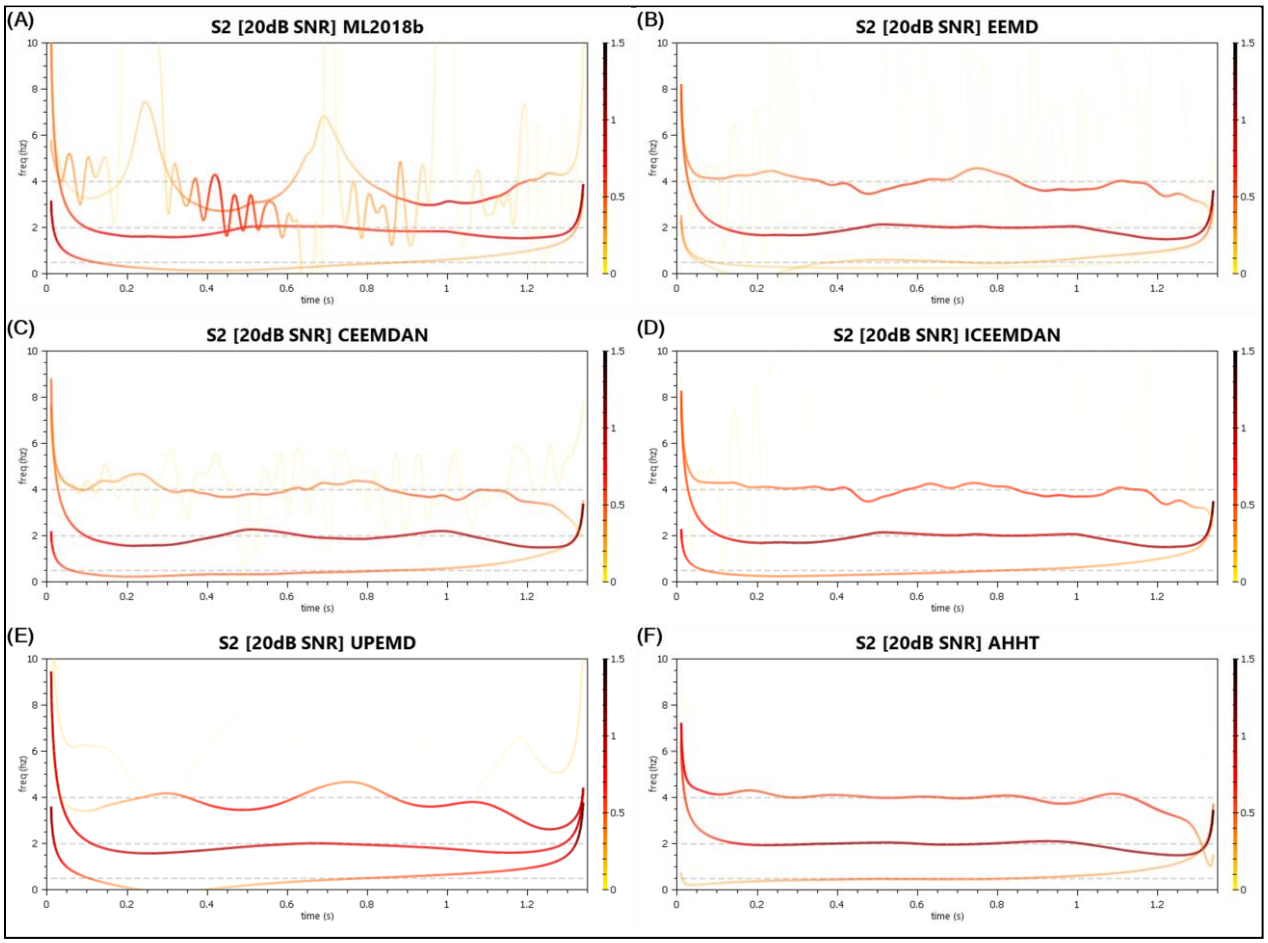


***Figure A-8 Signal 2 (20dB SNR) - Hilbert Spectral Decompositions***

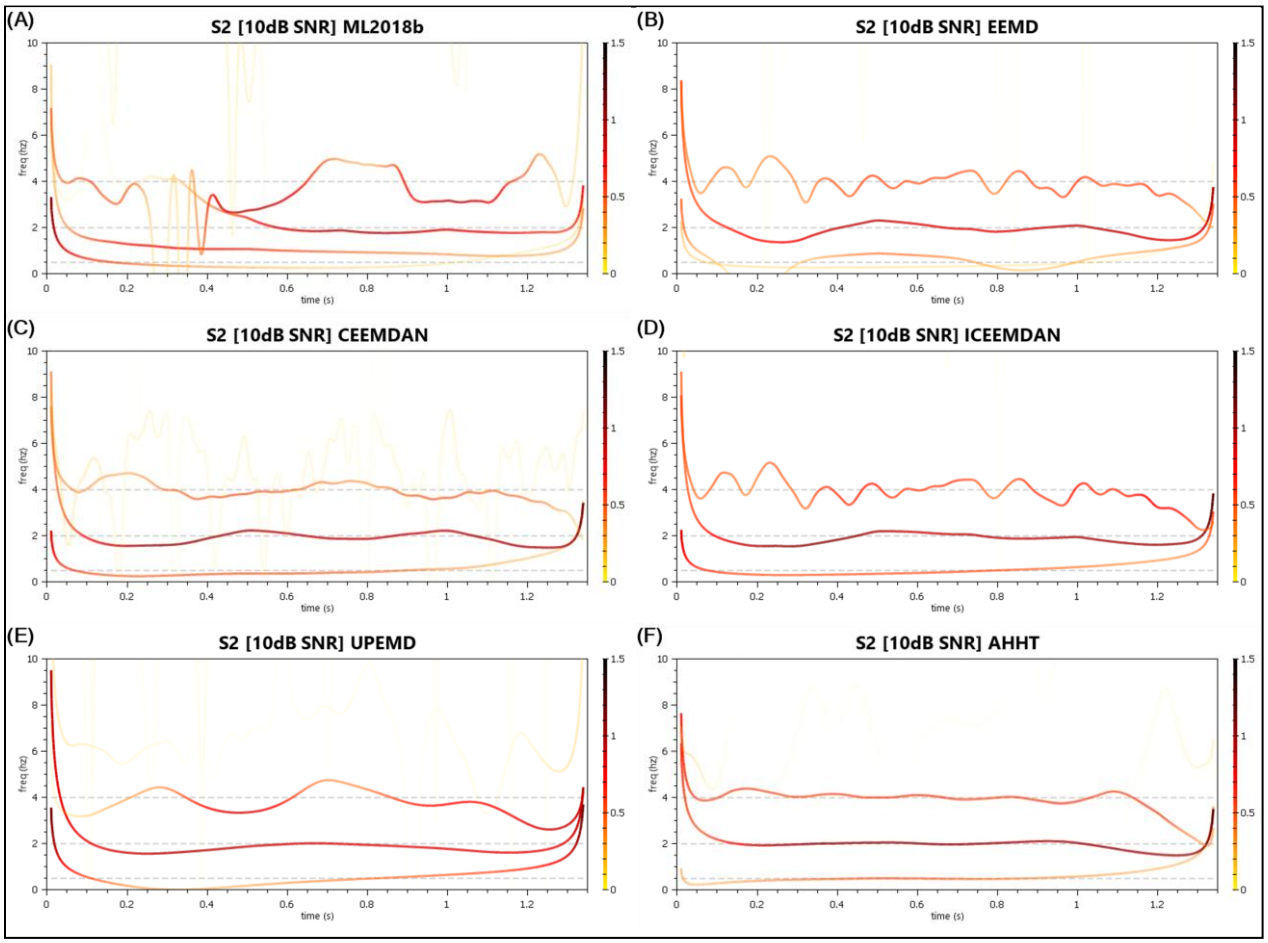


***Figure A-9 Signal 2 (10dB SNR) - Hilbert Spectral Decompositions***

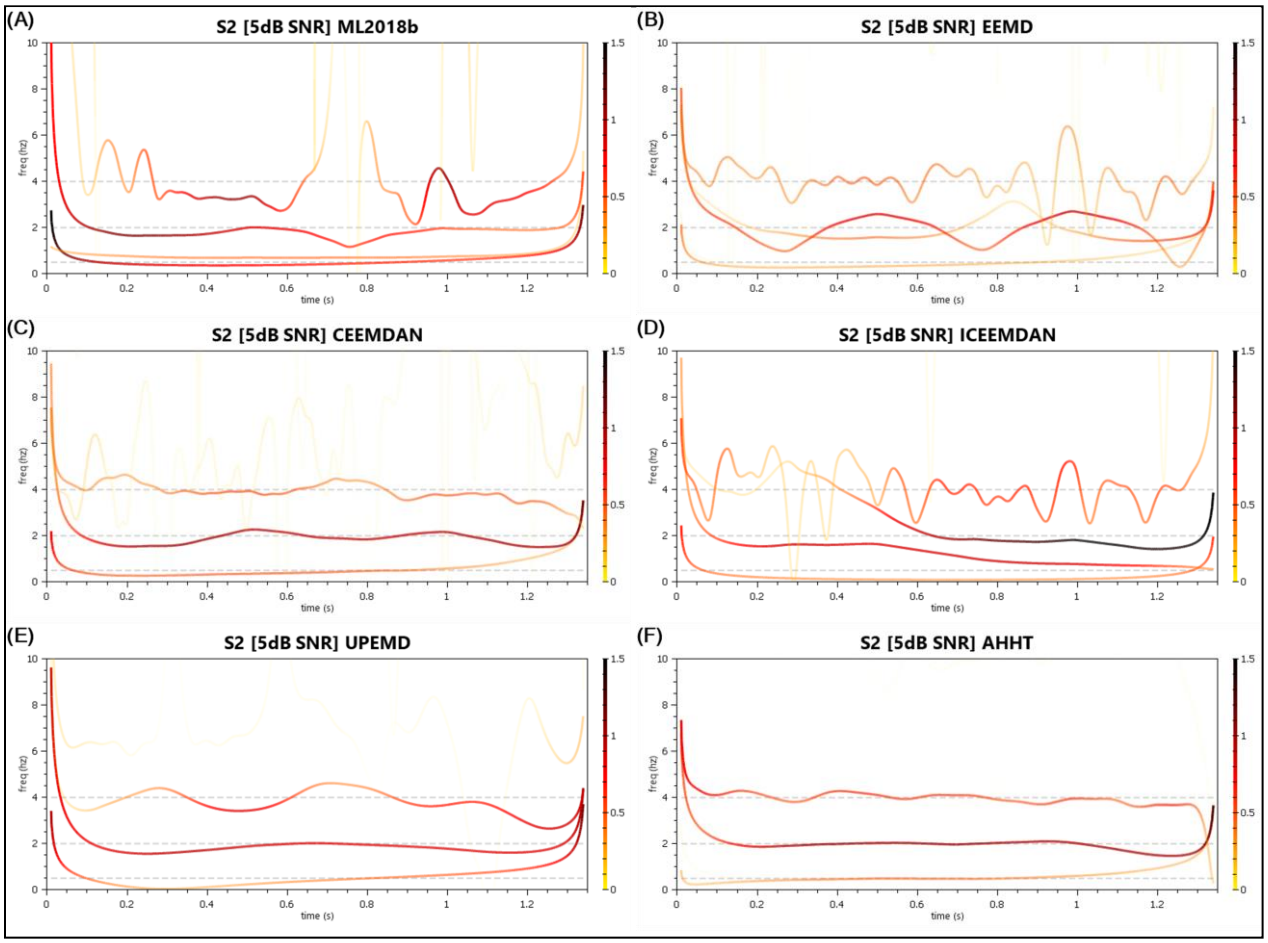


***Figure A-10 Signal 2 (5dB SNR) - Hilbert Spectral Decompositions***

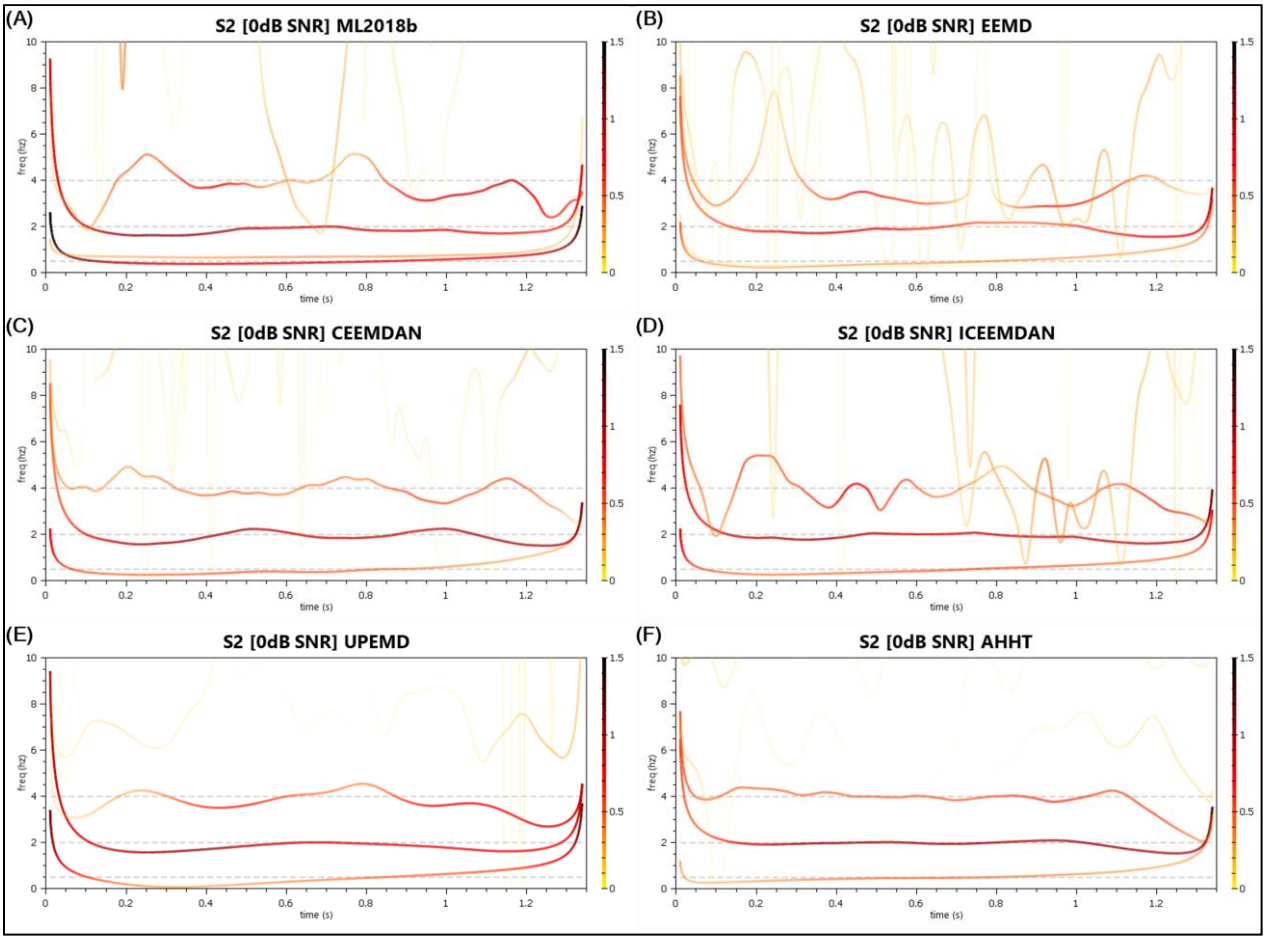


***Figure A-11 Signal 2 (0dB SNR) - Hilbert Spectral Decompositions***

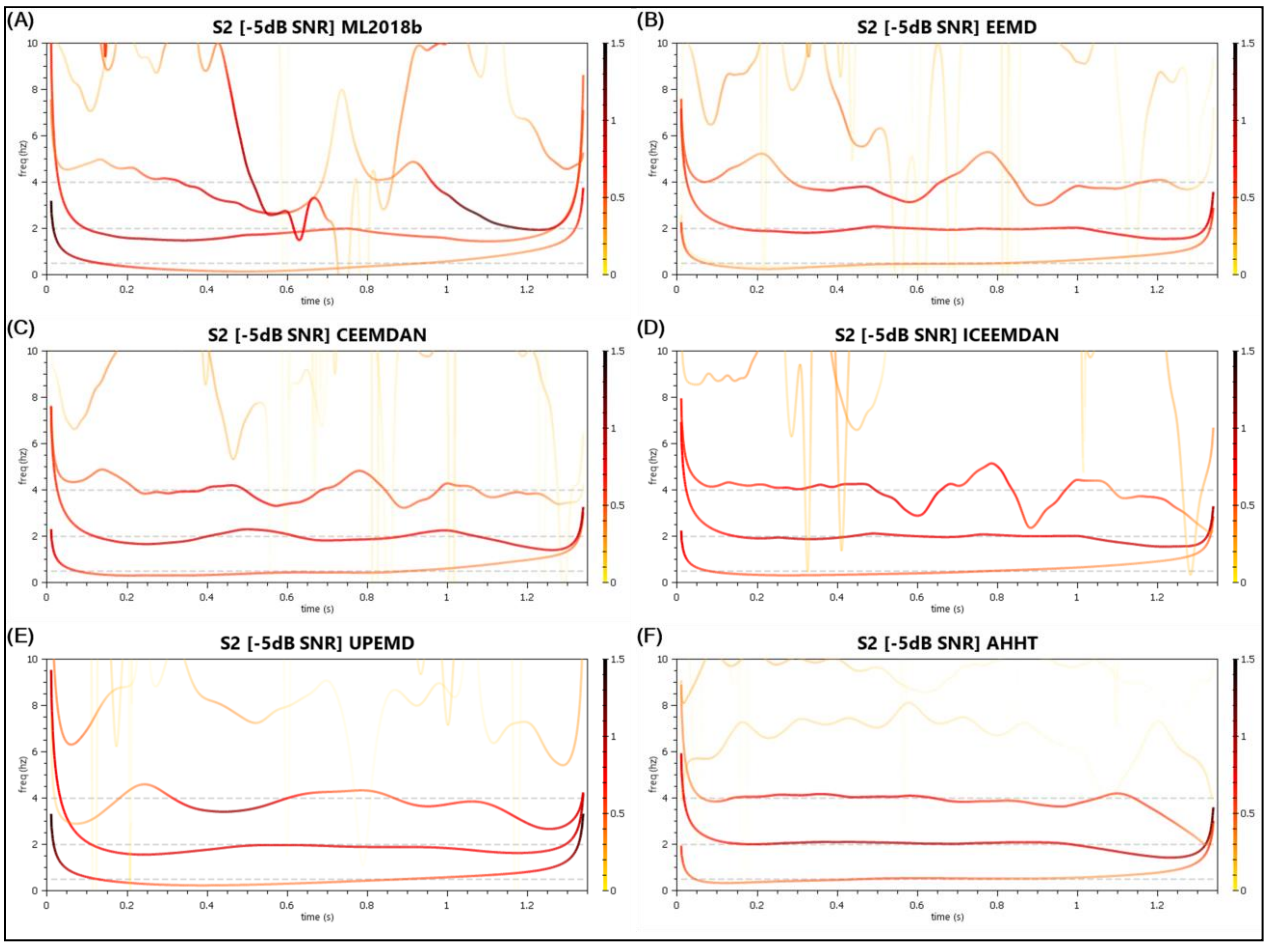


***Figure A-12 Signal 2 (-5dB SNR) - Hilbert Spectral Decompositions***

*Table A-2 Signal 2 (All) - IMF Counts and QoD Values*

| | MATLAB EMD | EEMD | CEEMDAN | ICEEMDAN | UPEMD | AHHT |
|---|---|---|---|---|---|---|
| **Signal #2 – 3 Component Signals** | | | | | | |
| # of IMFs + Res | 4 | 11 | 12 | 9 | 11 | 4 |
| $QoD_1$ | 0.076892 | 0.267081 | 0.168238 | 0.438313 | 0.194584 | **0.747296** |
| $QoD_2$ | 0.25541 | 0.177857 | 0.250678 | 0.083441 | 0.057665 | **0.0218** |
| **Signal #2 (20 dB SNR)** | | | | | | |
| # of IMFs + Res | 7 | 10 | 10 | 8 | 10 | 13 |
| $QoD_1$ | 0.062098 | 0.286238 | 0.321638 | 0.509038 | 0.173811 | **0.723826** |
| $QoD_2$ | 0.401694 | 0.341237 | 0.246312 | 0.160326 | 0.230322 | 0.246443 |
| **Signal #2 (10 dB SNR)** | | | | | | |
| # of IMFs + Res | 8 | 10 | 10 | 8 | 10 | 14 |
| $QoD_1$ | 0.100569 | 0.269905 | 0.300698 | 0.371098 | 0.182505 | **0.691487** |
| $QoD_2$ | 0.839138 | 0.639777 | 0.57363 | 0.491614 | 0.615343 | 0.781927 |
| **Signal #2 (5 dB SNR)** | | | | | | |
| # of IMFs + Res | 8 | 10 | 10 | 9 | 10 | 15 |
| $QoD_1$ | 0.098095 | 0.004382 | 0.343992 | 0.089494 | 0.191818 | **0.659632** |
| $QoD_2$ | 1.700549 | 1.197872 | 0.957972 | 2.111195 | 1.024908 | 1.320442 |
| **Signal #2 (0 dB SNR)** | | | | | | |
| # of IMFs + Res | 9 | 11 | 10 | 9 | 10 | 17 |
| $QoD_1$ | 0.138329 | 0.145568 | 0.280201 | 0.203106 | 0.194271 | **0.639027** |
| $QoD_2$ | 2.670128 | 1.88054 | 1.716002 | 1.873978 | 1.843343 | 2.520125 |
| **Signal #2 (-5 dB SNR)** | | | | | | |
| # of IMFs + Res | 8 | 11 | 10 | 9 | 10 | 17 |
| $QoD_1$ | 0.062024 | 0.219003 | 0.2337 | 0.258374 | 0.132853 | **0.39636** |
| $QoD_2$ | 3.326011 | 3.125181 | 3.062576 | 3.222284 | 3.211789 | 4.63286 |

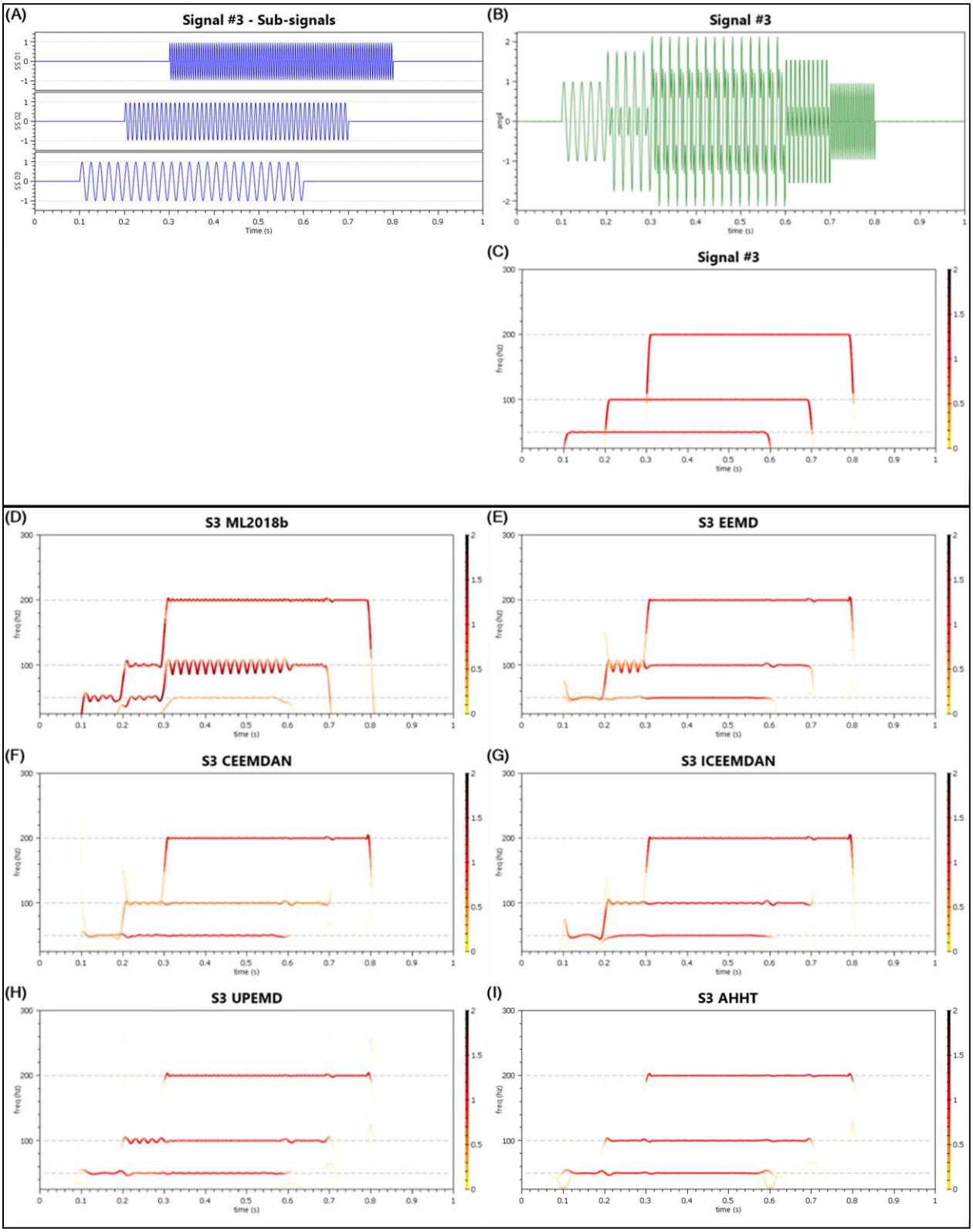


*Figure A-13 Signal 3 - Plot, Source Sub-Signals, Hilbert Spectral Decompositions*

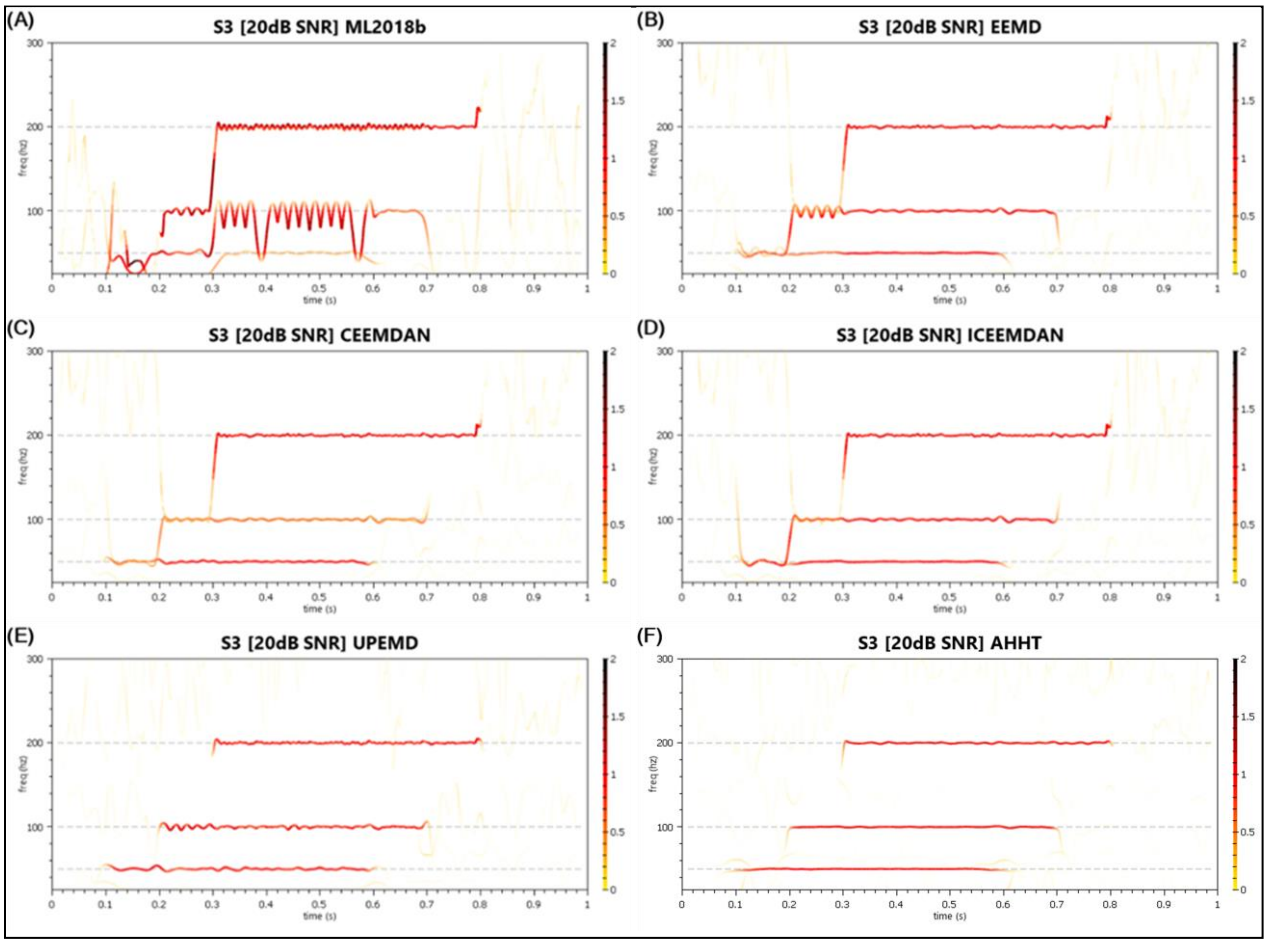


***Figure A-14 Signal 3 (20dB SNR) - Hilbert Spectral Decompositions***

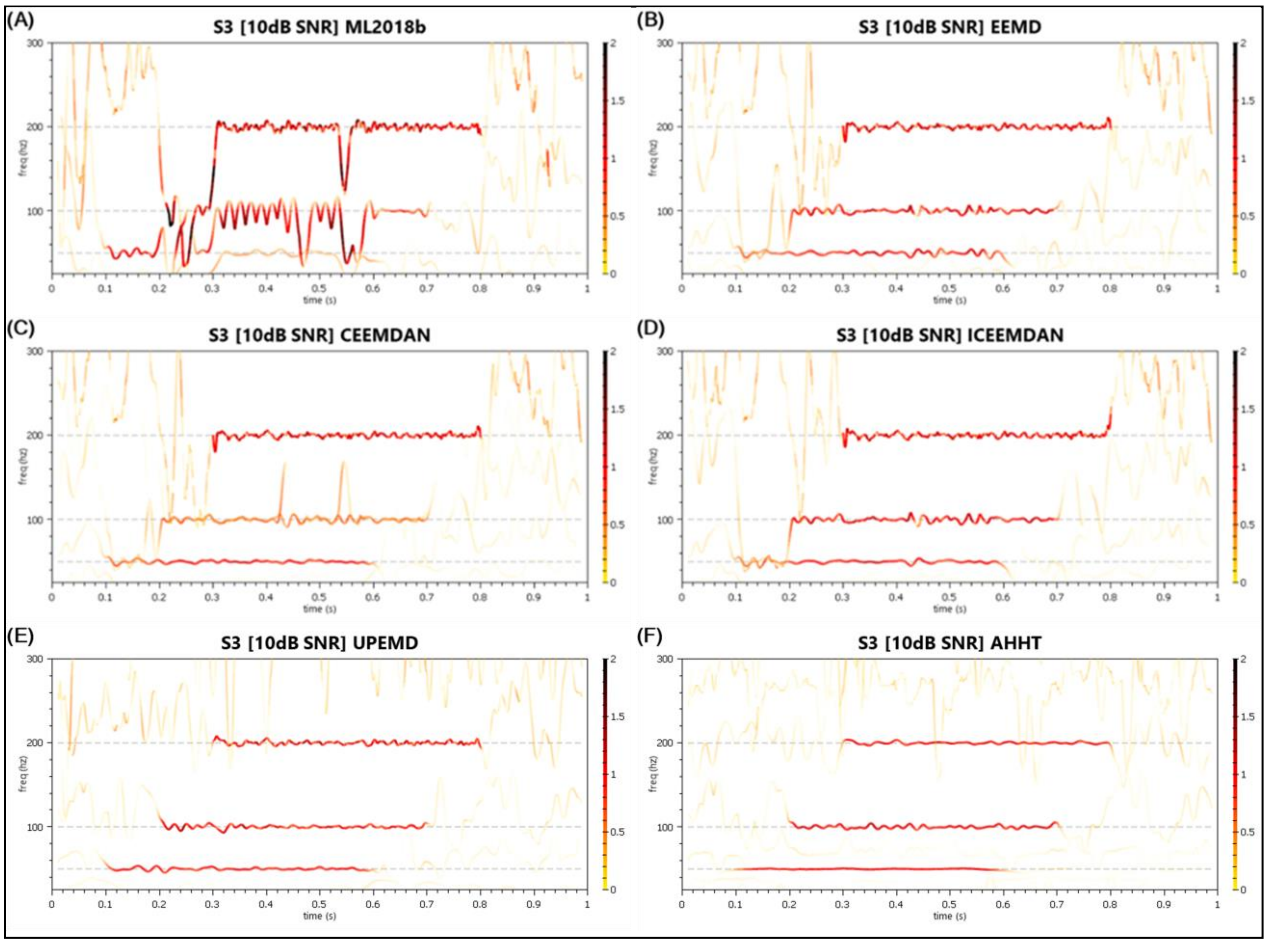


***Figure A-15 Signal 3 (10dB SNR) - Hilbert Spectral Decompositions***

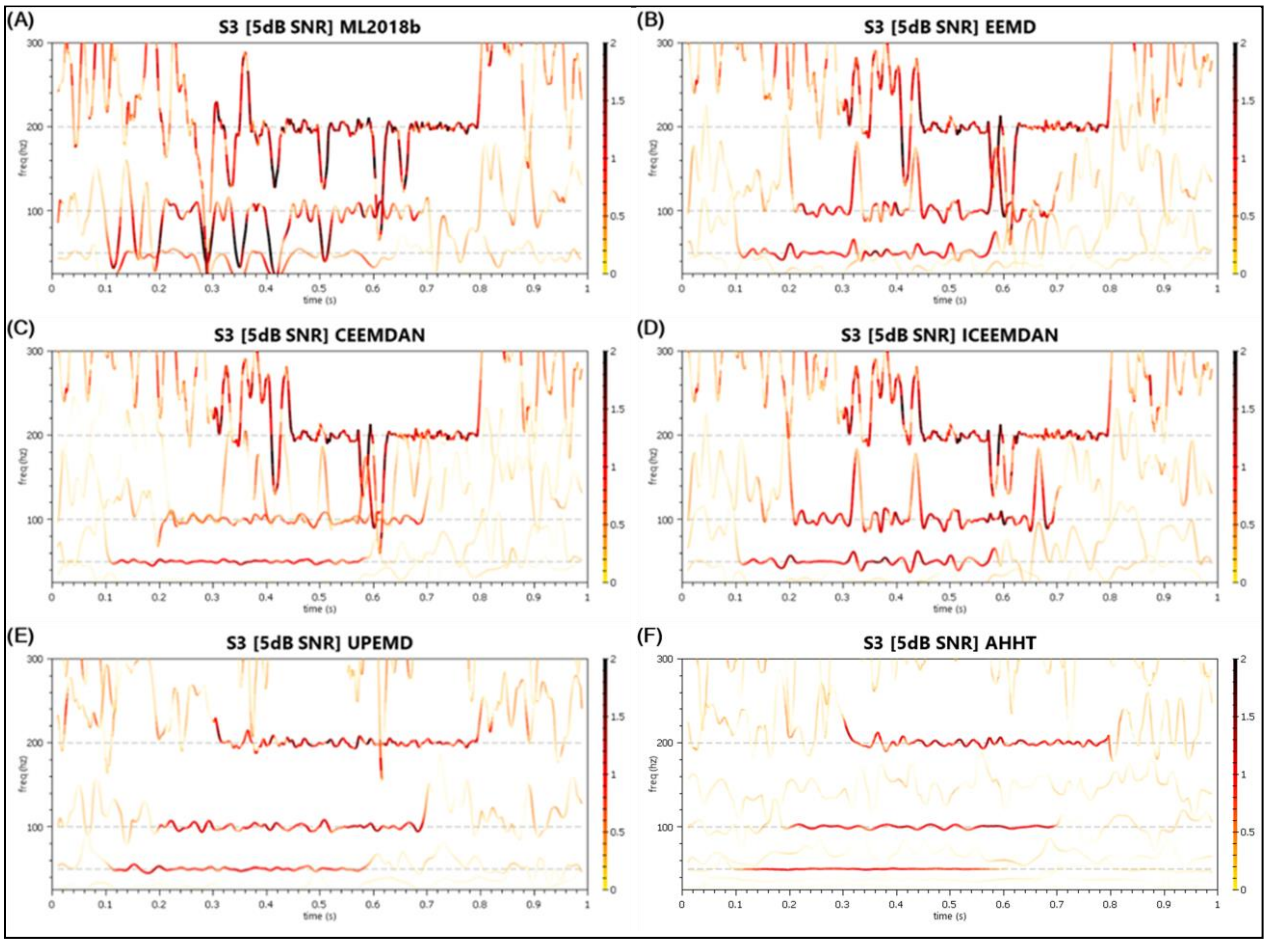


***Figure A-16 Signal 3 (5dB SNR) - Hilbert Spectral Decompositions***

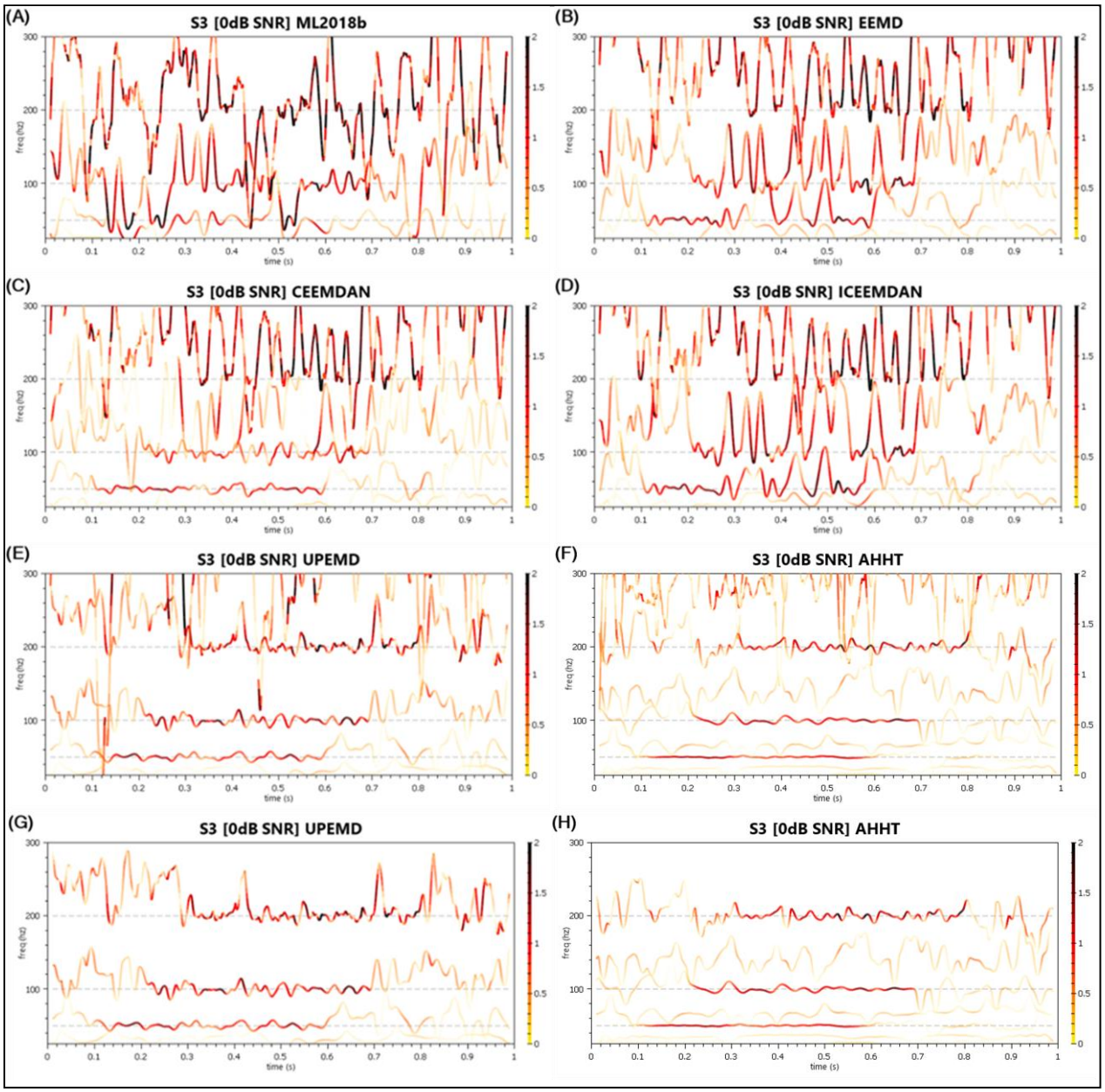


*Figure A-17 Signal 3 (0dB SNR) - Hilbert Spectral Decompositions (G – Top 1 IMF Removed, H – Top 2 IMFs Removed)*

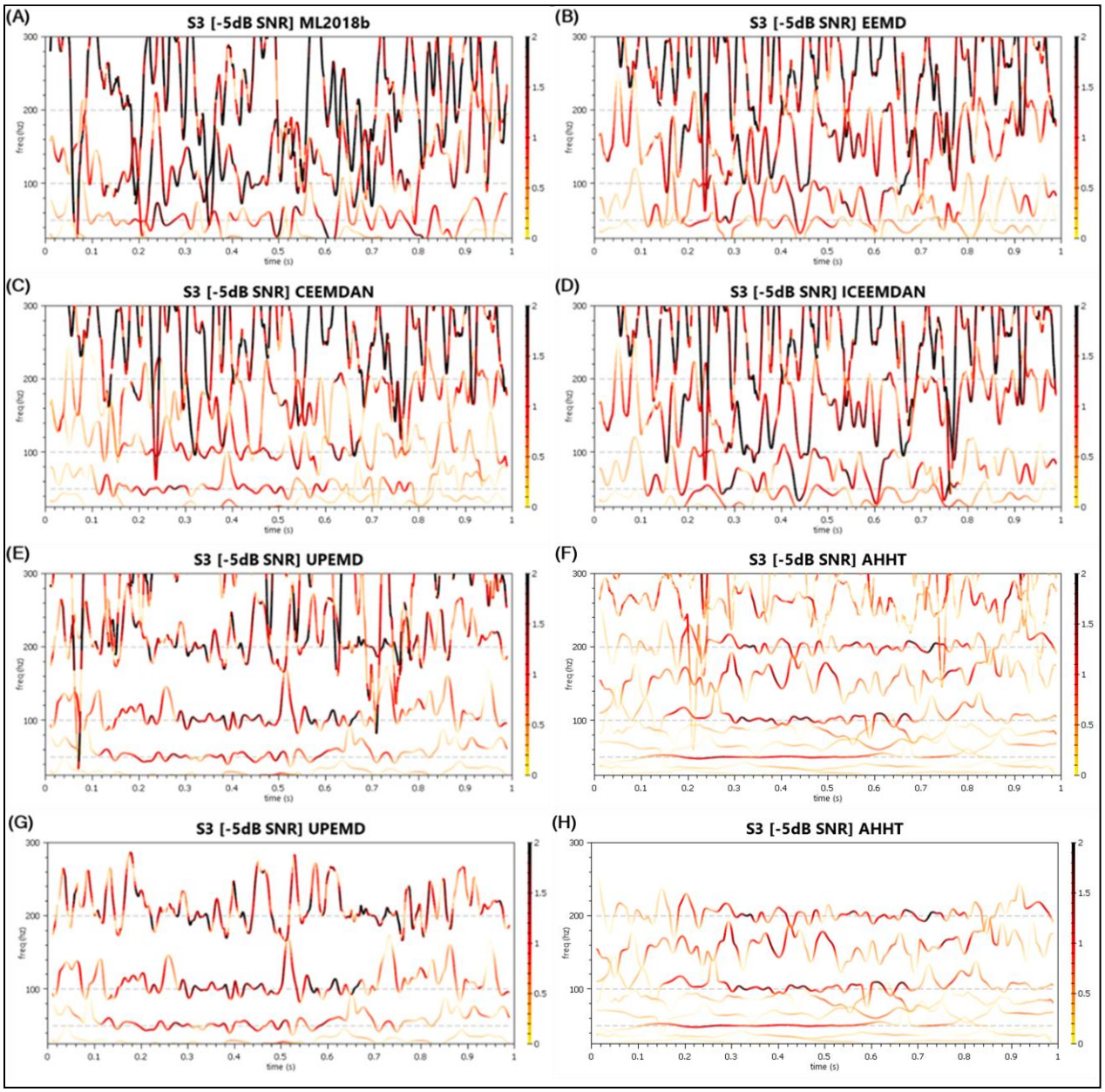


***Figure A-18 Signal 3 (-5dB SNR) - Hilbert Spectral Decompositions (G – Top 1 IMF Removed, H – Top 3 IMFs Removed)***

***Table A-3 Signal 3 (All) - IMF Counts and QoD Values***

| | MATLAB EMD | EEMD | CEEMDAN | ICEEMDAN | UPEMD | AHHT |
|---|---|---|---|---|---|---|
| **Signal #3 – 3 Component Signals** | | | | | | |
| # of IMFs + Res | 9 | 10 | 11 | 10 | 9 | 4 |
| $QoD_1$ | 0.020886 | 0.557792 | 0.37078 | 0.544032 | 0.529846 | **0.753141** |
| $QoD_2$ | 0.613839 | 0.10765 | 0.253335 | 0.174159 | 0.12163 | **0.051944** |
| **Signal #3 (20 dB SNR)** | | | | | | |
| # of IMFs + Res | 7 | 11 | 11 | 9 | 9 | 8 |
| $QoD_1$ | -0.00821 | 0.319809 | 0.198 | 0.347089 | 0.291731 | **0.510485** |
| $QoD_2$ | 0.320405 | 0.122919 | 0.630467 | 0.165799 | 0.19788 | 0.235395 |
| **Signal #3 (10 dB SNR)** | | | | | | |
| # of IMFs + Res | 8 | 11 | 10 | 8 | 9 | 8 |
| $QoD_1$ | -0.00556 | 0.106585 | 0.097331 | 0.151765 | 0.18288 | **0.385018** |
| $QoD_2$ | 0.401339 | 0.24 | 0.807162 | 0.30251 | 0.433253 | 0.527114 |
| **Signal #3 (5 dB SNR)** | | | | | | |
| # of IMFs + Res | 9 | 11 | 11 | 9 | 9 | 10 |
| $QoD_1$ | -0.02893 | 0.006274 | 0.052193 | 0.041124 | 0.089003 | **0.202904** |
| $QoD_2$ | 1.35883 | 0.347984 | 1.591972 | 0.439706 | 0.610421 | 0.989872 |
| **Signal #3 (0 dB SNR)** | | | | | | |
| # of IMFs + Res | 8 | 11 | 10 | 9 | 9 | 13 |
| $QoD_1$ | -0.01262 | -0.0225 | 0.007386 | -0.0209 | 0.015153 | **0.104714** |
| $QoD_2$ | 1.141699 | 2.033299 | 1.707571 | 1.70374 | 1.116571 | 2.027863 |
| **Signal #3 (-5 dB SNR)** | | | | | | |
| # of IMFs + Res | 9 | 11 | 10 | 9 | 9 | 18 |
| $QoD_1$ | -0.0105 | -0.08706 | -0.0411 | 0.001675 | -0.01545 | **0.076302** |
| $QoD_2$ | 2.838753 | 3.423026 | 3.264821 | 2.549948 | 2.836086 | 4.371667 |

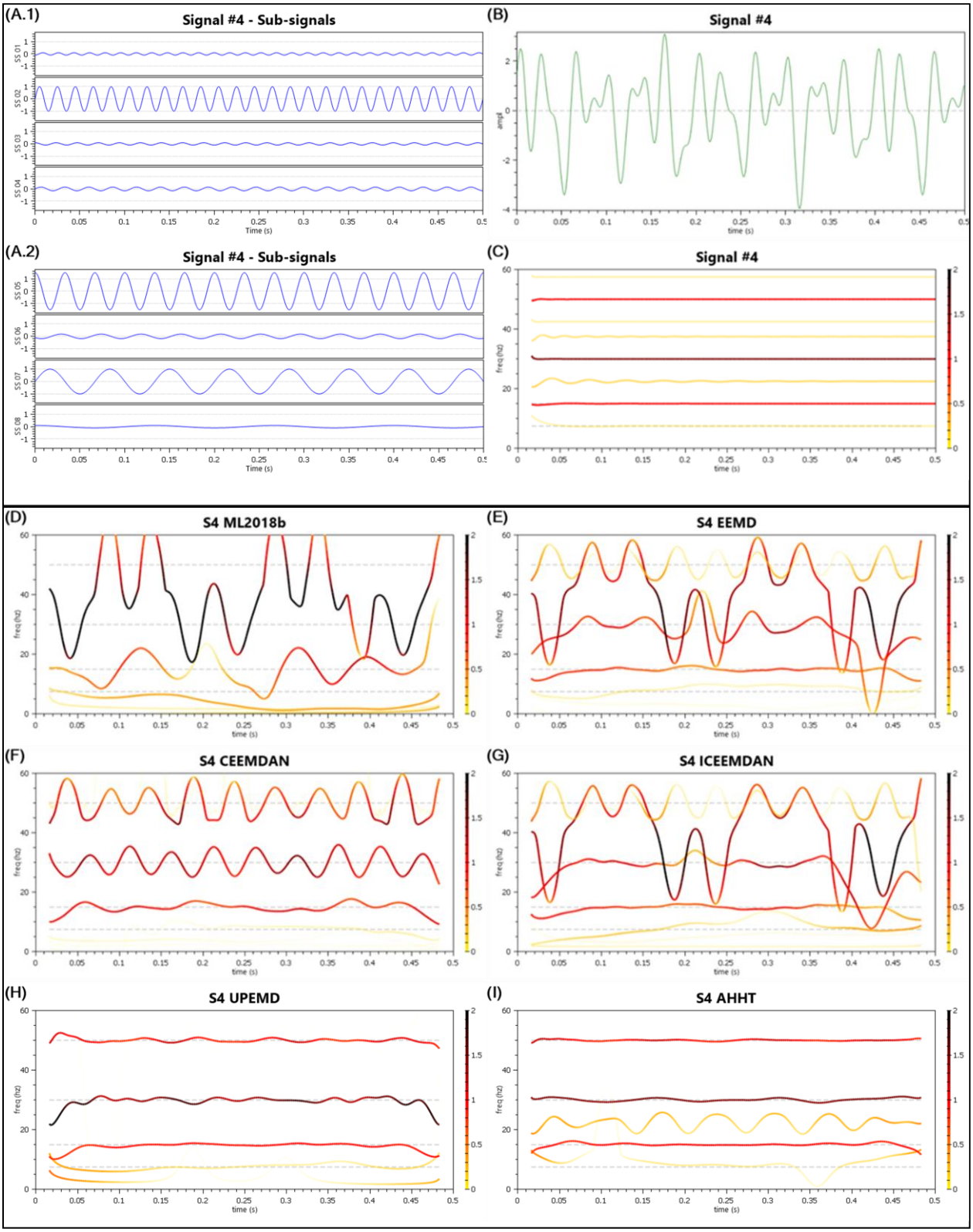


***Figure A-19 Signal 4 - Plot, Source Sub-Signals, Hilbert Spectral Decompositions***

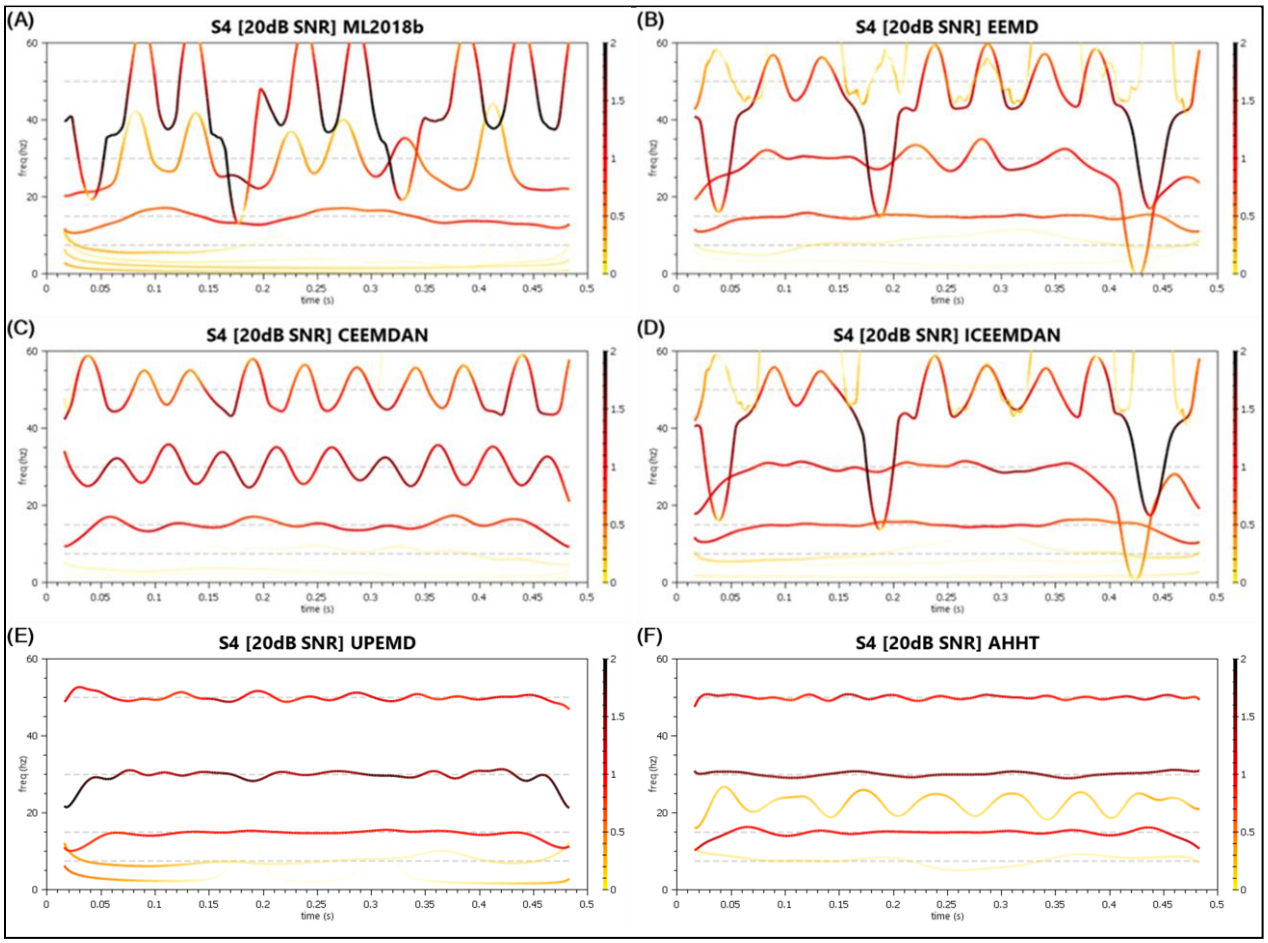


***Figure A-20 Signal 4 (20dB SNR) - Hilbert Spectral Decompositions***

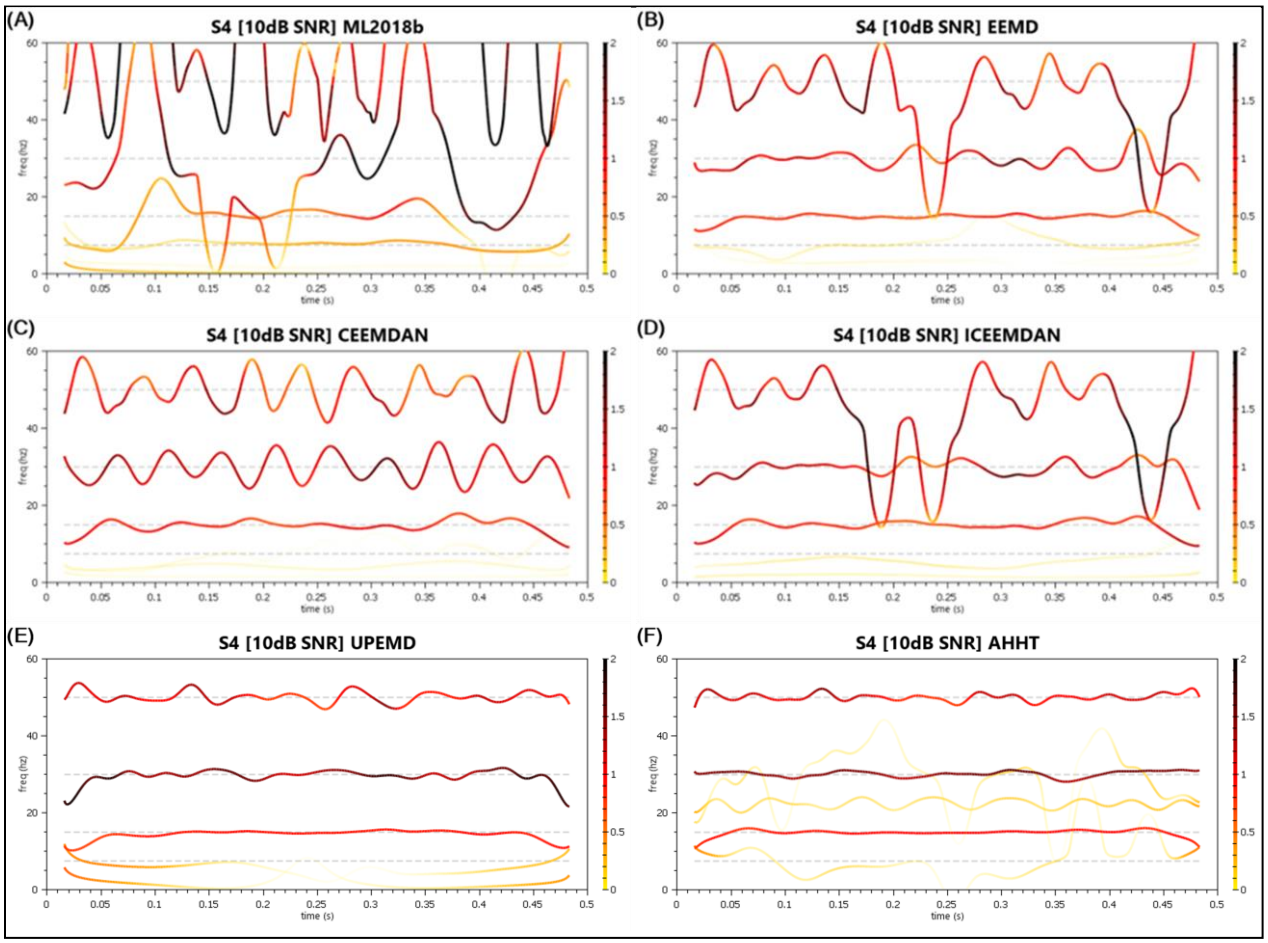


***Figure A-21 Signal 4 (10dB SNR) - Hilbert Spectral Decompositions***

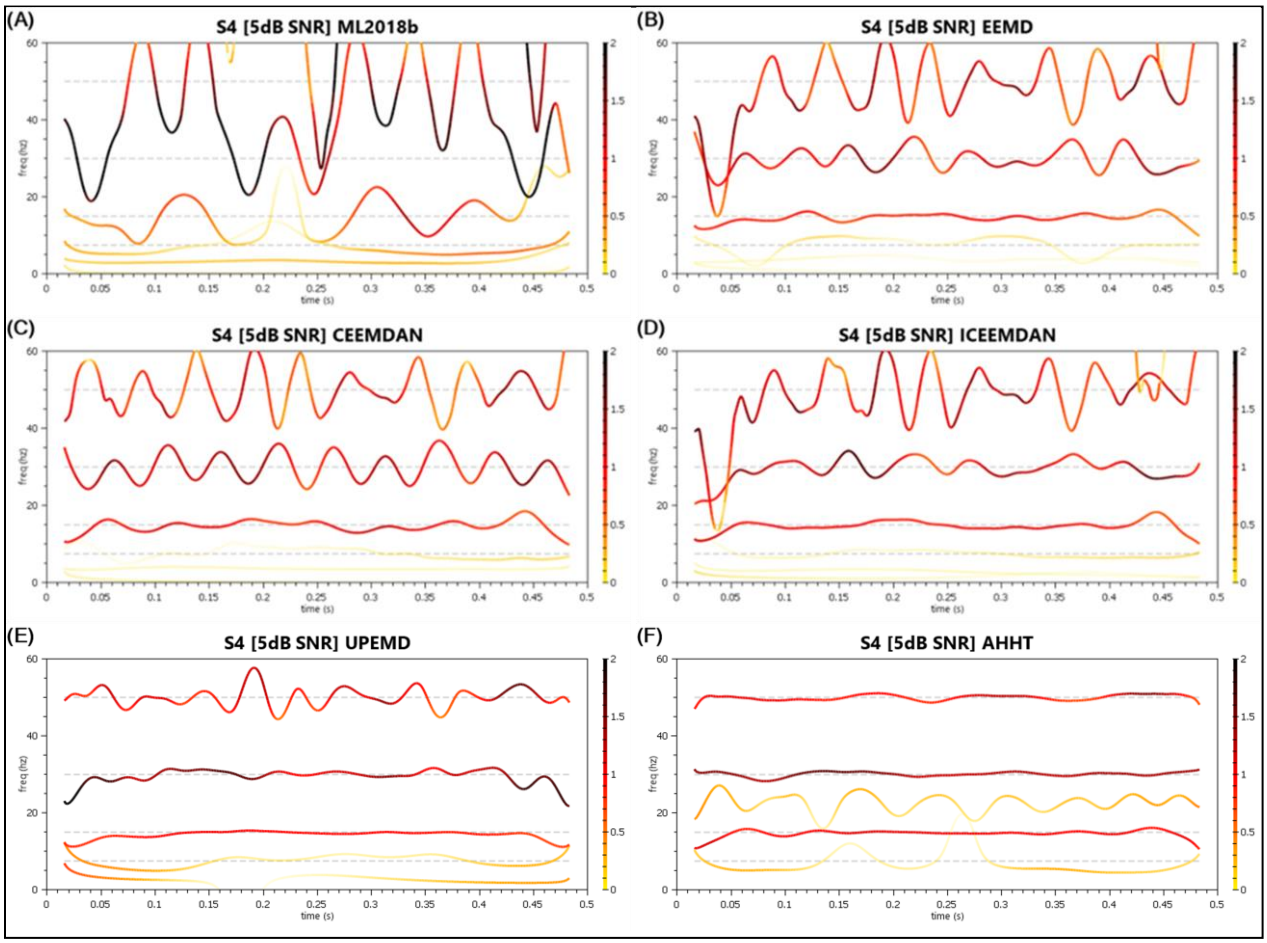


***Figure A-22 Signal 4 (5dB SNR) - Hilbert Spectral Decompositions***

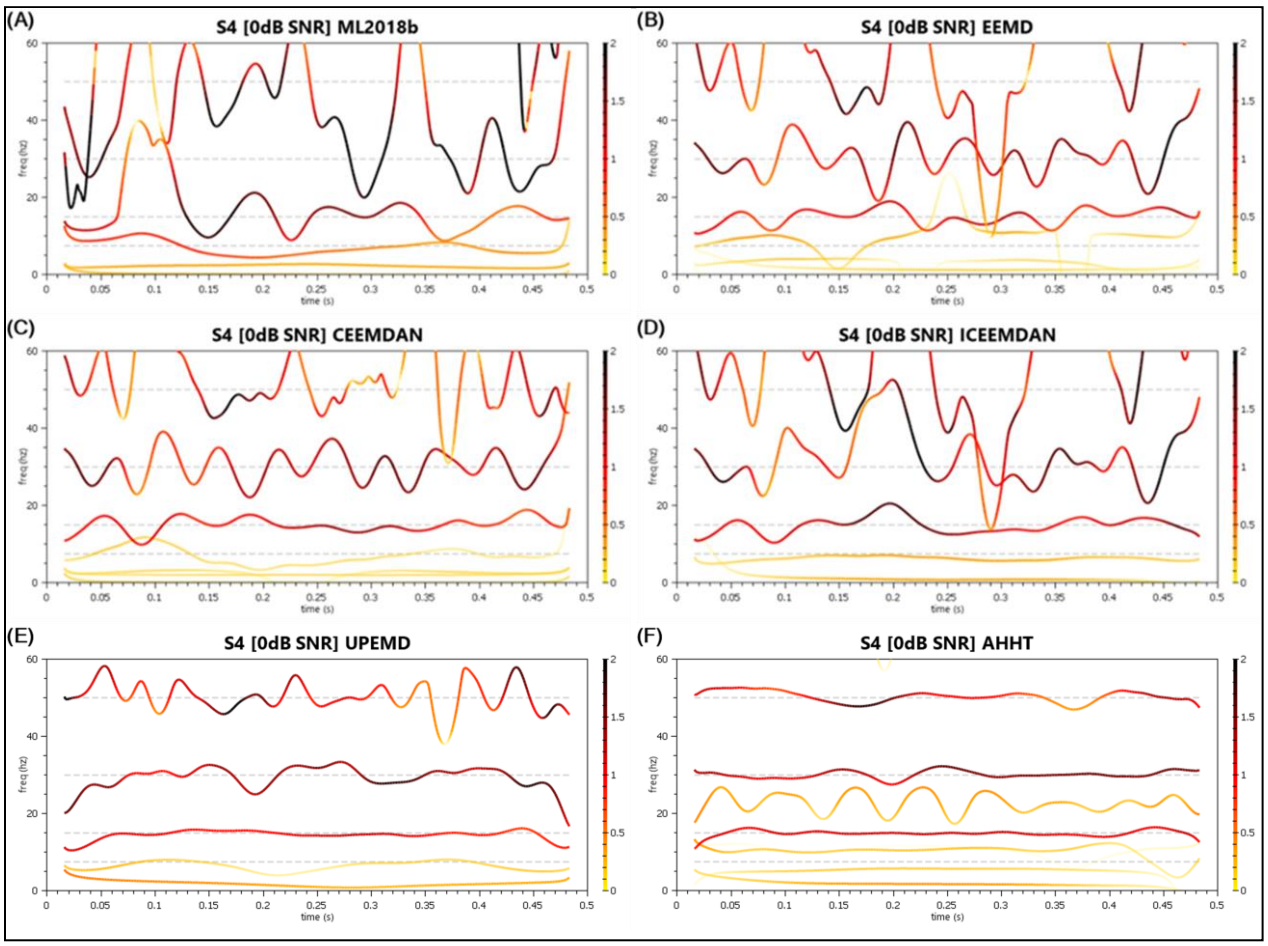


***Figure A-23 Signal 4 (0dB SNR) - Hilbert Spectral Decompositions***

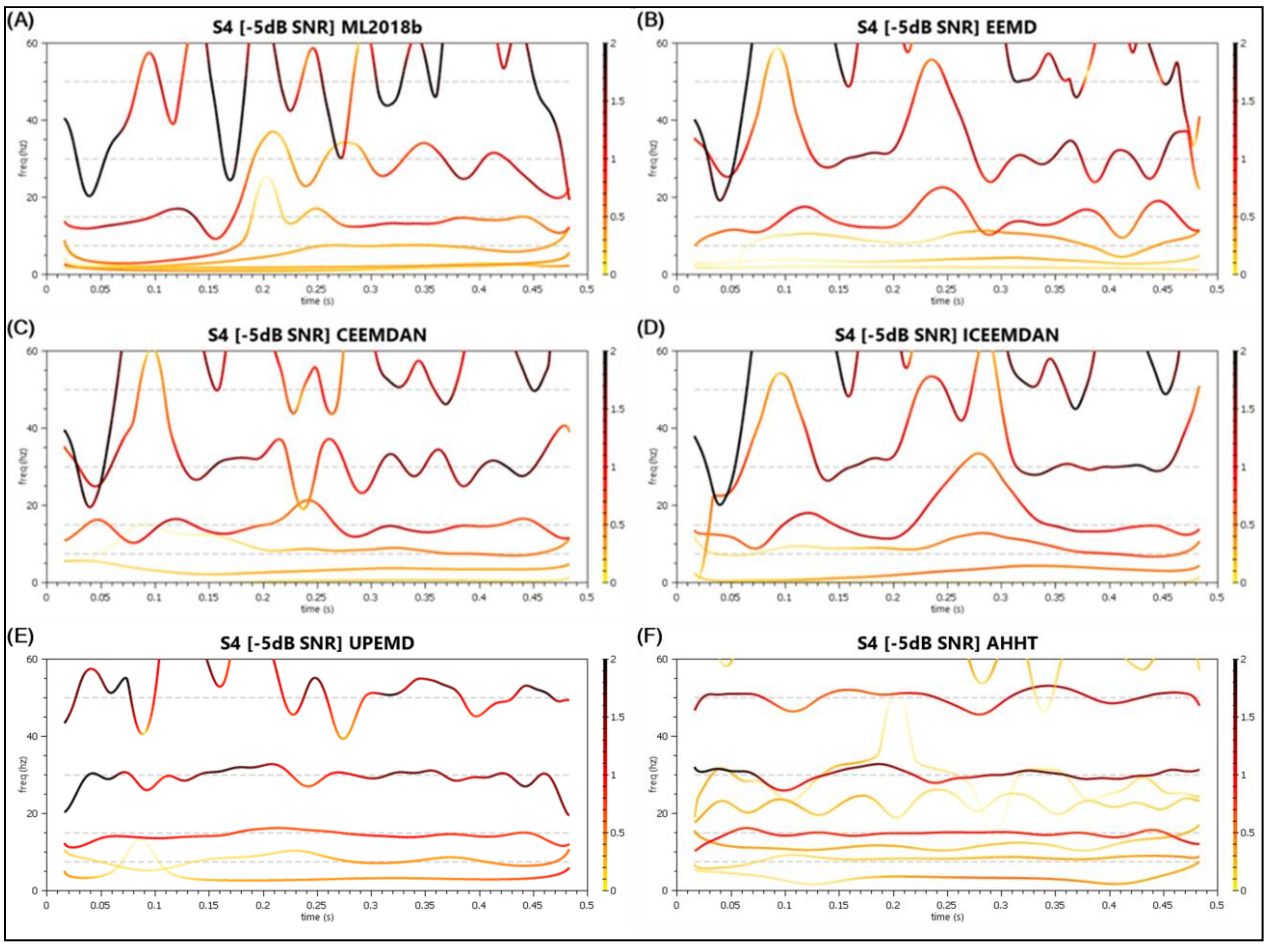


***Figure A-24 Signal 4 (-5dB SNR) - Hilbert Spectral Decompositions***

***Table A-4 Signal 4 (All) - IMF Counts and QoD Values***

| | MATLAB EMD | EEMD | CEEMDAN | ICEEMDAN | UPEMD | AHHT |
|---|---|---|---|---|---|---|
| **Signal #4 – 8 Component Signals** | | | | | | |
| # of IMFs + Res | 5 | 10 | 10 | 8 | 8 | 5 |
| $QoD_1$ | 0.005595 | 0.024312 | 0.060725 | 0.030793 | 0.198268 | **0.295797** |
| $QoD_2$ | 0.493316 | 0.04983 | 0.090839 | 0.113139 | 0.155964 | **0** |
| **Signal #4 (20 dB SNR)** | | | | | | |
| # of IMFs + Res | 8 | 10 | 10 | 8 | 8 | 9 |
| $QoD_1$ | 0.015475 | 0.030754 | 0.054051 | 0.04584 | 0.195282 | **0.314472** |
| $QoD_2$ | 0.394653 | 0.183965 | 0.237149 | 0.101842 | 0.43245 | 0.277699 |
| **Signal #4 (10 dB SNR)** | | | | | | |
| # of IMFs + Res | 7 | 10 | 9 | 7 | 8 | 11 |
| $QoD_1$ | 0.005865 | 0.052937 | 0.060017 | 0.05125 | 0.15364 | **0.274203** |
| $QoD_2$ | 0.672487 | 0.048135 | 0.125739 | 0.073667 | 0.504773 | 0.812328 |
| **Signal #4 (5 dB SNR)** | | | | | | |
| # of IMFs + Res | 9 | 10 | 9 | 8 | 8 | 12 |
| $QoD_1$ | 0.003798 | 0.070892 | 0.068167 | 0.111237 | 0.147371 | **0.232234** |
| $QoD_2$ | 1.220619 | 0.866165 | 1.069117 | 0.903985 | 1.334719 | 1.84262 |
| **Signal #4 (0 dB SNR)** | | | | | | |
| # of IMFs + Res | 8 | 10 | 10 | 7 | 8 | 15 |
| $QoD_1$ | 0.001887 | 0.040406 | 0.046947 | 0.035357 | 0.103671 | **0.138437** |
| $QoD_2$ | 2.550354 | 2.508192 | 2.744795 | 2.327903 | 2.84775 | 3.170976 |
| **Signal #4 (-5 dB SNR)** | | | | | | |
| # of IMFs + Res | 9 | 10 | 9 | 8 | 8 | 16 |
| $QoD_1$ | -0.00023 | 0.035635 | 0.03574 | 0.037776 | 0.075311 | **0.124583** |
| $QoD_2$ | 4.210165 | 4.536542 | 4.109397 | 4.830886 | 3.794886 | 6.85488 |

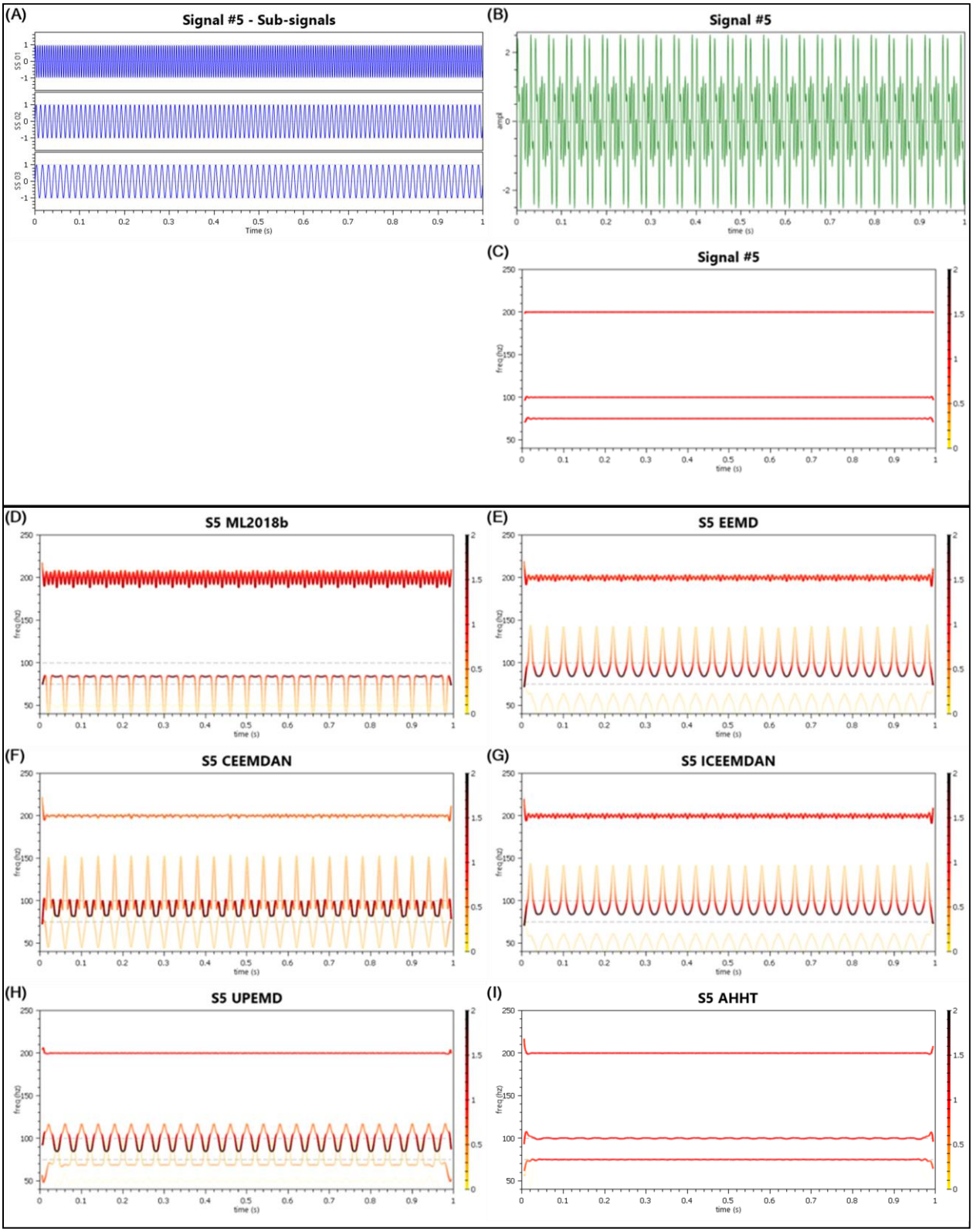


*Figure A-25 Signal 5 - Plot, Source Sub-Signals, Hilbert Spectral Decompositions*

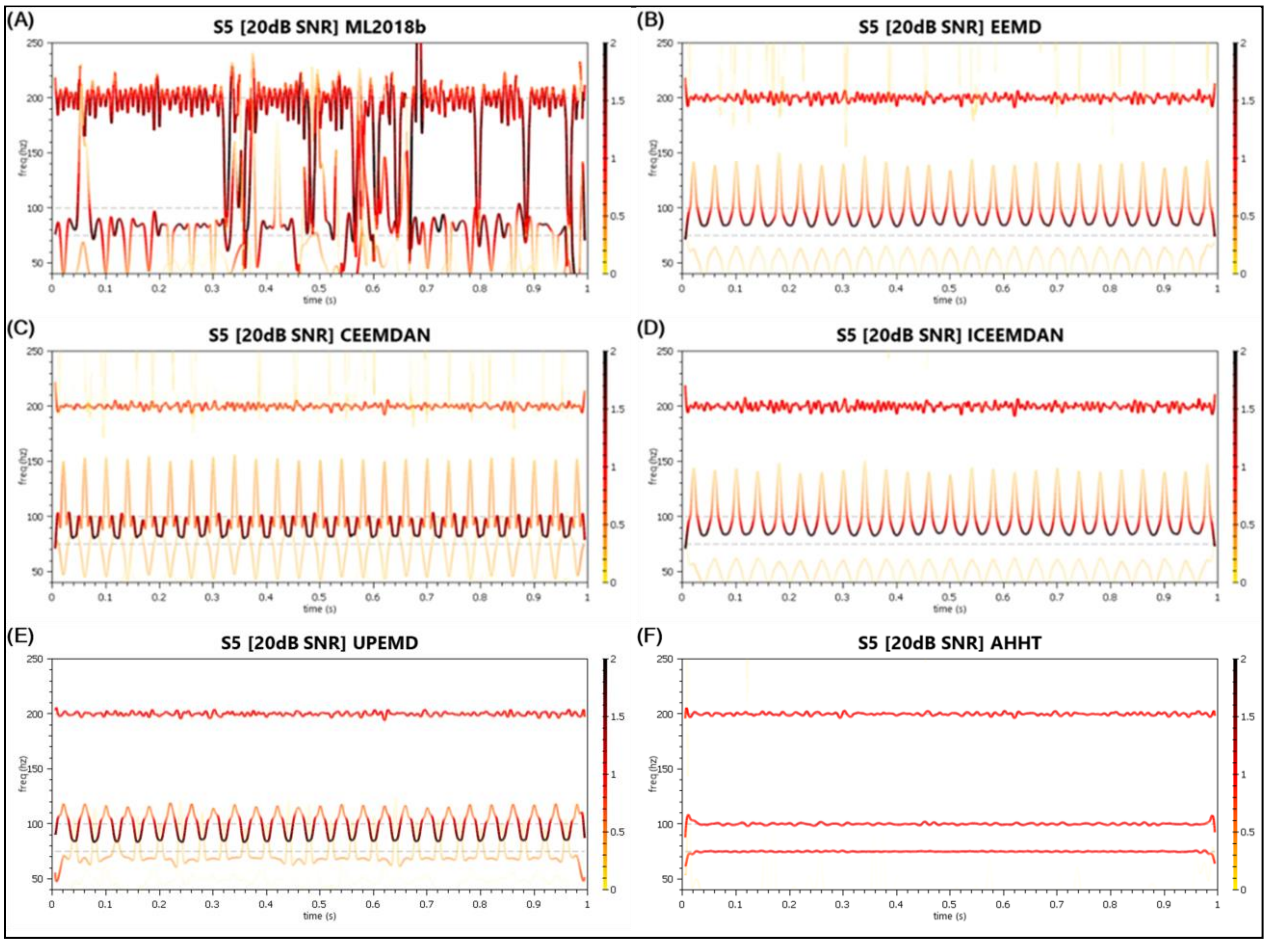


***Figure A-26 Signal 5 (20dB SNR) - Hilbert Spectral Decompositions***

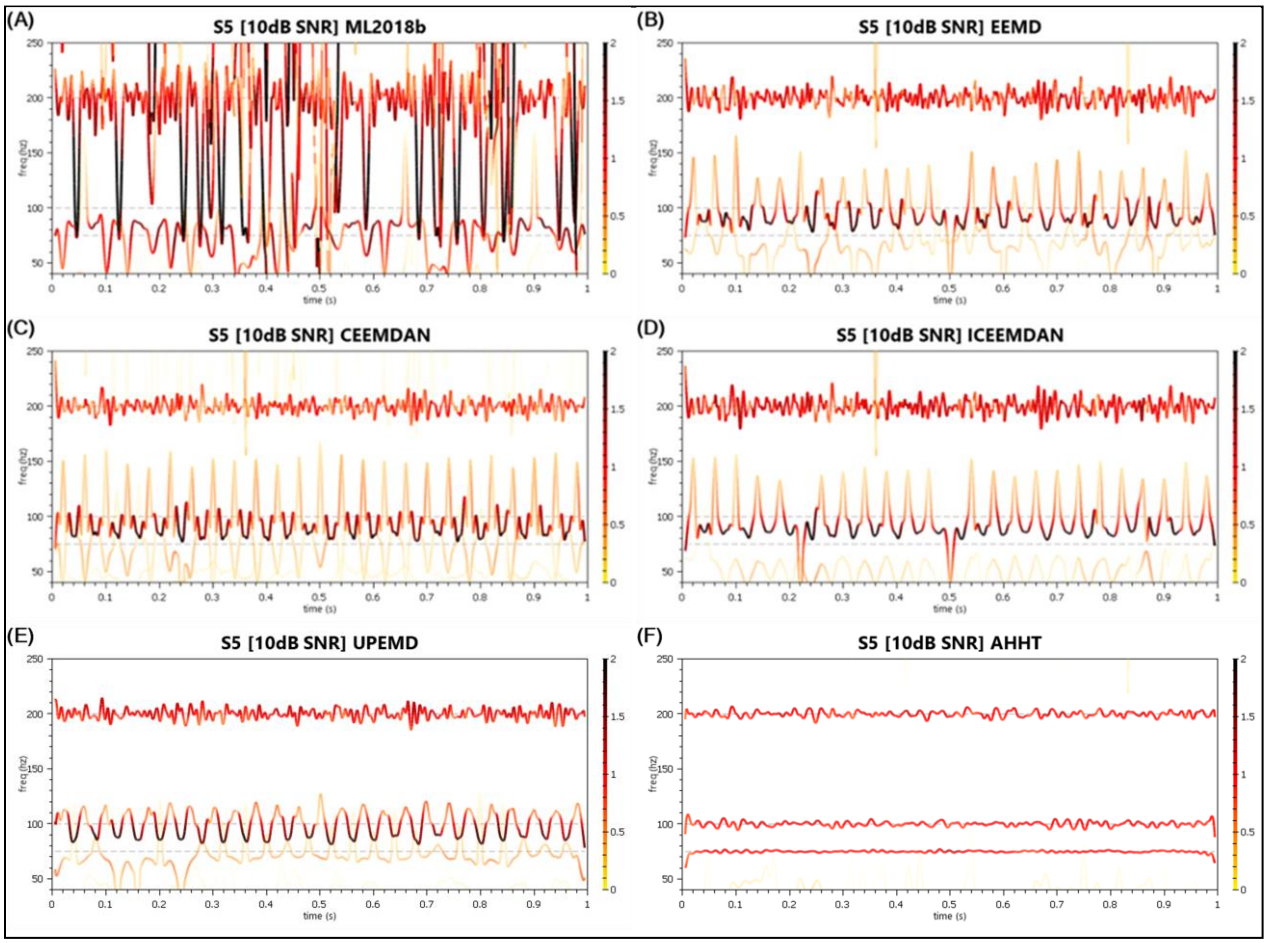


***Figure A-27 Signal 5 (10dB SNR) - Hilbert Spectral Decompositions***

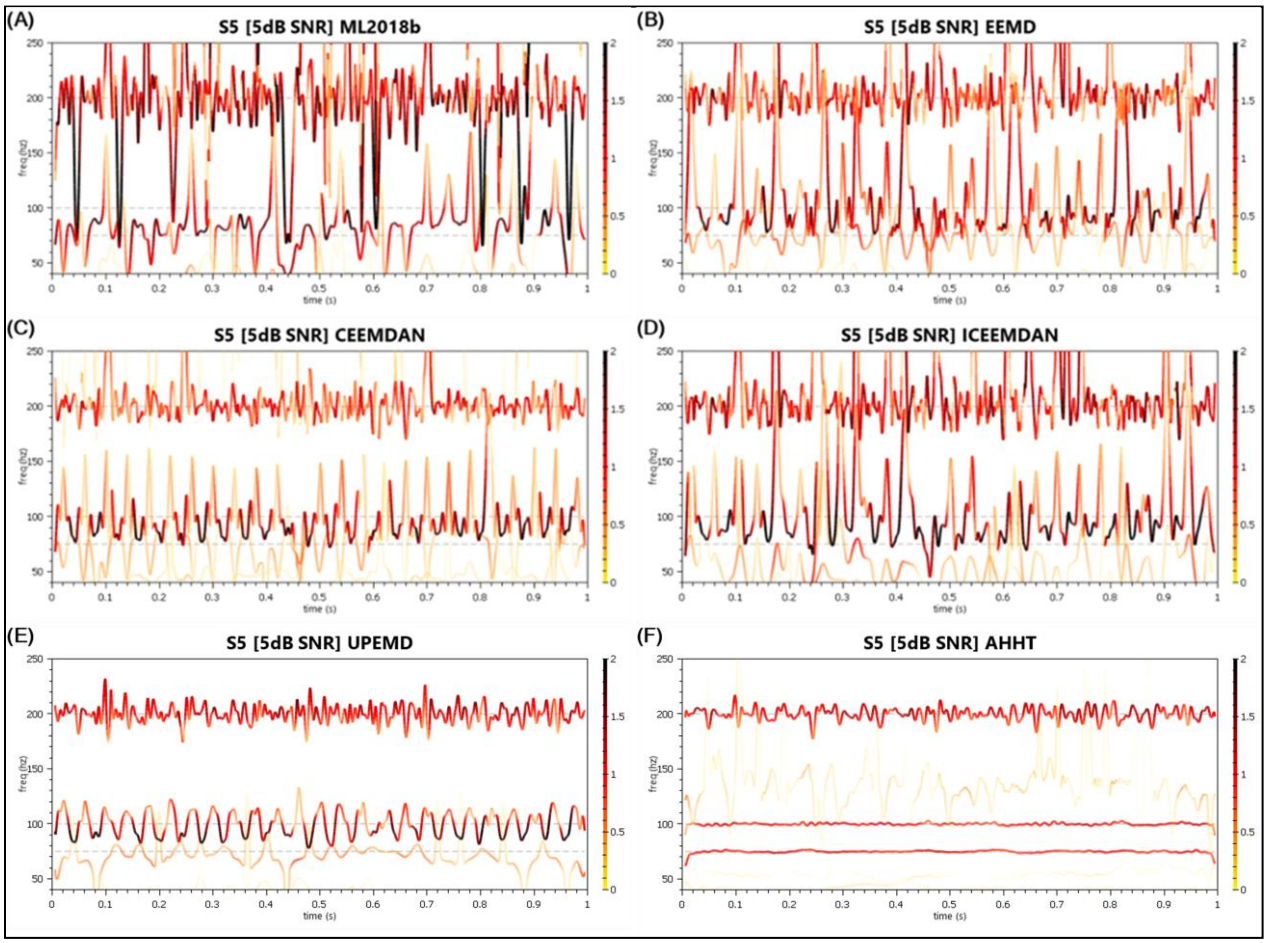


***Figure A-28 Signal 5 (5dB SNR) - Hilbert Spectral Decompositions***

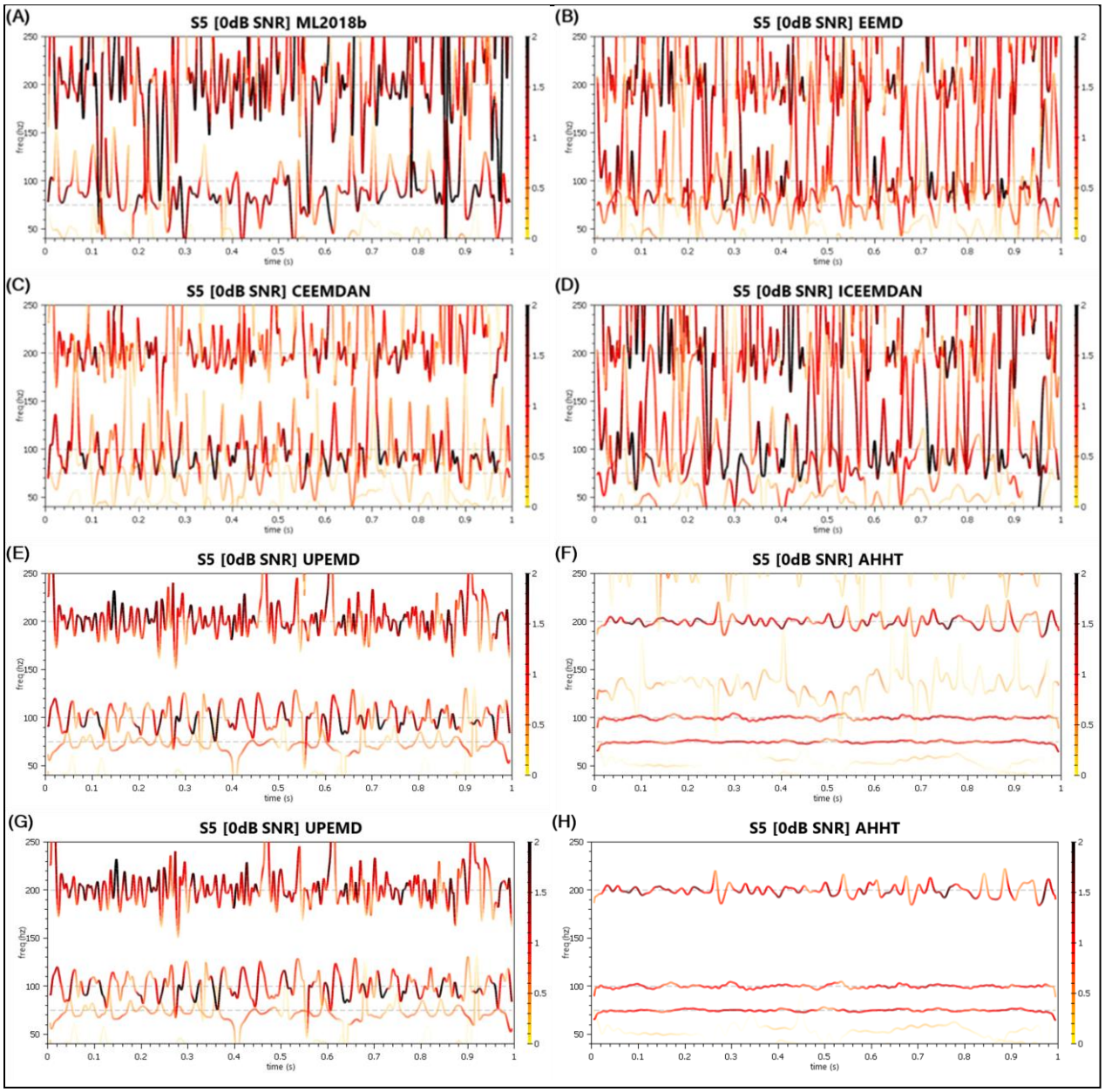


***Figure A-29 Signal 5 (0dB SNR) - Hilbert Spectral Decompositions***
***(G – Top 2 IMFs Removed: No Significant Difference, H – Top 6 IMFs + IMF #8 Removed)***

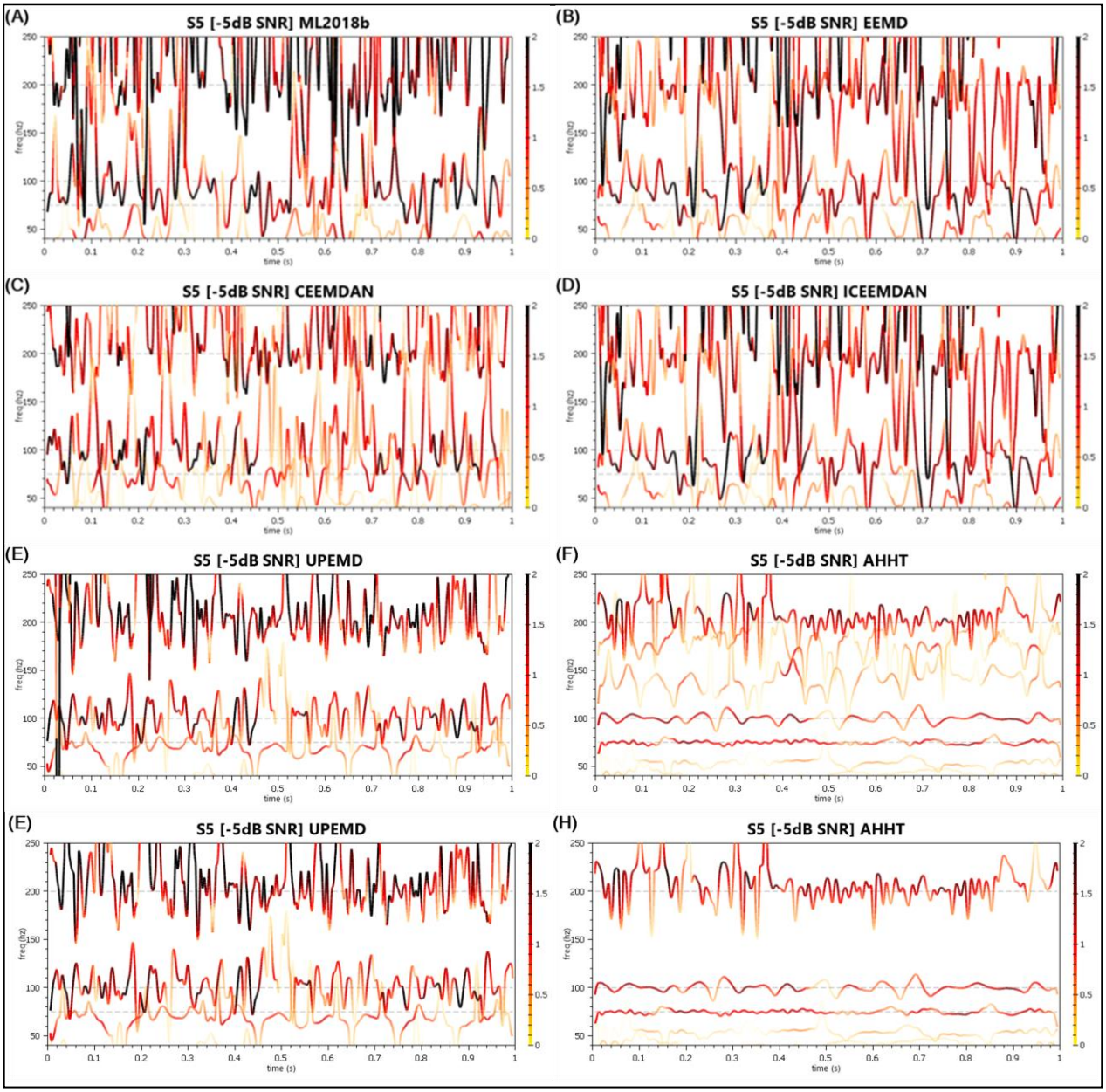


***Figure A-30 Signal 5 (-5dB SNR) - Hilbert Spectral Decompositions***
***(G – Top 2 IMFs Removed, H – Top 5 IMFs + IMFs #7 & #8 Removed)***

***Table A-5 Signal 5 (All) - IMF Counts and QoD Values***

| | MATLAB EMD | EEMD | CEEMDAN | ICEEMDAN | UPEMD | AHHT |
|---|---|---|---|---|---|---|
| **Signal #5 – 3 Component Signals** | | | | | | |
| # of IMFs + Res | 5 | 12 | 11 | 10 | 10 | 4 |
| $QoD_1$ | 0.10039 | 0.230145 | 0.021741 | 0.304136 | 0.320848 | **0.950357** |
| $QoD_2$ | 0.132166 | 0.289157 | 0.539182 | 0.272371 | 0.191616 | **0.007954** |
| **Signal #5 (20 dB SNR)** | | | | | | |
| # of IMFs + Res | 9 | 11 | 12 | 9 | 10 | 7 |
| $QoD_1$ | 0.038323 | 0.221079 | 0.035741 | 0.251931 | 0.289975 | **0.935122** |
| $QoD_2$ | 0.656645 | 0.381416 | 0.637039 | 0.3977 | 0.337138 | 0.223352 |
| **Signal #5 (10 dB SNR)** | | | | | | |
| # of IMFs + Res | 8 | 12 | 12 | 9 | 10 | 8 |
| $QoD_1$ | 0.033308 | 0.091251 | 0.091839 | 0.09175 | 0.190836 | **0.714732** |
| $QoD_2$ | 0.521943 | 0.799889 | 1.0263 | 0.738757 | 0.778061 | 0.774399 |
| **Signal #5 (5 dB SNR)** | | | | | | |
| # of IMFs + Res | 9 | 12 | 12 | 10 | 10 | 12 |
| $QoD_1$ | 0.0295 | 0.034119 | 0.057548 | 0.030567 | 0.121964 | **0.543822** |
| $QoD_2$ | 0.571785 | 1.007517 | 1.674875 | 1.175834 | 1.279064 | 1.774484 |
| **Signal #5 (0 dB SNR)** | | | | | | |
| # of IMFs + Res | 10 | 13 | 12 | 11 | 10 | 15 |
| $QoD_1$ | 0.016168 | 0.026883 | 0.032202 | 0.004074 | 0.0638 | **0.442115** |
| $QoD_2$ | 0.851994 | 1.811761 | 2.178548 | 2.07707 | 2.207894 | 3.620482 |
| **Signal #5 (-5 dB SNR)** | | | | | | |
| # of IMFs + Res | 10 | 11 | 12 | 11 | 10 | 16 |
| $QoD_1$ | 0.004273 | 0.0263 | 0.034754 | 0.0263 | 0.061062 | **0.242315** |
| $QoD_2$ | 3.304944 | 4.364467 | 4.016143 | 4.364467 | 3.810706 | 6.430541 |

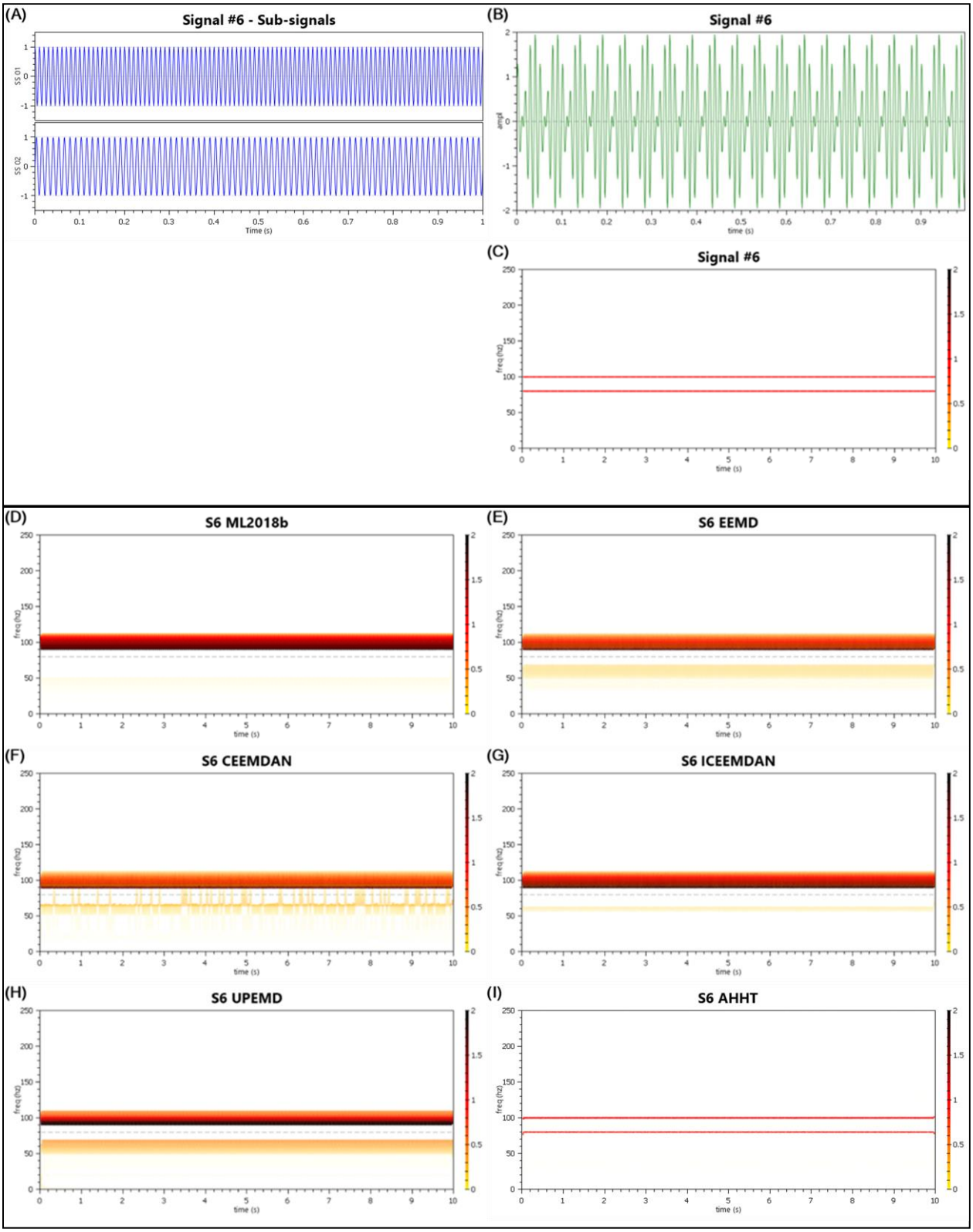


*Figure A-31 Signal 6 - Plot, Source Sub-Signals, Hilbert Spectral Decompositions*

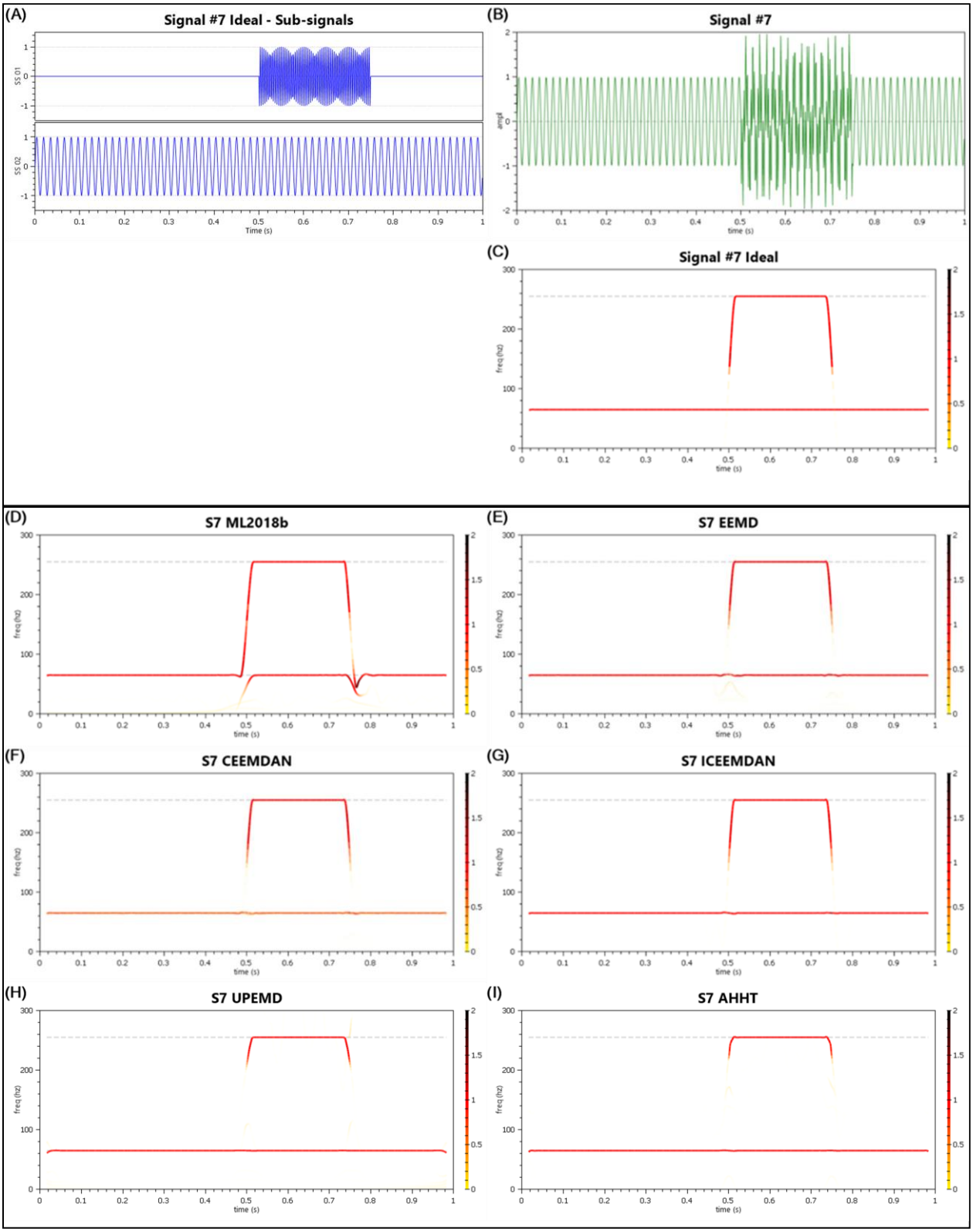


*Figure A-32 Signal 7 - Plot, Source Sub-Signals, Hilbert Spectral Decompositions*

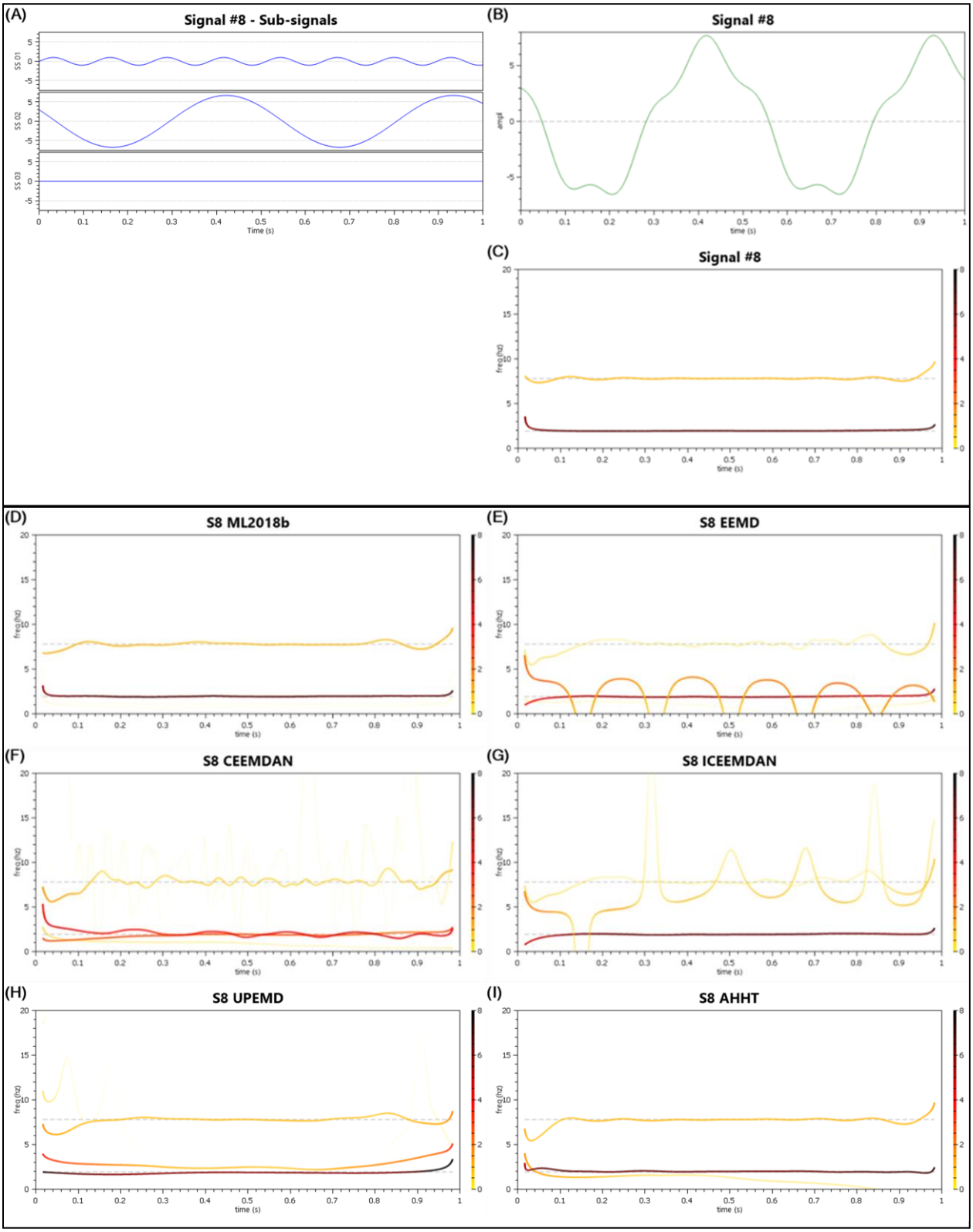


*Figure A-33 Signal 8 - Plot, Source Sub-Signals, Hilbert Spectral Decompositions*

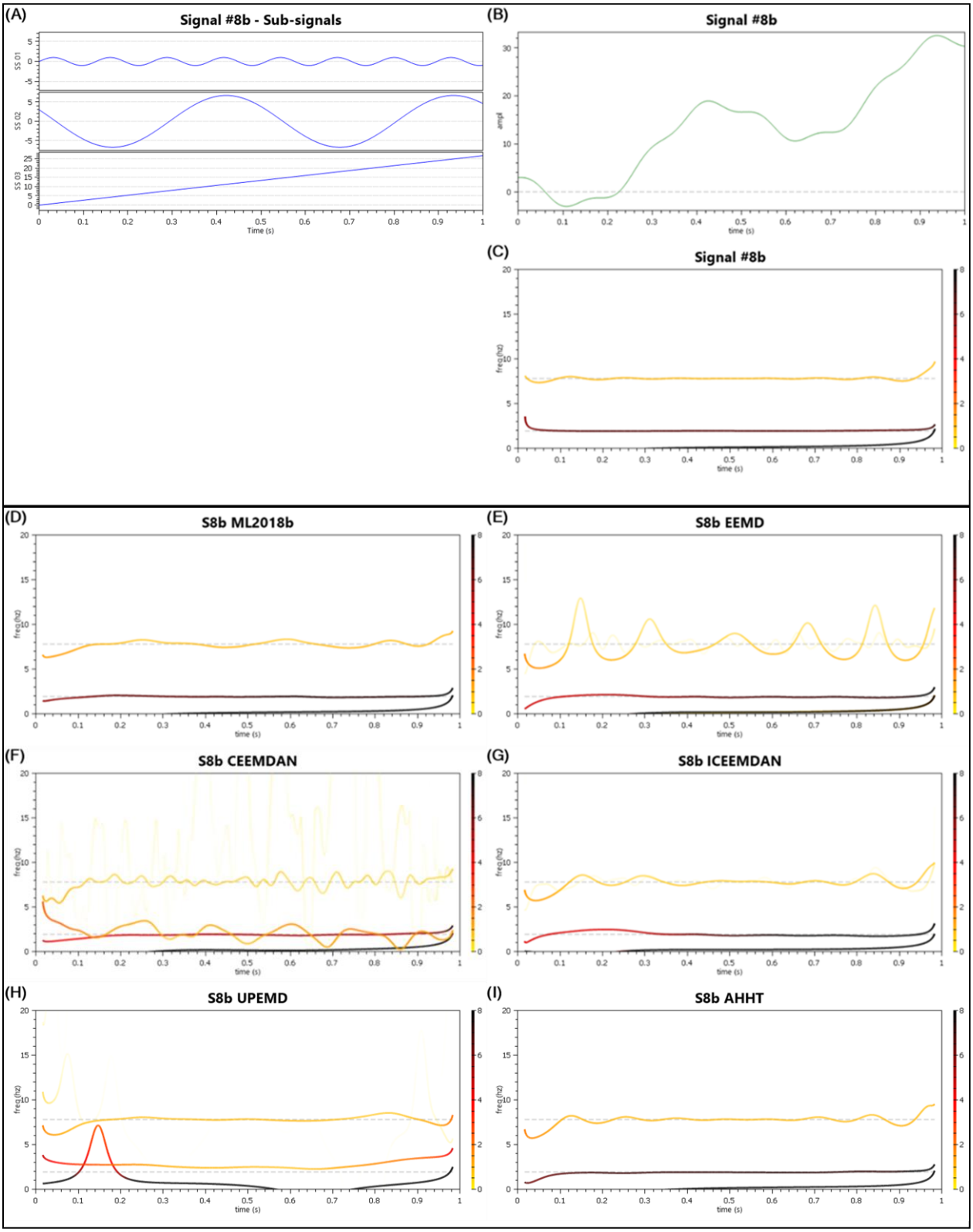


*Figure A-34 Signal 8b - Plot, Source Sub-Signals, Hilbert Spectral Decompositions*

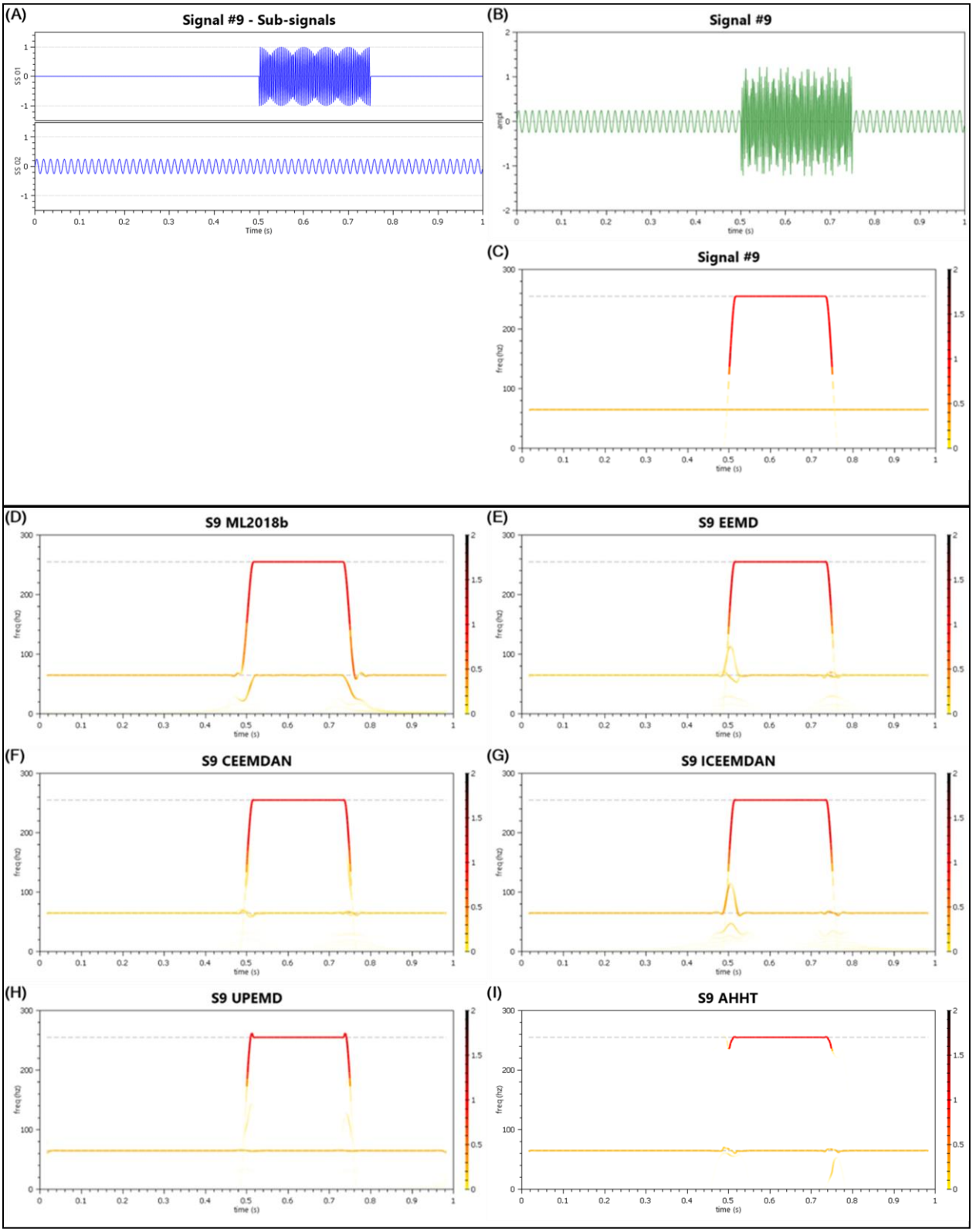


*Figure A-35 Signal 9 - Plot, Source Sub-Signals, Hilbert Spectral Decompositions*

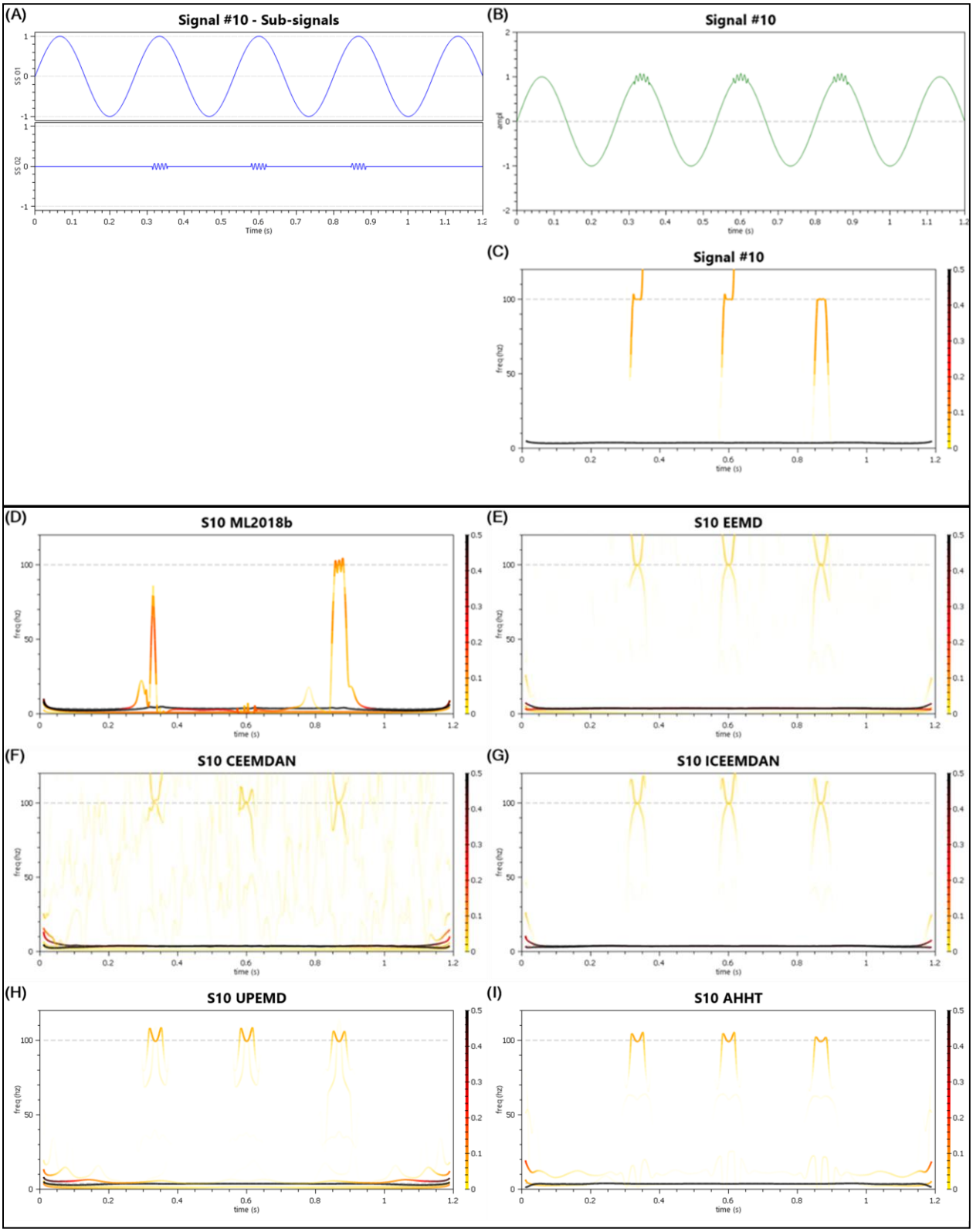


*Figure A-36 Signal 10 - Plot, Source Sub-Signals, Hilbert Spectral Decompositions*

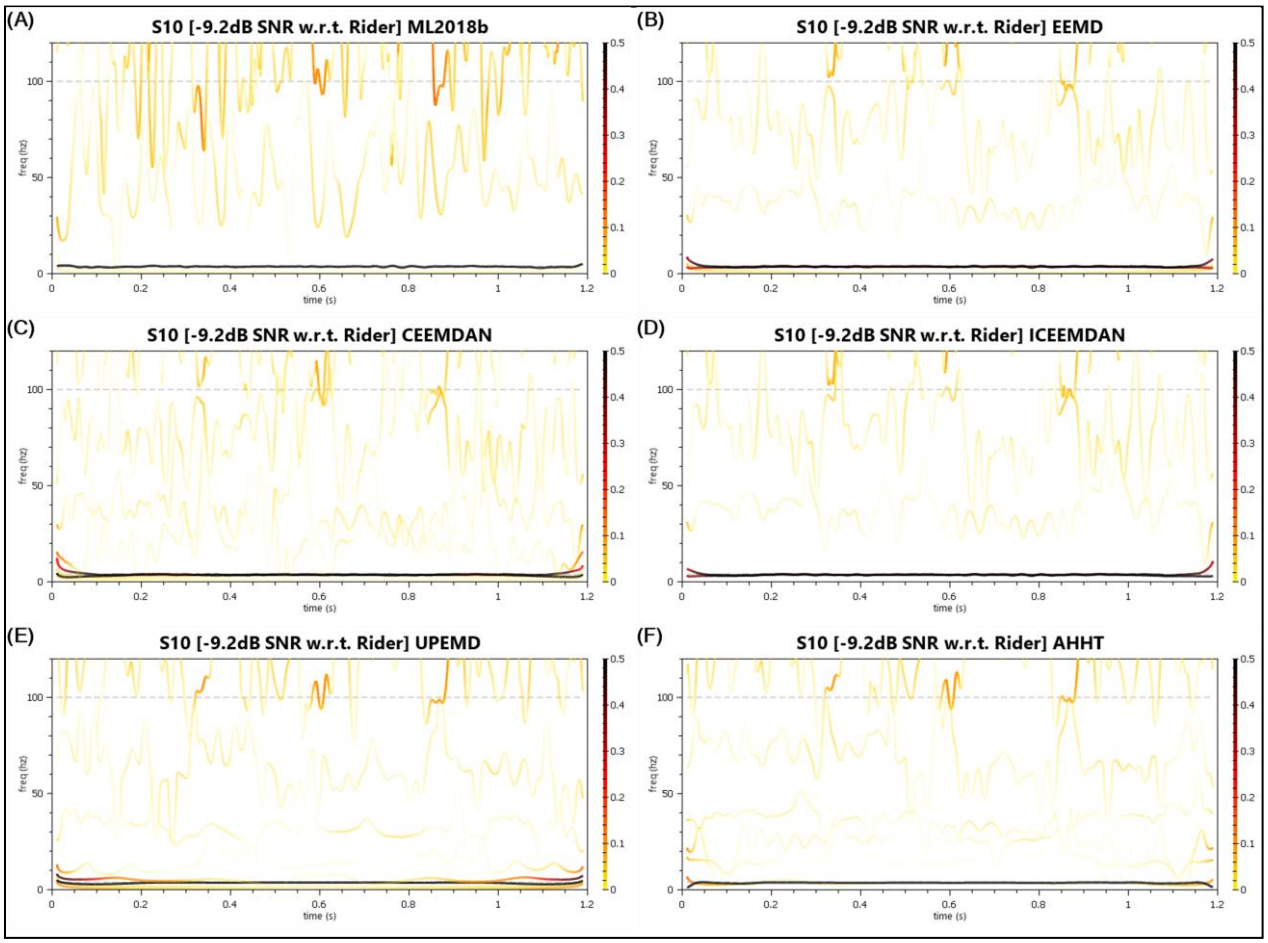


***Figure A-37 Signal 10 (-9.2dB SNR w.r.t. Rider) - Hilbert Spectral Decompositions***

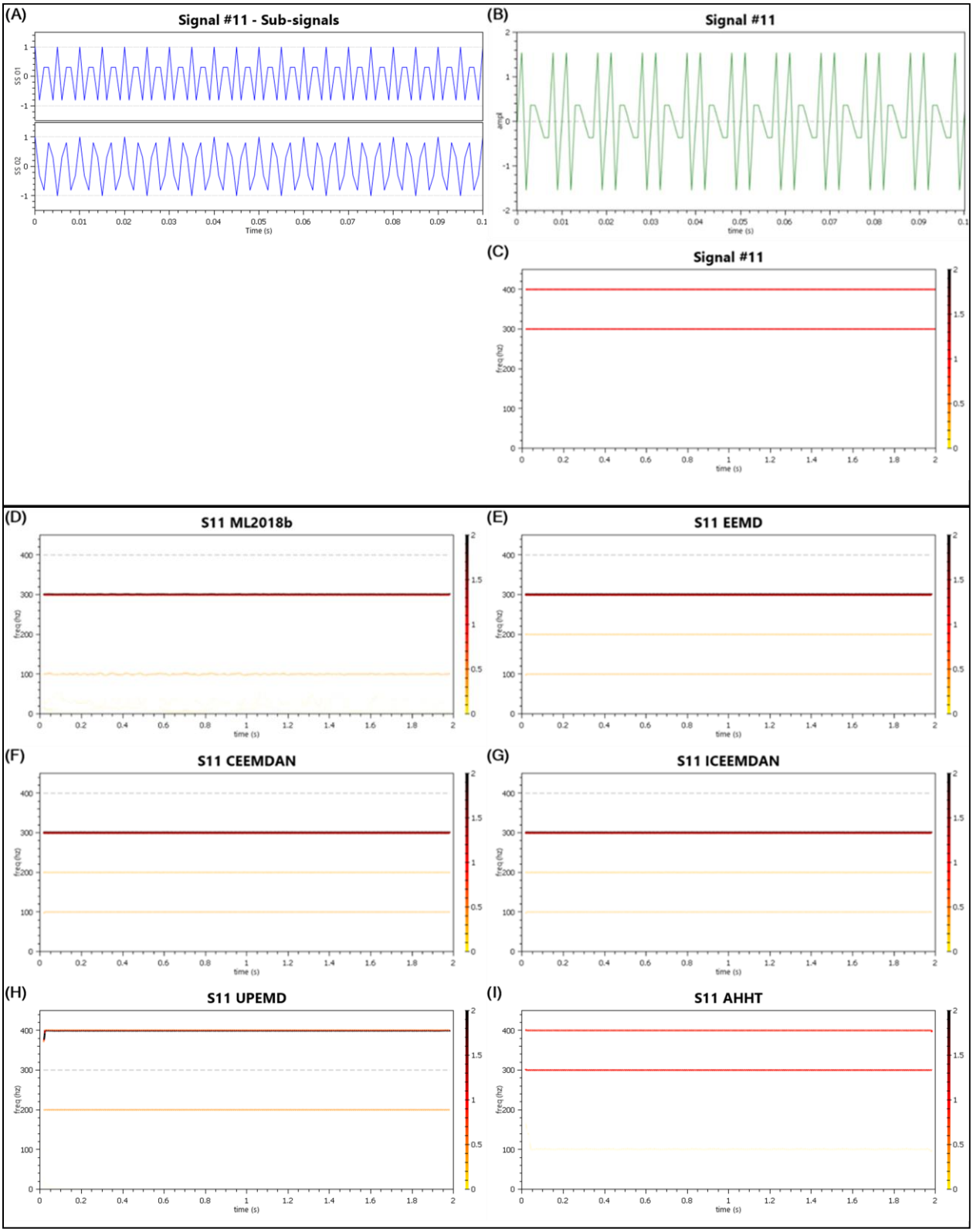


*Figure A-38 Signal 11 - Plot, Source Sub-Signals, Hilbert Spectral Decompositions*

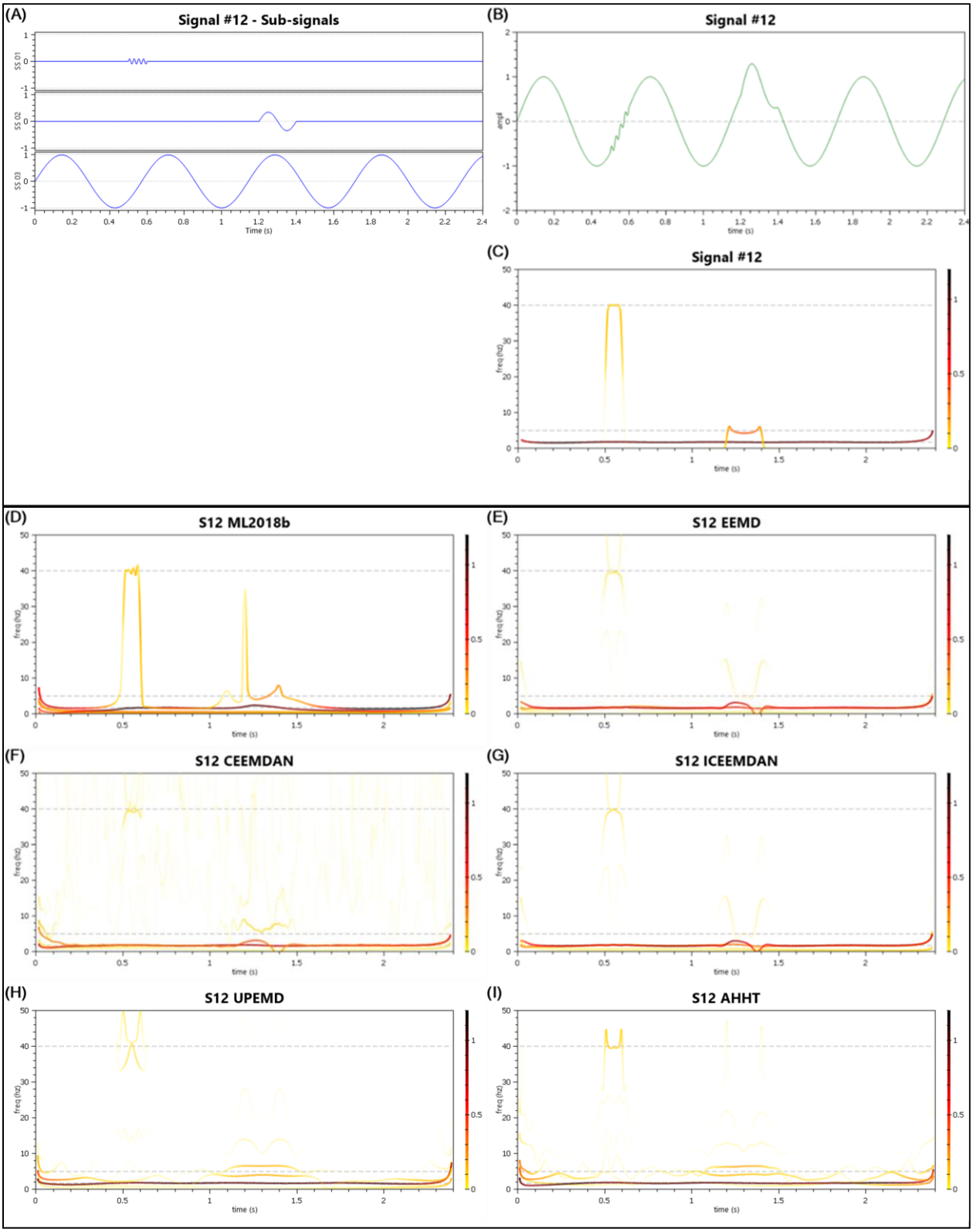


*Figure A-39 Signal 12 - Plot, Source Sub-Signals, Hilbert Spectral Decompositions*

***Table A-6 Signals #6 -> #12 - IMF Counts and QoD Values***

| | MATLAB EMD | EEMD | CEEMDAN | ICEEMDAN | UPEMD | AHHT |
|---|---|---|---|---|---|---|
| **Signal #6 – 2 Component Signals** | | | | | | |
| # of IMFs + Res | 3 | 15 | 16 | 14 | 13 | 5 |
| $QoD_1$ | 0.006497 | 0.023184 | 0.011612 | 0.017926 | 0.028354 | **0.89535** |
| $QoD_2$ | 0.03871 | 0.340859 | 0.423141 | 0.227672 | 0.428347 | **0.018928** |
| **Signal #7 – 2 Component Signals** | | | | | | |
| # of IMFs + Res | 8 | 10 | 11 | 2 | 9 | 5 |
| $QoD_1$ | 0.115095 | 0.863624 | 0.41947 | 0.923283* | 0.904884 | **0.924295** |
| $QoD_2$ | 0.128662 | 0.053114 | 0.313989 | **0*** | 0.094126 | 0.016248 |
| **Signal #8 – 2 Component Signals** | | | | | | |
| # of IMFs + Res | 4 | 9 | 10 | 7 | 9 | 3 |
| $QoD_1$ | **0.612176** | 0.047074 | 0.024415 | 0.275469 | 0.329786 | 0.569422 |
| $QoD_2$ | **0.159315** | 1.801686 | 3.219262 | 0.813113 | 1.717778 | 0.606953 |
| **Signal #8b – 2 Component Signals** | | | | | | |
| # of IMFs + Res | 3 | 9 | 10 | 8 | 9 | 3 |
| $QoD_1$ | 0.636169 | 0.346151 | 0.26351 | 0.298206 | 0.199724 | **0.654943** |
| $QoD_2$ | **0** | 0.997061 | 1.873362 | 0.149712 | 1.96271 | **0** |
| **Signal #9 – 2 Component Signals** | | | | | | |
| # of IMFs + Res | 7 | 11 | 10 | 11 | 9 | 3 |
| $QoD_1$ | 0.102185 | 0.46892 | 0.420989 | 0.874851 | 0.942162 | **0.902378** |
| $QoD_2$ | 0.07751 | 0.106619 | 0.11403 | 0.086259 | 0.032487 | **0.008494** |
| **Signal #10 – 2 Component Signals** | | | | | | |
| # of IMFs + Res | 5 | 10 | 11 | 6 | 10 | 6 |
| $QoD_1$ | 0.1037 | 0.037899 | 0.016519 | 0.038398 | 0.406582 | **0.591427** |
| $QoD_2$ | 0.228057 | 0.407359 | 0.576082 | 0.487356 | 0.204101 | **0.03929** |
| **Signal #10 (-9.2 dB SNR w.r.t. Riding Signal)** | | | | | | |
| # of IMFs + Res | 7 | 10 | 12 | 6 | 10 | 9 |
| $QoD_1$ | 0.453868 | -0.00497 | -0.01244 | 0.011398 | **0.460711** | 0.452966 |
| $QoD_2$ | **0.083734** | 0.535078 | 0.586462 | 0.52819 | 0.289933 | 0.126818 |
| **Signal #11 – 2 Component Signals** | | | | | | |
| # of IMFs + Res | 9 | 12 | 13 | 3 | 10 | 3 |
| $QoD_1$ | 0.013308 | 0.000238 | 0.000113 | 0.004813 | 0.000559 | **0.576315** |
| $QoD_2$ | 0.526655 | 0.61775 | 0.618331 | 0.494555 | 0.456143 | **0.055918** |
| **Signal #12 – 3 Component Signals** | | | | | | |
| # of IMFs + Res | 5 | 11 | 11 | 9 | 11 | 7 |
| $QoD_1$ | 0.033761 | 0.021324 | -0.02086 | -0.0067 | **0.272741** | 0.263005 |
| $QoD_2$ | 0.578082 | 0.435397 | 0.424518 | 0.404332 | 0.203293 | **0.120043** |

* The final IMF is really the residual. It was not an extracted IMF via sifting, though it matched well.

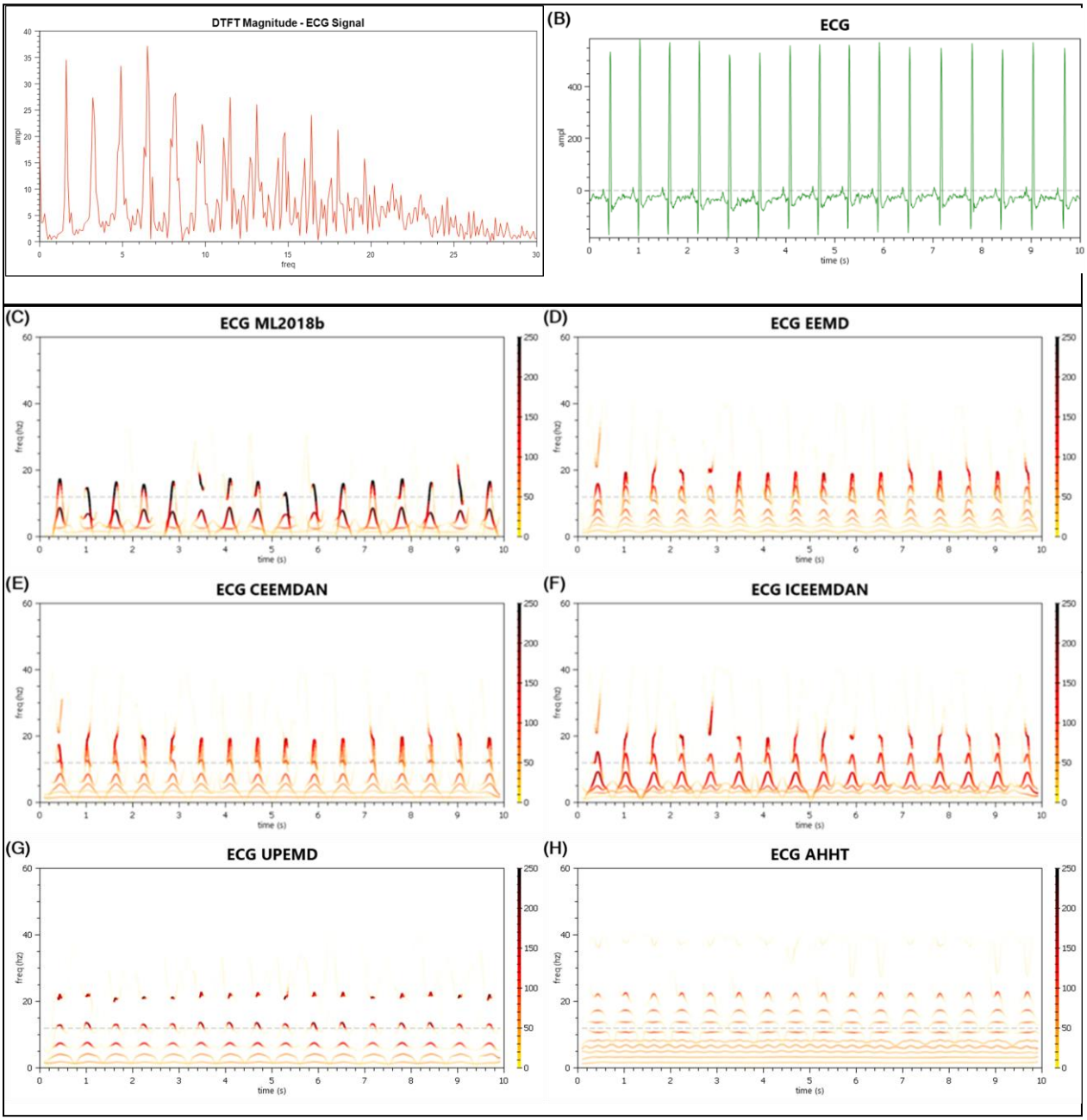


***Figure A-40 ECG Signal - Hilbert Spectral Decompositions***

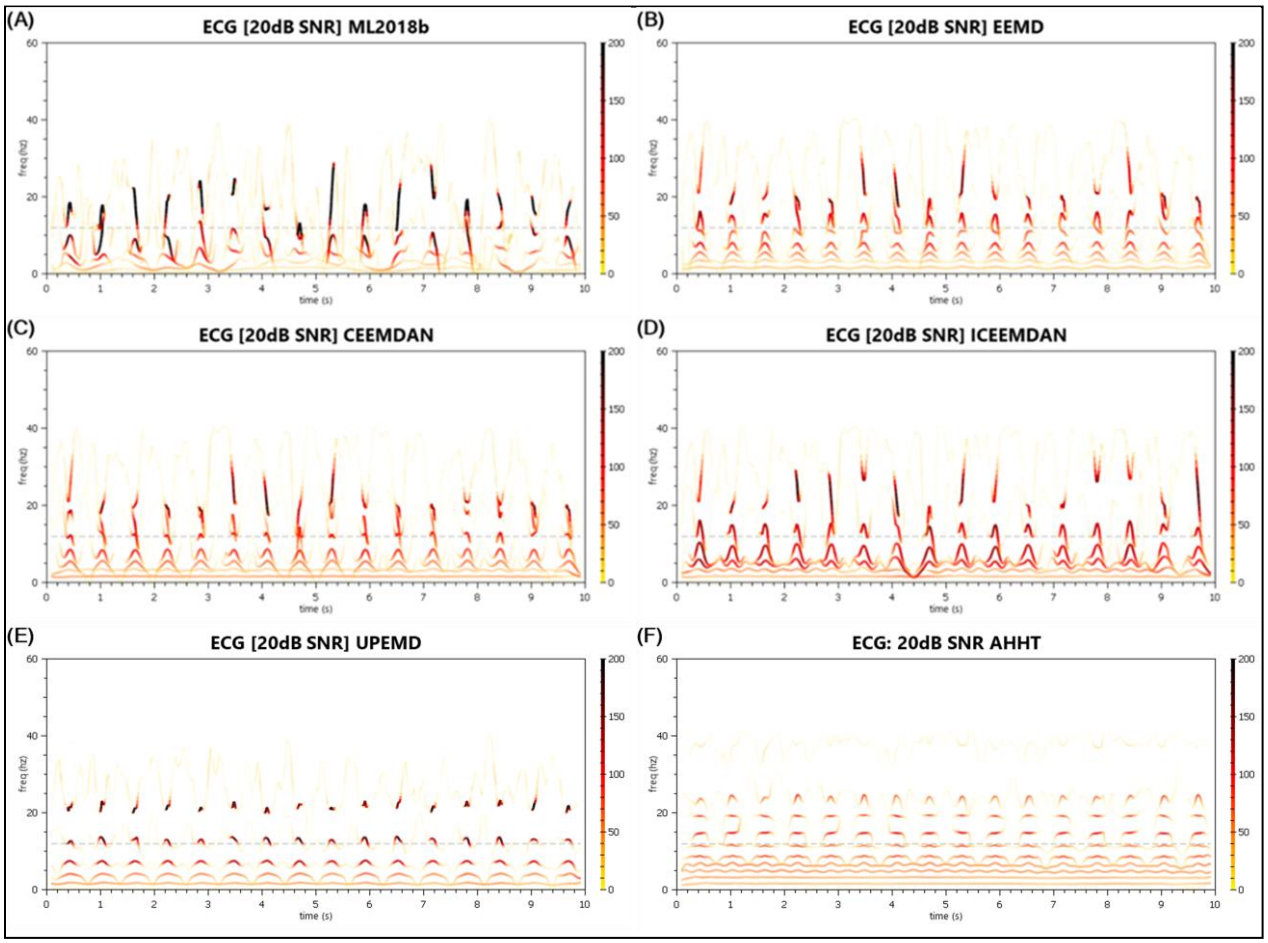


***Figure A-41 ECG Signal (20dB SNR) - Hilbert Spectral Decompositions***

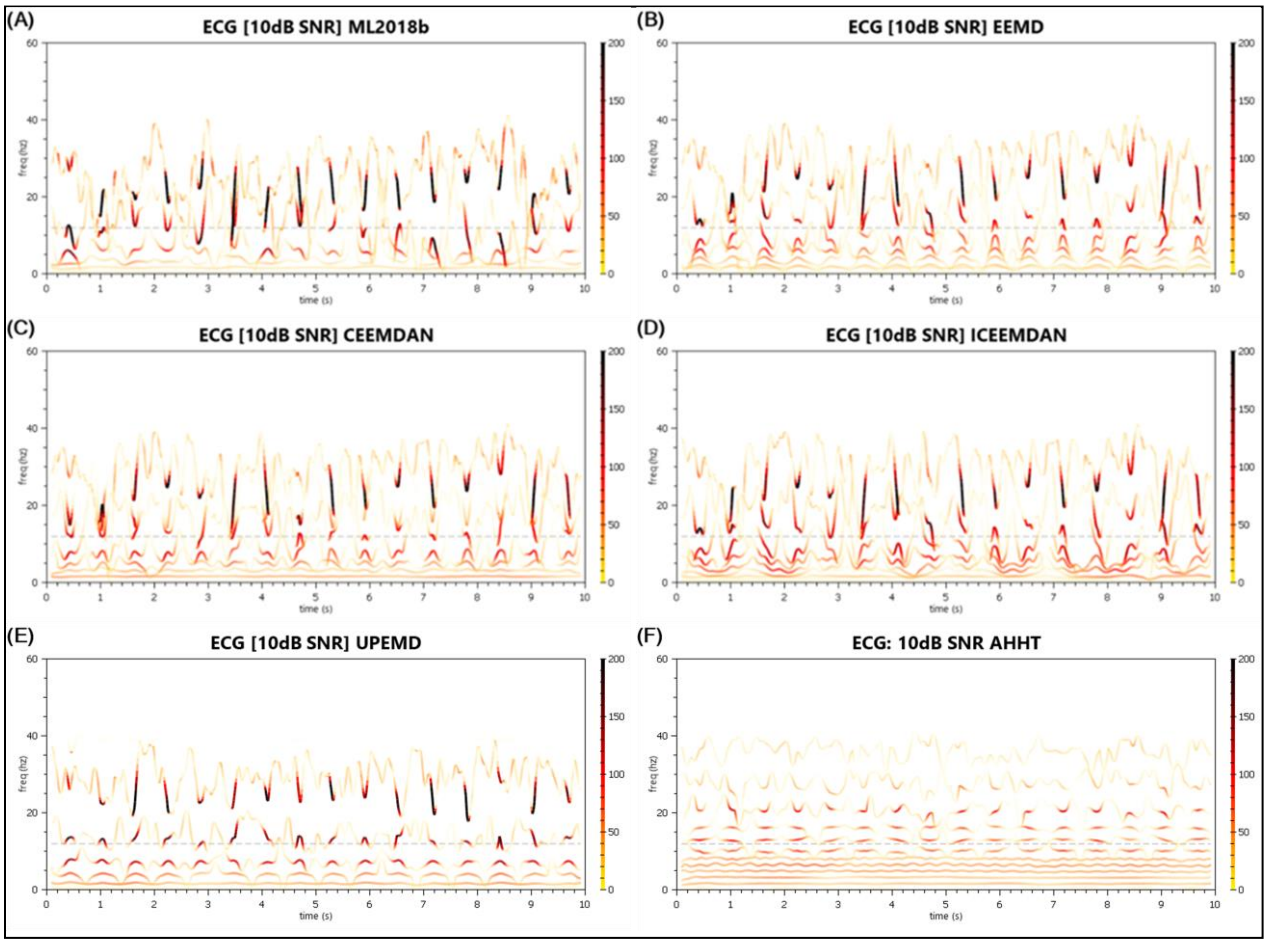


***Figure A-42 ECG Signal (10dB SNR) - Hilbert Spectral Decompositions***

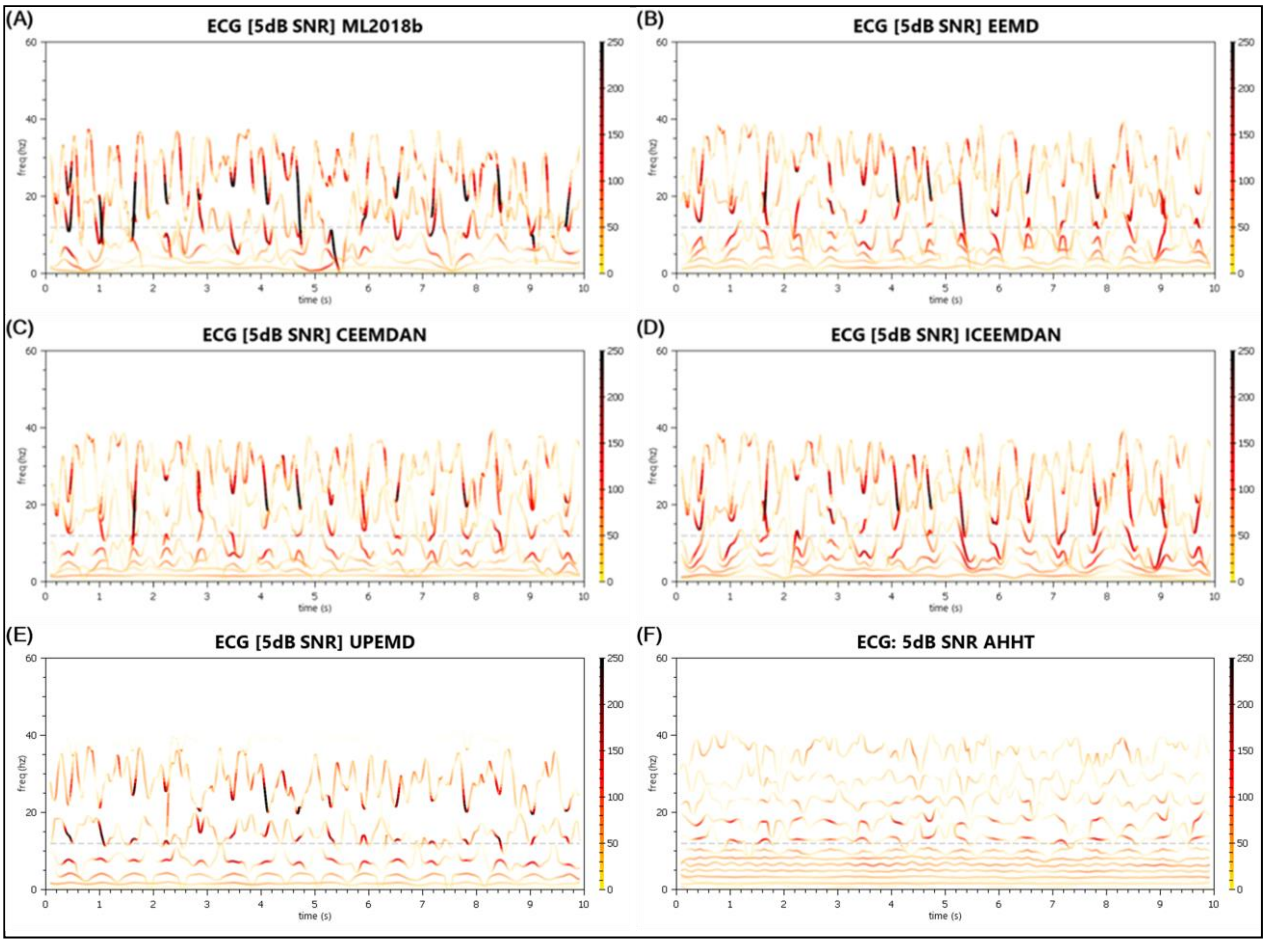


***Figure A-43 ECG Signal (5dB SNR) - Hilbert Spectral Decompositions***

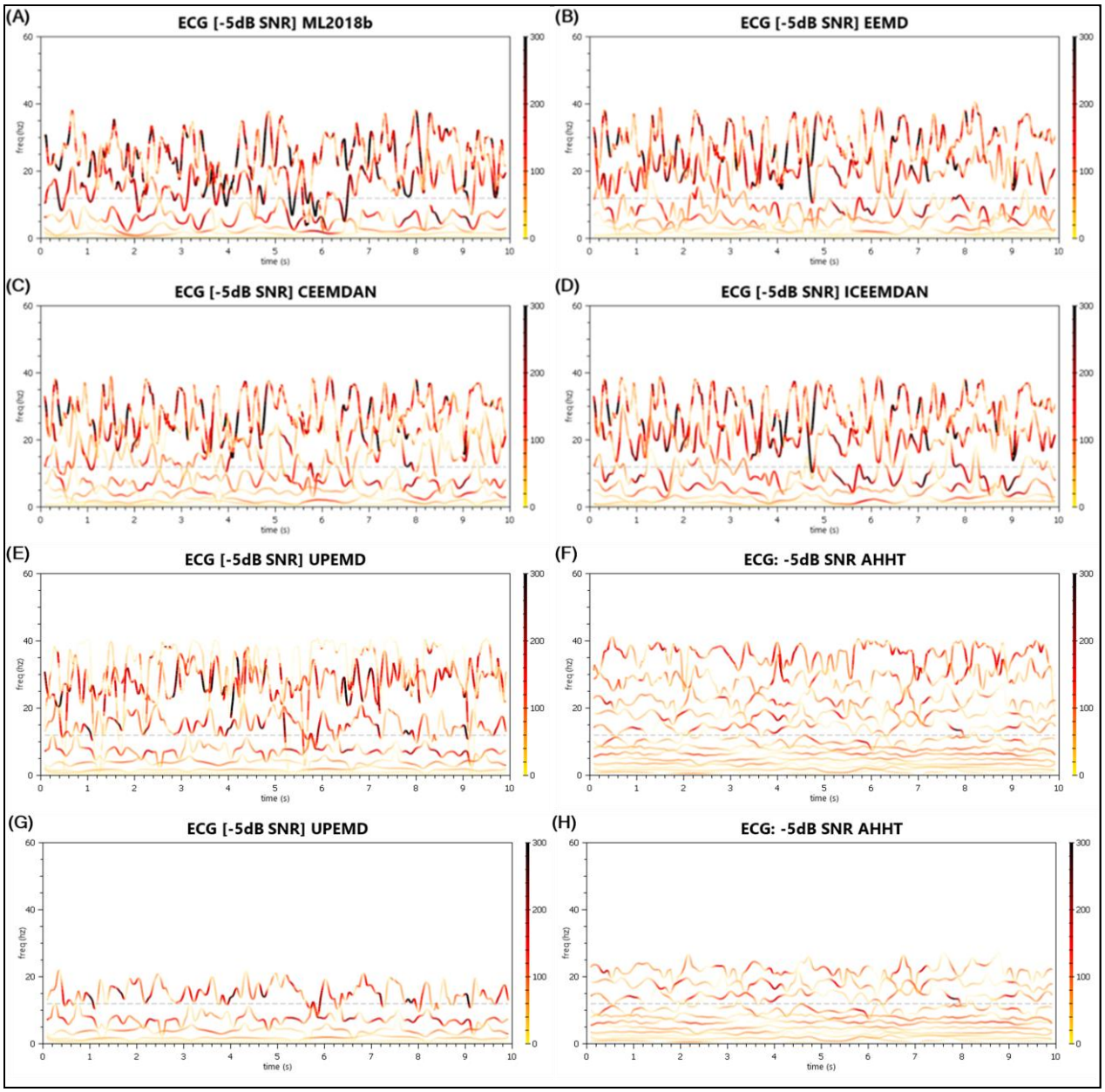


***Figure A-45 ECG Signal (-5dB SNR) - Hilbert Spectral Decompositions (G – Top 2 IMFs Removed, H – Top 2 IMFs Removed)***

# Appendix B

# Hilbert Spectrums of Select, Upsampled Signals

As discussed in Chapter 3.1, there is evidence in literature [51] [52] that for the EMD and, perhaps, the noise-assisted algorithms to show good results, it is necessary that the data be oversampled such that the sampling rate is >=10 times the component frequencies of interest. Although AHHT has demonstrated its ability to do significantly better than this, it is desirable to see how the other algorithms manage the decompositions of certain signals that did not meet this component-to-sampling-rate ratio.

In the plots included in this Appendix B, therefore, are the decompositions of Signal #1, Signal #3, Signal #5, Signal #6, Signal #7, and Signal #9, all sampled at 100 kHz. New noisy versions of Signals #1, #3, and #5 were also generated at this higher sampling frequency and decomposed. All other parameters of the decompositions were unchanged. As a result, the unchanged Kay windowing parameter used to evaluate the results leads to more frequency volatility in the Hilbert spectral plots than was apparent in prior results.

| **Signal #** | **Former Sampling Rate Over Highest Frequency Component** | **New Sampling Rate Over Highest Frequency Component** |
|---|---|---|
| **#1 + AGWN Versions** | 3.92x | 39.2x |
| **#3 + AGWN Versions** | 5x | 50x |
| **#5 + AGWN Versions** | 5x | 50x |
| **#6** | 10x | 100x |
| **#7** | 3.92 | 39.2 |
| **#9** | 3.92 | 39.2 |

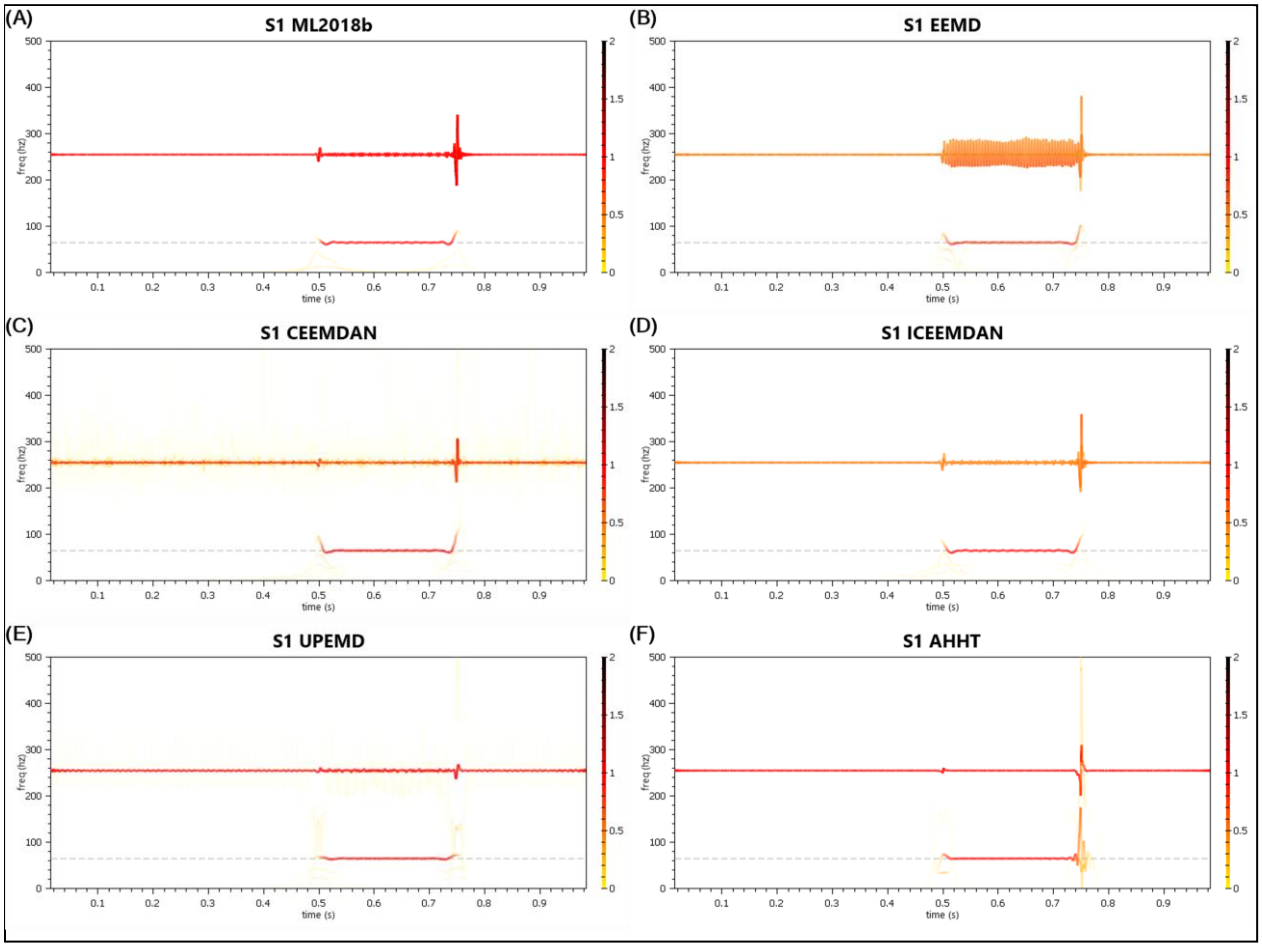


***Figure B-1 Upsampled Signal 1 - Plot, Source Sub-Signals, Hilbert Spectral Decompositions***

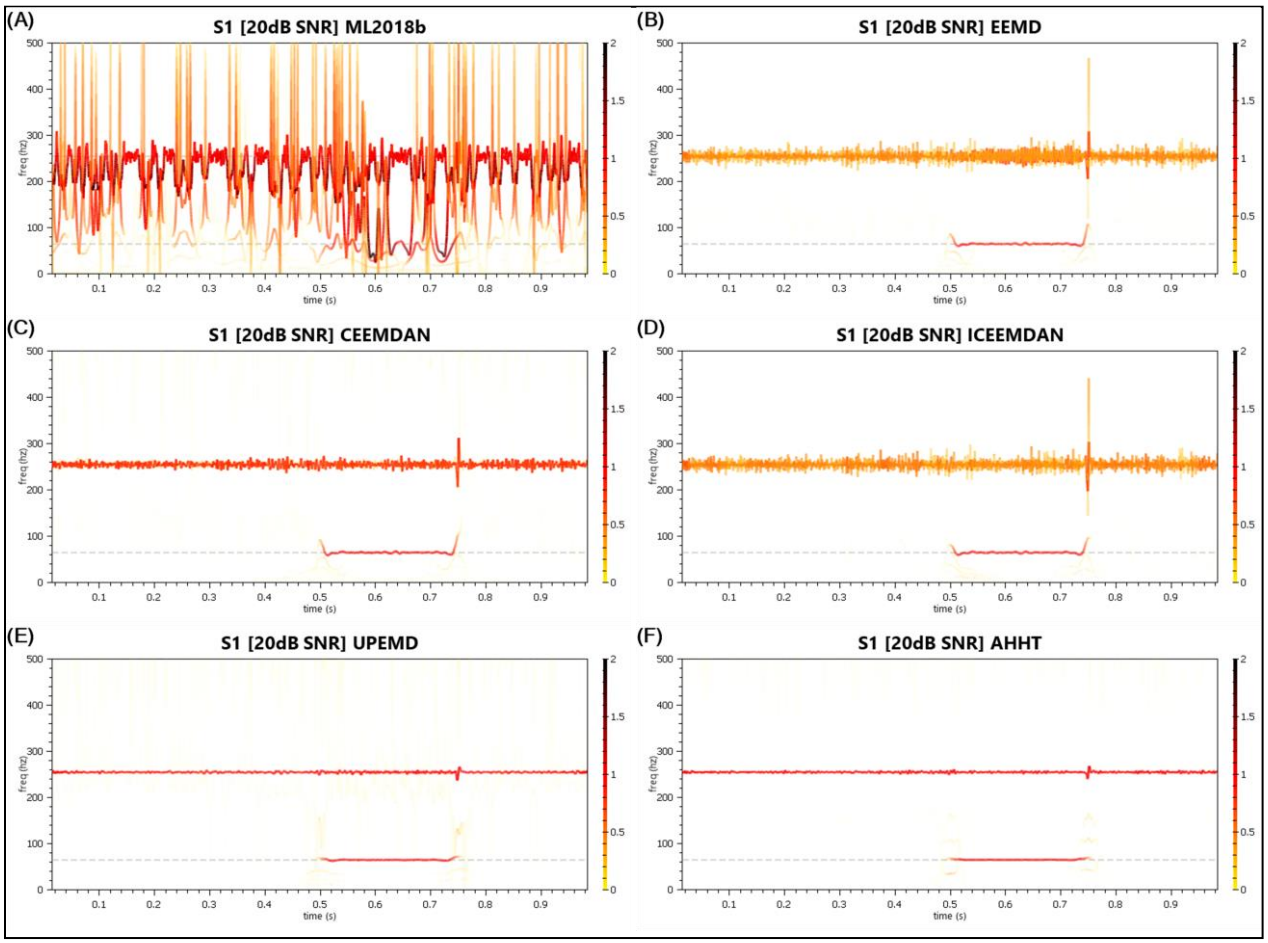


***Figure B-2 Upsampled Signal 1 (20dB SNR) - Hilbert Spectral Decompositions***

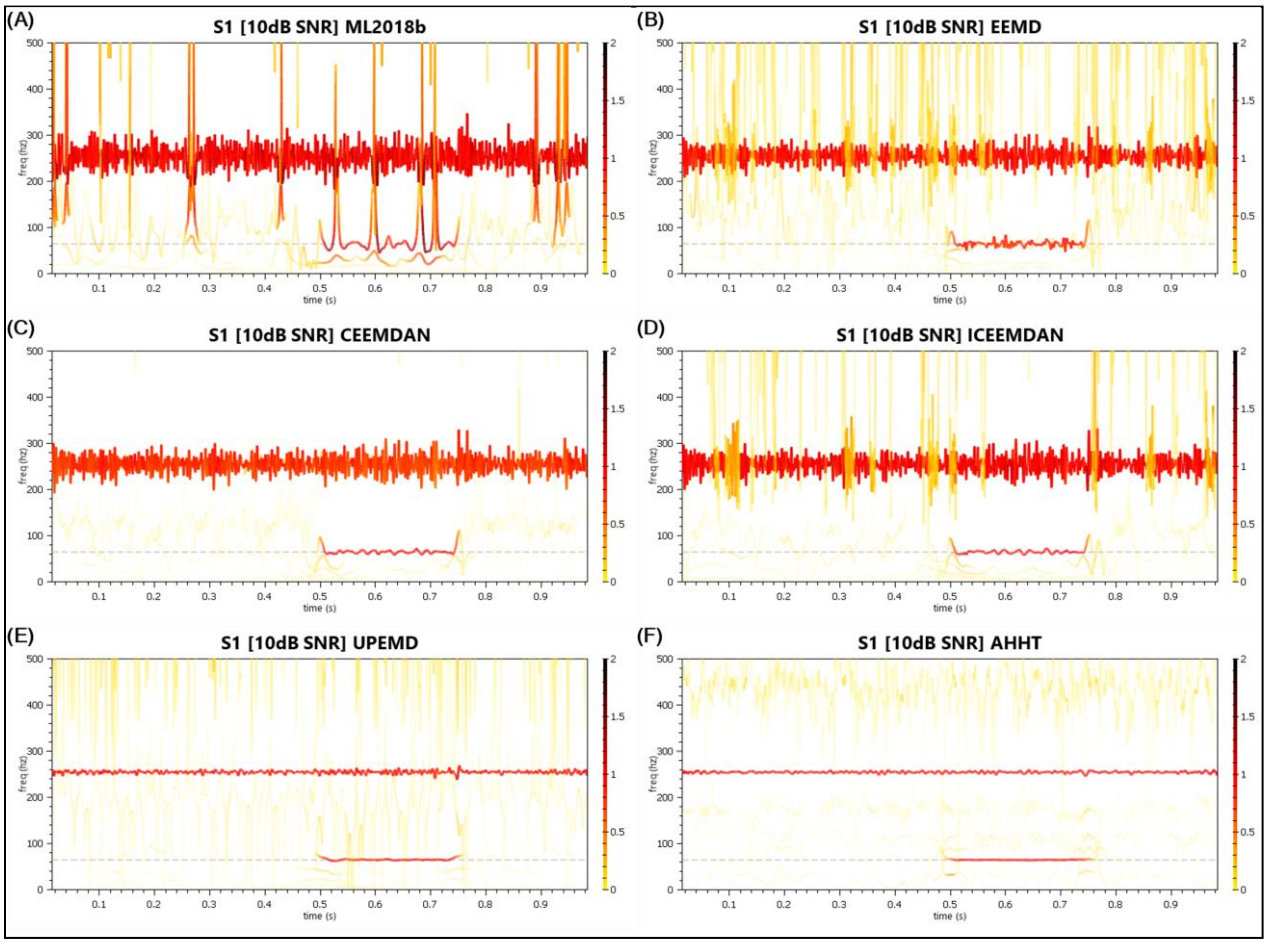


***Figure B-3 Upsampled Signal 1 (10dB SNR) - Hilbert Spectral Decompositions***

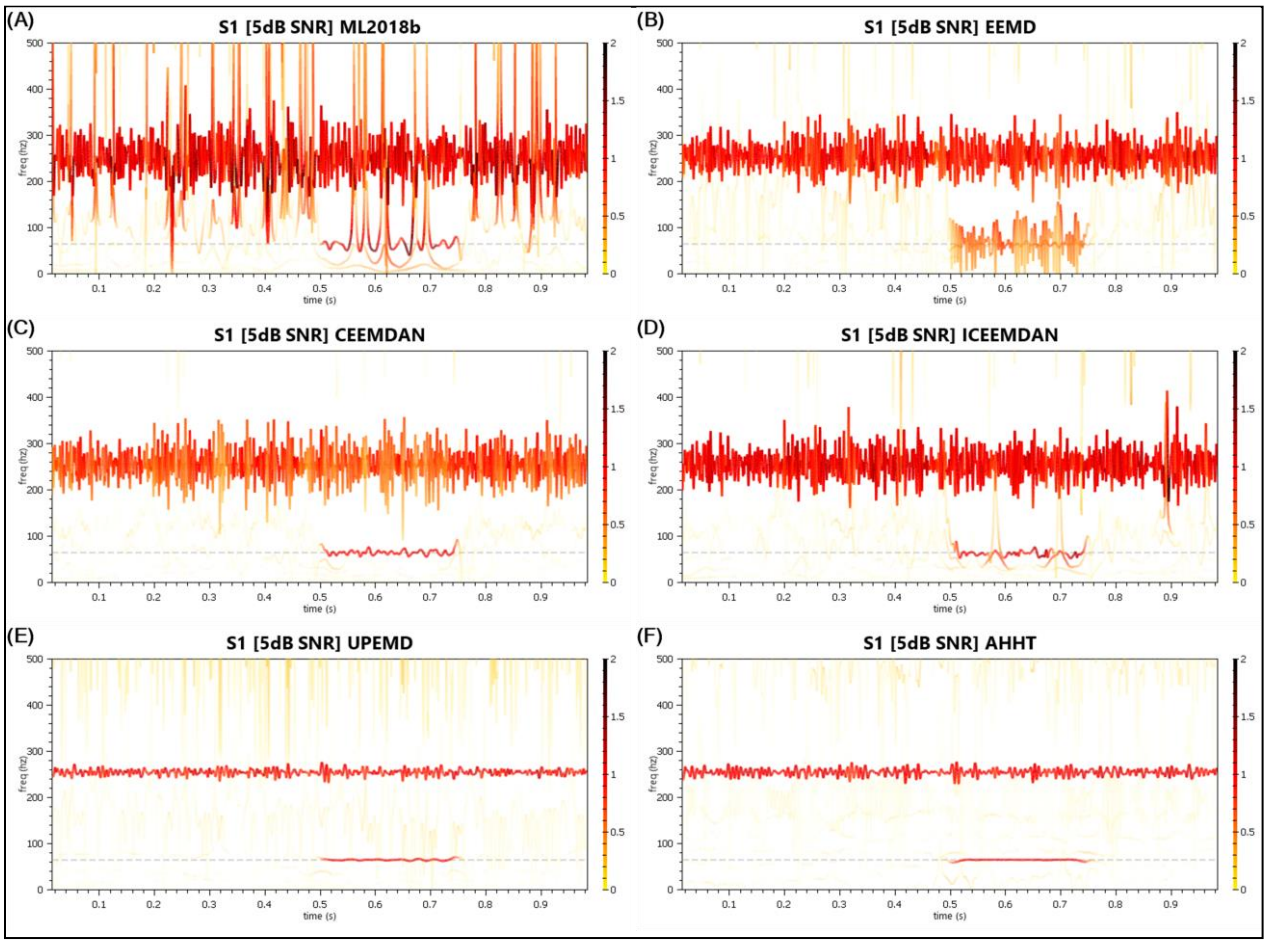


***Figure B-4 Upsampled Signal 1 (5dB SNR) - Hilbert Spectral Decompositions***

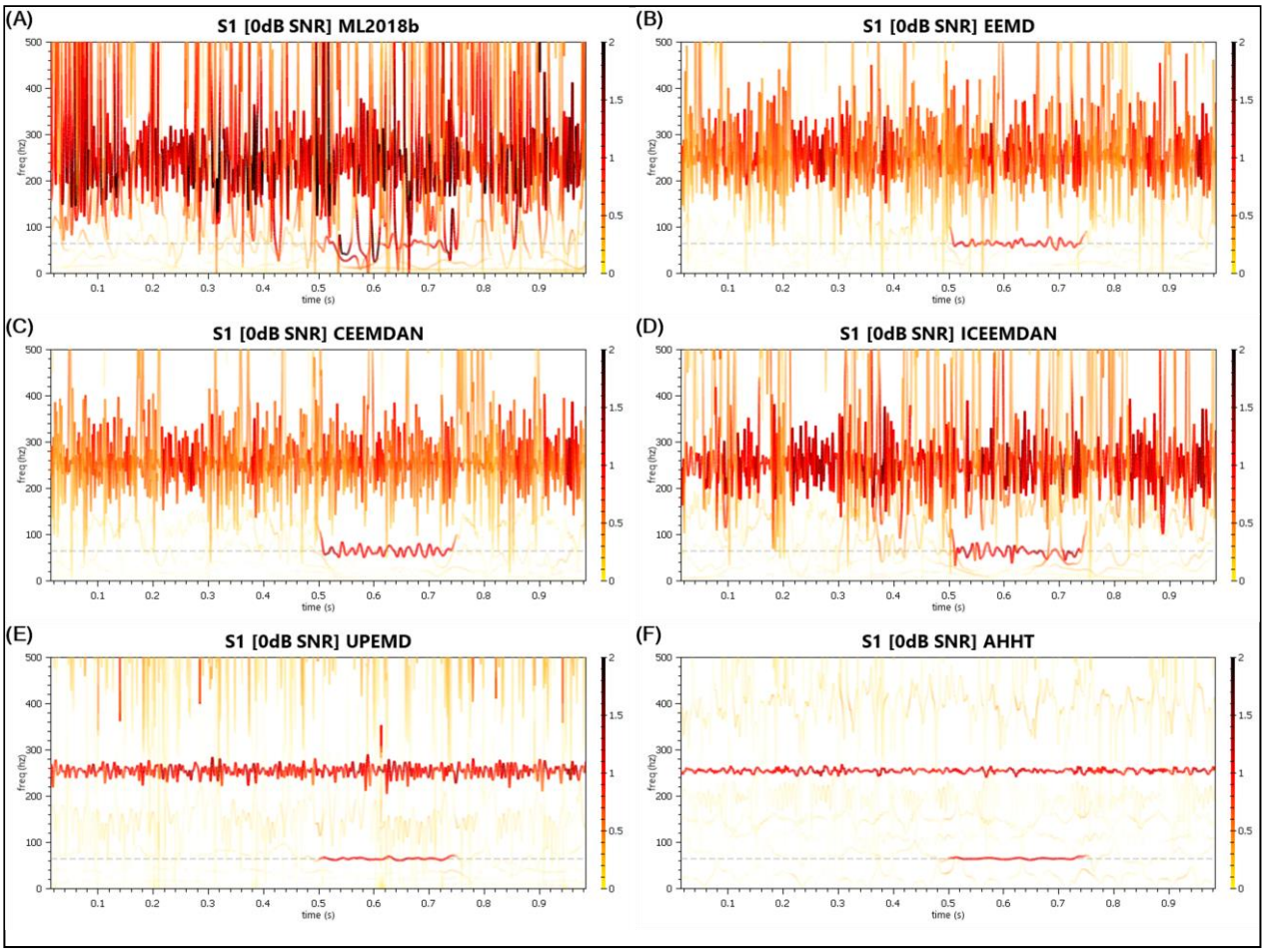


*Figure B-5 Upsampled Signal 1 (0dB SNR) - Hilbert Spectral Decompositions*

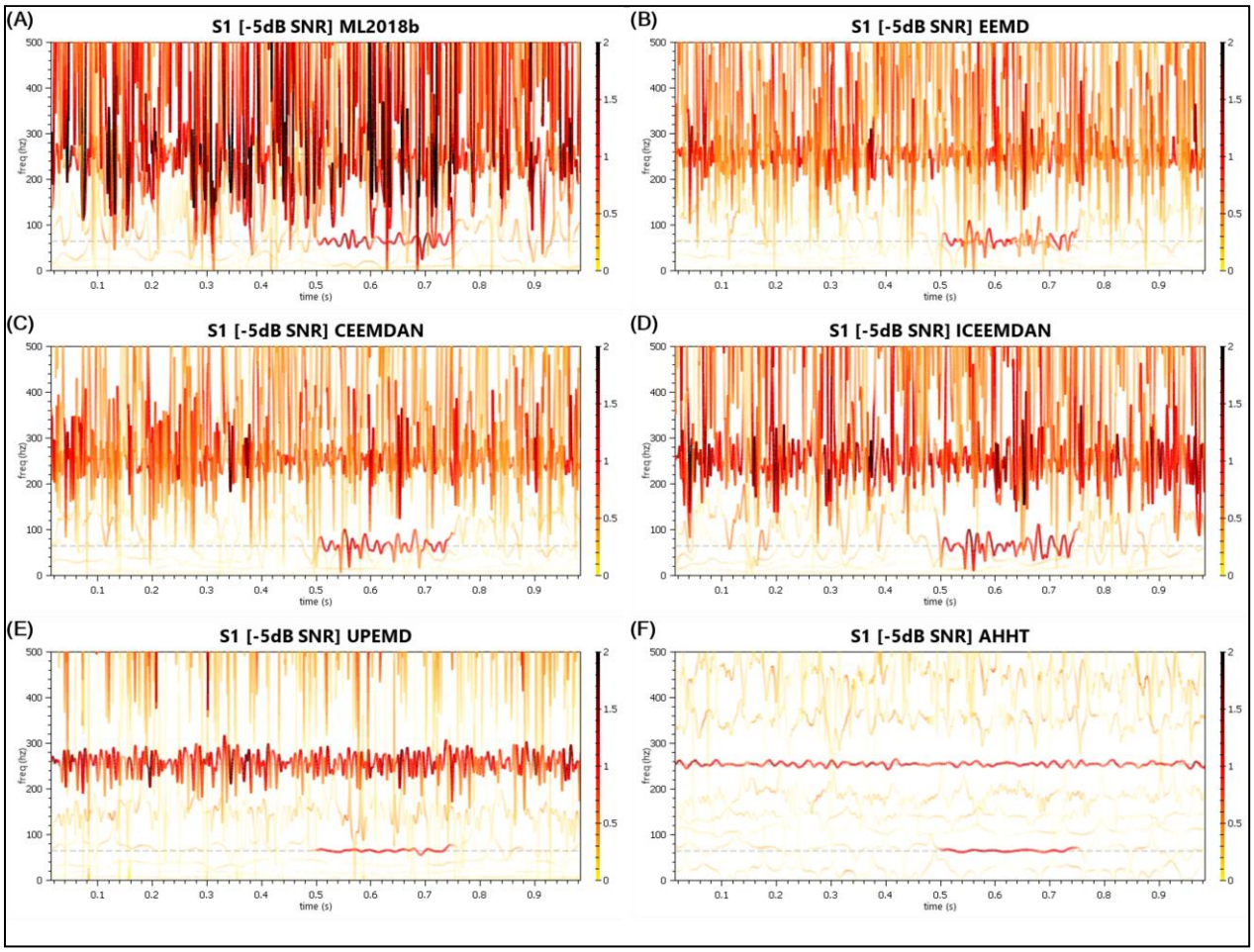


***Figure B-6 Upsampled Signal 1 (-5dB SNR) - Hilbert Spectral Decompositions***

*Table B-1 Upsampled Signal 1 (All) - IMF Counts and QoD Values*

| | MATLAB EMD | EEMD | CEEMDAN | ICEEMDAN | UPEMD | AHHT |
|---|---|---|---|---|---|---|
| **Upsampled Signal #1 – 2 Component Signals** | | | | | | |
| # of IMFs + Res | 6 | 14 | 14 | 16 | 13 | 4 |
| $QoD_1$ | **0.868725** | 0.145542 | 0.392584 | 0.376605 | 0.857015 | 0.856625 |
| $QoD_2$ | 0.082602 | 0.554312 | 0.307444 | 0.567087 | 0.101037 | **0.028142** |
| **Upsampled Signal #1 (20 dB SNR)** | | | | | | |
| # of IMFs + Res | 9 | 14 | 16 | 14 | 13 | 10 |
| $QoD_1$ | 0.05681 | 0.26267 | 0.368516 | 0.379566 | 0.838484 | **0.870377** |
| $QoD_2$ | 0.914563 | 0.4862 | 0.386762 | 0.600609 | 0.214223 | 0.19221 |
| **Upsampled Signal #1 (10 dB SNR)** | | | | | | |
| # of IMFs + Res | 10 | 14 | 14 | 12 | 13 | 12 |
| $QoD_1$ | 0.195671 | 0.309392 | 0.186869 | 0.495832 | 0.608957 | **0.721552** |
| $QoD_2$ | 0.56032 | 0.465815 | 0.646515 | 0.518533 | 0.507906 | 0.596597 |
| **Upsampled Signal #1 (5 dB SNR)** | | | | | | |
| # of IMFs + Res | 10 | 14 | 14 | 12 | 13 | 13 |
| $QoD_1$ | 0.076362 | 0.123028 | 0.109712 | 0.181031 | 0.413161 | **0.532673** |
| $QoD_2$ | 1.032561 | 1.067 | 1.06905 | 0.963152 | 0.854975 | 1.114567 |
| **Upsampled Signal #1 (0 dB SNR)** | | | | | | |
| # of IMFs + Res | 11 | 14 | 14 | 13 | 13 | 14 |
| $QoD_1$ | 0.013344 | 0.034739 | 0.016865 | 0.017597 | 0.264365 | **0.478996** |
| $QoD_2$ | 2.258857 | 1.70214 | 1.814807 | 1.971759 | 1.514179 | 2.104633 |
| **Upsampled Signal #1 (-5 dB SNR)** | | | | | | |
| # of IMFs + Res | 11 | 15 | 14 | 13 | 13 | 15 |
| $QoD_1$ | 0.008059 | -0.010539 | -0.014329 | 0.025526 | 0.167013 | **0.302609** |
| $QoD_2$ | 3.074593 | 2.823249 | 2.971801 | 3.103915 | 2.715245 | 3.835638 |

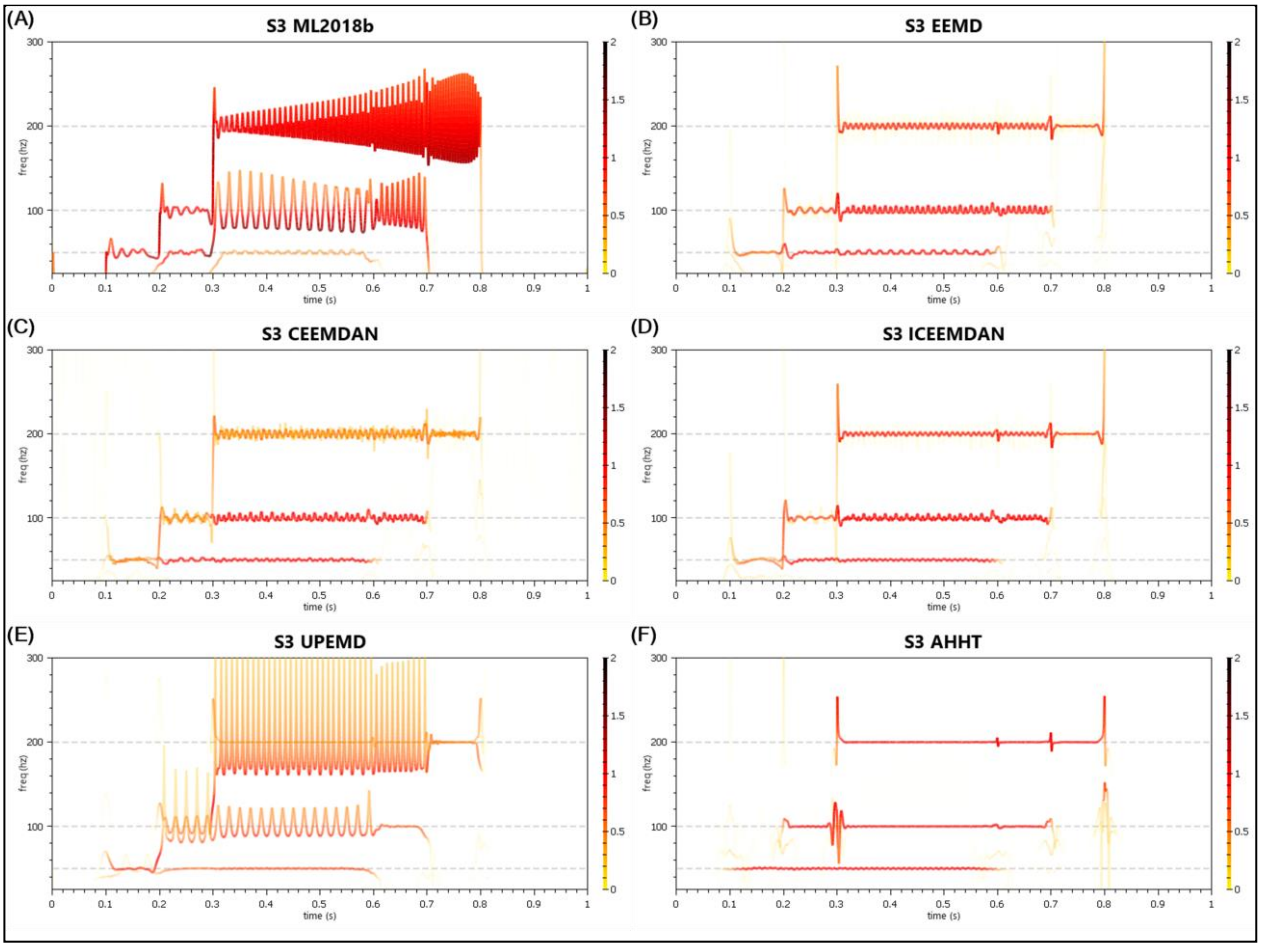


***Figure B-7 Upsampled Signal 3 - Plot, Source Sub-Signals, Hilbert Spectral Decompositions***

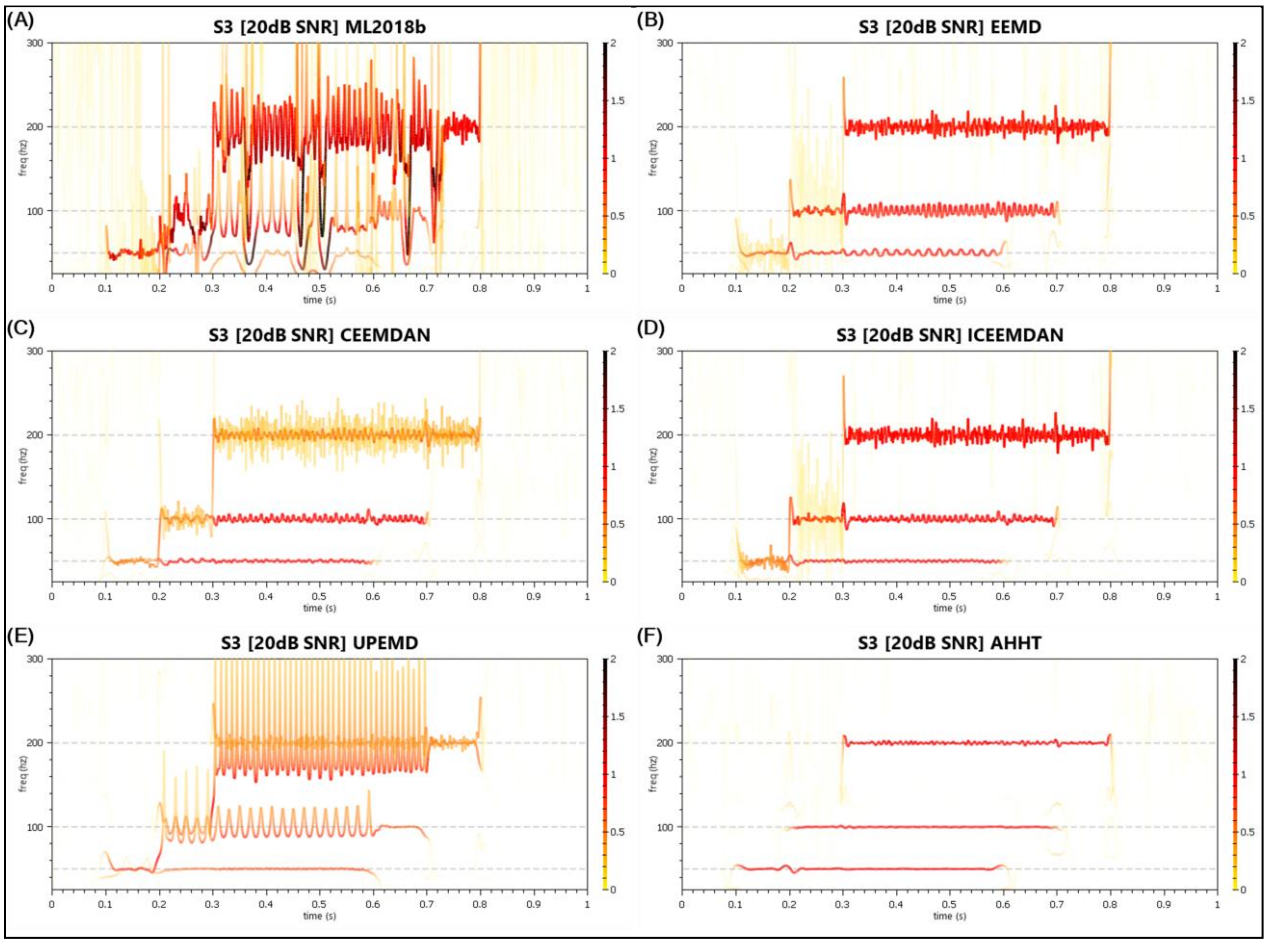


***Figure B-8 Upsampled Signal 3 (20dB SNR) - Hilbert Spectral Decompositions***

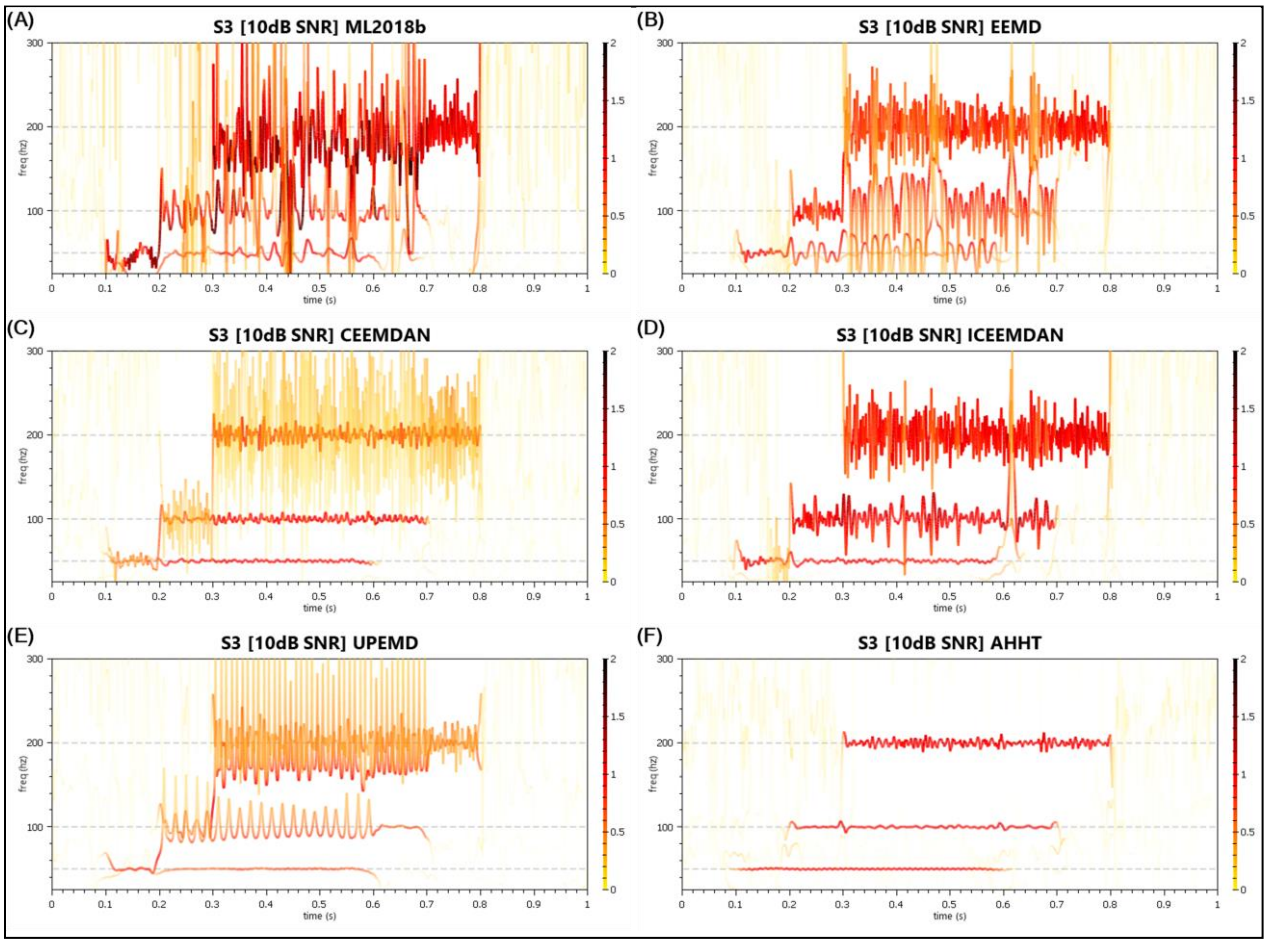


***Figure B-9 Upsampled Signal 3 (10dB SNR) - Hilbert Spectral Decompositions***

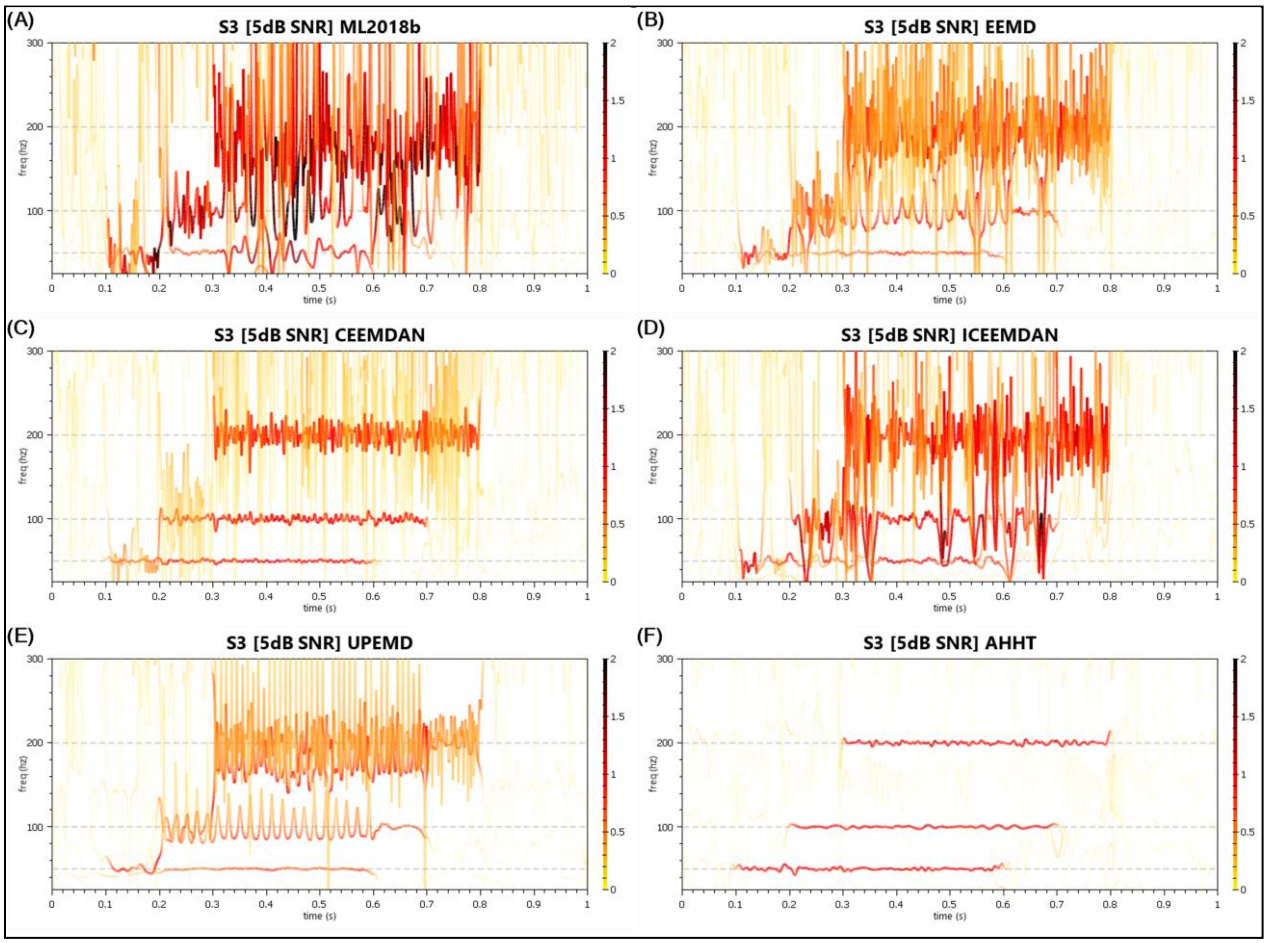


***Figure B-10 Upsampled Signal 3 (5dB SNR) - Hilbert Spectral Decompositions***

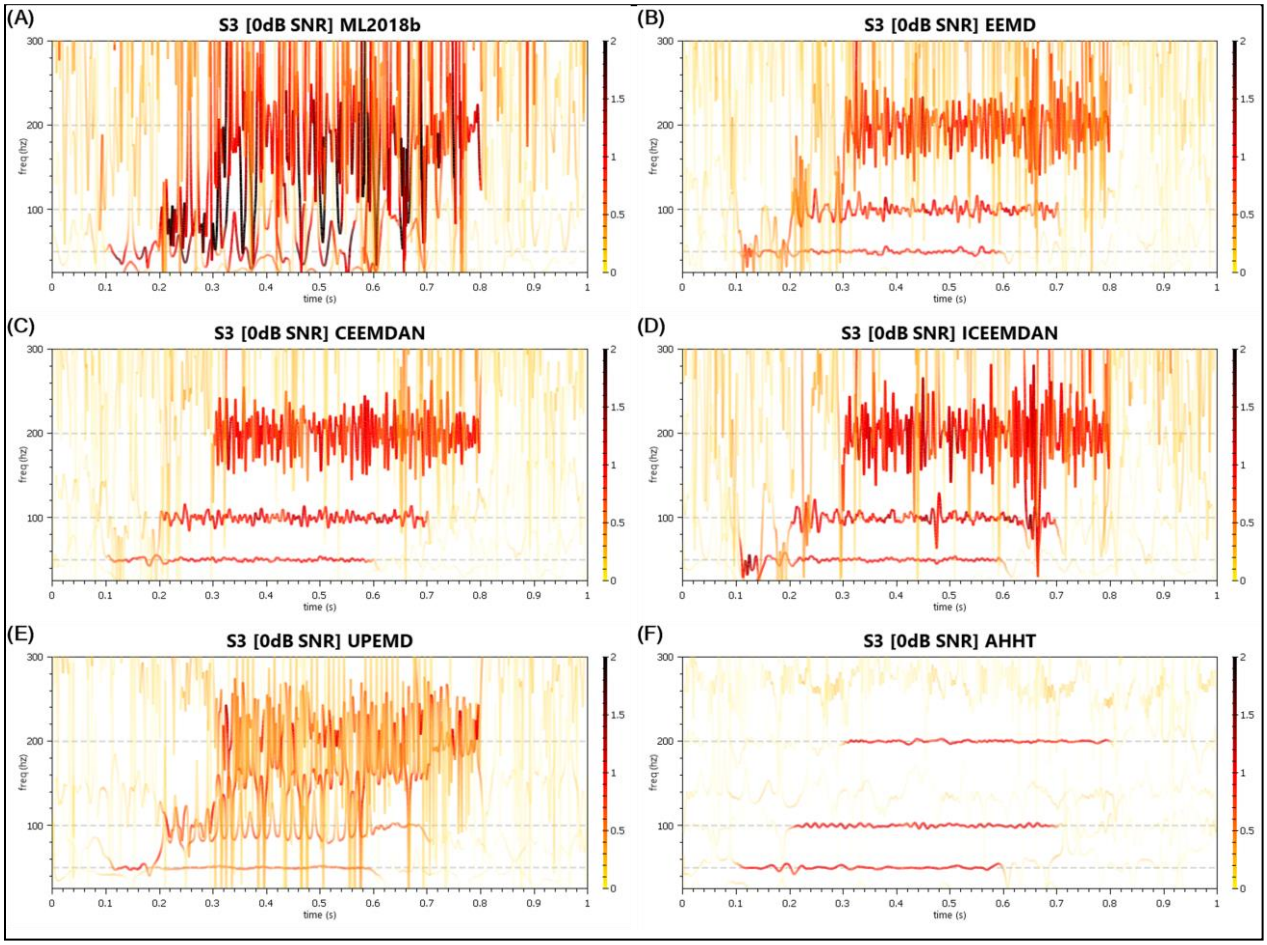


***Figure B-11 Upsampled Signal 3 (0dB SNR) - Hilbert Spectral Decompositions***

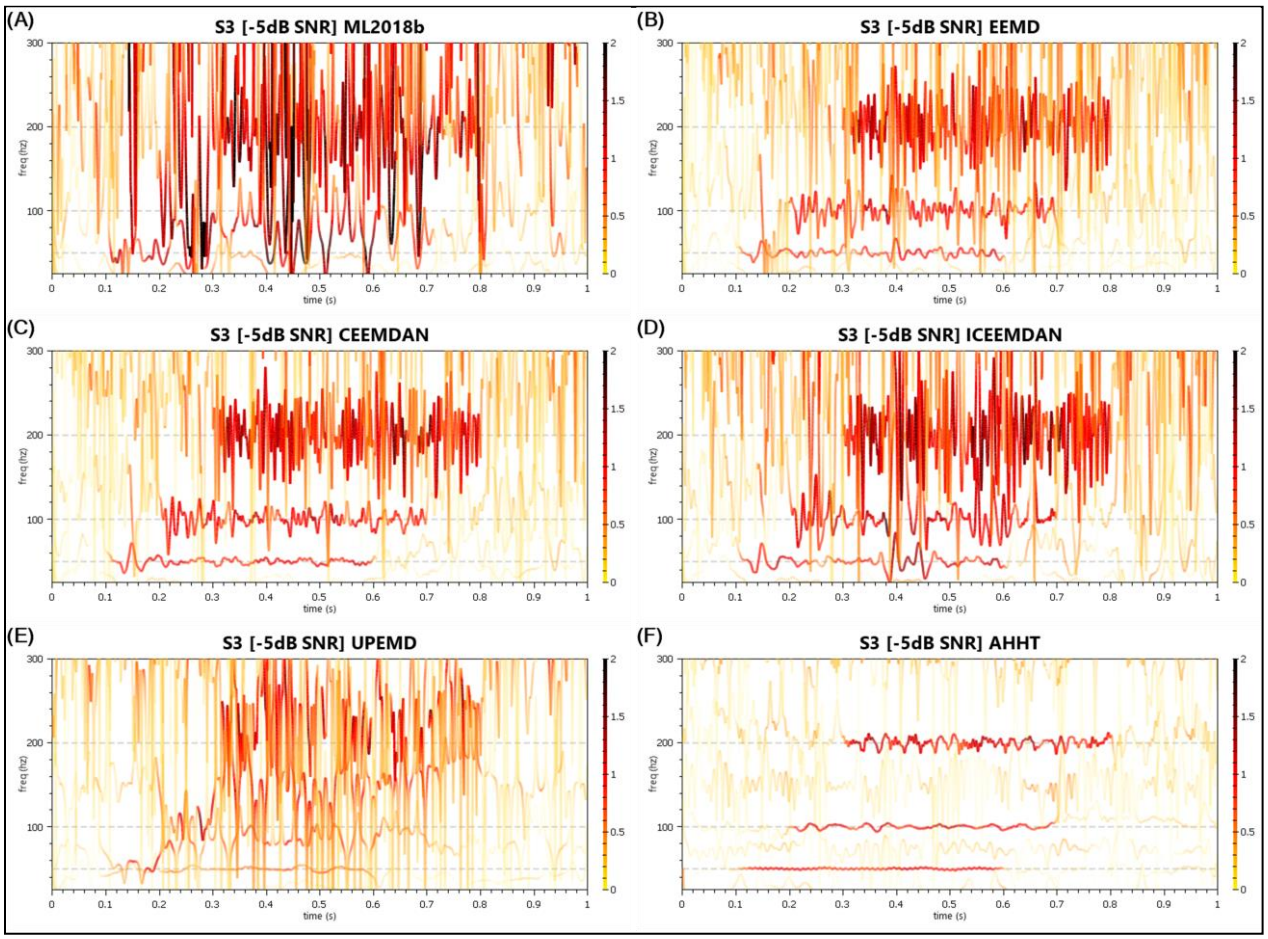


***Figure B-12 Upsampled Signal 3 (-5dB SNR) - Hilbert Spectral Decompositions***

***Table B-2 Upsampled Signal 3 (All) - IMF Counts and QoD Values***

| | MATLAB EMD | EEMD | CEEMDAN | ICEEMDAN | UPEMD | AHHT |
|---|---|---|---|---|---|---|
| **Upsampled Signal #3 – 3 Component Signals** | | | | | | |
| # of IMFs + Res | 9 | 14 | 14 | 13 | 13 | 6 |
| $QoD_1$ | 0.002503 | 0.524581 | 0.308413 | 0.598458 | -0.011024 | **0.726922** |
| $QoD_2$ | 0.328612 | 0.171052 | 0.285797 | 0.246136 | 0.603094 | **0.08977** |
| **Upsampled Signal #3 (20 dB SNR)** | | | | | | |
| # of IMFs + Res | 11 | 14 | 15 | 13 | 13 | 10 |
| $QoD_1$ | 0.034106 | 0.384791 | 0.315054 | 0.531643 | -0.002891 | **0.682995** |
| $QoD_2$ | 0.581167 | 0.260524 | 0.366137 | 0.316426 | 0.737913 | 0.223056 |
| **Upsampled Signal #3 (10 dB SNR)** | | | | | | |
| # of IMFs + Res | 10 | 14 | 15 | 13 | 13 | 11 |
| $QoD_1$ | 0.046304 | 0.047758 | 0.238852 | 0.251988 | 0.001073 | **0.516608** |
| $QoD_2$ | 0.611072 | 0.617726 | 0.63306 | 0.567058 | 1.054583 | 0.652612 |
| **Upsampled Signal #3 (5 dB SNR)** | | | | | | |
| # of IMFs + Res | 10 | 14 | 14 | 13 | 13 | 12 |
| $QoD_1$ | 0.017234 | -0.016161 | 0.239453 | 0.042693 | -0.007289 | **0.438046** |
| $QoD_2$ | 0.952904 | 1.019671 | 0.925741 | 1.233508 | 1.392858 | 1.134163 |
| **Upsampled Signal #3 (0 dB SNR)** | | | | | | |
| # of IMFs + Res | 11 | 14 | 15 | 12 | 13 | 14 |
| $QoD_1$ | -0.013231 | 0.108388 | 0.222107 | 0.189367 | -0.017107 | **0.360453** |
| $QoD_2$ | 2.043001 | 1.578886 | 1.600595 | 1.721697 | 2.41939 | 2.285595 |
| **Upsampled Signal #3 (-5 dB SNR)** | | | | | | |
| # of IMFs + Res | 11 | 15 | 15 | 13 | 13 | 16 |
| $QoD_1$ | -0.01126 | 0.073556 | 0.109807 | 0.070762 | -0.036035 | **0.250141** |
| $QoD_2$ | 3.282858 | 2.76823 | 2.890569 | 3.108276 | 3.314392 | 4.338824 |

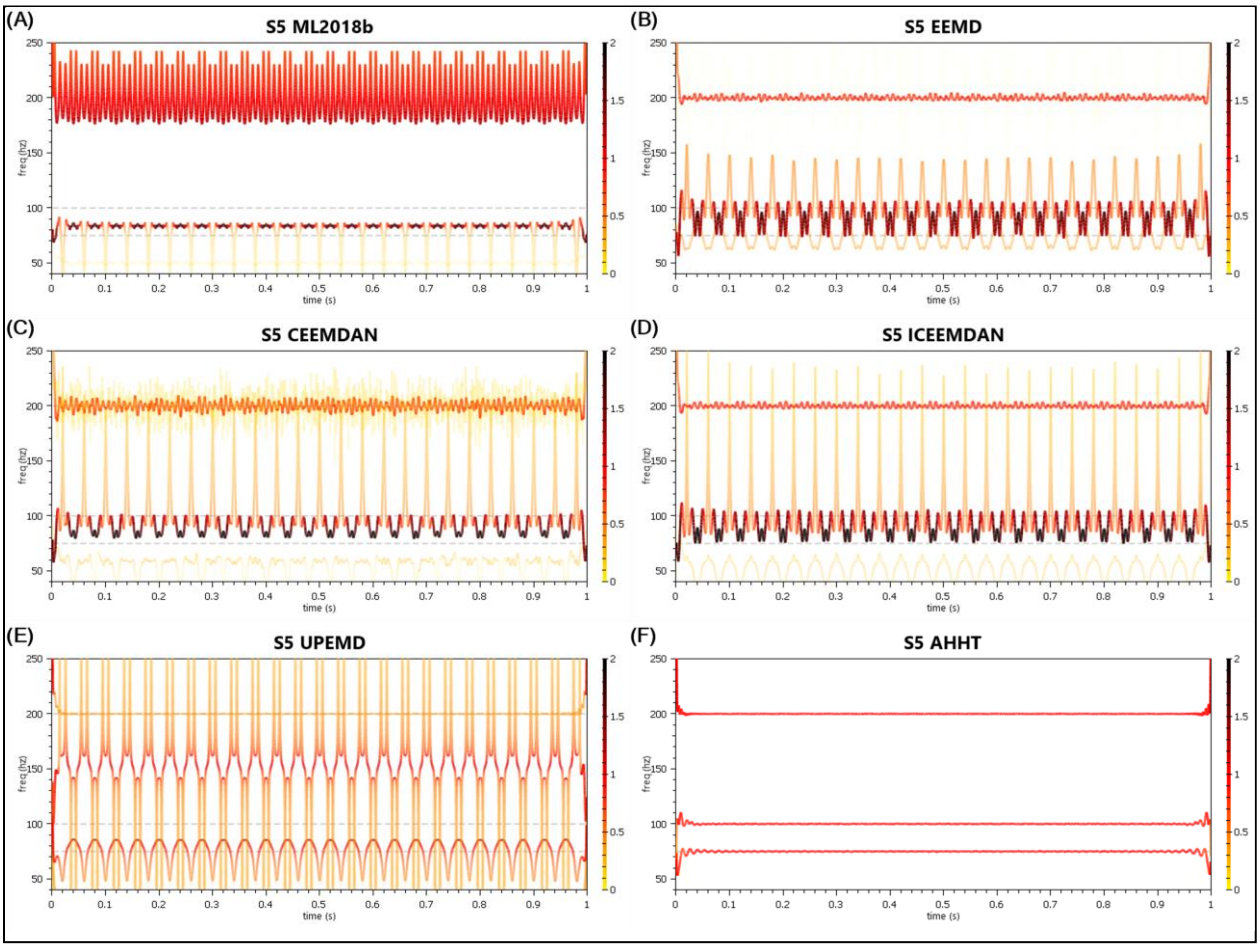


***Figure B-13 Upsampled Signal 5 - Plot, Source Sub-Signals, Hilbert Spectral Decompositions***

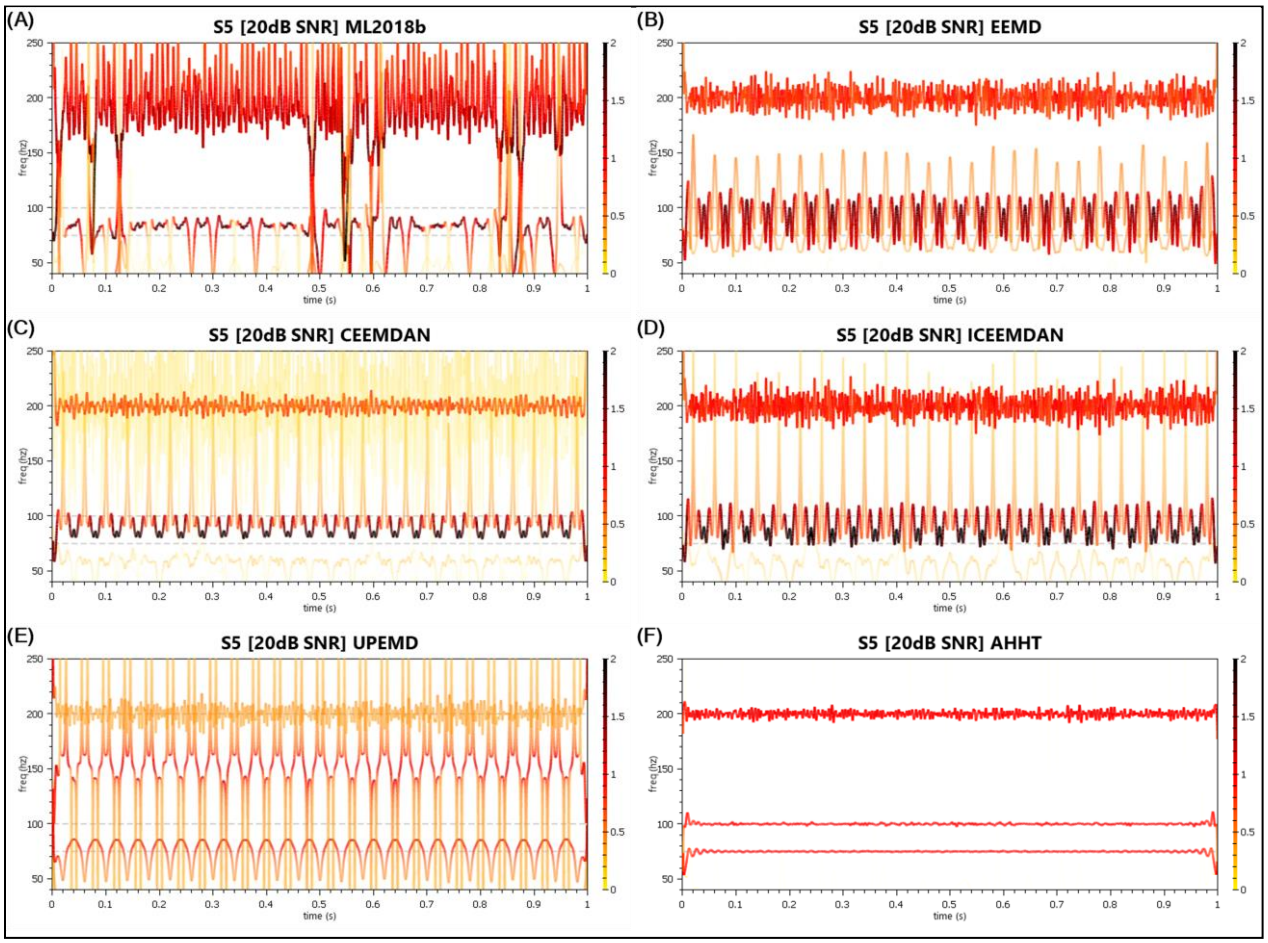


***Figure B-14 Upsampled Signal 5 (20dB SNR) - Hilbert Spectral Decompositions***

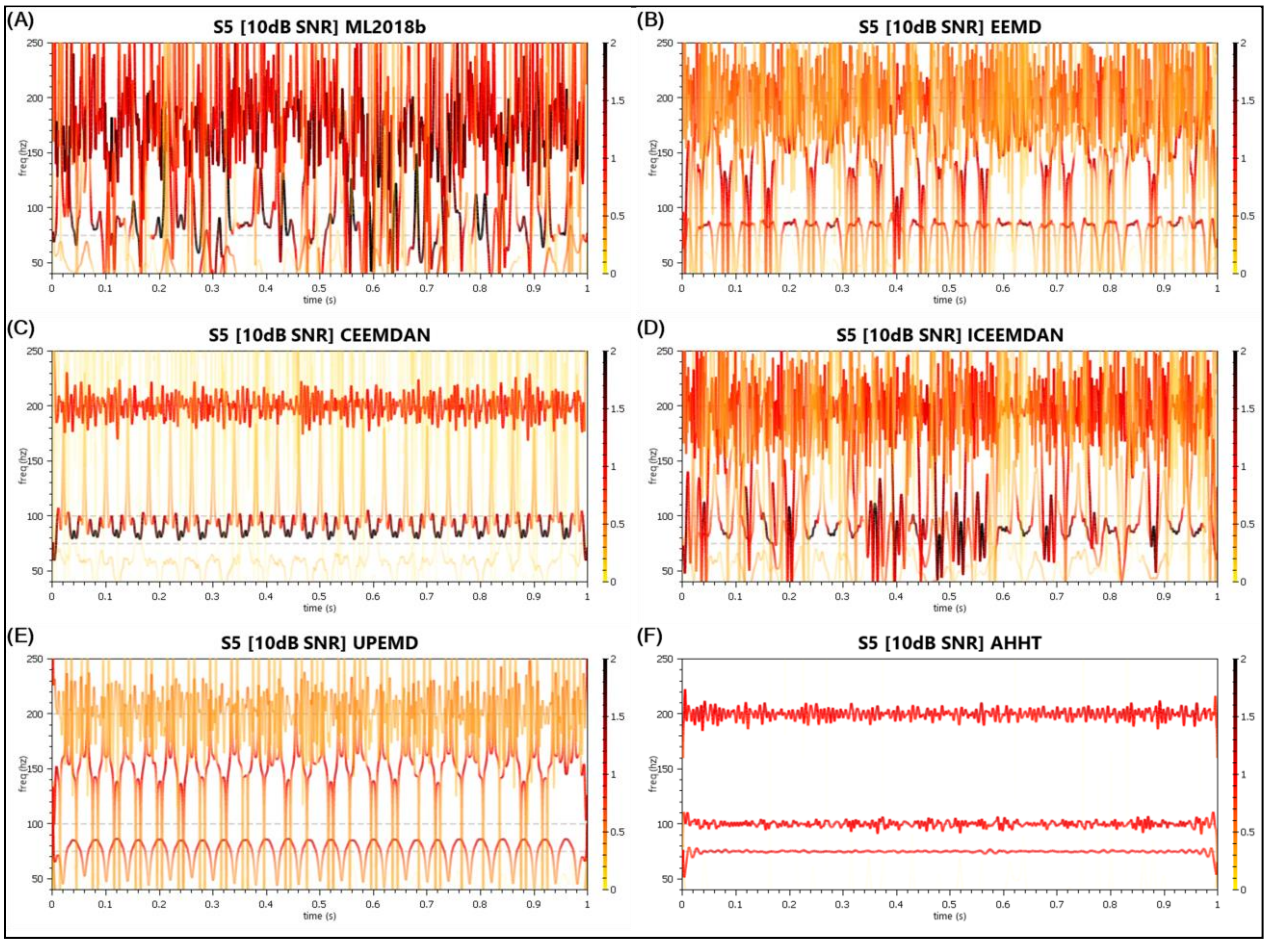


***Figure B-15 Upsampled Signal 5 (10dB SNR) - Hilbert Spectral Decompositions***

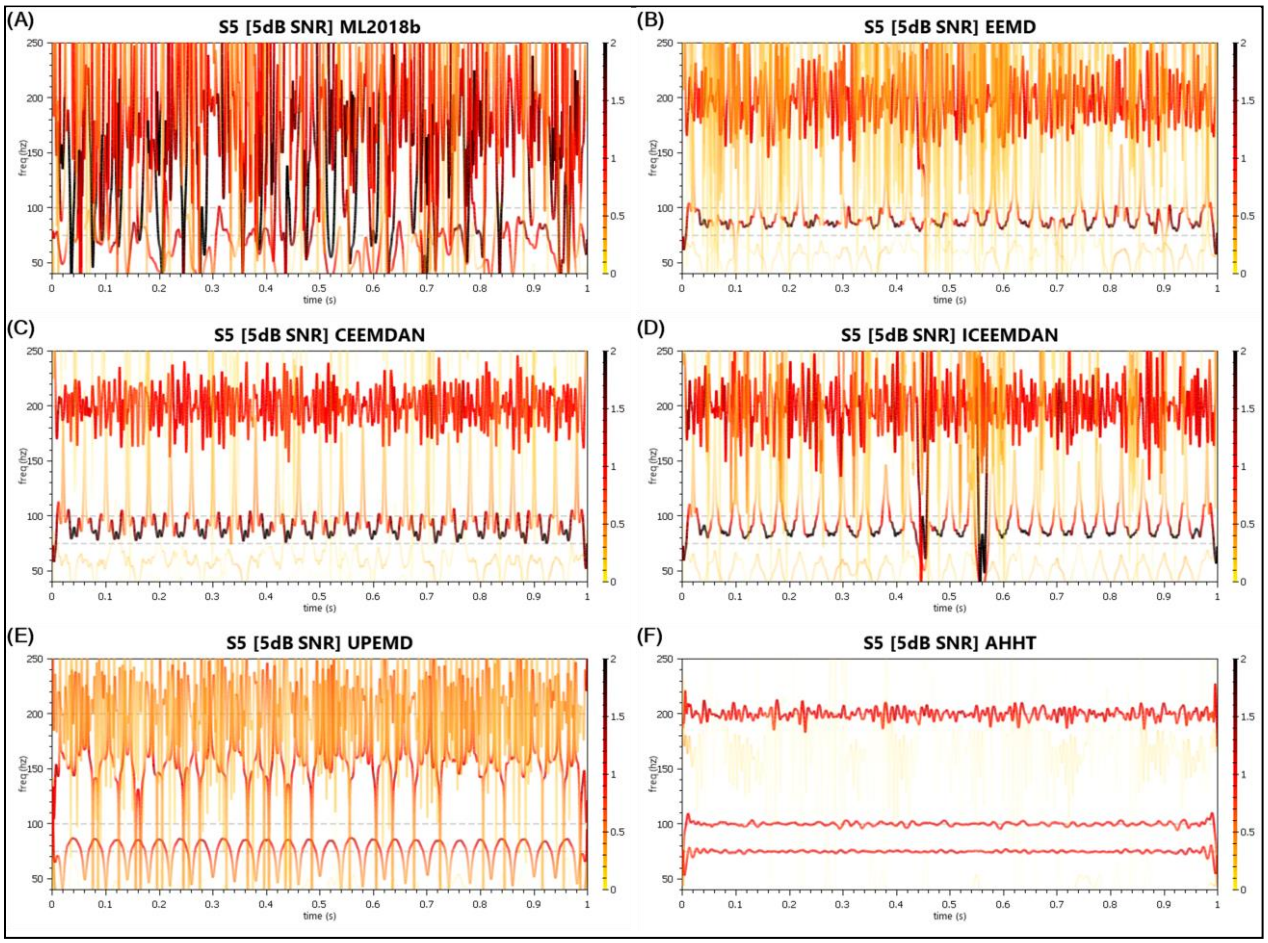


***Figure B-16 Upsampled Signal 5 (5dB SNR) - Hilbert Spectral Decompositions***

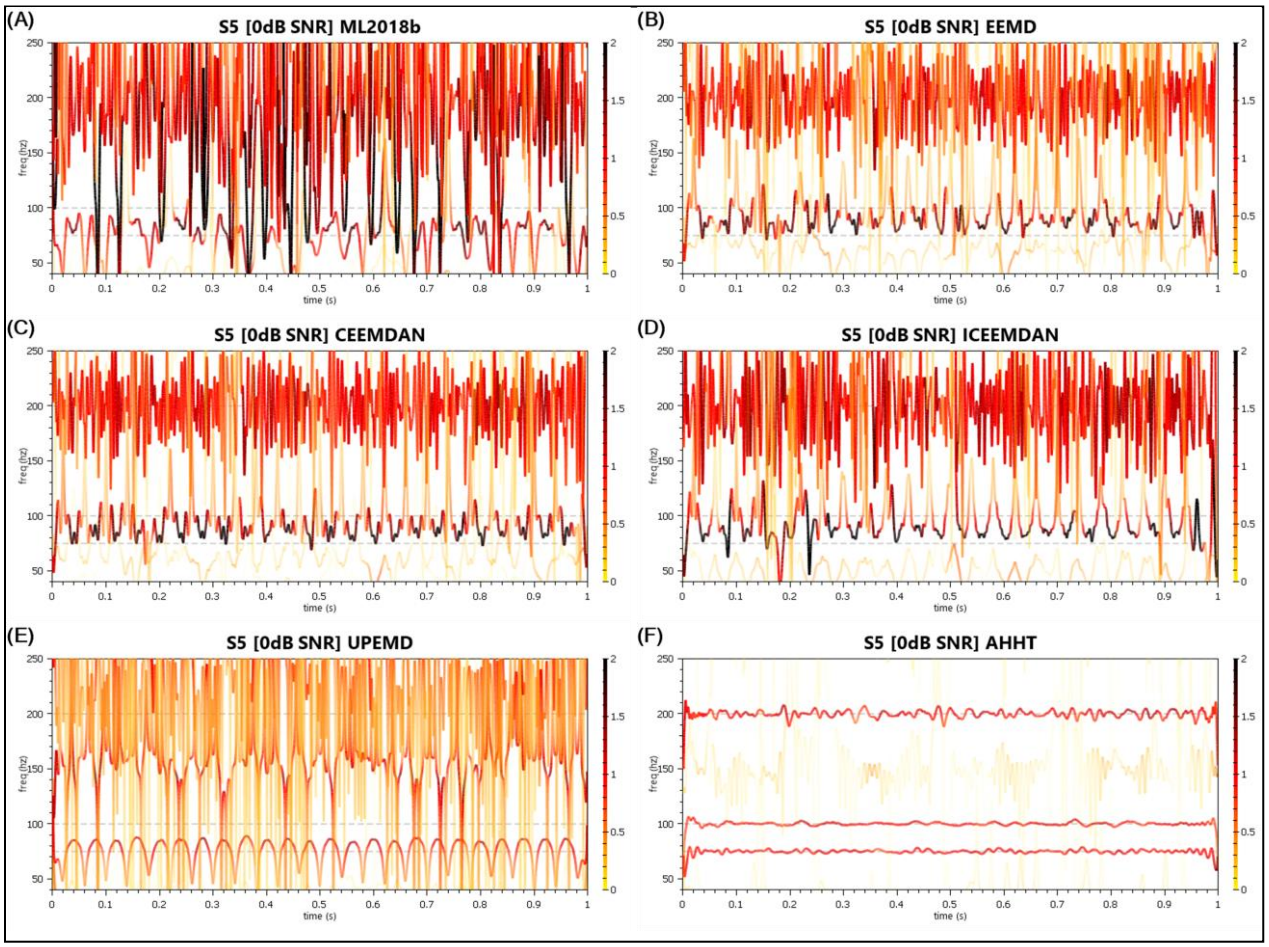


***Figure B-17 Upsampled Signal 5 (0dB SNR) - Hilbert Spectral Decompositions***

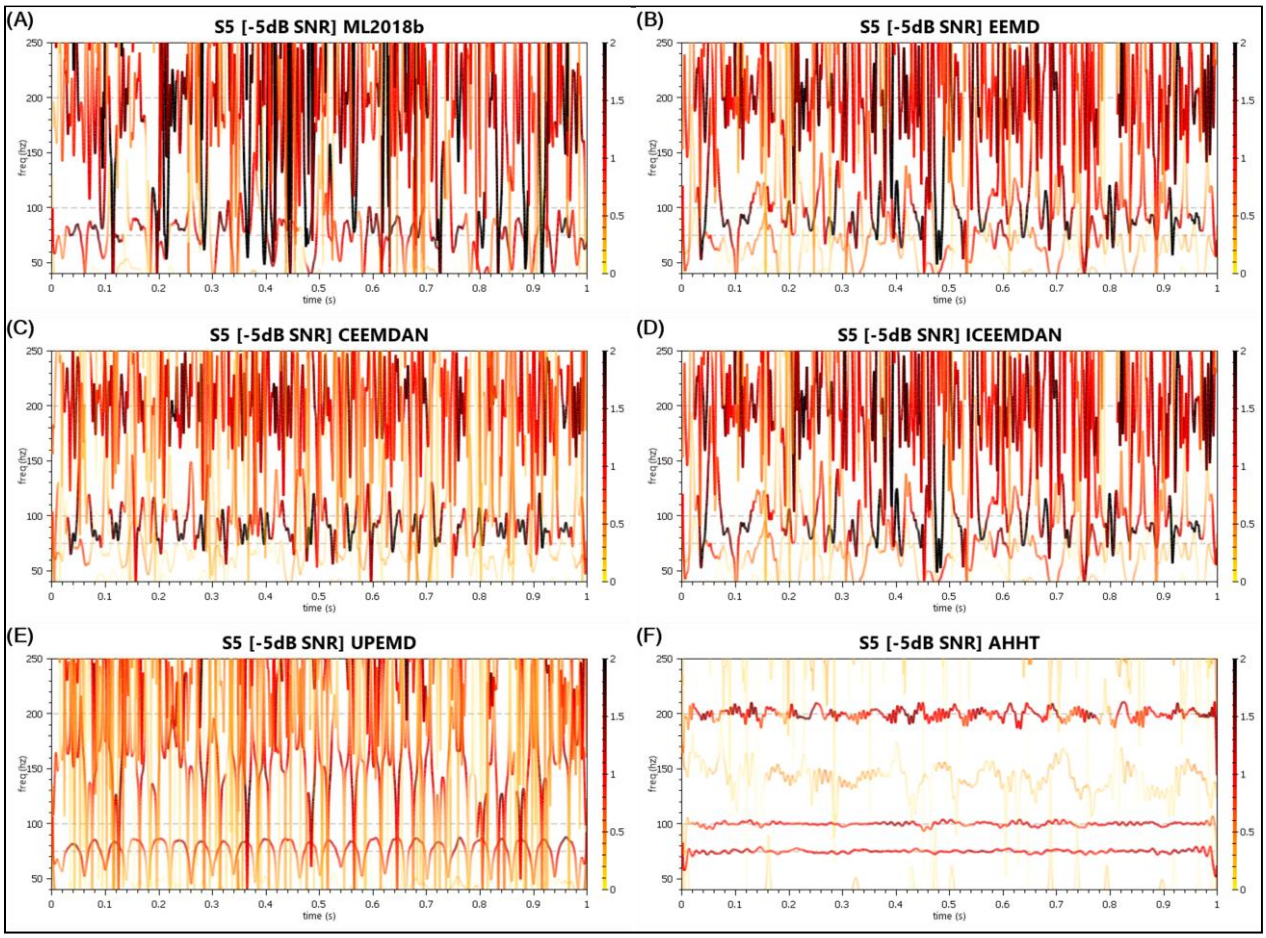


***Figure B-18 Upsampled Signal 5 (-5dB SNR) - Hilbert Spectral Decompositions***

*Table B-3 Upsampled Signal 5 (All) - IMF Counts and QoD Values*

| | MATLAB EMD | EEMD | CEEMDAN | ICEEMDAN | UPEMD | AHHT |
|---|---|---|---|---|---|---|
| **Upsampled Signal #5 – 3 Component Signals** | | | | | | |
| # of IMFs + Res | 5 | 14 | 15 | 12 | 13 | 4 |
| $QoD_1$ | 0.099468 | 0.140463 | 0.067864 | 0.195147 | 0.058406 | **0.960785** |
| $QoD_2$ | 0.146337 | 0.026829 | 0.400963 | 0.292686 | 0.791562 | **0.003888** |
| **Upsampled Signal #5 (20 dB SNR)** | | | | | | |
| # of IMFs + Res | 11 | 14 | 15 | 12 | 13 | 9 |
| $QoD_1$ | 0.060826 | 0.056062 | 0.077134 | 0.146958 | 0.058917 | **0.954664** |
| $QoD_2$ | 0.532281 | 0.183193 | 0.530977 | 0.524301 | 0.975465 | 0.236321 |
| **Upsampled Signal #5 (10 dB SNR)** | | | | | | |
| # of IMFs + Res | 11 | 15 | 14 | 12 | 13 | 10 |
| $QoD_1$ | 0.01825 | 0.008165 | 0.132134 | 0.009055 | 0.056097 | **0.888054** |
| $QoD_2$ | 1.054129 | 0.615296 | 0.912661 | 0.917231 | 1.397841 | 0.79096 |
| **Upsampled Signal #5 (5 dB SNR)** | | | | | | |
| # of IMFs + Res | 11 | 15 | 15 | 13 | 13 | 12 |
| $QoD_1$ | 0.023747 | 0.078392 | 0.145385 | 0.113101 | 0.05522 | **0.786199** |
| $QoD_2$ | 1.697752 | 1.418502 | 1.397869 | 1.526685 | 1.873004 | 1.579817 |
| **Upsampled Signal #5 (0 dB SNR)** | | | | | | |
| # of IMFs + Res | 11 | 14 | 15 | 12 | 13 | 13 |
| $QoD_1$ | 0.036805 | 0.079392 | 0.091727 | 0.072883 | 0.050284 | **0.683265** |
| $QoD_2$ | 2.08434 | 2.456669 | 2.449599 | 2.646384 | 2.824877 | 3.059121 |
| **Upsampled Signal #5 (-5 dB SNR)** | | | | | | |
| # of IMFs + Res | 11 | 12 | 15 | 12 | 13 | 15 |
| $QoD_1$ | 0.02941 | 0.037988 | 0.033628 | 0.037988 | 0.038889 | **0.422288** |
| $QoD_2$ | 4.392684 | 4.403106 | 4.096299 | 4.403106 | 4.706581 | 6.086905 |

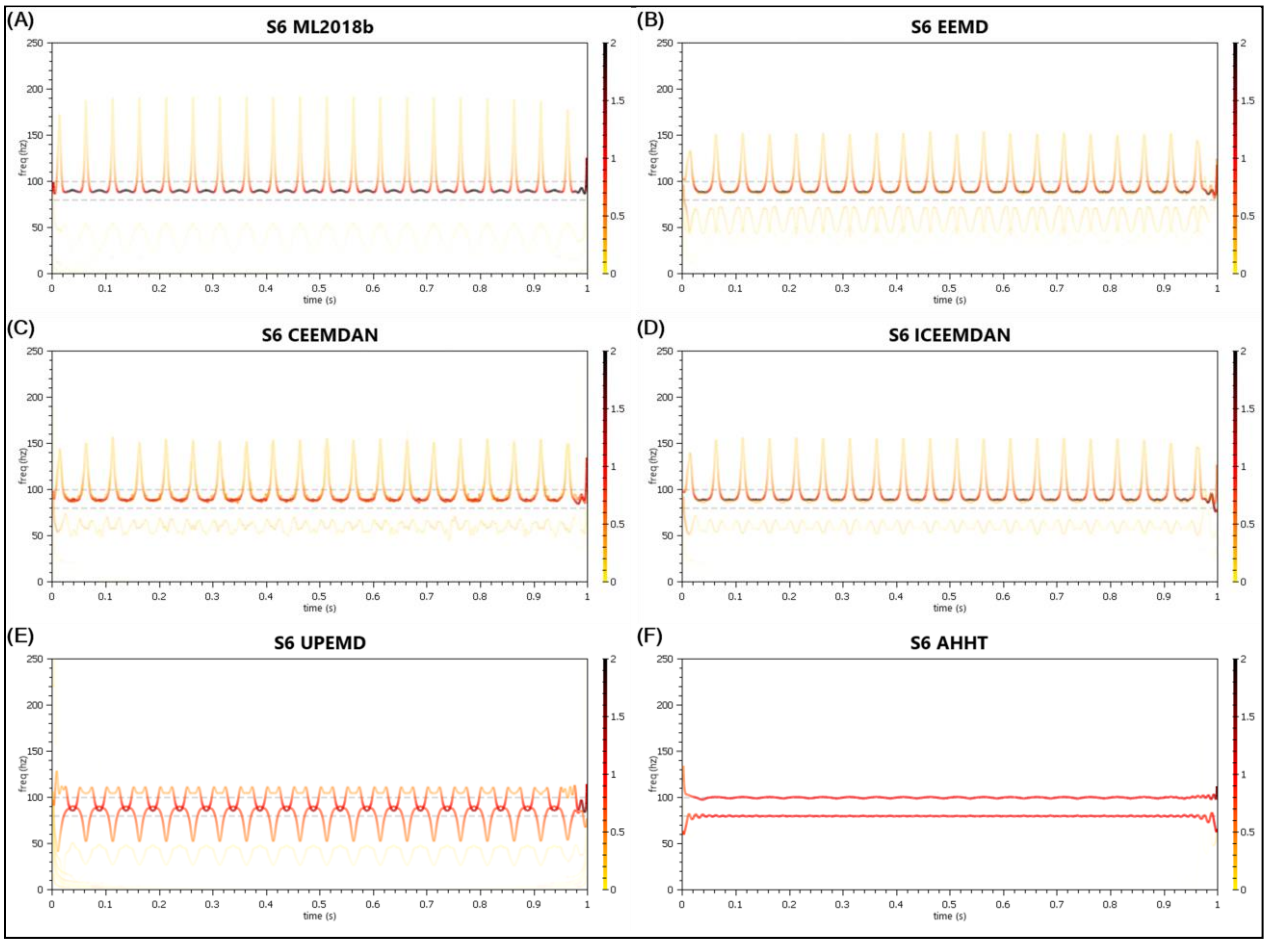


***Figure B-19 Upsampled Signal 6 - Hilbert Spectral Decompositions***

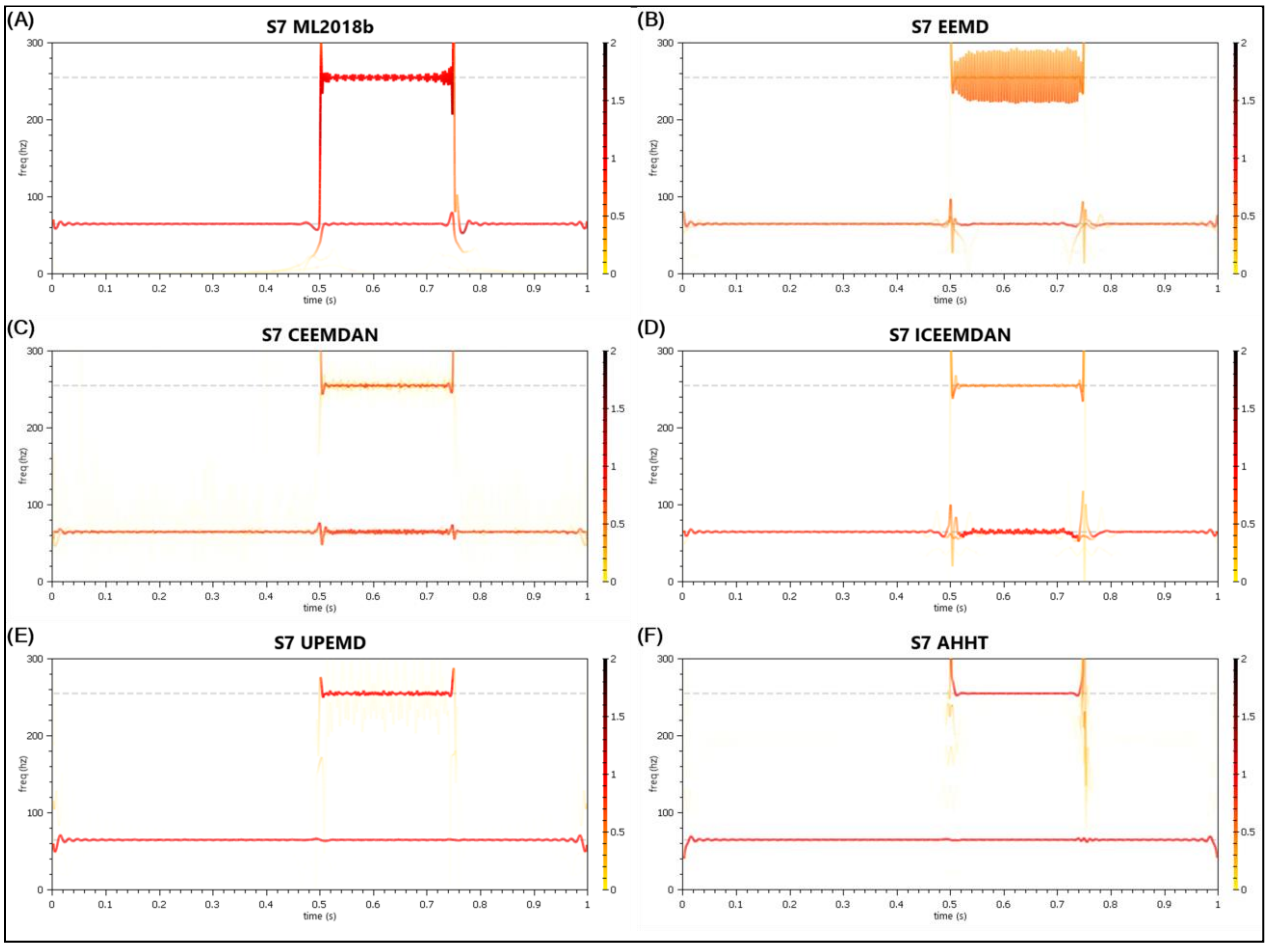


***Figure B-20 Upsampled Signal 7***

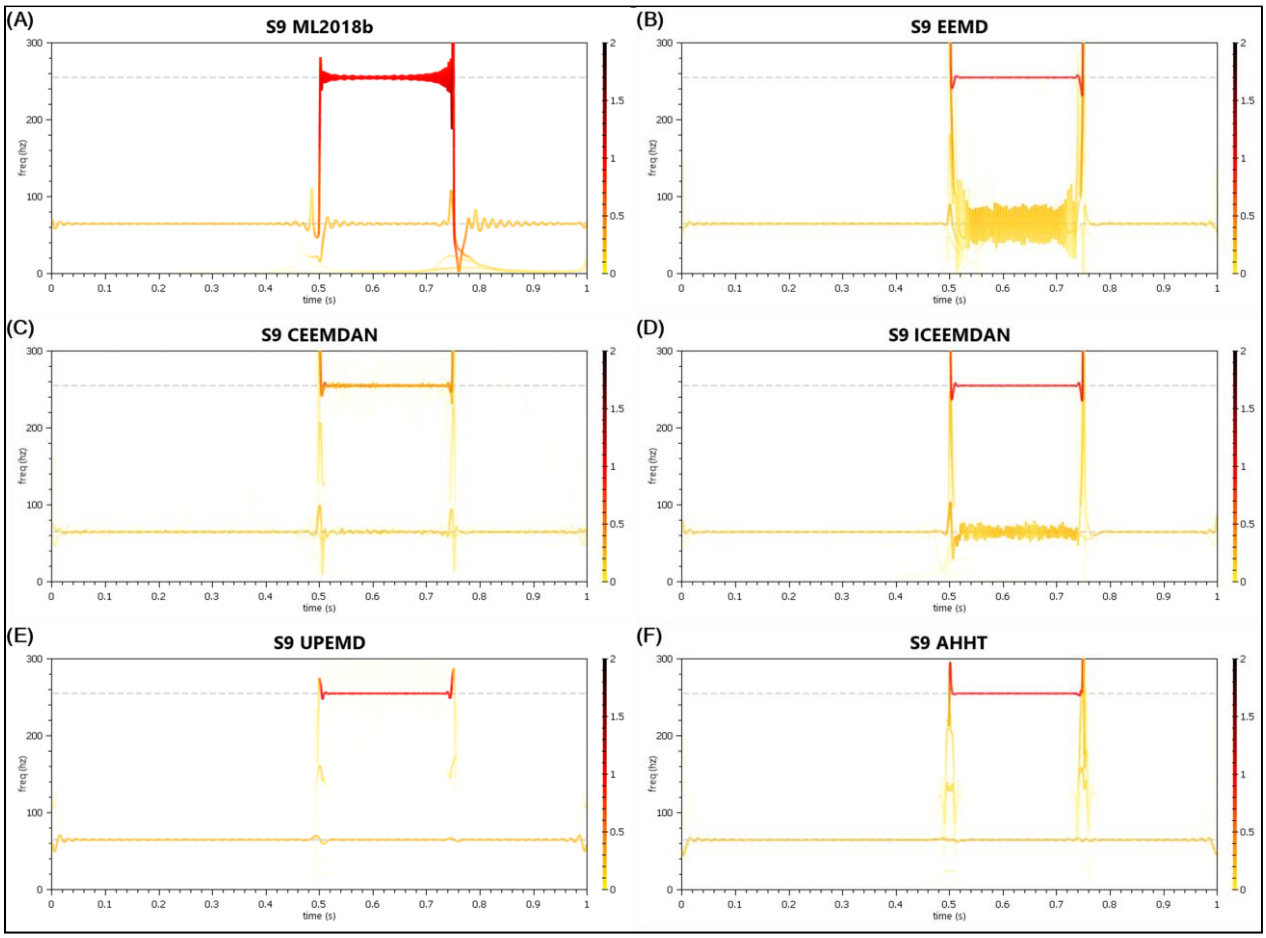


***Figure B-21 Upsampled Signal 9***

*Table B-4 Upsampled Signals 6, 7, 9 - IMF Counts and QoD Values*

| | MATLAB EMD | EEMD | CEEMDAN | ICEEMDAN | UPEMD | AHHT |
|---|---|---|---|---|---|---|
| **Upsampled Signal #6 – 2 Component Signals** | | | | | | |
| # of IMFs + Res | 7 | 15 | 14 | 14 | 13 | 3 |
| $QoD_1$ | 0.001286 | 0.011804 | -0.00072 | 0.010277 | 0.016403 | **0.897527** |
| $QoD_2$ | 0.211773 | 0.376739 | 0.240331 | 0.334099 | 0.218042 | **0.005306** |
| **Upsampled Signal #7 – 2 Component Signals** | | | | | | |
| # of IMFs + Res | 7 | 14 | 14 | 12 | 13 | 6 |
| $QoD_1$ | 0.114102 | 0.029503 | 0.076316 | 0.287624 | **0.915303** | 0.912855 |
| $QoD_2$ | 0.379488 | 0.372809 | 0.276192 | 0.258323 | **0.043887** | 0.048888 |
| **Upsampled Signal #9 – 2 Component Signals** | | | | | | |
| # of IMFs + Res | 7 | 15 | 15 | 13 | 13 | 6 |
| $QoD_1$ | 0.108405 | 0.535578 | 0.066222 | 0.739156 | **0.934624** | 0.926521 |
| $QoD_2$ | 0.182142 | 0.110145 | 0.138287 | 0.072851 | **0.02302** | 0.024974 |